NASA CONTRACTOR REPORT

NASA CR-1499

POTASSIUM TURBOALTERNATOR (KTA) PRELIMINARY DESIGN STUDY

Volume II - Alternator Parametric Design

Prepared by
GARRETT CORPORATION
Phoenix, Ariz.
for Lewis Research Center

NATIONAL AERONAUTICS AND SPACE ADMINISTRATION • WASHINGTON, D. C. • MARCH 1970

1. Report No. NASA CR-1499	2. Government Accession No.	3. Recipient's Catalog No.
4. Title and Subtitle POTASSIUM TURBOALTERNATOR (KTA) PRELIMINARY DESIGN STUDY II - ALTERNATOR PARAMETRIC DESIGN		5. Report Date March 1970 6. Performing Organization Code
7. Author(s)		8. Performing Organization Report No. APS-5317-R
9. Performing Organization Name and Address AiResearch Manufacturing Company of Arizona Phoenix, Arizona		10. Work Unit No. 11. Contract or Grant No. NAS 3-10934 13. Type of Report and Period Covered Contractor Report
12. Sponsoring Agency Name and Address National Aeronautics and Space Administration Washington, D.C. 20546		14. Sponsoring Agency Code

15. Supplementary Notes

Edited by R. A. Rachley

16. Abstract

The NASA is engaged in a research and technological investigation of high-temperature potassium Rankine cycle space power systems. As part of this program, AiResearch Manufacturing Company has performed a comprehensive analysis and preliminary design study of the potassium turboalternator component. The study was performed in two phases-a component performance and conceptual design analysis (Phase I) and a preliminary design study (Phase II). AiResearch was assisted by two subcontractors - Westinghouse Aerospace Electrical Division, which was responsible for the alternator design, and Westinghouse Astronuclear Laboratories, which provided technical assistance in the areas of turbine aerothermodynamic analysis and turbine material support. The report is presented in three volumes. Volume I covers the turbine and bearing parametrics, Phase I conceptual analysis and complete turboalternator configurations of Phase I. Volume II covers the Phase I alternator conceptual design. Volume III covers the detailed evaluation of the selected turboalternator assembly, which incorporates a ten-stage turbine and an alternator, each of which is straddle-mounted on potassium bearings with a flexible coupling between units. The KTA rotates at 19,200 rpm and produces 428 KWe, 480 V, 3 phase, 1600 hz electrical power.

17. Key Words (Suggested by Author(s))	18. Distribution Statement
Potassium turboalternator design Alternator, high temperature Refractory materials Rankine cycle	Unclassified - unlimited

19. Security Classif. (of this report)	20. Security Classif. (of this page)	21. No. of Pages	22. Price*
Unclassified	Unclassified	338	$3.00

*For sale by the Clearinghouse for Federal Scientific and Technical Information Springfield, Virginia 22151

Distribution of this report is provided in the interest of information exchange. Responsibility for the contents resides in the author or organization that prepared it.

FOREWORD

This report was prepared by the AiResearch Manufacturing Company of Arizona, A Division of The Garrett Corporation, and was originally issued as APS-5317-R. The activities discussed herein were conducted under NASA contract NAS 3-10934; Mr. E. E. Kempke of the Lewis Research Center Space Power Systems Division was the project manager for NASA, and Mr. R. A. Rackley directed the program at AiResearch and edited the final report.

The study was performed in two phases; a component performance and conceptual design analysis (Phase I) and a preliminary design study (Phase II). AiResearch was assisted by two subcontractors: Westinghouse Aerospace Electrical Division (WAED), which was responsible for the alternator design, and Westinghouse Astronuclear Laboratories (WANL), which provided technical assistance in the areas of turbine aerothermodynamic analysis and turbine material support. The report was issued in three volumes. Volume I covers the turbine and bearing Phase I conceptual analysis and complete turboalternator configurations of Phase I. Volume II covers the Phase I alternator conceptual design. Volume III covers the detailed evaluation of the turboalternator that resulted from the study.

The following individuals contributed to this program as specified: alternator design (WAED): Mr. T. C. Allen, Mr. A. E. King, Mr. C. C. Kouba, and Mr. J. L. McCabria; bearings and rotor dynamics (AiResearch): Mr. D. R. Chivens and Dr. L. A. Matsch; turbine aerodynamic and mechanical design (AiResearch): Dr. K. E. Boyd, Dr. C. S. Chang, Mr. C. A. Larson, and Mr. E. A. Mock; turbine aerothermodynamic and materials support (WANL): Mr. W. D. Pouchot and Mr. G. G. Lessman.

It should be noted that many of the bearing configurations, alternator variables, and turbine materials were initially identified during the analytical and experimental SNAP 50/SPUR program.

TABLE OF CONTENTS

LIST OF FIGURES

LIST OF FIGURES (Contd.)

LIST OF FIGURES (Contd.)

LIST OF FIGURES (Contd.)

LIST OF FIGURES (Contd.)

LIST OF TABLES

LIST OF TABLES (Contd.)

LIST OF TABLES (Contd.)

LIST OF TABLES (Contd.)

POTASSIUM TURBOALTERNATOR (KTA) PRELIMINARY DESIGN STUDY

II - ALTERNATOR PARAMETRIC DESIGN

1. INTRODUCTION AND SUMMARY

This report, submitted by The AiResearch Manufacturing Company of Arizona, A Division of The Garrett Corporation, presents the analysis and final results of a program conducted under NASA-Lewis Research Center contract NAS 3-10934, "Potassium Turboalternator Preliminary Design". The program was conducted in two phases; a component performance and conceptual design analysis (Phase I) and a preliminary design study (Phase II).

During the Phase I analysis, the individual turbine, alternator, bearings, and seals subcomponents were separately optimized. At the conclusion of the Phase I analyses at least four turboalternator configurations comprised of the optimized components were to be submitted to the NASA for their approval and selection. The Phase II effort was a detailed preliminary design of the turboalternator configuration(s) selected by the NASA at the end of Phase I.

Assisting AiResearch in the performance of the study were two subcontractors. Westinghouse Aerospace Division was responsible for the alternator electrical and mechanical design and analysis (exclusive of bearings). Westinghouse Astronuclear Laboratory supplied technical support in the anlysis of condensation formation and blade moisture collection, executed a detailed erosion analysis of the final turbine configuration, and provided the complete turbine materials support.

This report is in three volumes. Volume I contains the Phase I turbine, bearing, and rotor dynamic analysis as well as a definition of the KTA configurations defined at the end of Phase I. Volume II

contains the alternator conceptual design and analysis for Phase I. Volume III presents the final KTA configuration and the supporting analyses on the individual components.

The priorities observed in the component optimization were as ranked in descending order below:

(a) High reliability

(b) Ease of development

(c) Maximum energy conversion efficiency

(d) Minimum weight

1.1 Phase I Guidelines and Specifications

The pertinent alternator design specifications for Phase I were defined as follows:

(a) Design power output - 600 kva (450-kw_e, three-phase, at a 0.75 lagging load power factor)

(b) Maximum continuous load rating - 733 kva (550 kw_e)

(c) Overload - 1000 kva (900 kw_e at 0.9 lagging load power factor) for 5 sec

(d) Speed capability (percent of design speed) - 0 to 120

(e) The alternator design to the maximum extent feasible shall reduce to a minimum any adverse effects due to unbalanced magnetic forces

(f) The speed (frequency) control of the alternator is presently considered to be the parasitic-load type, and frequency regulation is anticipated to be ±1 percent of design frequency for a change in external load from 10 percent to maximum load (550 kw_e).

(g) Specification MIL-G-6099A (ASG), per the latest revision in effect at the start of the study, shall apply to the following:

(1) Waveform - Paragraph 4.5.16. In addition, the total RMS harmonic content of the line-to-neutral voltage wave, when the alternator is operating into a purely resistive load, shall be less than 5 percent from 10 to 100 percent maximum load (550 kw_e).

(2) Phase balance - Paragraphs 4.5.10, 4.5.10.1, and 4.5.10.2 except that Paragraph 4.5.10.1 is amended to read " ... the individual phase voltages shall not deviate from the average by more than 1.5, 3, and 6 percent, respectively."

(3) Output voltage modulation - Paragraph 4.5.13 except that modulation shall not exceed 0.5 percent.

(4) Overload - 1000 kva at 0.9 lagging load power factor for 5 sec

(5) Short-circuit capacity - Paragraph 4.5.12 for a minimum time of 5 sec

(h) Design Life - Three years minimum, with growth to 5 years as an ultimate objective.

(i) Environmental Specifications - Applicable portions of the component design requirements of NASA Specification Numbers P1224-1 and P1224-2, dated January 31, 1967, per the latest revision on date of beginning of the study.

(j) Radiation Environment - 10^7 rad, 10^{11} fast neutrous (>1 Mev)

(k) Radial gap alternator configuration

The major alternator design variables to be investigated in the conceptual design study (Phase I) and their ranges were:

(a)	Frequency:	800 to 2000 Hz in multiples of 400 Hz
(b)	Speed:	16000 to 32000 rpm
(c)	Voltage:	To be based on Westinghouse experience in prior studies. (As indicated in Section 2.4, System Design Variable Screening Studies, the selected voltage range was 120 to 1200 v Line-to-Neutral)
(d)	Coolants:	Stator - Liquid potassium or NaK - Organic liquid selected for organic bearing lubricant during study (Coolants above not to be mixed in same machine) Rotor - Liquid potassium - Organic liquid selected for organic bearing lubricant during study (Coolants above not to be mixed in same machine)

(e) Coolant Temperatures: Stator - Liquid potassium or NaK, 800° to 1100°F. (Stator hot-spot temperature to be 1100° to 1300°F)

- Organic - to be determined

Rotor - Liquid potassium 800° to 1100°F

- Organic - to be determined

The alternator conceptual designs presented in this report were determined through a process of elimination and optimization of candidate designs. Initially, parametric screening studies were carried out to eliminate all but the most desirable candidates. These parametric screening studies were concerned with

(1) Significant alternator internal design variables selection (which can exert significant influence on system considerations)

(2) Rotor materials selection

(3) Alternator/system design variables such as voltage, speed, frequency, and coolant temperature.

Separate rotor and stator detail design screening analyses were carried out in parallel with the parametric screening studies. Three of the most promising candidate designs were selected from the screening studies and were subjected to additional optimization studies to arrive at the three conceptual designs.

In addition, certain correlative studies not directly involved in the conceptual design process were performed.

The parametric screening studies, the detailed rotor and stator design screening analyses, the selection of base designs, the electrical and mechanical conceptual design analyses, and the correlative studies on the subjects of major sections which follow. Recommendations of the conceptual designs to be selected for further study in the Phase II preliminary design studies are also presented.

2. PARAMETRIC SCREENING STUDIES

2.1 Introduction

2.1.1 Background

Parametric screening studies of alternator design variables were performed to determine the values required to meet the primary design objectives within the specification requirements.

Studies were performed by calculating a complete generator design for each incremental value of a given parameter within a specified range. In this manner, all aspects of the alternator design which affects the primary design objectives, the specification requirements, and material limitations could be comparatively evaluated.

Designs were compared on the basis of alternator weight and efficiency to achieve minimum system weight within the bounds of materials and specification limitations. Primary criteria and considerations used in evaluating the designs are listed in Table 1. In those cases where alternator efficiency increased as alternator weight increased, a system weight penalty per kilowatt of loss criteria was required to aid in selection of the optimum parametric value. A specific weight penalty of 20 lb/kw was assumed. It was found that an increased weight penalty would not have significantly changed the choice of parameters because the 20 lb/kw was already predominate in the influence the penalty had on the choices.

TABLE 1

CONSIDERATIONS FOR SCREENING DESIGNS

Reliability
Ease of Development
Efficiency
Weight
Rotor Stress
Rotor Losses
Maximum Allowable Rotor Coolant Temperature
Turns per Coil
Conductor Temperature
Voltage Unbalance
Overload and Three-Phase Short Circuit Performance
Voltage Ionization and Breakdown
Magnetic Unbalance Rotor Forces
Voltage Waveform
Required Field Power
Rotor Weight

The design objectives of high reliability and ease of development were primary considerations in design trade-off selection. For example, the choice of two-conductor-per-slot designs and 120-deg phase belts were based primarily on these two objectives since this type of winding does not require intricate end extension crossover connections with the relatively stiff Inconel-clad silver conductors. This is an important feature considering that the silver in the conductor joint must not be exposed through the cladding material for reasons of silver migration through the insulation. Comparison of two- and four-conductor-per-slot coils is shown in Figure 1. The comparison of 120- and 60-deg phase belt windings is shown in Figure 2.

2 CONDUCTORS PER SLOT

4 CONDUCTORS PE

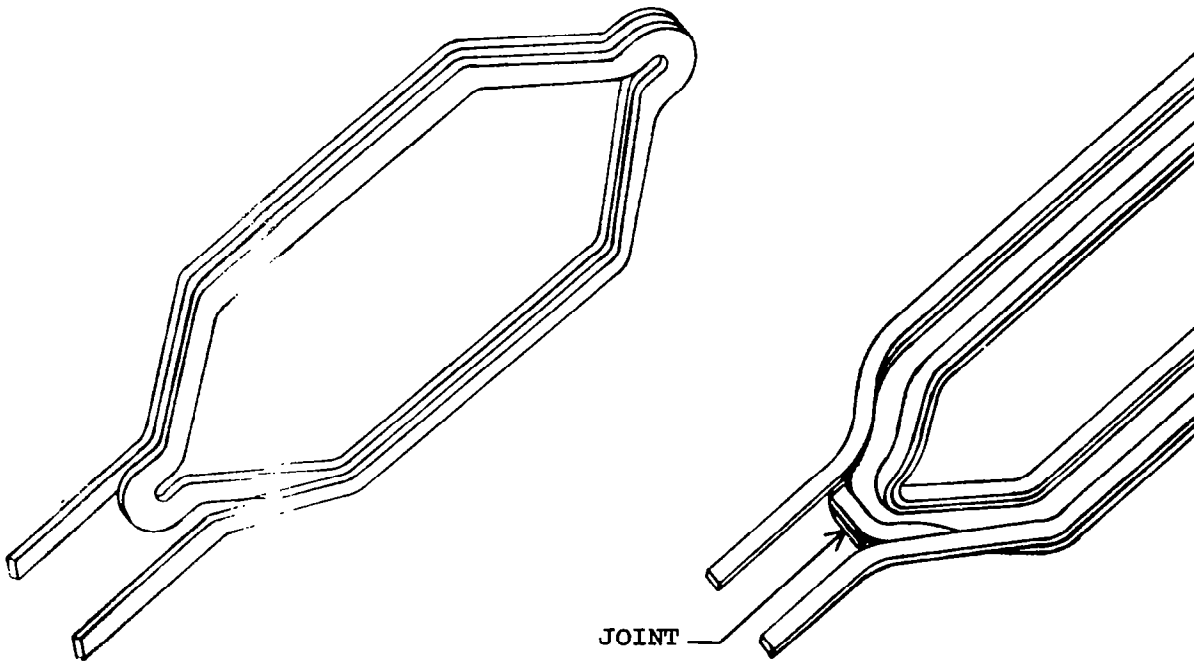

COIL SCHEMATICS

FIGURE 1

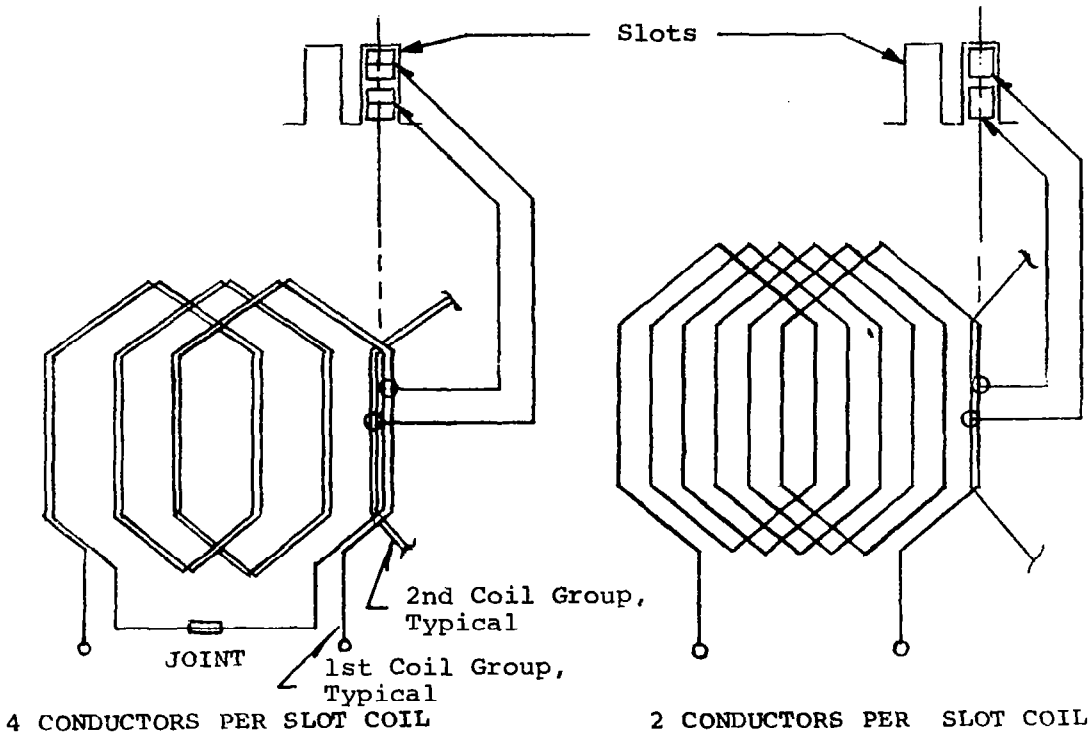

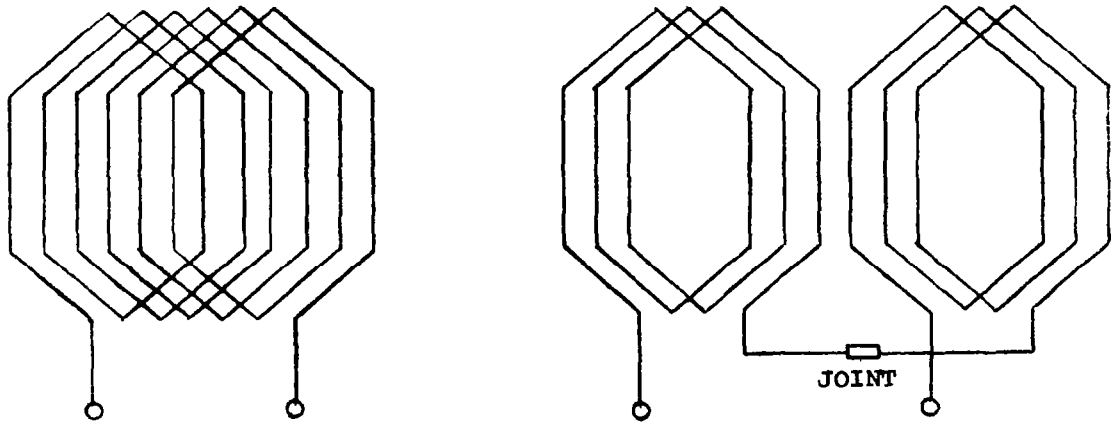

COIL CONFIGURATIONS

FIGURE 2

Minimization of rotor pole face losses and magnetic unbalance rotor forces by proper selection of design parameters was also directed toward increasing reliability and easing required development. Low pole face losses eliminate the need for elaborate rotor cooling schemes and reduced rotor magnetic forces alleviate the design requirements for the bearings. The comparative field power required for each design was taken into account as a secondary consideration because of its effect on voltage regulator-exciter (VRE) design. The VRE design requirements were not within the specific scope of this study.

In addition to the stator hot spot, another major mechanical design screening parameter is the rotor stress. Those designs giving too high stress during the screening studies were eliminated from further consideration for the conceptual designs. The particular criterion for establishing whether the stress was too high or not was changed during the screening studies, so a few words of explanation are in order as to exactly what criterion was used.

In the past, the Westinghouse Aerospace Electrical Division has carried out similar analytical screening studies[1*] where the selection criterion was as follows:

> "The average tangential stress in the rotor core is calculated based on the rotor core dimensions. This stress is then increased by a stress concentration factor to account for the rotor poles attached to the core; the factor is dependent upon the number of rotor poles. This stress is then compared to the allowable stress that will cause less than 0.2-percent creep strain over the design life of the rotor. Those alternators

*Superscript numbers refer to References in Section 8.

having calculated average tangential rotor stresses in excess of the allowable were said to be 'stress-limited' and considered impractical."

This same criterion was proposed and used at the start of the screening studies for the KTA alternator. However, during the course of the studies, it became apparent that the above approximation was not sufficient for making a sound judgment. The basic reasons for this were that the designs at the lower temperatures were not creep-strength limited, and there were several borderline cases that defied selection based on the previous criterion. As a result, a more comprehensive criteria was established and the rotor stresses were analyzed in detail rather than as a single average value.

The detail calculated rotor stress used was the maximum equivalent (or Von Mises) stress that occurs under the pole on a plane (r-z direction) through its center; this is the most crucial and usually the largest stress area to be considered in the alternator design. The Von Mises stress relationship was used to relate the biaxial stresses occurring in the rotor to the uniaxial, maximum allowable material stress. The criterion for the material stress limit was expressed in terms of the following considerations:

(a) The stress within the rotor at 20-percent overspeed shall not exceed 90 percent* of the ultimate tensile strength of the material.

*Later in the studies, when H-11 had been selected as the rotor material, the 90-percent limit was changed to 87 percent. This is because the 87-percent line corresponds to the 72-percent yield-strength limit; thus, any design meeting one of the two limits automatically met the other.

(b) The stress within the rotor at design speed shall not exceed 72 percent of the 0.2-percent offset yield strength of the material.

(c) The creep strain for 3-years operation shall be less than that required for the pole tips and bore seal to rub. The allowable strain must be determined from the initial dimensions of the actual alternator design. At the early stages of the design study, it was assumed that a maximum of 0.5-percent creep strain would be permissible.

Any design which did not meet any one of these three criteria were considered over-stressed and were dropped from further consideration. The calculation procedures used for determining the maximum principle stresses and the Von Mises stress are summarized in Appendix B of Reference 2.

Other major design criteria which were used in the screening processes concern windage and pole face losses. The pole face calculation procedures used in the screening studies are based upon those reported in Reference 3. The windage losses were initially calculated using the results of Reference 4.

Later, an improved method was derived and correlated with the original data of Smith[5]. The improved method gave more accurate results and is summarized in Appendix A.

Since separate studies were not carried out to determine configurations that minimized the windage and pole face losses until after the base designs had been selected, it was necessary to carry out the screening studies using fixed configurations that give minimal losses.

Unless these losses were calculated as abnormally high (tens of kilowatts), the values were not used as separate criteria for retaining or discarding a design. Rather, the calculated values were simply lumped with the rest of the losses for overall efficiency and system weight considerations.

The goal of the screening studies was to keep these rotor losses near or below the 1-kw (each) level. This level was not selected because of efficiency considerations, but rather because these losses occur in the sensitive rotor cooling circuit. It was recognized that losses above 1 kw would obviate the chances of a simple, reliable rotor cooling configuration being sufficient.

The screening studies were carried out in successive stages according to recognized areas of separation. They were in order of their occurrence:

(a) Internal Variables: These are the parameters of interest to the alternator designer that do not directly effect choice of external system parameters.

(b) Rotor Materials: Because of the significant influence the choice of rotor material has on the design limitations and performance, separate selection studies are required which compare materials in actual designs.

(c) System Design Variables: These are the parameters of interest to both the alternator designer and system designers.

(d) Organic Coolant: Because of the multitude of fluids available and because there are related influences between the

coolant and alternator design, separate comparative studies were made to evaluate the choices.

2.1.2 Selection of Coolant Temperatures

One of the intents of the screening study was to determine the best coolant temperature from the standpoint of the alternator design. Because of the interdependence between the alternator design, the initial materials selection, and the limited temperature capabilities of the materials, it was necessary to assign the coolant temperature the role of a dependent variable. That is, preselected fixed values were chosen and a family of parametric data were calculated about them. Later discussion will illustrate why it is not practical to consider coolant temperature a continuously variable parameter. Also, because of the dependence of the coolant temperature on system weight, the final recommendations were based on system as well as alternator considerations.

The ranges of coolants and temperatures to be considered in the study were:

(a) Organic Coolant:

Rotor and Stator - Coolant temperatures based on capabilities of fluids under consideration

(b) Alkali Metal Coolant:

Rotor - 800° and 1100°F Potassium

Stator - 800° and 1100°F Potassium, NaK

For the various fluids considered, it was assumed that the flow could be specified so that the bulk temperature rise through the alternator would remain constant. A weighted average of film drop was used for the various organic coolants considered; a film temperature drop of 1.0°F was used for the potassium and NaK coolants. The

purpose of these simplifications were to fix the heat-sink temperature conditions. This allowed the alternator temperature calculations to be made independent of a particular fluid or cooling scheme, thereby minimizing the number of calculations required in the preliminary stages. As a result, the discussions relate to 400, 800, and 1100°F alternators (Sections 2.3.1 and 2.5) without reference to the corresponding fluid whatever it may be.

2.2 Internal Design Variable Screening Studies

2.2.1 Background

It is generally recognized that system weight and performance is affected by the choice of alternator-electrical system variables such as frequency, speed, and voltage as well as the internal design variables. Therefore, a series of trial designs were performed to comparatively evaluate the resulting trends for these variables over a specific range. The trends were used to select the approximate values required to meet the specification requirements and primary design objectives prior to performing the frequency, speed, and voltage investigations. Candidate rotor materials were screened during the trial design studies at the lowest speed, highest frequency combination in order to prevent premature elimination of a candidate for reason of excessive rotor stress at a higher speed or lower frequency. The following basic design factors were held constant at 733 kva for the internal design variable studies:

Load power factor, lagging	0.75
Frequency	1600
Speed, rpm	16000
Voltage, L-N	480
Rotor material	Hiperco-27 for 400°F coolant H-11 forging for 800°F coolant 1BS1 for 1100°F coolant
Armature magnetic material	0.004-in. thick Hiperco 27
Stator frame material	Hiperco 27 forgings
Electric conductor material	Anadur insulated Inconel-clad silver
Slot liner material	99.5% alumina
Pole face configuration	Slotted
Armature hot-spot temperature limits	1100° to 1300°F

The screening studies were performed for three coolant temperatures. The lowest temperature (400°F) was for an organic coolant and the two higher temperatures (800° and 1100°F) were for an alkali metal coolant. A temperature excursion study in the range of 200° to 600°F for organic coolants was performed to determine possible design benefits from other than 400°F.

Nine internal design variables, out of a possible 28, were chosen for inclusion in the study. The variables selected were those that would significantly affect the application design goals and specification requirements and that required the knowledge of parametric trends to establish application trade-off information for the selection of optimum values. The values for other parameters were chosen based on established aerospace alternator design and manufacturing procedures and material properties and limitations.

The internal design parameters included in the screening studies are listed in Table 2. The internal design variables held constant for the trial design screening studies and their values are given in Table 3.

2.2.2 Results of Internal Design Parametric Screening Studies

Results of the direct axis synchronous reactance "Xd" studies for coolant temperatures of 400°, 800°, and 1100°F are given in Tables 4, 5, and 6, respectively. Results indicated that an increase in the voltage unbalance limit from 6 to 9 percent for the study was desirable since the specified 6-percent voltage unbalance required the value of per unit Xd be less than 0.7 at the expense of increased alternator weight, thereby restricting the parametric study to relatively heavier low Xd machines. A per-unit Xd of about 1.0 required the voltage unbalance limit (for 2/3 single-phase load) to be increased to 9 percent. It was requested and granted that the phase unbalance be increased to 9 percent.

Rotor and stator hot-spot temperatures, rotor stress at 16,000 rpm, overload and three-phase short circuit limitations were found to have relatively little influence on the choice of Xd. Both two and four conductor-per-slot designs were examined for the 800° and 1100°F coolant temperatures. Two conductor per slot designs have the advantage of a simpler winding configuration, better transfer of the armature heat load from the slots, and a higher number of armature slots for a given Xd which reduces pole face loss. The disadvantage in this application is that the maximum Xd is limited to a relatively low value due to a practical limit in the maximum number of slots, resulting in heavier designs.

A per-unit Xd range of 0.7 to 1.0 was selected for the three coolant temperatures for use in the remaining studies based on the best combinations of alternator weights and efficiency occurring in this range.

TABLE 2

STUDY VARIABLES

Design Variable	Range of Variable
Direct axis synchronous reactance "Xd"	0.25 - 1.6 per unit
Armature winding current density	3000 - 9200 amp/in.^{2}
Armature core flux density	20 - 110 kL/in.^{2}
Armature teeth flux density	80 - 130 kL/in.^{2}
Rotor core flux density	Range selected according to material
Radial gap	0.10 - 0.16 in.
Stator leakage flux	8 - 24%
Rotor leakage flux	4 - 6%
Phase belt	60 and 120 deg

TABLE 3

FIXED VARIABLES

Design Variable	Value
Parallel paths	6
Conductors in parallel	2
Pitch factor	0.666 or 0.8
Skew	0
Slot configuration	Semi-Closed Slot
Clearance between end turns	0.075 in.
Armature conductor insulation thickness	0.011 in.
Ceramic slot cell thickness	0.021 in.
Slot clearance depth	0.020 in.
Slot clearance width	0.018 in.
Conductor configuration	Rectangular
Ratio of tooth width to slot pitch	0.475
Armature stacking factor	0.9
Armature lamination thickness	0.004 in.
Damper bars on rotor	None
Field width clearance (for cooling fins, insulation, etc.)	0.268 in.
Field height clearance (for cooling fins, insulation, etc.)	0.493 in.
Pole embrace	0.667
Pole face configuration	Grooved
Field current density	4000 amp/in.^{2}

TABLE 4

RESULTS OF Xd STUDY - 400°F COOLANT

Conditions: 733 kva, 16000 rpm, 1600 Hz, 480 v (L-N), 120-deg phase belts, radial gap = 0.14 in. j = 6000 amp/in.^{2}, Rotor core flux density = 130 kl/in.^{2}

No. Slots	Xd P.U.	Electrical Weight, lb	Efficiency, %	Voltage Unbalance, %	Armature Hot-Spot, °F	Field Current Ratios	
						Overload	3Ø Short
4 Conductors per Slot							
162	1.54	819	89.0	15.09	876	1.23	1.74
144	1.22	799	91.5	11.57	810	1.16	1.58
126	0.87	827	92.0	8.18	768	1.10	1.35
108	0.69	915	92.1	6.33	741	1.06	1.20
90	0.49	957	91.2	4.52	772	1.03	0.96
72	0.34	1062	89.4	3.12	790	1.00	0.73

TABLE 5

RESULTS OF Xd STUDY - 800°F COOLANT

Conditions: 733 kva, 16,000 rpm, 1600 Hz, 480 v (L-N), 60-deg phase belts

No. Slots	Xd P.U.	Electrical Weight, lb	Efficiency, %	Voltage[1] Unbalance, %	Armature Hot-Spot, °F	Field Current Ratios	
						Overload	3Ø Short
4 Conductors per Slot							
162	1.44	768	90.7	12.83	1188	1.20	1.765
144	1.18	786	92.2	10.28	1114	1.14	1.615
126	0.92	815	92.3	7.95	1098	1.10	1.465
108	0.69	857	91.9	5.90	1105	1.06	1.21
90	0.48	917	90.8	4.09	1096	1.02	0.941
72	0.32	1046	87.7	2.78	1098	0.99	0.602
2 Conductors per Slot							
198	0.65	942	91.9	5.69	1081	1.05	1.13
180	0.57	1018	92.2	4.91	1047	1.04	1.05
162	0.50	1126	91.9	4.26	1044	1.03	0.948
144	0.42	1244	91.2	3.53	1042	1.02	0.834
126	0.35	1413	89.5	2.90	1056	1.00	0.726
108	0.25	1508	87.6	2.10	1058	0.993	0.555

(1) at 0, 0, 2/3 rated-amperes per phase

TABLE 6

RESULTS OF Xd STUDY - 1100°F COOLANT

Conditions: 733 kva, 16,000 rpm, 1600 Hz, 480 v
120-deg phase belts, radial gap - 0.1

No. Slots	Xd P.U.	Electrical Weight, lb	Efficiency, %	Voltage Unbalance, %	Armature Hot-Spot, °F	Fi Ov
4 Conductors per Slot						
180	1.57	882	89.8	14.04	1465	
162	1.29	872	91.2	11.36	1449	
144	1.02	872	91.7	8.85	1434	
126	0.77	948	91.3	6.64	1436	
108	0.56	1018	89.4	4.78	1416	
2 Conductors per Slot						
216	0.66	1051	91.4	5.78	1384	
198	0.59	1135	91.8	5.08	1365	
180	0.51	1211	91.7	4.38	1360	
162	0.46	1364	91.2	3.88	1359	

Results of the armature winding phase belt study are summarized in Table 7. The choice of phase belts is independent of temperature; therefore, the study performed for 800°F is applicable to the 400° and 1100°F coolant temperatures. A phase-belt angle of 120 deg was selected despite a slight weight and efficiency penalty because 120-deg belt windings eliminate the crossover connections and joints required for 60-deg phase belts. This improves reliability and ease of development relative to the use of clad silver conductors.

Tables 8, 9, and 10 present results of the current density studies performed for coolant temperatures of 400°, 800°, and 1100°F. A current density of 7000 amp/in.^{2} was selected for the 400°F organic fluid coolant temperature based on minimum system weight. A current density of 6000 amp/in.^{2} for the 800°F coolant temperature gave maximum efficiency and near minimum alternator weight while limiting armature hot-spot temperatures below 1100°F. A current density of 6000 amp/in.^{2} was also chosen for the 1100°F coolant temperature based on near-minimum system weight and a voltage unbalance less than 9 percent. A current density of about 2500 amp/in.^{2} would be required to reduce armature hot-spot temperatures below 1300°F, resulting in a severe increase in system weight and a voltage unbalance above 9 percent. Alternate choices are to (1) Operate at a higher current density (6000 amp/in.^{2}) and reduce hot-spot temperatures by an improved cooling configuration for the windings (2) Use a simple configuration such as required for the 800°F coolant (conduction to stator stacks and radiation off end-turns to stator frame) and allow the hot spot to go as high as 1500°F and use a conductor capable of the temperature, e.g., CUBE* alloy insulated with plasma-arc sprayed alumina.

Results of the flux density studies for the three coolant temperatures are given in Tables 11, 12, and 13. Tooth densities of 130,

*Handy and Harman's dispersioned-strengthened copper alloy[12]

TABLE 7

RESULTS OF PHASE BELT STUDY

Conditions: 733 kva, 16,000 rpm, 1600 Hz, 480 v (L-N), 800°F coolant temperature, 180 slots, 2 conductors per slot

PHBLT, deg	Xd P.U.	Electrical Weight, lb	Efficiency %	Voltage Unbalance, %	Field Current Ratio		Pitch	Armature Hot-Spot, °F
					Overload	3Ø Short		
60	0.57	1018	92.2	4.91	1.04	1.05	0.666	1047
120	0.55	1064	91.9	4.75	1.04	1.01	0.800	1072

TABLE 8

RESULTS OF CURRENT DENSITY STUDY – 400°F COOLANT

Conditions: 733 kva, 16,000 rpm, 1600 Hz, 480 v (L-N), 120-deg phase belts, 126 slots, 4 conductors per slot

Current Density, amp/in.^{2}	Electrical Weight, lb	Efficiency, %	Voltage Unbalance, %	Field Current Ratios		Armature Hot-Spot, °F
				Overload	3Ø Short	
3933	892	91.4	8.61	1.1	1.36	712
5061	864	91.9	8.39	1.1	1.38	739
5753	842	92.1	8.20	1.1	1.35	768
7472	817	92.0	8.09	1.1	1.34	865
8332	807	91.9	8.05	1.1	1.34	923
9217	800	91.7	8.03	1.1	1.34	988

TABLE 9

RESULTS OF CURRENT DENSITY STUDY - 800°F COOLANT

Conditions: 733 kva, 16,000 rpm, 1600 Hz, 480 v (L-N), 180 slots, 120-deg phase belts, 2 conductors per slot

Current Density, amp/in.^{2}	Xd P.U.	Electrical Weight, lb	Efficiency, %	Voltage Unbalance, %	Field Current Ratios		Armature Hot-Spot, °F
					Overload	3Ø Short	
3933	0.55	1099	91.6	4.87	1.04	1.01	1017
5061	0.55	1074	91.8	4.77	1.04	1.01	1045
5753	0.55	1064	91.9	4.75	1.04	1.01	1072
7472	0.54	1048	91.6	4.74	1.04	1.01	1144
8543	0.54	1042	91.4	4.76	1.04	1.01	1204

TABLE 10

RESULTS OF CURRENT DENSITY STUDY - 1100°F COOLANT

Conditions: 733 kva, 16,000 rpm, 1600 Hz, 480 v (L-N), 120-deg phase belts, 144 slots, 4 conductors per slot, radial gap = 0.13 in.

Current Density, amp/in.^{2}	Xd P.U.	Electrical Weight, lb	Efficiency, %	Voltage Unbalance, %	Armature Hot-Spot, °F	Field Current Ratios	
						Overload	3Ø Short
9217	1.00	825	90.6	8.83	1645	1.3	1.23
8332	1.01	833	91.0	8.82	1591	1.3	1.23
7472	1.01	842	91.3	8.82	1539	1.3	1.22
5753	1.01	851	91.6	8.76	1434	1.6	1.12
5061	1.03	882	91.7	8.93	1398	1.3	1.20
3933	1.08	956	92.0	9.30	1342	1.2	1.37
3070	1.11	980	91.3	9.73	1317	1.3	1.3

TABLE 11

RESULTS OF FLUX DENSITY STUDIES - 400°F COOLANT

Conditions: 733 kva, 16,000 rpm, 1600 Hz, 480 v (L-N), 120-deg phase belts, j = 7000 amp/in.^{2}, 126 slots, 4 conductors per slot, radial gap = 0.14 in.

Flux Density, kl/in.^{2}	Electrical Weight, lb	Efficiency, %	Voltage Unbalance, %	Field Current Ratios		Armature Hot-Spot, °F	Xd P.U.
				Overload	3Ø Short		
Armature Core Flux Density							
20	1164	93.2	8.04			1020	0.85
30	967	92.9	8.07			948	0.86
40	889	92.6	8.08			910	0.86
50	845	92.3	8.09			883	0.86
60	817	92.0	8.09			865	0.86
70	797	91.7	8.10			853	0.86
80	782	91.4	8.10			844	0.86
90	771	91.1	8.11			837	0.86
100	762	90.9	8.11			829	0.86
110	756	90.6	8.11			824	0.86
Tooth Flux Density							
89	1077	91.3	11.65	1.18	1.58	828	1.26
99	981	91.6	10.33	1.15	1.52	837	1.11
110	867	91.8	8.92	1.12	1.41	853	0.95
120	817	92.0	8.09	1.10	1.34	865	0.86
130	775	92.1	7.36	1.09	1.27	882	0.79
Rotor Core Flux Density							
80.1	855[a]	92.1	6.88	1.07	1.10[b]		0.77
100.2	830	92.1	7.37	1.08	1.10		0.80
118.9	844	92.1	8.08	1.08	1.11		0.87
130.2	817	92.0	8.09	1.10	1.14		0.86
140.3	821	91.9	8.38	1.12	1.20		0.89
160.3	819	91.4	8.70	1.16	1.28		0.91

(a) Corresponding rotor weights are 381, 346, 344, 316, 315, and 294 lb

(b) At 10-percent overvoltage instead of at 3Ø short

TABLE 12

RESULTS OF FLUX DENSITY STUDIES - 800°F COOLANT

Conditions: 733 kva, 16,000 rpm, 1600 Hz, 480 v (L-N), 120-deg phase belts, j = 6000 amp/in.^{2}

Flux Density, Kl/in.^{2}	Electrical Weight, lb	Efficiency, %	Voltage Unbalance, %	Field Current Ratios		Armature Hot-Spot, °F	Xd P.U.
				Overload	3Ø Short		
Armature Core Flux Density (180 slots, 2 conductors per slot)							
20	1583	93.9	4.72	1.03	1.01	1144	
30	1297	93.5	4.73	1.04	1.02	1121	
40	1191	93.0	4.74	1.04	1.02	1112	
50	1130	92.6	4.74	1.04	1.01	1090	
60	1091	92.3	4.75	1.03	1.01	1074	
70	1064	91.9	4.75	1.04	1.01	1072	
80	1044	91.6	4.75	1.04	1.00	1062	
90	1028	91.3	4.75	1.03	1.00	1058	
100	1016	91.0	4.75	1.04	1.00	1056	
110	1007	90.7	4.75	1.04	.98	1049	
Tooth Flux Density (126 slots, 4 conductors per slot)							
80	1226	91.5	11.86	1.17	1.63	1110	1.34
90	1101	92.0	10.36	1.14	1.56	1126	1.16
100	1005	92.2	9.18	1.11	1.49	1126	1.03
110	937	92.2	8.29	1.09	1.43	1128	0.93
120	885	92.3	7.51	1.09	1.36	1134	0.85
130	833	92.3	6.79	1.08	1.25	1143	0.78
Rotor Core Flux Density (H-11 Rotor, Air Gap = 0.13, 126 slots, 4 conductors per slot)							
70	898 (a)	92.1	7.22	1.12 (b)		1161	0.83
80	833	92.3	7.41	1.14		1134	0.84
90	886	92.2	7.85	1.39		1132	0.88
95	874	92.0	7.73	1.84		1133	0.86
100	891	91.3	7.97	2.90		1134	0.89

(a) Corresponding rotor weights are 420, 386, 379, 354, and 353 lb
(b) At 10 percent overvoltage instead of at overload

TABLE 13

RESULTS OF FLUX DENSITY STUDIES - 1100°F COOLANT

Conditions: 733 kva, 16,000 rpm, 1600 Hz, 480 v (L-N), 120-deg phase belts, $j = 6000$ amp/in.^{2}, 144 slots, 4 conductors per slot, radial gap = 0.14 in.

Flux Density, kl/in.^{2}	Electrical Weight, lb	Efficiency, %	Voltage Unbalance, %	Field Current Ratios		Armature Hot-Spot, °F	Xd P.U.
				Overload	3Ø Short		
Armature Core Flux Density							
20	1277	93.1	8.44			1479	0.97
30	1060	92.9	8.49			1461	0.97
40	975	92.7	8.51			1449	0.97
50	931	92.5	8.53			1438	0.97
60	903	92.3	8.54			1436	0.97
70	884	92.2	8.55			1432	0.98
80	870	92.0	8.55			1429	0.98
90	858	91.8	8.55			1427	0.98
100	850	91.6	8.56			1423	0.98
110	844	91.3	8.56			1422	0.98
Tooth Flux Density							
129.6	870	90.7	7.49	2.04	0.8	1436	0.87
120.3	884	92.2	8.55	1.27	1.23	1432	0.98
110.0	930	92.2	9.61	1.21	1.42	1429	1.09
100.1	999	92.3	10.79	1.21	1.57	1427	1.21
89.7	1095	92.0	12.38	1.25	1.67	1427	1.37
84.1	1154	91.9	13.38	1.27	1.69	1425	1.49
Rotor Core Flux Density							
45.2	954 (a)	92.0	7.7			1438	0.90
50.2	942	92.1	8.18			1438	0.95
56.2	911	92.1	8.29			1438	0.95
60.4	903	92.1	8.54			1438	0.97
70.4	870	92.1	8.74			1440	0.99

(a) Corresponding rotor weights are 497, 483, 450, 440, and 408 lb

120, and 115 kilolines/in.^{2} were selected for coolant temperatures of 400°, 800°, and 1100°F, respectively, based on minimum system weight, voltage unbalance, and proximity to magnetic saturation of the teeth.

An armature core flux density of 60 kilolines/in.^{2} was chosen for the 400° and 800°F coolant temperatures and 70 kilolines/in.^{2} for the 1100°F based on near-minimum system weight, low armature conductor temperature, and near-minimum stator outside diameter. Alternator weight and stator O.D. increase rapidly for density values below 60 kilolines/in.^{2} and although a slightly lighter system weight is indicated for a lower core density (considering a weight penalty of 100 lb/kw), the higher values were retained since very large core depths may not be fully utilized by the high frequency (1600 Hz) flux wave.

The rotor materials selected for the 400°, 800° and 1100°F coolant temperatures for the internal design parametric screening studies were Hiperco 27, premium quality H-11 (AMS 6487), and 1BS1 experimental alloy based on a preliminary assessment of the required material strength and magnetic properties for the specified coolant temperatures. Final selection of rotor materials was performed in a latter stage of the study. Selected densities for the 400°F coolant temperature, Hiperco 27 rotor, the 800°F coolant temperature, H-11 rotor, and the 1100°F coolant temperature, 1BS1 rotor were 130, 80, and 60 kilolines/in.^{2}, respectively, based on the best combination of alternator weight and efficiency, rotor weight, and field current ratios for a 10-percent overvoltage condition which is a measure of the proximity of the rated operating density to the saturation level of the rotor material.

Radial gap study results are tabulated in Tables 14 and 15. The choice of radial gap (0.140 in.) for the 400° and 800°F coolant temperatures was based on achieving minimum weight and maximum efficiency at reasonable levels of rotor stress, pole face loss, and voltage

TABLE 14

RESULTS OF RADIAL GAP STUDY - 400°F COOLANT

Conditions: 733 kva, 16,000 rpm, 1600 Hz, 480 v (L-N), 120-deg phase belts, j = 7000 amp/in.^{2}, 1260 slots, 4 conductors per slot

Radial Gap, in.	Electrical Weight, lb	Efficiency, %	Voltage Unbalance, %	Rotor Weight, lb	Xd P.U.
0.16	783	92.2	6.66	304	0.71
0.15	787	92.2	7.11	306	0.76
0.14	769	92.1	7.35	290	0.79
0.13	772	92.0	7.90	293	0.85
0.12	757	91.9	8.20	276	0.89
0.10	771	91.6	9.70	296	1.10

TABLE 15

RESULTS OF RADIAL GAP STUDY - 800°F COOLANT

Conditions: 733 kva, 16,000 rpm, 1600 Hz, 480 v (L-N), 120-deg phase belts, j = 6000 amp/in.^{2}, 126 slots, 4 conductors per slot

Radial Gap, in.	Electrical Weight, lb	Efficiency, %	Voltage Unbalance, %	Rotor Weight, lb	Xd P.U.
0.12	894	91.7	8.10	397	0.92
0.13	880	91.8	7.42	386	0.84
0.14	872	91.8	6.83	378	0.77
0.16	891	91.7	6.21	395	0.70

unbalance. Where a choice existed between two alternatives (0.130 or 0.140 in.) of near-equal overall designs, the largest was chosen to minimize magnetic unbalance forces, provide increased radial clearance, and reduce pole face loss. Results of the 800°F studies are applicable to the 1100°F coolant designs.

Results of the leakage flux study for the 800°F coolant are tabulated in Table 16 and are applicable to the 400° and 1110°F coolant designs since leakage flux is independent of temperature. A stator leakage of 20 percent of the main path flux and a rotor leakage of 5 percent of the rotor useful flux were chosen based on minimum weights and maximum efficiencies consistent with acceptable rotor stress and voltage unbalance values.

A summary of the selected design variables resulting from the internal design variable parametric studies is presented in Table 17.

2.3 Rotor Materials Screening Studies

2.3.1 Background

Various rotor alloys were investigated to determine the best rotor material for the three coolant temperatures, 400°, 800°, and 1100°F. A complete generator design was calculated for various values of rotor core flux density incorporating the internal design parameters selected from the previous studies. After selecting the optimum rotor core flux density for each material, generator designs were compared on the basis of efficiency, weight, rotor material limitations, and specification requirements. The candidate materials selected for the rotor materials screening studies, the applicable coolant temperatures, and the maximum hot spot (pole face) temperatures allowed based on material property limitations are summarized in Table 18.

TABLE 16

RESULTS OF LEAKAGE FLUX STUDIES

Conditions: 733 kva, 16,000 rpm, 1600 Hz, 480 v (L-N), 800°F coolant, 120-deg phase belts, j = 6000 amp/in.^{2}, 4 conductors per slot

Leakage Flux, percent	Electrical Weight, lb	Efficiency, percent	Voltage Unbalance, percent	Rotor Weight, lb	Xd P.U.
Stator Leakage Flux (126 slots)					
24.0	870	91.8	6.99	370	
20.0	868	91.8	6.89	374	
16.0	872	91.8	6.77	382	
12.0	883	91.7	6.68	396	
8.0	903	91.8	6.26	415	
Rotor Leakage Flux (126 slots)					
4.3	875	91.6	6.55	389	0.75
4.9	896	91.6	7.08	404	0.80
5.1	875	91.8	6.90	376	0.77
5.3	887	91.8	7.11	384	0.79
5.8	911	91.8	7.45	399	0.83
6.4	887	91.9	7.45	371	0.82
Rotor Leakage Flux (144 slots)					
4.3	810	91.8	8.87	348	1.00
4.9	814	91.8	9.19	336	1.02
5.1	829	91.8	9.53	347	1.06
5.3	837	91.8	9.78	351	1.08
5.8	852	91.8	10.18	358	1.12

TABLE 17

SUMMARY OF RESULTS OF PARAMETRIC SCREENING STUDIES

Parameter	Coolants	
	400°F	800°F
Internal Design Variables		
Direct Axis Synchronous Reactance, Xd	0.7 - 1.0	0.7 - 1.05
Phase Belt-deg, pitch	120, 0.8	120, 0.8
Armature current density, amp/in.^{2}	7000.	6000.
Armature core flux density, kl/in.^{2}	60.	60.
Armature tooth flux density, kl/in.^{2}	130.	120.
Rotor core flux density, kl/in.^{2}	130.*	80.
Radial gap, in.	0.14	0.14
Stator leakage flux, %	20.	20.
Rotor leakage flux, %	5.	5.

*For Hiperco-27 rotor material. After later rotor materials and stress analy the rotor material for 400°F coolant was changed to H-11 steel. The flux de reoptimized for the H-11 at 400°F and a value of 90 kl/in.^{2} was selected.

TABLE 18

MATERIALS EXAMINED DURING ROTOR MATERIALS SCREENING STUDIES

	Coolant Temp., °F	Maximum Hot-Spot Temp., °F
15% Ni Maraging Steel - specified in work statement; age-hardenable high-strength steel with reasonably good magnetic properties; limited to organic coolant temperatures due to low curie temperature that is time-temperature dependent; properties summarized in Reference 7.	400	700
Hiperco-27 Alloy - high permeability soft magnetic alloy; usually considered a stator material; applicable to high temperature but strength limited; properties summarized in Reference 7.	400 800	900
H-11 Steel at 45 R_C - high-strength tool steel softened somewhat to improve magnetic properties; considerable data available on this alloy; properties summarized in Reference 6 and 7.	400 800	950
1AS2 Alloy - precipitation-hardened developmental alloy; identified by heat on Contract NAS3-6465; represents improvement over H-11 steel but is too brittle in its present developmental state; large forging techniques need to be developed also; properties summarized in Reference 8.	800	1025
NIVCO - originally developed as a turbine blading material; adapted as a magnetic rotor alloy even though its combined magnetic and mechanical properties are barely adequate; represents only readily available materials capable of operation over 800°F coolant temperature; properties summarized in Reference 7.	800 1100	1200
1BS1 Alloy - precipitation-hardened developmental alloy: identified by heat on Contract NAS3-6465; represents improvement over NIVCO; only requires development of large forging techniques to make it readily available for designs; properties summarized in Reference 8.	1100	1300
NASA "Superalloy" - 7.5 w, 2.5 Fe, 1 Ti, 0.5 Zr, 0.5 C; developmental alloy; magnetic property data supplied in private communication with NASA LRC personnel; considered similar to 1BS1 alloy per Abstract BG-6, International Congress on Magnetism, September 11 to 15, 1967, Boston, Mass.	1100	-
D.S. 27% Fe-Co - dispersion-strengthened developmental alloy; applicable to very high temperatures only because not competitive with lower temperature alloys at lower temperatures; properties summarized in Reference 8.	1100	1300

While the list might appear short relative to the importance of the rotor material on the design outcome, one must recognize it as the result of a number of related rotor materials screening and selecting studies which have been completed over the past decade[1,6,7,8,9]. Earlier studies involved little more than screening a number of candidates based upon their magnetic and mechanical property data alone and the acquisition of additional data and development on the most promising candidates. Later studies[1] involved screening materials in actual alternator designs over the 500°- to 1400°F-coolant temperature range.

Also, at the lower coolant temperatures, it must be recognized there exist a large number of possible candidates. In order to limit the amount of analyses required to arrive at a selection, a bracketing process was used. This was possible because, as a general rule, materials having superior magnetic properties are weak structurally and those having superior mechanical properties are weak magnetically; in between, there are a host of materials having intermediate properties in both areas. By evaluating designs that bracket the spectrums from superior magnetics to superior strength, it was expected that some insight could be gained on intermediate properties that would give design improvements. Hiperco-27 and H-11 steel were considered bracketing materials. As seen later, the differences in designs between these two alloys were so small as to obviate the need for examining intermediate materials. The reasons for the small difference are related to the influence the stator design has on the minimum possible size (Section 2.3.2).

Relative to the mechanical design aspects of alternator rotor design, rotor materials, and coolant temperature, one finds the rotor materials selection to be very dependent upon and limited by peak operating temperatures that are a function of coolant temperature and the rotor losses. This dependency is so great that as

little as 100°F difference in coolant temperature can result in significantly different material choices and resulting designs. Fortunately, for the temperatures of interest to the KTA alternator, the temperature areas giving significant changes can be identified by various plateaus. As a result, a single coolant temperature can be used to represent all the results that could be obtained for all temperatures on that plateau, and the amount of analyses required to obtain the results are, therefore, minimized.

For purposes of the present discussion, the dependencies and plateaus are best illustrated by the data summarized on Figure 3. On that figure are listed the various rotor materials analyzed in the KTA study and the rotor core temperature which, for the discussion, may be taken as the coolant temperature. This is because the KTA alternator rotor losses will be minimized, thereby minimizing the temperature gradient in the core. The indicating bars on the figure show the various temperature limitations of the alloys. The "likely" and "too-high" temperatures are self-explanatory. The "too-low" bar illustrates where the temperature is too low to fully utilize the magnetic and mechanical capabilities of the high-temperature alloy; there are alloys with lower temperature limitations that are better suited. For example at 800°F, the H-11 steel gives lower alternator electric specific weight (electrical weight divided by electrical rating) and has higher allowable limiting stress than the NIVCO or 1BS1 alloy. At 900°F, however, the H-11 must be completely ruled out due to loss of creep strength, and the NIVCO or 1BS1 alloy must be used. Thus, the 800°F temperature is too low for proper utilization of the NIVCO-type alloy.

The criterion which decides whether the temperature is "too-high", "too-low" or "likely" is based upon the data shown within the indicating bars, the maximum allowable pole tip temperature, the magnetic properties (typical data shown on Figure 4), and a considerable amount of experienced design judgement. The limiting stress values and

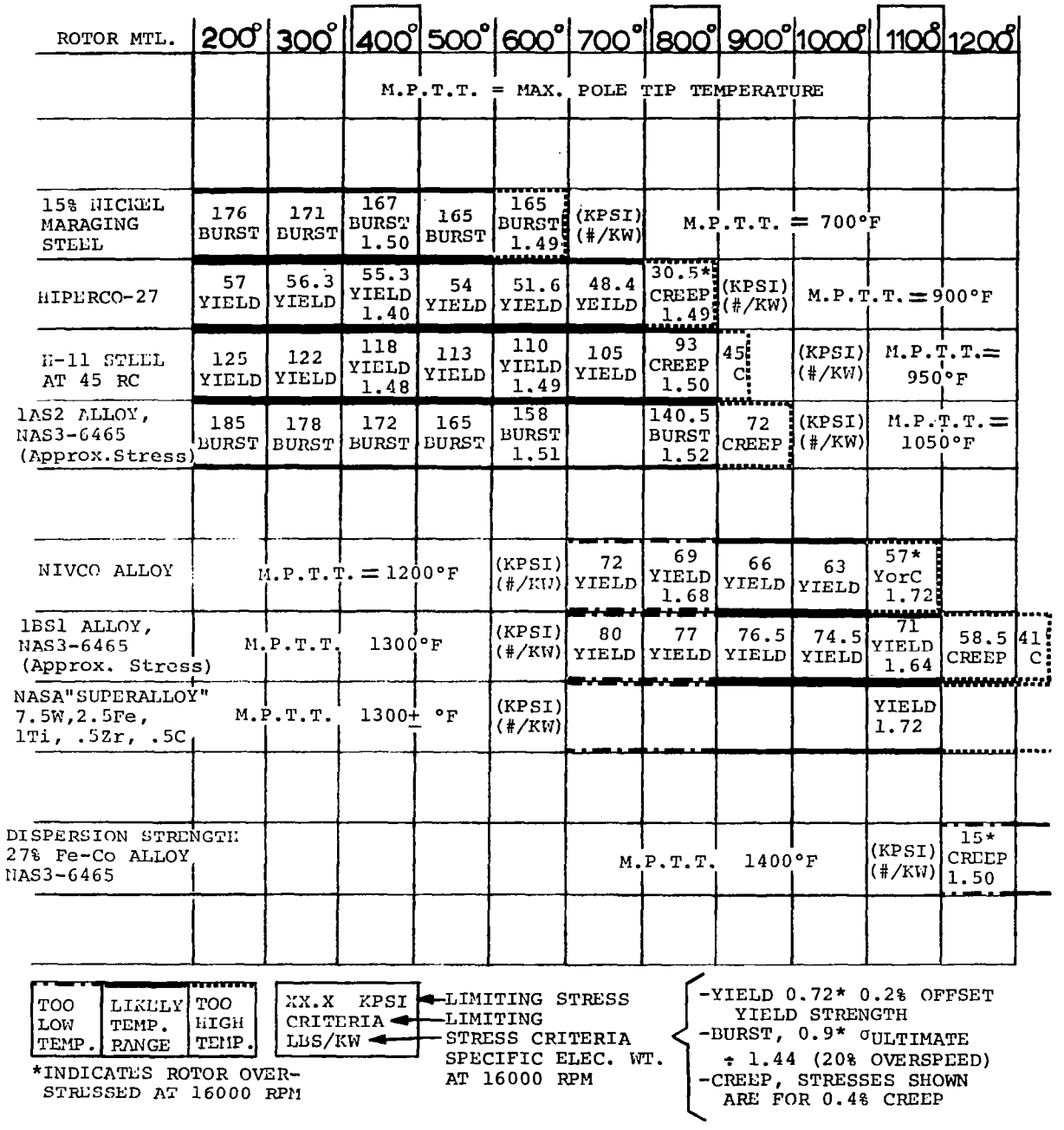

ROTOR MATERIAL TEMPERATURE COMPARISON

FIGURE 3

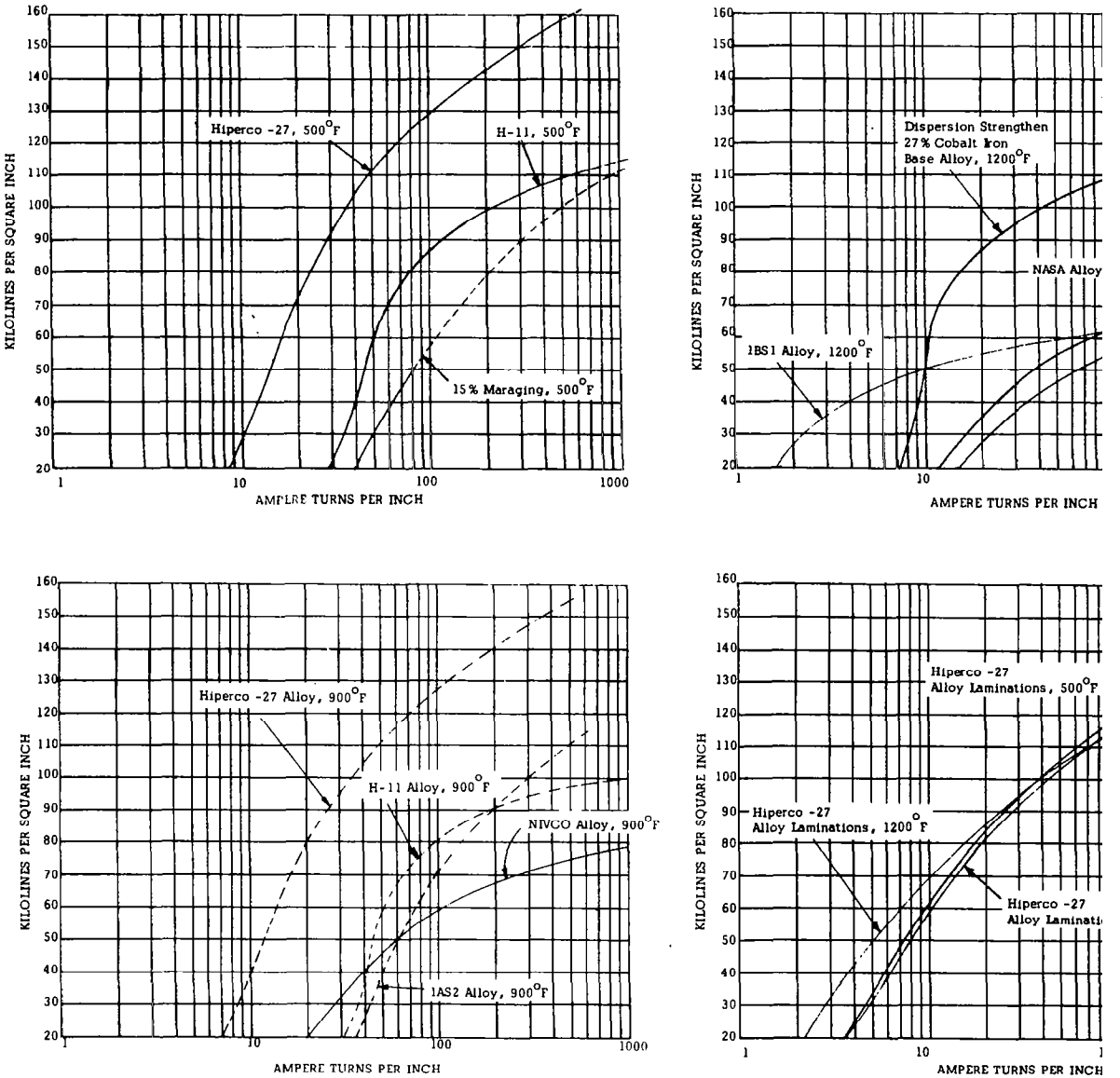

TYPICAL MAGNETIZATION CURVES

FIGURE 4

and criteria are based on published property data and the three stress criteria of Section 2.1. The maximum pole tip temperature is based upon judgement relative to both magnetic and mechanical design limitations. For instance, the 700°F limit for maraging steel is due to magnetic limitations. The opposite is true for the 900°F limit for Hiperco-27; it is creep strength limited. For the H-11 steel and 1AS2 alloy, both limitations are cause for specified maximums.

Relative to the limiting stress criteria shown, the temperature at which the design becomes creep-limited is generally the temperature at which it is first considered too high. This is because, of the three criteria, creep limitations are the least desirable. Notable exceptions shown on the chart concern H-11 steel, 1BS1 alloy, and dispersioned-strengthened 27-percent Fe-Co alloy. The H-11 may still be considered safe at 800°F because considerable creep data is available to permit reasonable design predictions. However, the data that is available is not considered precise enough for accurate, reliable design prediction over 3 to 5 years of life. If the 800°F were used in the KTA alternator design, long-term data would have to be taken from samples made from the same forging that would be used to fabricate the actual alternator rotor. The 1BS1 alloy is shown as creep-limited and too high at 1200°F; since it is still superior to the dispersioned-strengthened 27-percent Fe-Co alloy, the latter must be listed as too low at 1200°F. As a result, the 1200°F temperature appears as a "no-man's-land" without any likely material.

Relative to the magnetic properties which are now shown on Figure 3, an indirect comparison of their effects can be made by examining the specific weights. For instance, the first four materials have better magnetic properties and have correspondingly lower specific weights than do the last four. This result is not always true, and it should not be taken at face value. For instance, the Hiperco-27 alloy is recognized as a superior magnetic alloy over the H-11 steel, but the specific weights are similar. This is due to

stator design considerations influencing the minimum rotor size. Such effects can never be known until actual designs are made, and these effects serve to illustrate why comparison of magnetic and mechanical properties alone is inadequate in making the final selection of the rotor material.

An overall view of the discussion above and the distribution of the indicating bars on Figure 3 indicates there are several plateaus of temperatures and corresponding materials. The most obvious are the materials and temperatures in the 200° and 800°F range, the 900° to 1100°F range, and above 1200°F. Within the 200° to 800°F range, there are two subtle ranges over 200° to 600°F and 600° to 800°F. As a result, the following three coolant temperatures were selected to represent designs that could cover a 200° to 1100°F range for the entire study.

(a) 400°F - Organic coolant temperature
- Applicable to 200° to 600°F range
- Examined: 15 percent Ni Maraging Steel
  Hiperco-27
  H-11

(b) 800°F - Alkali metal coolant temperature
- Applicable to 600° to 800°F coolant
- Examined: Hiperco-27
  H-11 Steel
  1AS2 Alloy
  NIVCO

(c) 1100°F - Alkali metal coolant temperature
- Applicable to 900° to 1100°F coolant
- Examined: NIVCO
  1BS1 Alloy
  NASA "Superalloy"
  DS 27 percent Fe-Co Alloy

2.3.2 Results of Rotor Materials Studies

The 400°F-coolant temperature rotor materials screening study results are presented in Table 19. The Hiperco-27 and H-11 rotor materials gave generator designs with the best combination of weight efficiency, required field power and rotor losses. Both the Hiperco-27 alloy and H-11 rotor materials were included in the 400°F-coolant temperature speed studies.

The two materials are rather deverse in their magnetic and mechanical properties. The Hiperco-27 is a superior magnetic steel with low strength properties, and H-11 is considered a high strength steel with adequate magnetic properties. The trend in comparative properties for each of these steels is typical of most alloys. Thus, the H-11 and Hiperco-27 alloys can be said to bracket a host of intermediate steels which are recognized to have better magnetic properties but less stength than H-11 or better strength but worse magnetic properties than Hiperco-27.

The bracketing was done in an attempt to illustrate any "gains" or "losses" that might be associated with intermediate materials without actually having to look at them in detail. As seen by the small differences between the H-11 and Hiperco-27 designs, the bracketing appears justified. It can be concluded then, that if a Hiperco-27 rotor material design is overstressed and in need of a higher strength material, that material might as well be H-11 rather than a lesser known intermediate.

There are several reasons for the differences, but at the risk of oversimplifying, it may be stated that the minimum rotor diameter at a certain point is more dependent on stator design considerations. Thus, using an improved magnetic alloy beyond this point to shrink the rotor further results in little benefit with regard to generator weight. Field power is somewhat less, however. It was found during

TABLE 19

ROTOR MATERIALS STUDY - 400°F COOLANT

Conditions: 733 kva, 16,000 rpm, 1600 Hz, 480 v (L-N), 120-deg phase belts, 126 slots, $j = 7000$ amp/in.^{2}, radial gap = 0.14 in.

Rotor Material	Electrical Weight, lb	Rotor Weight, lb	Efficiency, %	Voltage Unbalance, %	Field Current Ratios			F P
					Overload	3Ø Short	Overvoltage	
Hiperco 27	769	290	91.9	7.35	1.08	1.27	1.15	3
H-11	815	341	91.8	6.51	1.07	1.27	1.12	4
15% Maraging	828	351	91.2	6.41	1.06	1.07	1.15	6

TABLE 20

ROTOR MATERIALS STUDY - 800°F COOLANT

Conditions: 733 kva, 16,000 rpm, 1600 Hz, 480 v (L-N), 120-deg phase belts, 4 conductors per sl 144 slots, $j = 6000$ amp/in.^{2}, radial gap = 0.14 in.

Rotor Material	Electrical Weight, lb	Rotor Weight, lb	Efficiency, %	Voltage Unbalance, %	Field Current Ratios			F
					Overload	3Ø Short	Overvoltage	
H-11	829	347	91.8	9.53	1.12	1.54	1.14	5
NIVCO	926	457	91.3	8.26	1.11	1.28	1.19	6
1AS2	838	353	91.7	9.50	1.12	1.51	1.11	5
Hiperco 27	818	299	91.2	11.75	1.20	1.58	1.15	5

TABLE 21

ROTOR MATERIALS STUDY- 1100°F COOLANT

Conditions: 733 kva, 16,000 rpm, 1600 Hz, 480 v (L-N), 120-deg phase belts, 144 slots, $j = 6000$ amp/in.^{2}, radial gap = 0.14 in.

Rotor Material	Electrical Weight, lb	Rotor Weight, lb	Efficiency, %	Voltage Unbalance, %	Field Current Ratios			I
					Overload	3Ø Short	Overvoltage	
1BS1	905	457	92.2	9.06	1.22	1.34	1.37	
NIVCO	947	499	91.8	8.54	1.15	1.27	1.25	
DS27CO	826	333	91.8	11.35	1.19	1.65	1.21	
NASA Alloy	945	487	92.3	9.19	1.17	1.43	1.26	

the 400°F-speed screening studies that the best alternator designs with Hiperco-27 rotor material occurred when the flux density in the rotor was less that the material capability.

Rotor materials study results at the 800°F-coolant condition are tabulated in Table 20. Four materials were examined, two of which could be candidates, H-11 alloy and 1AS2 alloy. These are comparable as far as generator size and efficiency goes but the 1AS2 shows more potential in overspeed, overload (to saturation), and long-term stability. The 1AS2 alloy is still in the development stage, however, with only rudimentary properties known compared to the extensive property data available for H-11. Thus, H-11 was the present choice. The fourth material, Hiperco-27, failed stress-wise even at the low 16,000-rpm speed. It was mainly examined for academic purposes to see the effect of minimizing the rotor size with a good magnetic material, and thereby bracketing the sizes between those obtainable with Hiperco-27 and those of higher strength and lesser magnetic properties.

It may appear that the choice of H-11 was based on a very limited comparison. Actually, the initial selection of H-11 is based on past studies[6] where H-11 was compared with five other materials having greater strength and lower magnetic properties and/or vice versa. Literally speaking, then, it is the choice of nine possible candidates.

Rotor material screening studies for the 1100°F-coolant temperature are given in Table 21. Of the four rotor materials investigated, only the experimental alloy 1BS1 could be recognized as a candidate. Material strength data for the "NASA alloy" was not available; therefore, its suitability as a candidate could not be determined. The material creep strength of the NIVCO and dispersion strengthened 27-percent cobalt alloys were less than the induced rotor stress at 16,000 rpm, which eliminated them from further consideration. The 1BS1 alloy is currently in the developmental stage; therefore, its

use as a design material in the KTA application is not in accordance with the design guideline priority, ease of development.

Comparative stresses, not shown on the tables, were used to determine the applicability of the material to speed and strength limitations. Typical stress plots for the rotors and materials selected are presented in Section 2.4.

Based on the results of the above alternator screening analyses (the later stress analyses and consultations with magnetic materials experts), the choices of rotor materials for the three coolant temperatures were made. These are summarized in Table 22, along with brief statements of primary considerations leading to the choices.

2.4 System Design Variable Screening Studies

The objective of the system design variable screening studies was to find the optimum combination of alternator frequency, speed, and voltage for each of the three specified coolant temperatures on the basis of meeting the specification requirements and of achieving the primary design objectives.

The range and specific values for the system design variables are set forth below.

Speed, rpm	16000 to 32000
Frequency, Hz	800, 1200, 1600, 2000
Voltage, L-N	120, 240, 480, 720, 960, 1200

The speeds listed below correspond to the specified frequencies and integral pole pairs.

TABLE 22

ROTOR MATERIALS CHOICE SUMMARY

800°F Coolant:	H-11 - First Choice 1. Considerable data and is readily avai 2. Still insufficient creep data for 800° designs. Requires 3-year data for hi
	1AS2 - Shows most promise for improvement; needs 1. Reduce brittleness by further develop 2. Large forging techniques undefined 3. More data needed for reliable design
1100°F Coolant:	1BS1 - First Choice; needs development 1. Large forging techniques undefined 2. More data needed for reliable design
	NIVCO - Considered possible alternate 1. Almost as good as 1BS1-type 2. Must be considered only available mat 900°- to 1100°F-coolant temperature r
400°F Coolant:	Either H-11 or Hiperco-27 - First Choice 1. Both showed applicability 2. Carried both on system speed and freq 3. They bracket host of intermediate can

Hz	Poles	Speeds
800	4,6	24000, 16000
1200	6,8	24000, 18000
1600	6,8,10,12	32000, 24000, 19200, 16000
2000	8,10,12,14	30000, 24000, 20000, 17143

The parametric data relating speed, frequency, and voltage to electrical alternator weight and efficiency were determined in an iterative cycling procedure whereby

(a) Frequency is varied at a fixed speed and voltage

(b) Speed is varied at a fixed frequency(s) and voltage

(c) Voltage is varied at a fixed speed and frequency

The fixed values were initially selected according to optimum values determined on contract AT(04-3)-679[1], and in the case of the frequency study, the requirement for a common speed for all frequencies. As the cycling proceeded, new values were chosen from data generated in the studies.

2.4.1 Information Pertinent to Design Selection from the Standpoint of Electromagnetic Design Characteristics

The frequency and speed studies for the 400°F organic coolant are summarized in Tables 23 and 24, respectively. A frequency of 1600 Hz results in minimum system weight while providing a good compromise between armature hot-spot temperature, rotor pole face loss, and field power; therefore, 1600 Hz is the primary choice for frequency. Based on the same criteria, slight differences make 2000 Hz a secondary choice.

TABLE 23

SUMMARY OF FREQUENCY STUDY - 400°F COOLANT

Conditions: 733 kva, 24,000 rpm, 480 v (L-N), 120-deg phase belts, j = 7000 amp/in.^{2}, Hiperco-27 rotor, radial gap = 0.14 in.

Frequency, Hz	Electrical Weight, lb	Efficiency, %	Field Power, w	Voltage Unbalance, %	Armature Hot Spot, °F	Conductors per Slot	Rotor Weight, lb	Fie 3Ø
800	933	87.5	4170	8.51	1263	2	243	1
1200	748	91.7	3070	6.85	1033	2	242	1
1600	626	91.6	2904	7.97	928	2	207	1
2000	661	91.4	2489	5.52	851	2	236	1

TABLE 24

SUMMARY OF SPEED STUDIES - 400°F COOLANT

Conditions: 733 kva, 480 v (L-N), 120-deg phase belts, j = 7000 amp/in.^{2}, radial gap = 0.14 in.

Speed, rpm	Frequency, Hz	Rotor Material	Electrical Weight, lb	Efficiency, %	Voltage Unbalance, %	Armature Hot Spot, °F	Conductors per Slot	Rotor Weight, lb	Field C 3Ø Shor
16,000	1600	Hiperco-27	860	91.9	5.76	826	4	340	1.13
19,200	1600	Hiperco-27	762	91.7	6.42	853	2	290	1.26
24,000	1600	Hiperco-27	626	91.6	7.97	928	2	207	1.43
32,000	1600	Hiperco-27	552	91.3	7.10	1053	2	171	1.42
16,000	1600	H-11	731	91.9	8.60	948	4	288	1.44
19,200	1600	H-11	777	91.7	6.23	862	2	305	1.24
24,000	1600	H-11	643	91.8	7.09	943	2	235	1.38
32,000	1600	H-11	533	91.0	9.00	1108	2	180	1.63
17,143	2000	Hiperco-27	767	91.5	5.70	808	4	304	1.08
20,000	2000	Hiperco-27	664	91.7	6.06	849	4	253	1.15
24,000	2000	Hiperco-27	661	91.4	5.52	851	2	236	1.10
30,000	2000	Hiperco-27	546	91.5	6.22	914	2	182	1.26
17,143	2000	H-11	688	90.8	8.99	918	4	277	1.41
20,000	2000	H-11	720	91.2	5.54	850	4	306	1.17
24,000	2000	H-11	619	90.9	6.52	889	2	252	1.32
30,000	2000	H-11	505	90.7	7.58	975	2	182	1.44

Four speed studies were required for the 400°F oganic coolant to consider both candidate rotor materials, i.e., Hiperco-27 and premium quality H-11 (AMS 6487) at frequencies of 1600 and 2000 Hz. Results of the speed studies are shown in Table 24. The preferred combination of speed, frequency, and rotor material for the 400°F-coolant temperature, based on generator electromagnetic design considerations and minimum system weight, is 24,000 rpm at a frequency of 1600 Hz for either a Hiperco-27 or H-11 rotor material. The Hiperco-27 generator design is slightly lighter (15 lb) but does not have as large a stress safety factor as the H-11 design. A discussion of rotor stress considerations is presented in the next section. The second alternate choice is 30,000 rpm, 2000 Hz, H-11 rotor material, and the third is 32,000 rpm, 1600 Hz, H-11 rotor material.

The 30,000 rpm, 2000 Hz, Hiperco-27 rotor material design was obviously overstressed and, therefore, was excluded from electrical-mechanical design preference consideration. The 16,000, 17,143, and 20,000 rpm designs have the undesirable four-conductors-per-slot winding configuration; therefore, these design points would be the least desirable in this application. A summary of design points listed in order of preference based on electromagnetic design considerations is presented in Table 25.

Results of the frequency study for a coolant temperature of 800°F are shown in Table 26. A frequency of 1600 Hz gave the best combination of generator weight and efficiency and was the primary choice. Results of the speed study at a frequency of 1600 Hz is given in Table 27. Very little weight or efficiency difference exists between the 16,000- and 19,200-rpm designs. Also the armature hot-spot temperatures are very close. Voltage unbalance (for a 2/3 single-phase load) for the 16,000-rpm design exceeds the preliminary guideline limit of 9 percent, whereas the 19,200-rpm design is well below this limit. The primary reason for this is that the 16,000-rpm design has four conductors per slot (i.e., two turns per coil), whereas the

TABLE 25

SELECTED SPEEDS AND FREQUENCIES - 400°F COOLANT

Order of Electro-Magnetic Design Preference	Speed, rpm	Frequency, Hz	Rotor Material	Electrical Weight, lb	Efficiency, %	Conductors per Slot	Voltage Unbalance, %	Rotor Radial ΔT, °F*	A F T
1	24,000	1600	H-11	643	91.8	2	7.09	95	
2	24,000	1600	Hiperco-27	626	91.6	2	7.97	39	
3	19,200	1600	Hiperco-27	762	91.7	2	6.42	26	
4	19,200	1600	H-11	777	91.7	2	6.23	44	
5	30,000	2000	H-11	505	90.7	2	7.58	107	
6	32,000	1600	H-11	533	91.0	2	9.00	356	
7	20,000	2000	Hiperco-27	664	91.5	4	6.06	113	

*Temperature difference between calculated pole tip temperature and coolant temperature in rotor bore.

TABLE 26

SUMMARY OF FREQUENCY STUDY - 800°F COOLANT

kva	Frequency, Hz	Speed, rpm	Electrical Weight, lb	Efficiency, %	Approx. Avg. Rotor Stress, psi	Rotor Radial ΔT, °F	Armature Hot-Spot Temp., °F	Conductors per Slot
733	800	24,000	1079	84.0	88,096		1288	2
733	1200	24,000	758	91.2	79,510	364	1269	2
733	1600	24,000	701	91.5	78,498	95	1189	2
733	2000	24,000	676	90.6	77,824	50	1161	2

TABLE 27

SPEED STUDY- 800°F COOLANT - 1600 HZ

kva	Frequency, Hz	Speed, rpm	Electrical Weight, lb	Efficiency, %	Approx. Avg. Rotor Stress, psi	Rotor Radial ΔT, °F	Armature Hot-Spot Temp., °F	Conductors per Slot
733	1600	16,000	829	91.8	38,728	81	1164	4
733	1600	19,200	844	91.7	55,520	45	1161	2
733	1600	24,000	701	91.6	78,498	95	1189	2
733	1600	32,000	573	90.4	124,344	362	1281	2

TABLE 28

SPEED STUDY - 800°F COOLANT - 2000 HZ

kva	Frequency, Hz	Speed, rpm	Electrical Weight, lb	Efficiency, %	Approx. Avg. Rotor Stress, psi	Rotor Radial ΔT, °F	Armature Hot-Spot Temp., °F	Conductors per Slot
733	2000	17,143	753	90.8	44,064	54	1186	4
733	2000	20,000	761	91.0	62,651	383	1148	4
733	2000	24,000	676	90.6	77,821	50	1157	2
733	2000	30,000	566	90.4	110,676	106	1203	2

19,200 rpm and higher speed designs have two-conductors-per-slot (i.e., one turn per coil). Also the direct axis synchronous reactance Xd is higher (1.06) for the 16,000- than for the 19,200-rpm design, which has an Xd of 0.77. As a general rule, generator weight decreases with increasing Xd. Had a two-conductor-per-slot design been chosen for the 16,000-rpm speed, its weight would be somewhat over 1000 lb, efficiency about 91.9 percent, and voltage unbalance about 6 percent. Four-conductor-per-slot designs investigated for speeds of 19,200 rpm and higher were inferior because of lower generator efficiency, higher rotor stress, and rotor losses. Also a two-conductor-per-slot design is preferable from the standpoint of ease of winding development with the stiff clad-silver conductor. Because of the basic simplicity of a one-turn coil winding with 120-deg phase belts, no end extension joints with clad-silver conductors are required.

The 24,000-rpm speed design provides the best combination of generator weight and efficiency of all the speeds investigated at a frequency of 1600 Hz and meets other electrical system requirements regarding voltage unbalance, three-phase short circuit, and overload. The 32,000-rpm speed design has the lowest generator weight but suffers the disadvantages of lower generator efficiency, high armature hot-spot temperature, higher rotor losses, and a voltage unbalance exceeding the 9 percent guideline limit. Temporarily disregarding any rotor stress limitations, the 24,000-rpm design would be the preferred design at a frequency of 1600 Hz (based on generator electromagnetic design considerations) with the 19,200-rpm design the second choice.

Results of the speed study at a frequency of 2000 Hz are given in Table 28. Again, temporarily neglecting any rotor stress considerations, the 30,000-rpm design would be selected as the best generator electromagnetic design at a frequency of 2000 Hz, with the 24,000-rpm design the second choice and the 20,000 as the third choice.

The selected speed points for the two frequencies are summarized in Table 29. It must be remembered that the selections are based on generator electromagnetic design and that stress limits were ignored in these choices. Stress limitations are covered in the next section of this report. If speeds greater than 24,000 rpm are excluded from consideration, the order of preference would be as shown in Table 30.

Grooved solid pole faces were assumed for the above designs. It should be noted here that there is some question regarding the accuracy of the load harmonic component of pole face losses as calculated by Barello's method. The calculation for the other component of pole face loss (tooth ripple) is considered reliable because the applicable value of permeability is used. Barello uses a constant value of permeability equal to 2000 in his equation, which may not be applicable to high-strength steels such as H-11 alloy. The use of laminated pole faces joined to the pole body would reduce the calculated tooth ripple component of pole face loss and assure that the calculated load harmonic component is not greater than the presently calculated value. The use of laminated pole tips joined to the pole body is considered feasible but is contrary to the ease of development design requirements.

Below a speed of 24,000, the 19,200-rpm, 1600-Hz design is preferred over the 20,000-rpm, 2000-Hz design not only because of higher efficiency but also because the winding is a two-conductor-per-slot winding, whereas the 20,000-rpm, 2000-Hz design is a four-conductor-per-slot winding. With the use of 120-deg phase belts, no crossover or conductor joints, other than to the terminal or bus bar, are required. Also the two conductors in the slot are separated by phase insulation, whereas with the four, two conductors lay together separated by insulation only. It is possible to form a four-conductor-per-slot winding without making joints, but experience with certain aircraft generator designs indicates voltage dielectric breakdown problems can become excessive with this configuration.

TABLE 29

SELECTED SPEEDS AND FREQUENCIES - 800°F COOLANT

Order of E.M. Design Preference	kva	Speed, rpm	Frequency, Hz	Electrical Weight, lb	Efficiency, %	Conductors per Slot	Voltage Unbalance, %	Rotor Radial ΔT, %	A B T
1	733	24,000	1600	701	91.6	2	7.78	95	
2	733	30,000	2000	566	90.4	2	8.32	106	
3	733	24,000	2000	676	90.6	2	7.32	50	
4	733	19,200	1600	844	91.7	2	6.77	45	
5	733	20,000	2000	761	91.0	4	5.78	383	

TABLE 30

SELECTED SPEEDS AND FREQUENCIES - 800°F COOLANT

Order of E.M. Design Preference	kva	Speed, rpm	Frequency, Hz	Electrical Weight, lb	Efficiency, %	Conductors per Slot	Voltage Unbalance, %	Rotor Radial ΔT, %	A B T
1	733	24,000	1600	701	91.6	2	7.78	95	
2	733	24,000	2000	676	90.6	2	7.32	50	
3	733	19,200	1600	844	91.7	2	6.77	45	
4	733	20,000	2000	761	91.0	4	5.78	383	

Results of the frequency study for a coolant temperature of 1100°F are shown in Table 31. A frequency of 1600 Hz gave the best combination of generator weight and efficiency, with 2000 Hz a close second choice. Speed studies were run for both 1600- and 2000-Hz frequencies as was done for the 800°F studies. Windage losses are not included in the 1100°F-coolant temperature efficiency values (they are in the 800°F-coolant temperature efficiency values) because their magnitudes (approximately 40 kw at 16,000 rpm) were so high other generator losses were reduced to secondary importance. The high loss is caused by the high saturated vapor pressure of potassium at 1100°F-coolant temperature. Results of the speed studies are given in Tables 32 and 33.

Designs were selected using the same considerations as applied to the 800°F coolant temperature design selections. Considering generator electromagnetic design factors only and temporarily neglecting rotor stress limitations, the speed and frequency combinations in order of preference are given in Table 34.

If speeds greater than 19,200 rpm are excluded from consideration, the order of preference would be as shown in Table 35.

As stated previously, windage losses are not included in the efficiency values for the 1100°F study because they are prohibitively high. Methods designed to reduce windage losses for the 1100°F-coolant temperature require separate evaluation regarding system penalties and are discussed more fully in Section 4.2.

Results of the voltage studies for coolant temperatures of 400° and 800°F are summarized in Tables 36 and 37, respectively.

The establishment of a safe working voltage for inorganically insulated magnet wire requires consideration of several important

TABLE 31

SUMMARY OF FREQUENCY STUDY - 1100°F COOLANT

kva	Frequency, Hz	Speed, rpm	Electrical Weight, lb	Efficiency, %	Approx. Avg. Rotor Stress, psi	Rotor Radial ΔT, °F	Armature Hot-Spot Temp., °F	Conductors per Slot
733	800	24,000	1200	71.7	126,893	207	1467	2
733	1200	24,000	836	91.3	105,509	242	1486	2
733	1600	24,000	770	92.7	104,168	1025	1434	2
733	2000	24,000	749	92.3	103,096		1413	2

TABLE 32

SPEED STUDY -1100°F COOLANT - 1600 Hz

kva	Frequency, Hz	Speed, rpm	Electrical Weight, lb	Efficiency, %	Approx. Avg. Rotor Stress, psi	Rotor Radial ΔT, °F	Armature Hot-Spot Temp., °F	Conductors per Slot
733	1600	16,000	905	92.2	52,317	112	1431	4
733	1600	19,200	935	92.7	74,256	973	1411	2
733	1600	24,000	770	92.7	104,168	207	1434	2
733	1600	32,000	627	91.4	163,833	231	1492	2

TABLE 33

SPEED STUDY - 1100°F COOLANT - 2000 Hz

kva	Frequency, Hz	Speed, rpm	Electrical Weight, lb	Efficiency, %	Approx. Avg. Rotor Stress, psi	Rotor Radial ΔT, °F	Armature Hot-Spot Temp., °F	Conductors per Slot
733	2000	17,143	868	92.0	60,697	112	1447	4
733	2000	20,000	837	91.0	82,997	973	1416	4
733	2000	24,000	749	92.3	103,096	107	1413	2
733	2000	30,000	622	92.4	145,384	231	1438	2

TABLE 34

SELECTED SPEEDS AND FREQUENCIES - 1100°F COOLANT

Order of E.M. Design Preference	kva	Speed, rpm	Frequency, Hz	Electrical Weight, lb	Efficiency, %	Conductors per Slot	Voltage Unbalance, %	Rotor Radial ΔT, %
1	733	30,000	2000	622	92.4	2	8.16	231
2	733	24,000	1600	770	92.7	2	7.68	242
3	733	24,000	2000	749	92.3	2	7.07	107
4	733	19,200	1600	935	92.7	2	6.57	96
5	733	17,143	2000	868	92.0	4	8.95	112
6	733	16,000	1600	905	92.2	4	9.06	202

TABLE 35

SELECTED SPEEDS AND FREQUENCIES - 1100°F COOLANT

Order of E.M. Design Preference	kva	Speed, rpm	Frequency, Hz	Electrical Weight, lb	Efficiency, %	Conductors per Slot	Voltage Unbalance, %	Rotor Radial ΔT, %
1	733	19,200	1600	935	92.7	2	6.57	96
2	733	17,143	2000	868	92.0	4	8.95	112
3	733	16,000	1600	905	92.2	4	9.06	202

TABLE 36

SUMMARY OF VOLTAGE STUDY - 400°F COOLANT

Conditions: 733 kva, 1600 Hz, 24,000 rpm, H-11 rotor material

Voltage, L-N	Electrical Weight, lb	Efficiency, %	Voltage Unbalance, %	Armature Hot-Spot, °F	Conductors per Slot	Xd P.U.	Rotor Radial ΔT, °F	Field 3 Ø S
120	544	83.4	10.10	1234	2	1.19	> 400	3.0
240	646	88.7	6.61	1053	2	0.79	> 400	1.3
480	643	91.8	7.09	943	2	0.85	95	1.3
720	598	91.7	8.43	1047	4	1.01	194	1.5
960	659	91.4	7.27	1027	4	0.87	84	1.4
1200	658	91.3	7.42	1031	6	0.89	136	1.4

TABLE 37

SUMMARY OF VOLTAGE STUDY - 800°F COOLANT

Conditions: 733 kva, 1600 Hz, 19,200 rpm, H-11 rotor material

Voltage, L-N	Electrical Weight, lb	Efficiency, %	Voltage Unbalance, %	Armature Hot-Spot, °F	Conductors per Slot	Xd P.U.	Rotor Radial ΔT, °F	Field 3 Ø S
120	693	85.8	9.76	1296	2	1.12	> 850	1.6
240	849	90.3	6.29	1161	2	0.73	848	1.2
480	837	91.6	6.75	1161	2	0.77	45	1.3
720	783	92.0	7.96	1180	4	0.92	76	1.4
960	829	91.7	6.93	1164	6	0.80	193	1.3
1200	823	91.6	7.91	1184	8	0.91	126	1.4

factors. These are insulation composition, material form, and operating temperature. As a result of testing and evaluation performed on contract NAS3-4162 and NAS3-6465, magnet wire insulation based upon served glass fiber with additional inorganic fillers and glassy binders has been selected as best for operation at temperatures of 900° to 1300°F. This insulation is known as Anadur and is produced by Anaconda Wire and Cable Company. The fully processed form of this insulation does not achieve complete density, but is porous; therefore, a designer must consider that the insulation serves as spacing rather than a complete insulating barrier. The glass-based binders in this composition begin to lose electrical insulation resistance at 1000°F and are very poor insulators above 1300°F. Thus, the electrical stresses of voltage potential must be kept low if high current losses are to be avoided. The total electric strength of Anadur, 0.0068-in. thick at 1100°F is approximately 400 volts; this results in a typical value of about 60 v/mil. This form of insulation must be used with supplemental ground and phase insulation composed of high purity aluminum oxide. For efficient utilization of available conductor and insulation volume in a magnetic core, the ceramic supplemental insulation must be of minimum thickness consistent with production and winding capabilities. The electric strength of aluminum oxide at 1100°F varies from about 60 to 150 v/mil. For high purity alumina, about 0.018-in. thick, typical electric strength is about 100 v/mil at 1100°F.

In order to assure a margin of safety to compensate for insulation defects created in processing, mechanical shock in operation, and transient overvoltages, an approximate operating limit of 500 v at temperature is recommended. Electrical current leakage with accompanying excessive losses may result if higher operational voltage level is attempted.

The selected voltage for the 400 and 800°F-coolant temperatures is 480 v (L-N) based on the considerations discussed above and the

combination of generator weight, efficiency, conductors per slot, and rotor temperature rise (i.e., from rotor coolant passage to the pole faces) from the parametric studies. A two-conductor-per-slot winding configuration is considered desirable with regard to ease of development and reliability of the armature winding.

The voltage study for 1100°F coolant was held pending a decision of further pursual of the design in Phase I. The decision was made to delete the 1100°F cooled/lubricated alternator base design from further consideration, and the 1100°F-coolant condition voltage studies were not performed.

2.4.2 Information Pertinent to Design Selection from the Stand-Point of Rotor Stresses

Two rotor materials were selected for further evaluation as a result of the 400°F rotor materials screening studies; they were H-11 and Hiperco-27 steel. The H-11 was selected over 15 percent Ni-maraging steel as a possible high-speed rotor material. The Hiperco-27 steel was selected to show the maximum "gains" that could be achieved with a very good magnetic rotor steel, recognizing that it may not work in an actual high-speed design. As seen by comparing the designs at equivalent conditions in the speed and frequency studies, the Hiperco-27 offers only slight improvements in weight and efficiency over those with H-11 steel.

The stress limitations which these materials impose upon a high-speed rotor are summarized in Figures 5 and 6. These limitations are given in terms of the allowable stress intensity at design speed and were based upon the considerations given in Section 2.1.

The properties for Hiperco-27 steel were taken from NASA-CR-54091[7]. The properties for H-11 steel were taken from NASA-CR-50491 and AFAPL-TR-66-127[6]. Since H-11 is known to undergo

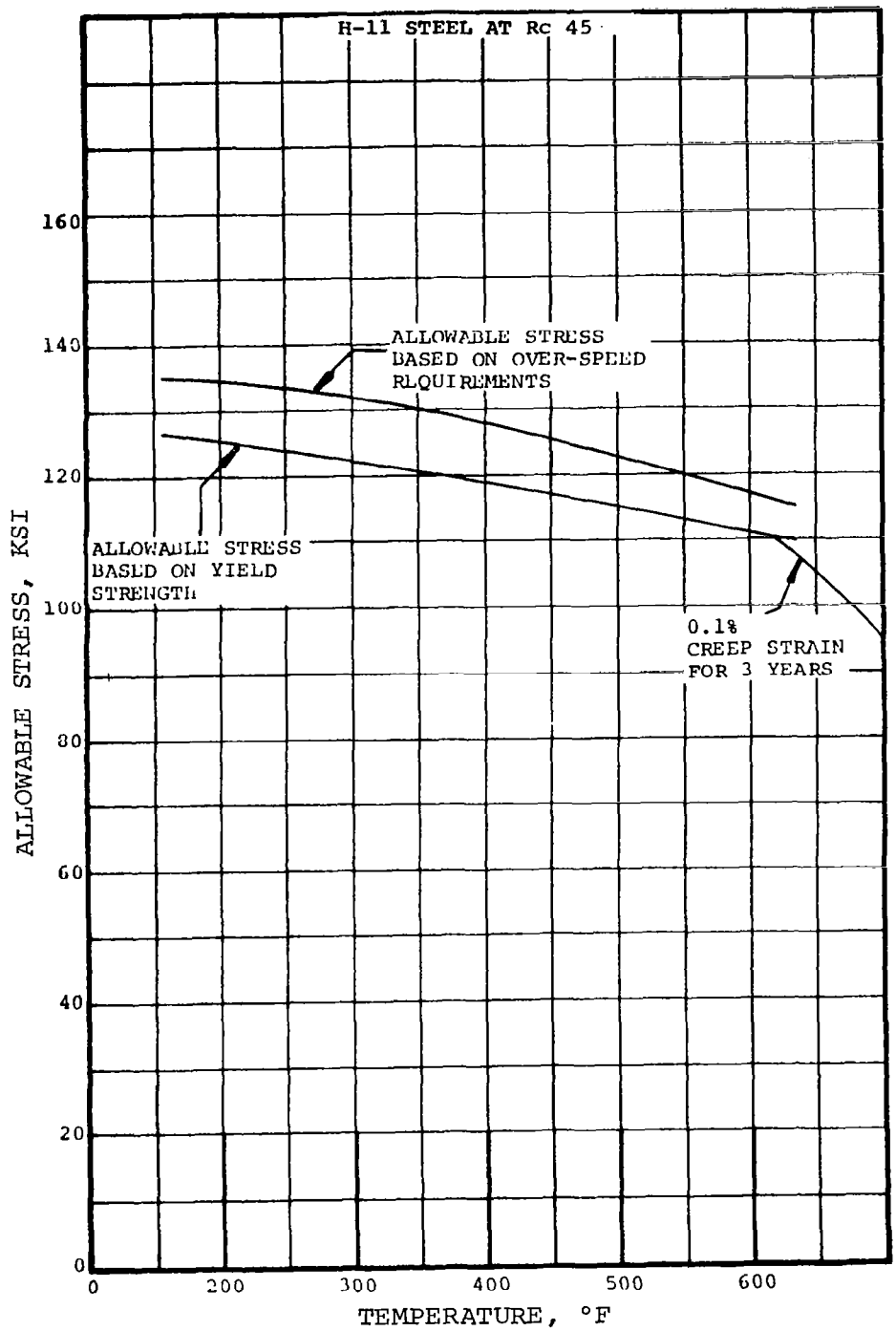

INTERPRETATION OF H-11 STEEL PROPERTY DATA AT A HARDNESS OF R_C 45

FIGURE 5

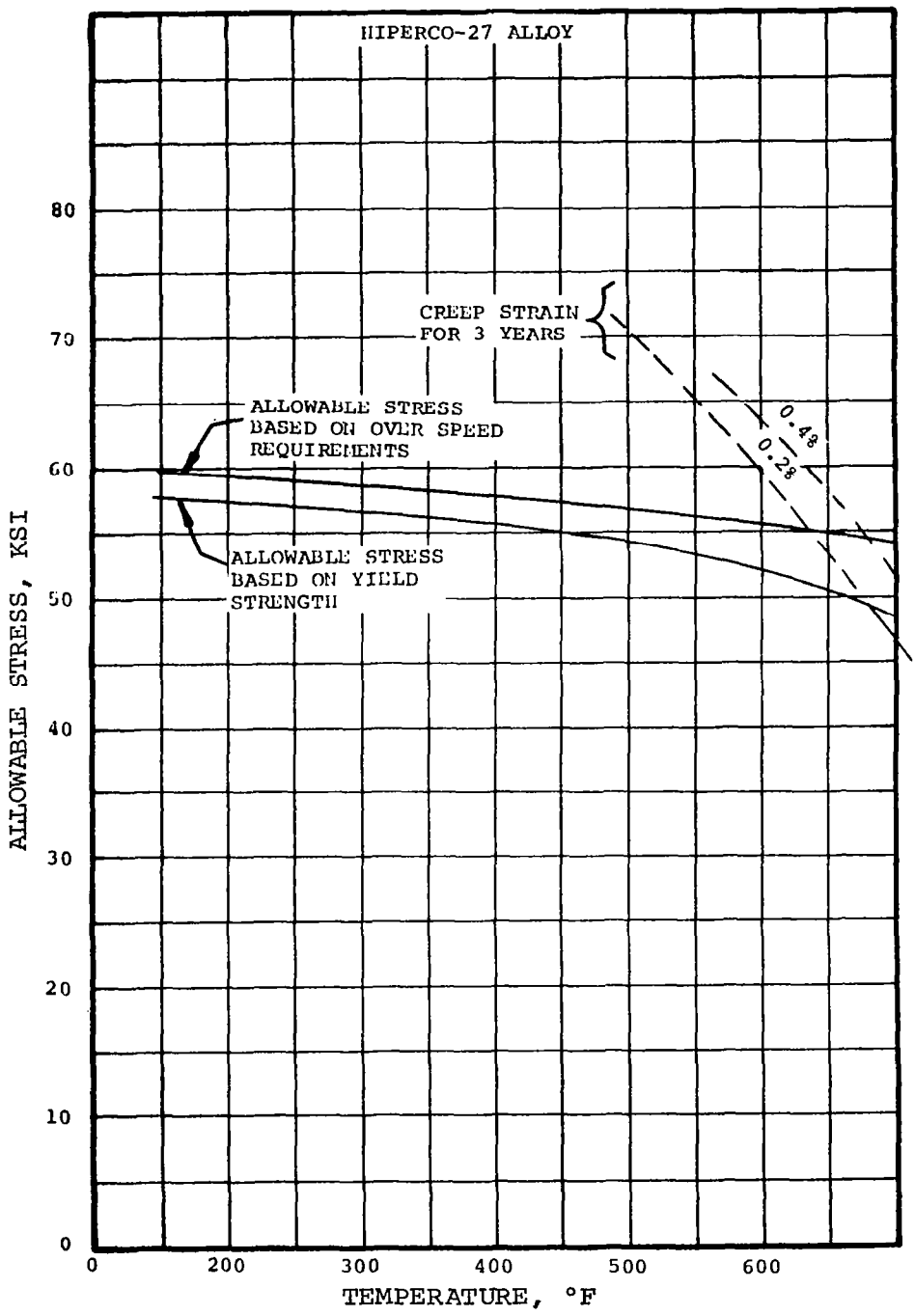

INTERPRETATION OF HIPERCO-27 PROPERTY DATA

FIGURE 6

aging, the H-11 strengths shown can be expected to be less at the end of 3 years.

The calculated rotor stress is the maximum equivalent (Von Mises) stress that occurs under the pole on a plane (r-z direction) through its center; this is the most crucial and usually the largest stress area to be considered in the alternator rotor design (see Figures 7 to 12). The Von Mises stress relationship is used to relate the biaxial stresses occurring in the rotor to the uniaxial, maximum allowable material stress to the maximum Von Mises stress - is used for comparison of various designs. For both Hiperco-27 and H-11 rotor material at 400°F coolant, the limiting stress criteria turns out to be the yield strength consideration.

Table 48 of the next section is a summary of alternator designs for a coolant temperature of 400°F. The first columns give a picture of pertinent electromagnetic (EM) and mechanical design criteria. The latter columns give a summary of the mechanical stress picture and the resulting overall order of design preference.

For the H-11 alloy rotor, the stress is barely unacceptable at 30,000 rpm but certainly acceptable at speeds of 24,000 or below. The stresses in the 30,000-rpm case could be made lower by designing specifically for the lowest possible stress at the expense of other electromagnetic and mechanical design criteria. However, data of the parametric studies which indicate this could be done also indicate the stress could only be lowered a few thousand psi, the result of which would be to make the speed barely acceptable with a small safety factor. From a reliability standpoint then, it would still be low order of overall preference.

For the Hiperco-27 alloy rotor, the stress is barely unacceptable at 19,200 rpm but acceptable at the speeds below this (17,143 or 16,000 rpm). The safety factor for the 19,200 rpm, Hiperco-27 is of

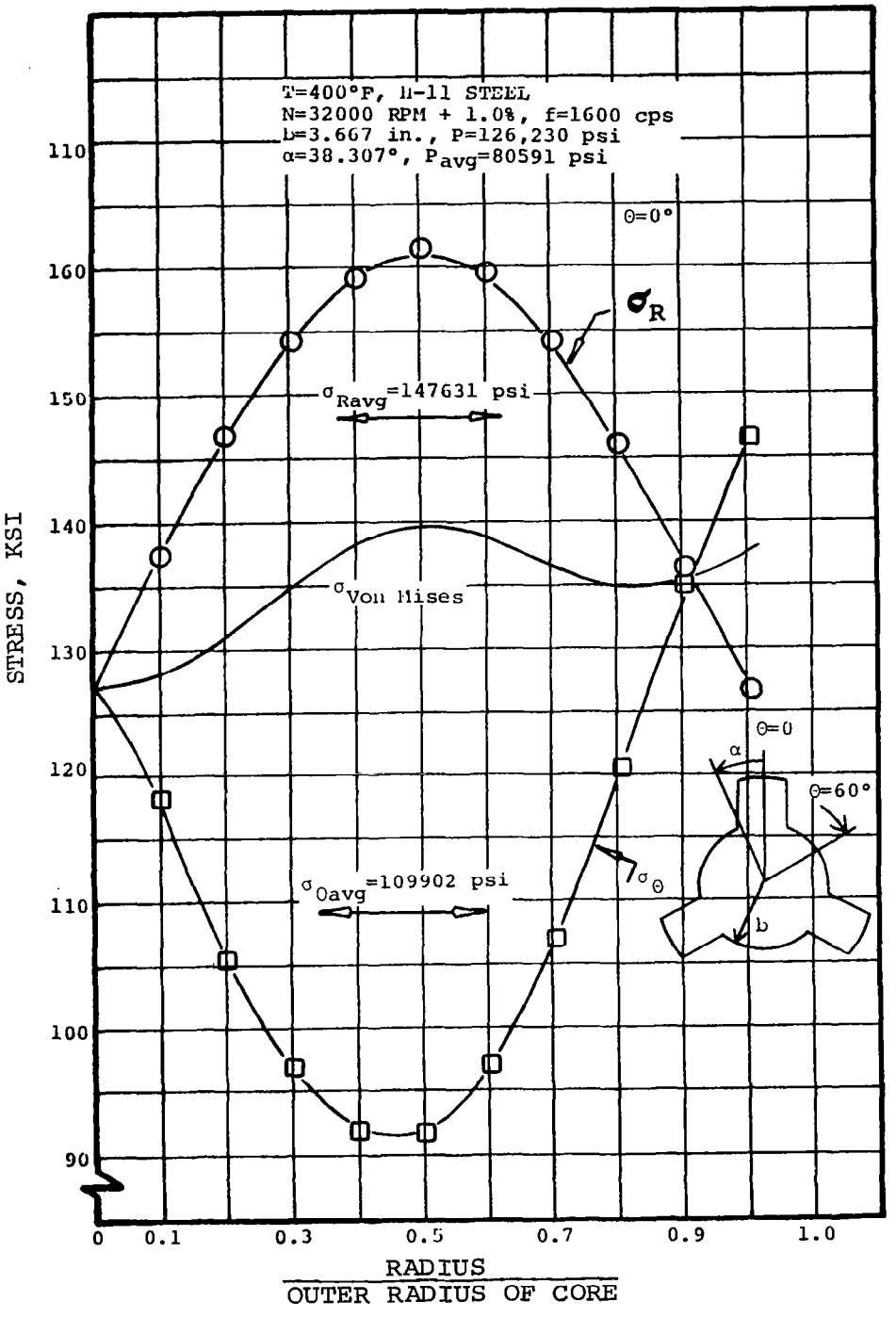

ROTOR STRESS AT θ = 0 DEG, 400°F COOLANT, 32,000 RPM

FIGURE 7

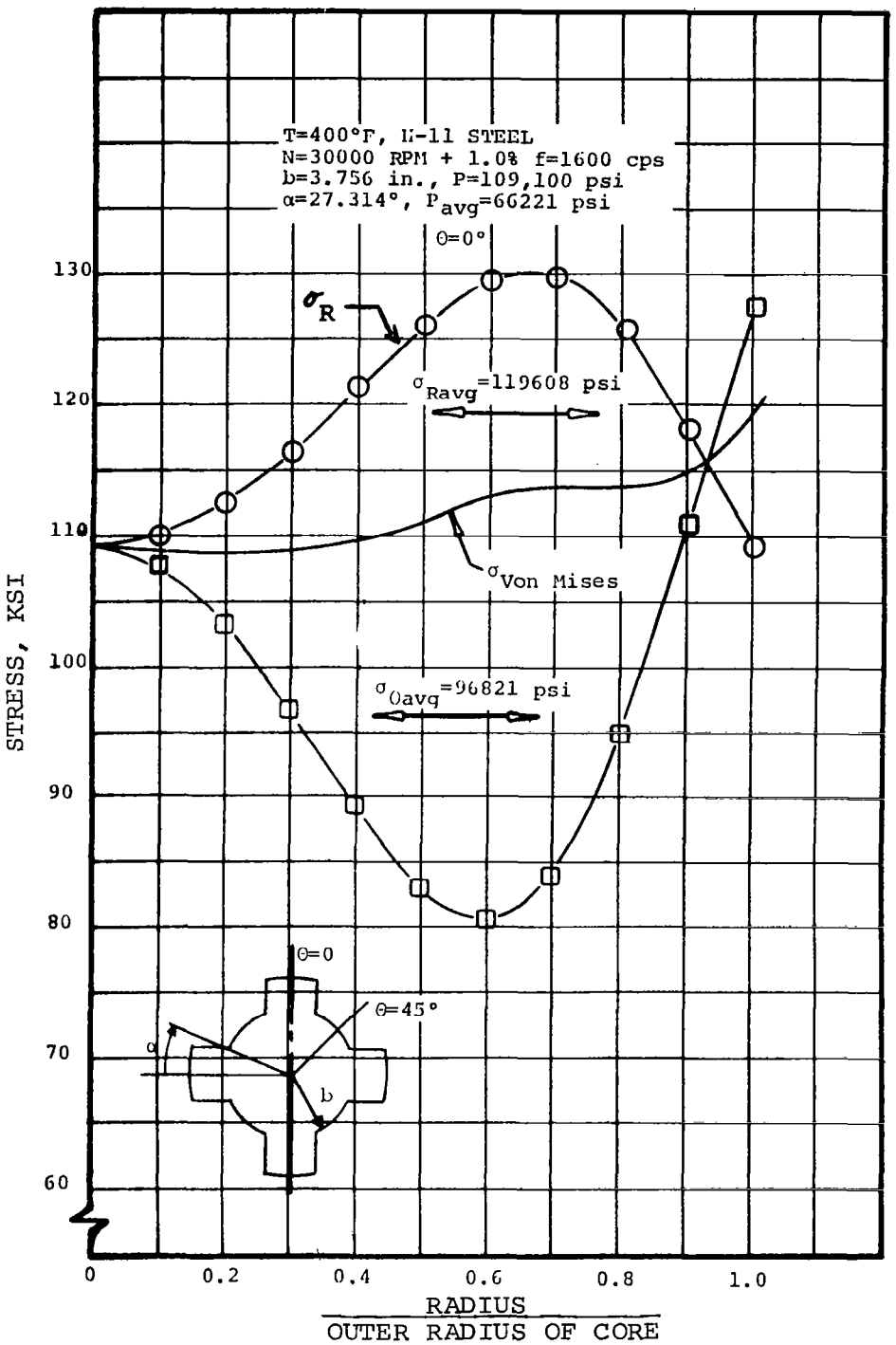

ROTOR STRESS AT θ = 0 DEG, 400°F COOLANT, 30,000 RPM

FIGURE 8

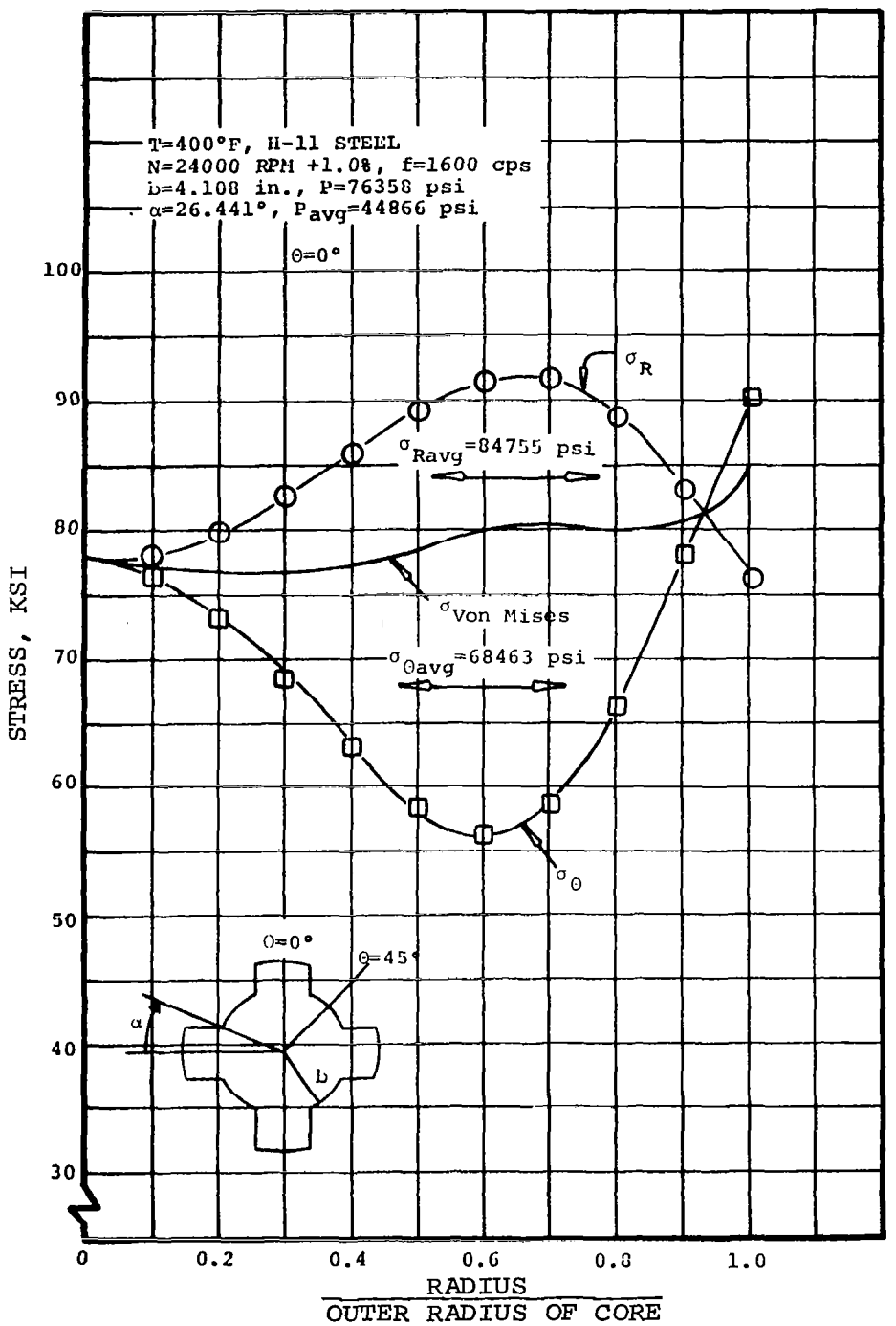

ROTOR STRESS AT θ = 0 DEG, 400°F COOLANT, 24,000 RPM

FIGURE 9

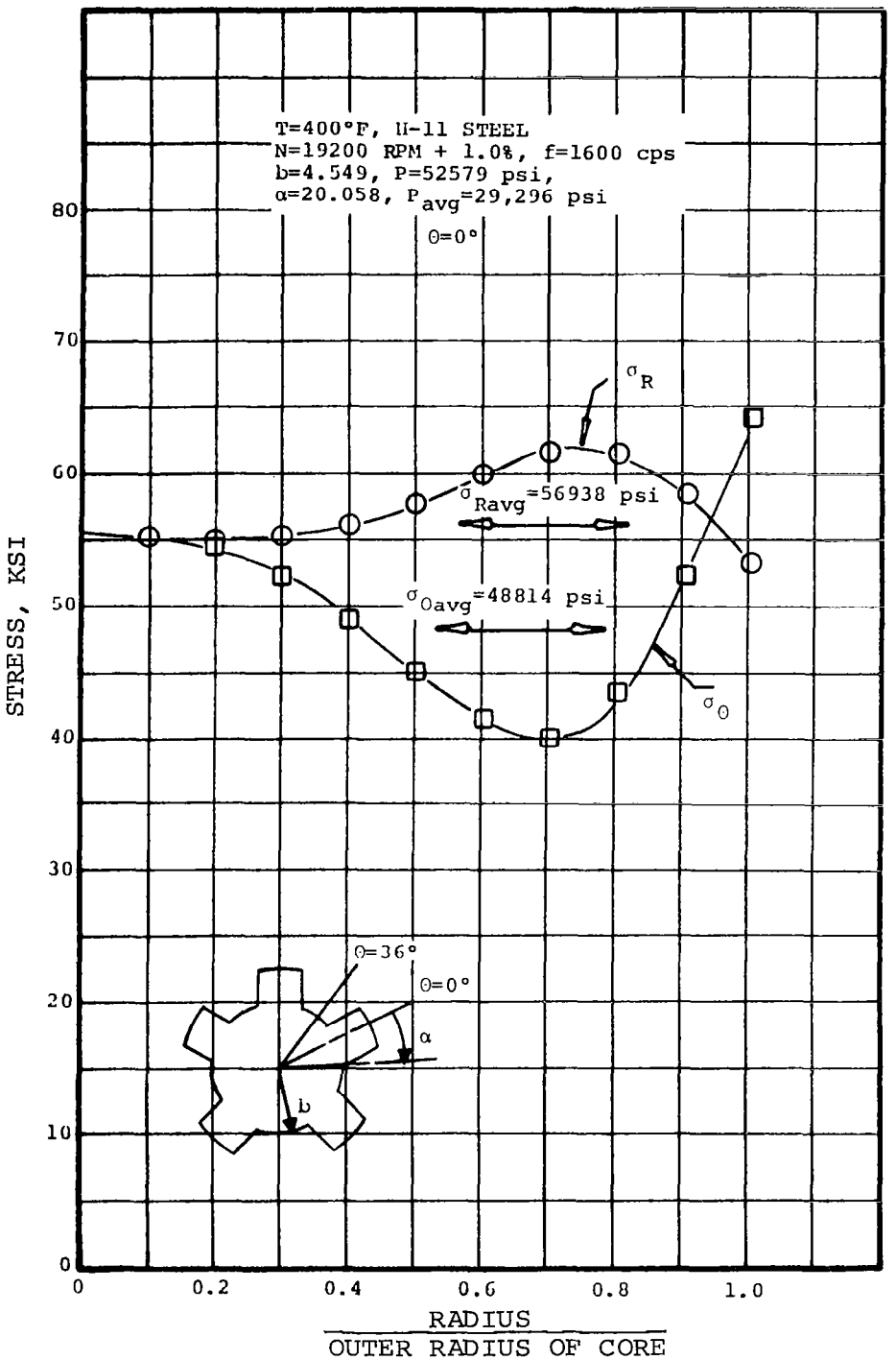

ROTOR STRESS AT θ = 0 DEG, 400°F COOLANT, 19,200 RPM

FIGURE 10

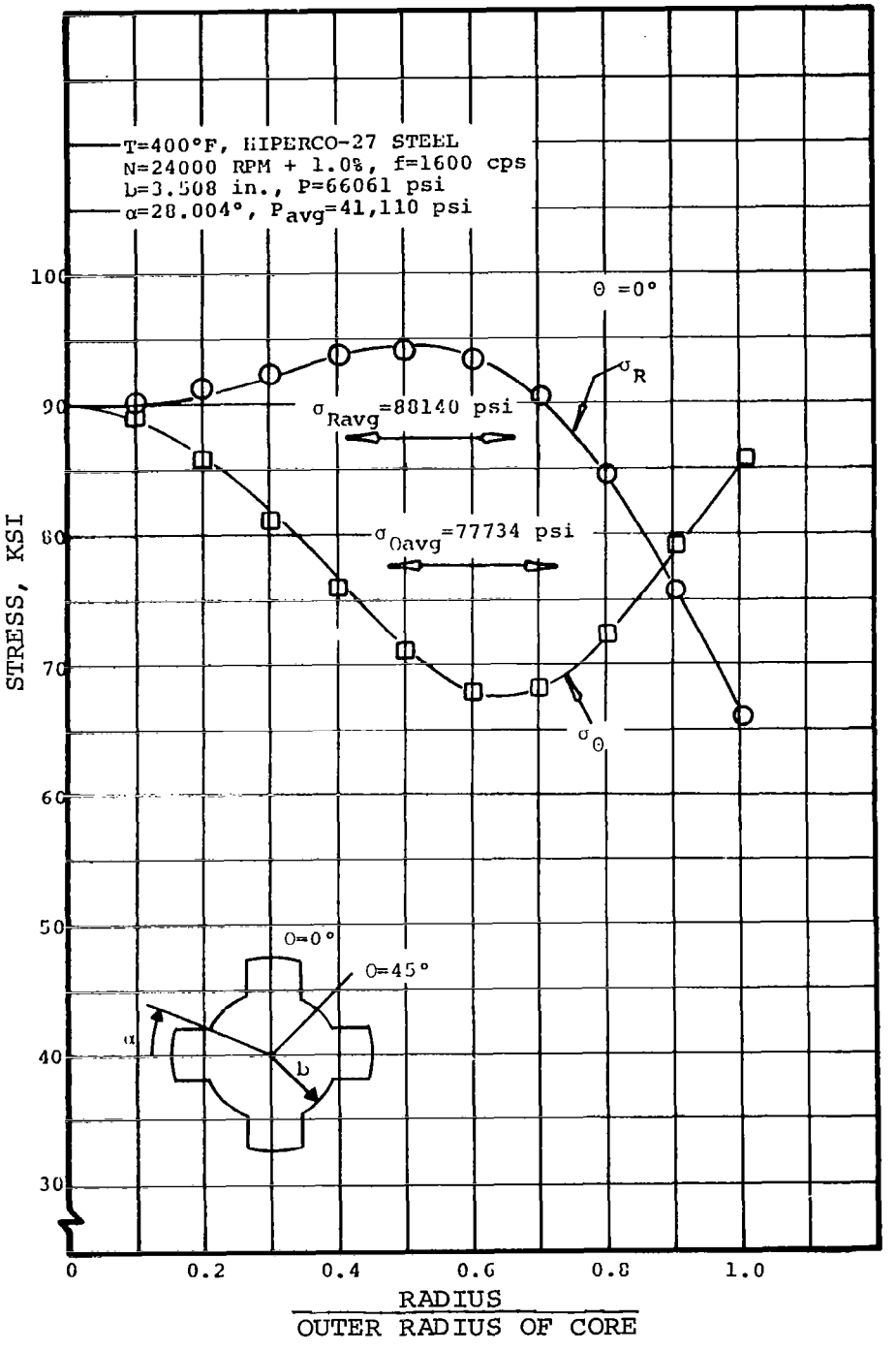

ROTOR STRESS AT θ = 0 DEG, 400°F COOLANT, 24,000 RPM

FIGURE 11

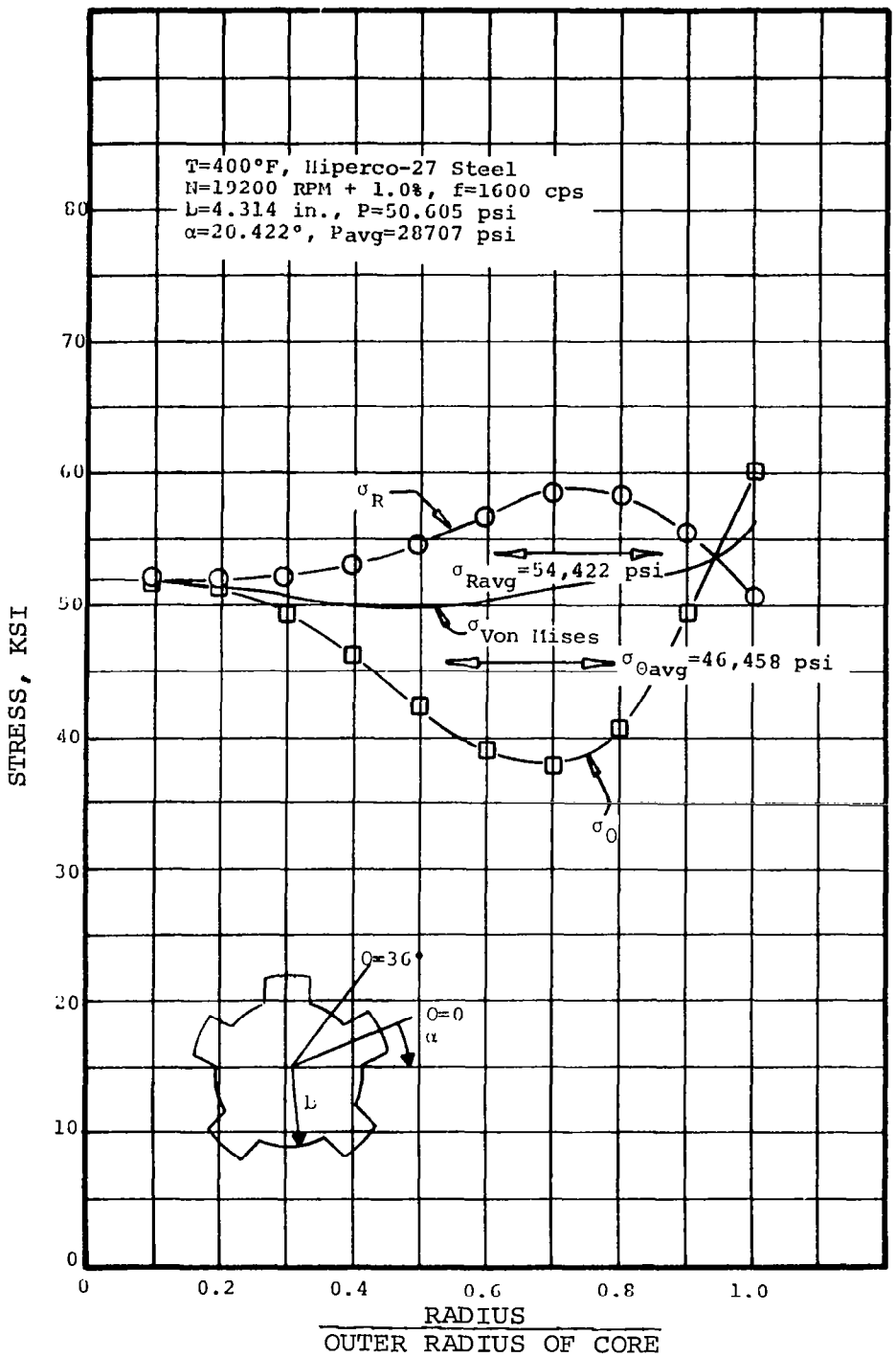

ROTOR STRESS AT θ = 0 DEG, 400°F COOLANT, 19,200 RPM

FIGURE 12

the same order of magnitude as that for the 30,000 rpm, H-11 design so the remarks above for making the H-11 design "barely acceptable" are applicable to the Hiperco.

An alternate approach to making the 19,200-rpm, Hiperco-27 design more acceptable might be to substitute a slightly higher strength material (likewise for the 30,000-rpm H-11 case) which would undoubtedly have lower magnetic capabilities. However, substituting an intermediate, less known material between H-11 (high strength, low magnetics) and Hiperco (low strength, high magnetics) does not appear warranted since the difference between the designs at these extremes are small.

A review of the strength properties of H-11 steel and of the 1BS1 precipitation-hardened alloy (modified cobalt base) was made for the 800°- and 1100°F-coolant temperature design condition. An interpretation of the available data for each material is graphically summaried in Figures 13 and 14, respectively. The strength data for H-11 steel was taken from Report No. AFAPL-TR-66-127[6] and NASA-CR-54091[7]. Only a limited amount of data was available for the precipitation-hardened, modified cobalt base alloy since only a few experiments were performed under Contract NAS3-6465[8]. The objectives of these experiments were to determine the relative merits of this type of material and not to determine the necessary property data for the design of a rotor. Therefore, the information present in Figure 14 cannot be used for the purpose of designing a rotor. The data only represents a "best estimation" of the property data that is required for the design of a rotor for a 3-year life. Similarly, considerable extrapolation of the creep data for H-11 steel, shown on Figure 13, was necessary to obtain the creep strength for the 3-year time period. Thus, the creep information given is only a "best estimate" of the creep data that is required for the design of a rotor for a 3-year operation. Inasmuch as H-11 is known to undergo aging, the strengths shown can be expected to be less at the end of 3 years. The extent of the aging is unknown at this time.

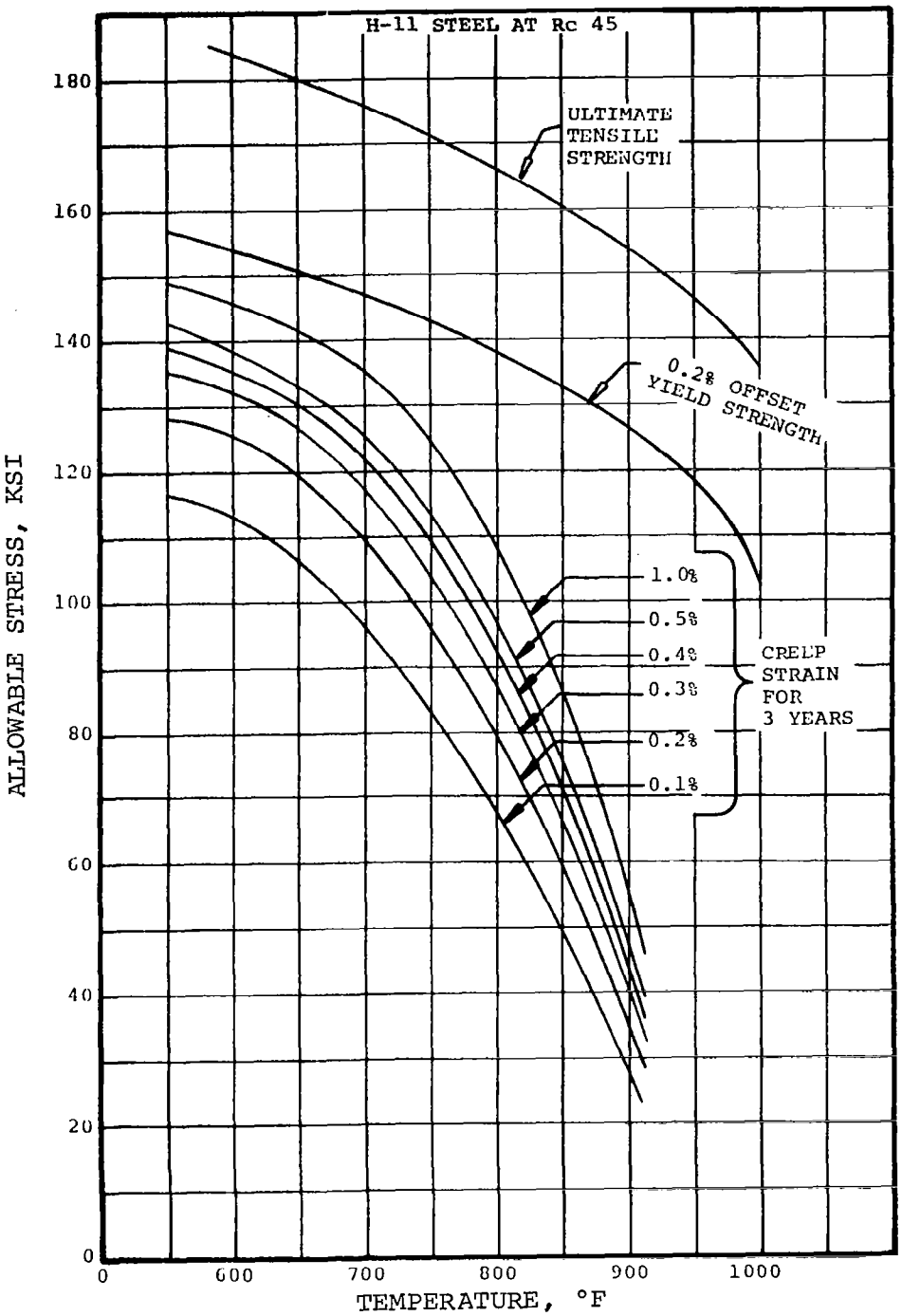

INTERPRETATION OF H-11 STEEL PROPERTY DATA AT A HARDNESS OF R_C 45

FIGURE 13

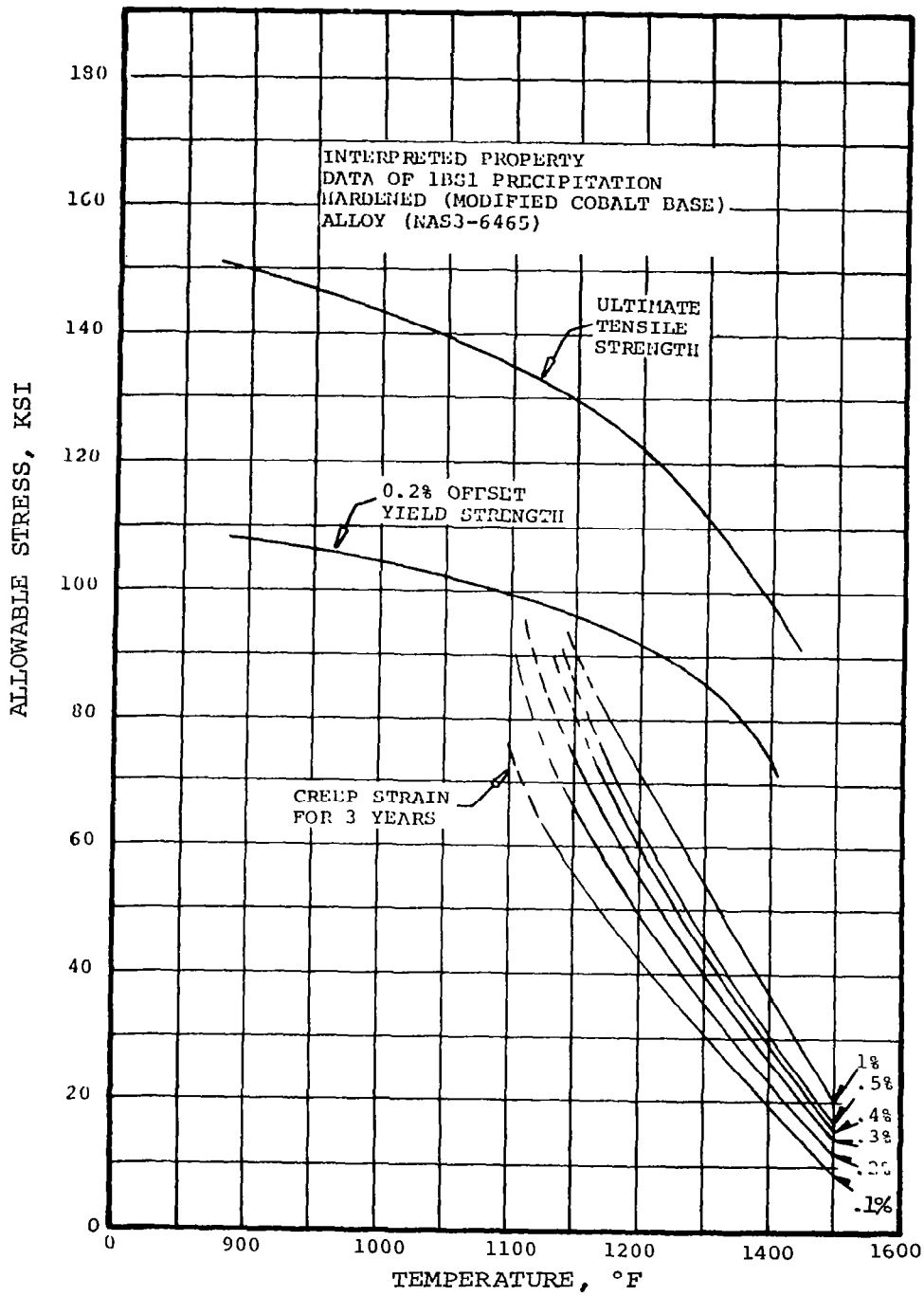

INTERPRETATION OF 1BS1 PRECIPITATION-HARDENED
ALLOY PROPERTY DATA

FIGURE 14

The stress distribution for the alternator rotors listed in Table 47 of the next section were calculated by the procedure outlined in Appendix B of Reference 2. Four stress profiles for each rotor are graphically illustrated in Figures 17 through 40. These stress profiles represent the following:

(a) The radial stress distribution which would exist within the rotor core if the centrifugal forces due to the poles were uniformly distributed around the outer boundary of the rotor core.

(b) The radial and tangential stress distributions in the rotor core on a radial plane (r-z) through the radial centerline of the poles.

(c) The radial and tangential stress distributions in the rotor core on a radial plane (r-z) midway between the radial centerline of adjacent poles.

(d) The average tangential and radial stress with respect to the radius of the rotor core that exists around the core.

In general, the maximum stress intensity occurs under the poles. Therefore, the biaxial tensile stresses at this location were converted into an equivalent stress so a comparison with the uniaxial tensile date from Figures 15 and 16 could be made. The equivalent stress is shown only for the cases where the acceptability of the design is questionable.

On the basis of a comparison between the actual stresses and the stress limitations of the materials, the following conclusions are justified for the 800° and 1100°F designs:

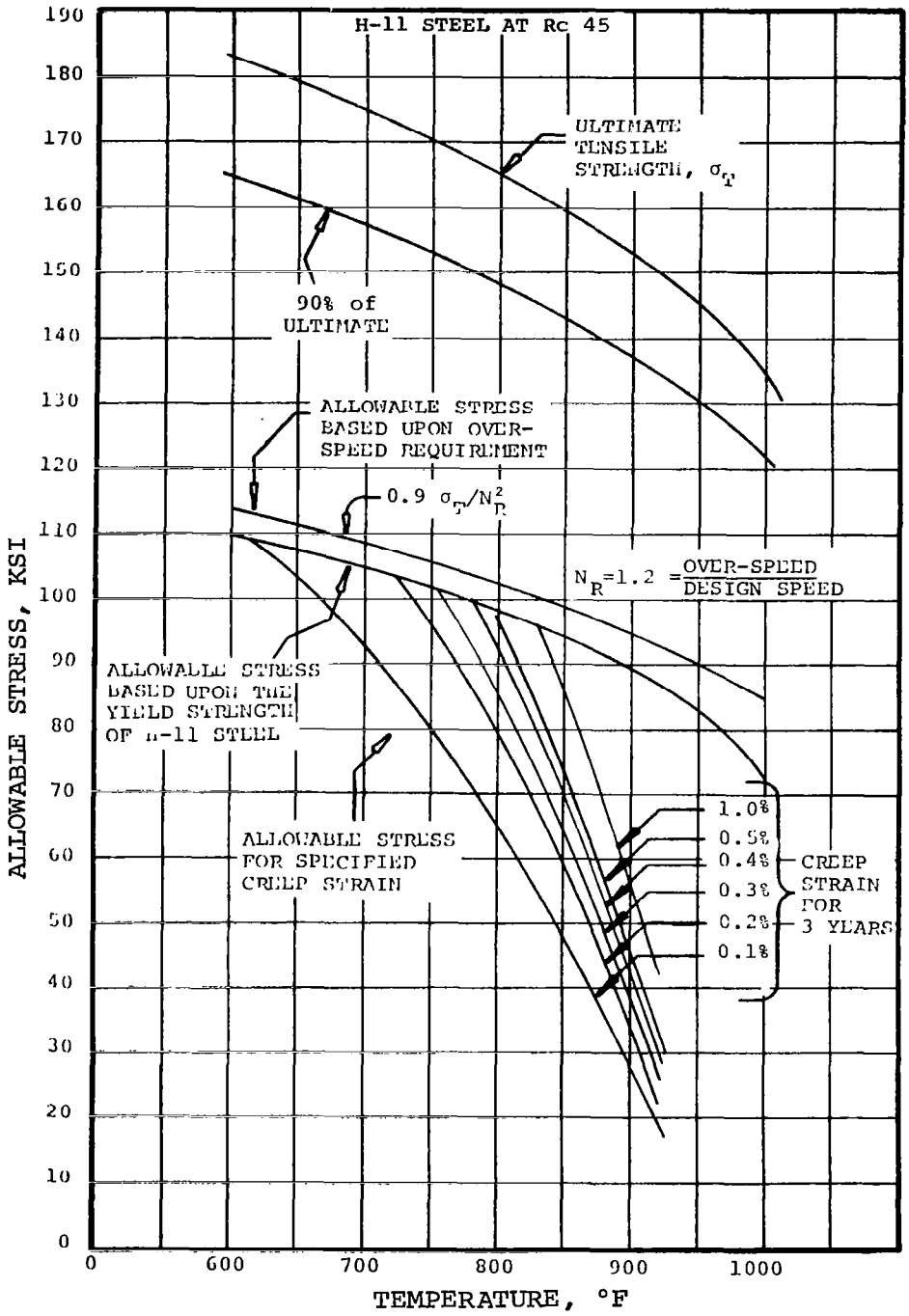

INTERPRETATION OF H-11 STEEL PROPERTY DATA AT A HARDNESS OF R_C 45

FIGURE 15

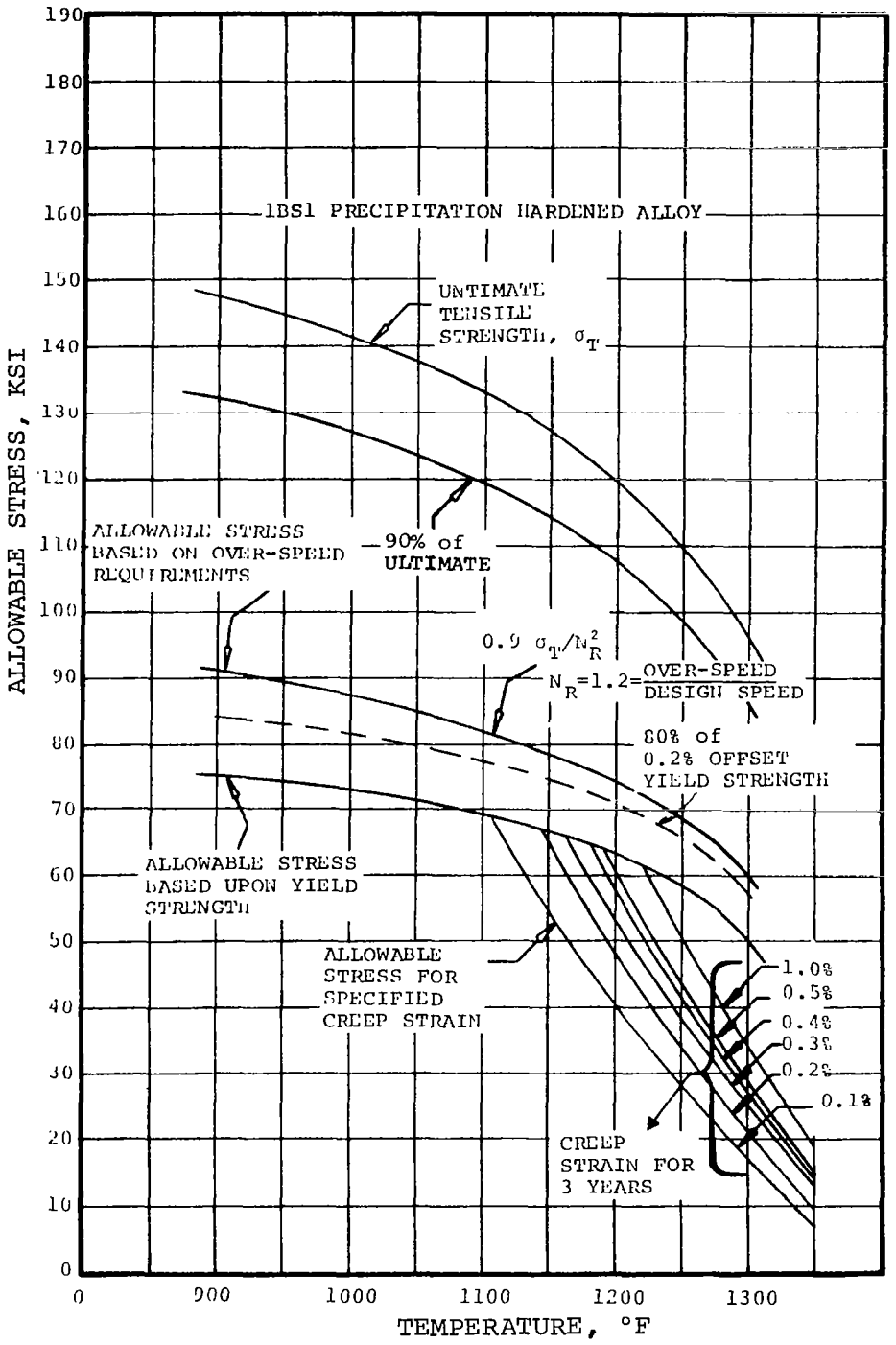

INTERPRETATION OF 1BS1 PRECIPITATION-HARDENED ALLOY PROPERTY DATA

FIGURE 16

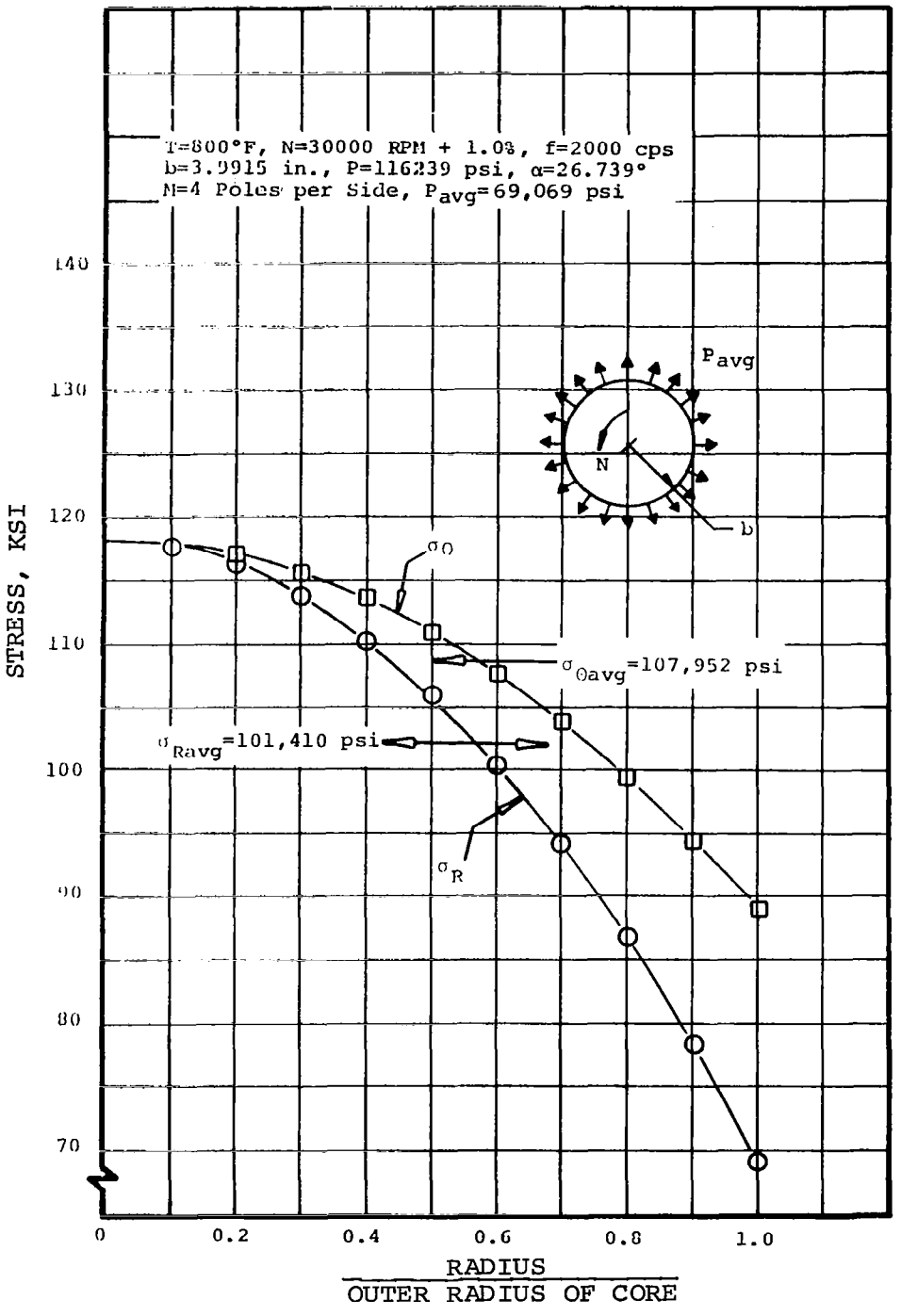

ROTOR STRESS AT UNIFORM LOAD,
800°F COOLANT, 30,000 RPM

FIGURE 17

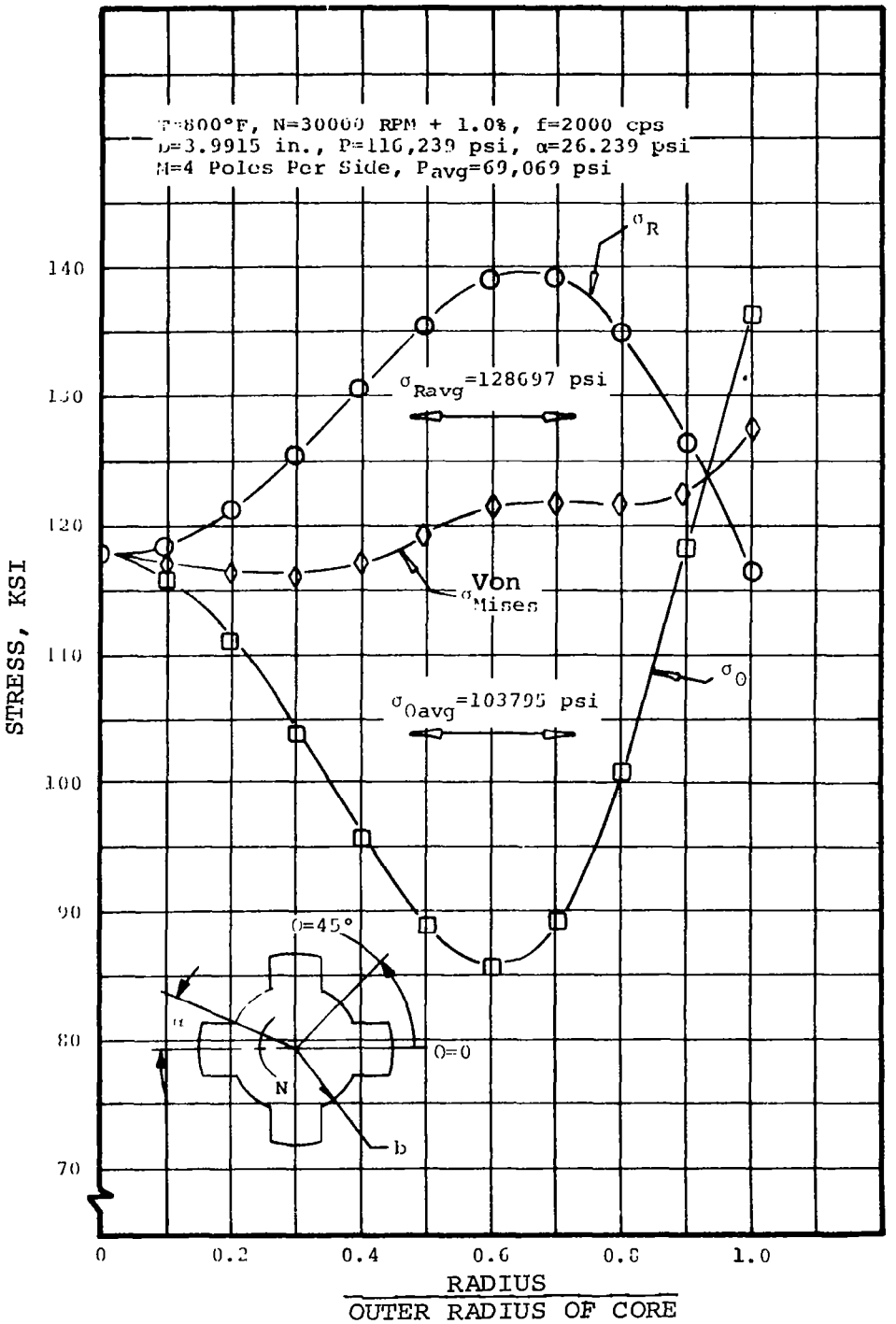

ROTOR STRESS AT θ = 0 DEG, 800°F COOLANT, 30,000 RPM

FIGURE 18

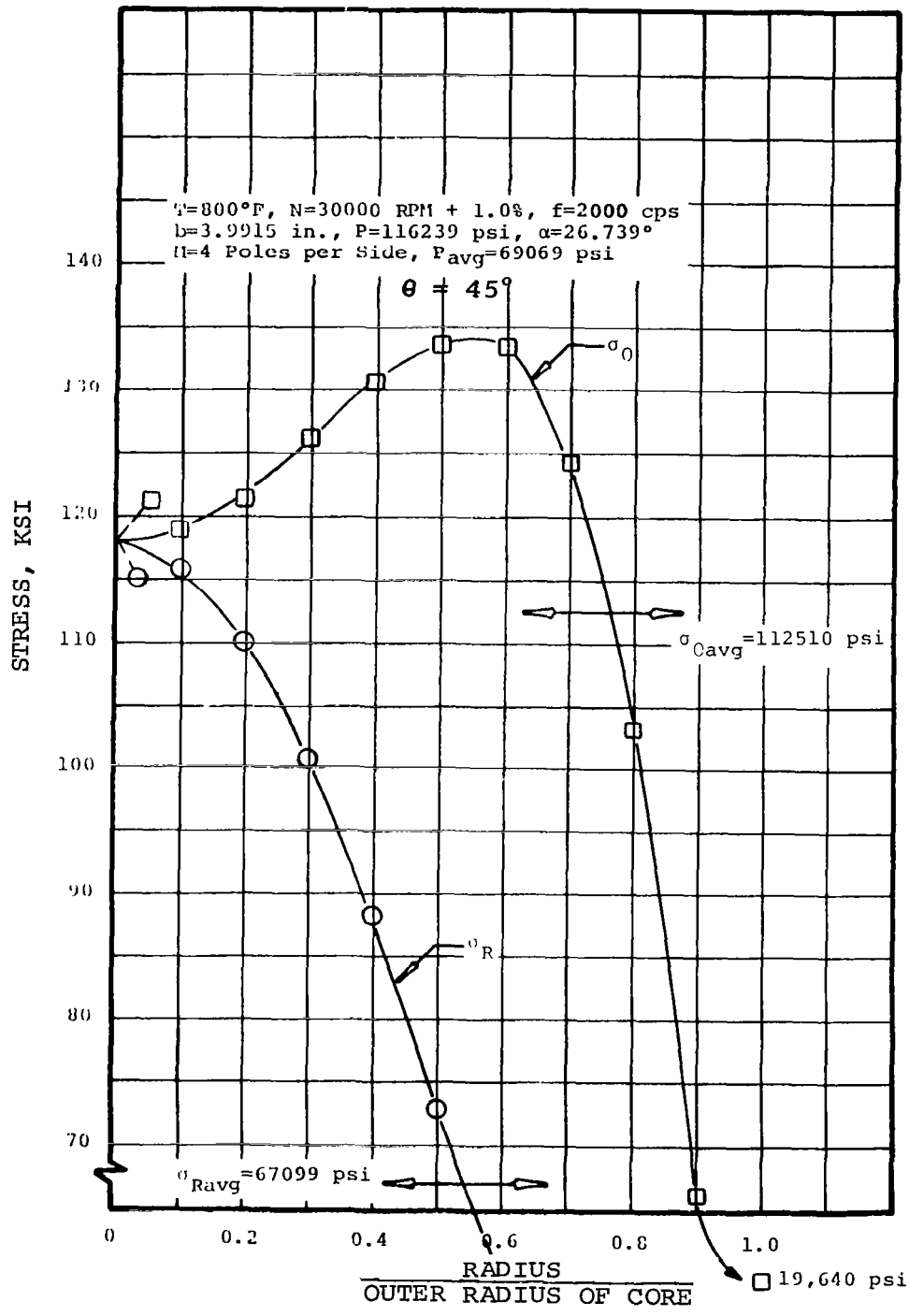

ROTOR STRESS AT θ = 45 DEG, 800°F COOLANT, 30,000 RPM

FIGURE 19

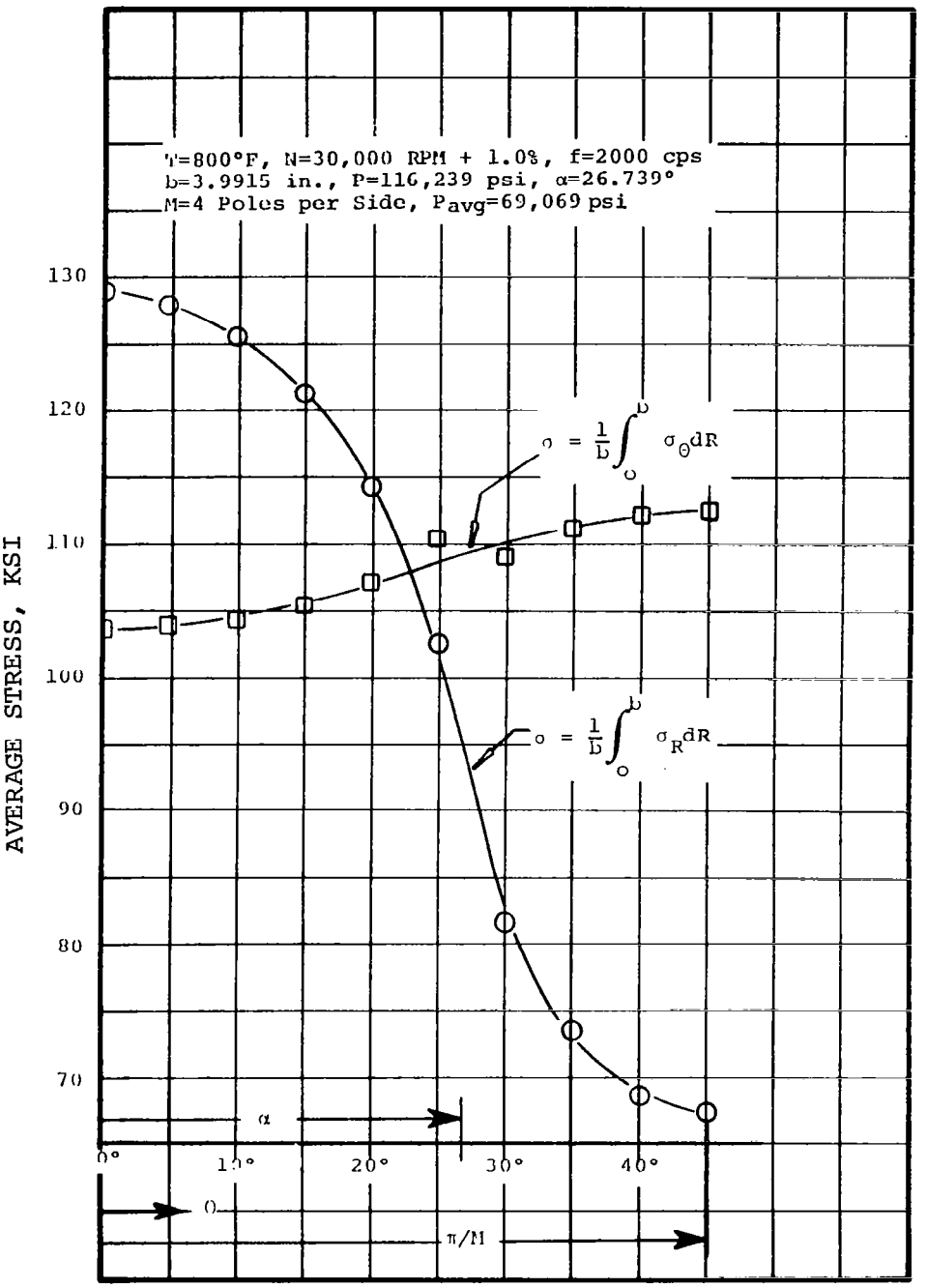

ROTOR STRESS (AVERAGE) AS A FUNCTION OF θ,
800°F COOLANT, 30,000 RPM

FIGURE 20

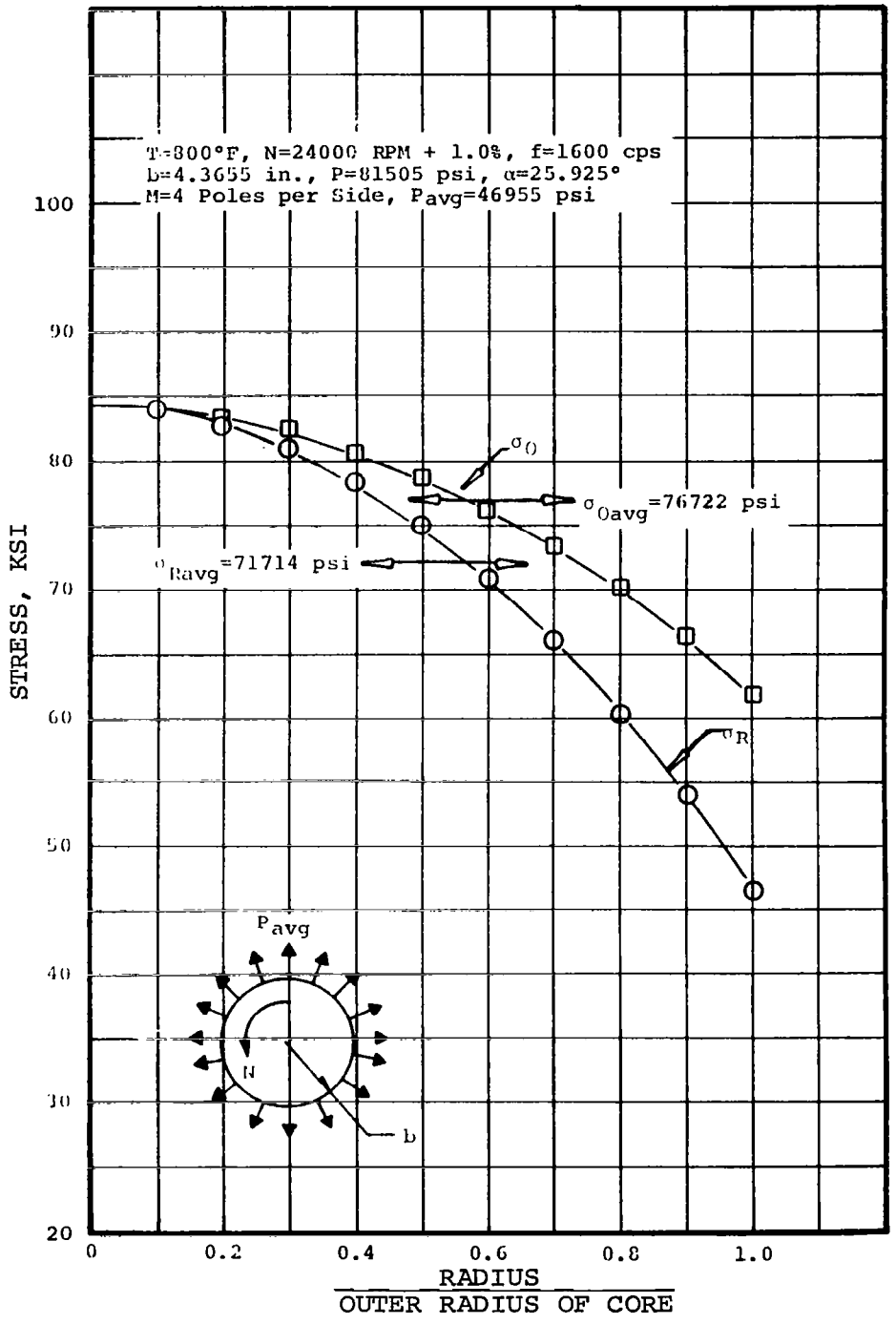

ROTOR STRESS AT UNIFORM LOAD,
800°F COOLANT, 24,000 RPM

FIGURE 21

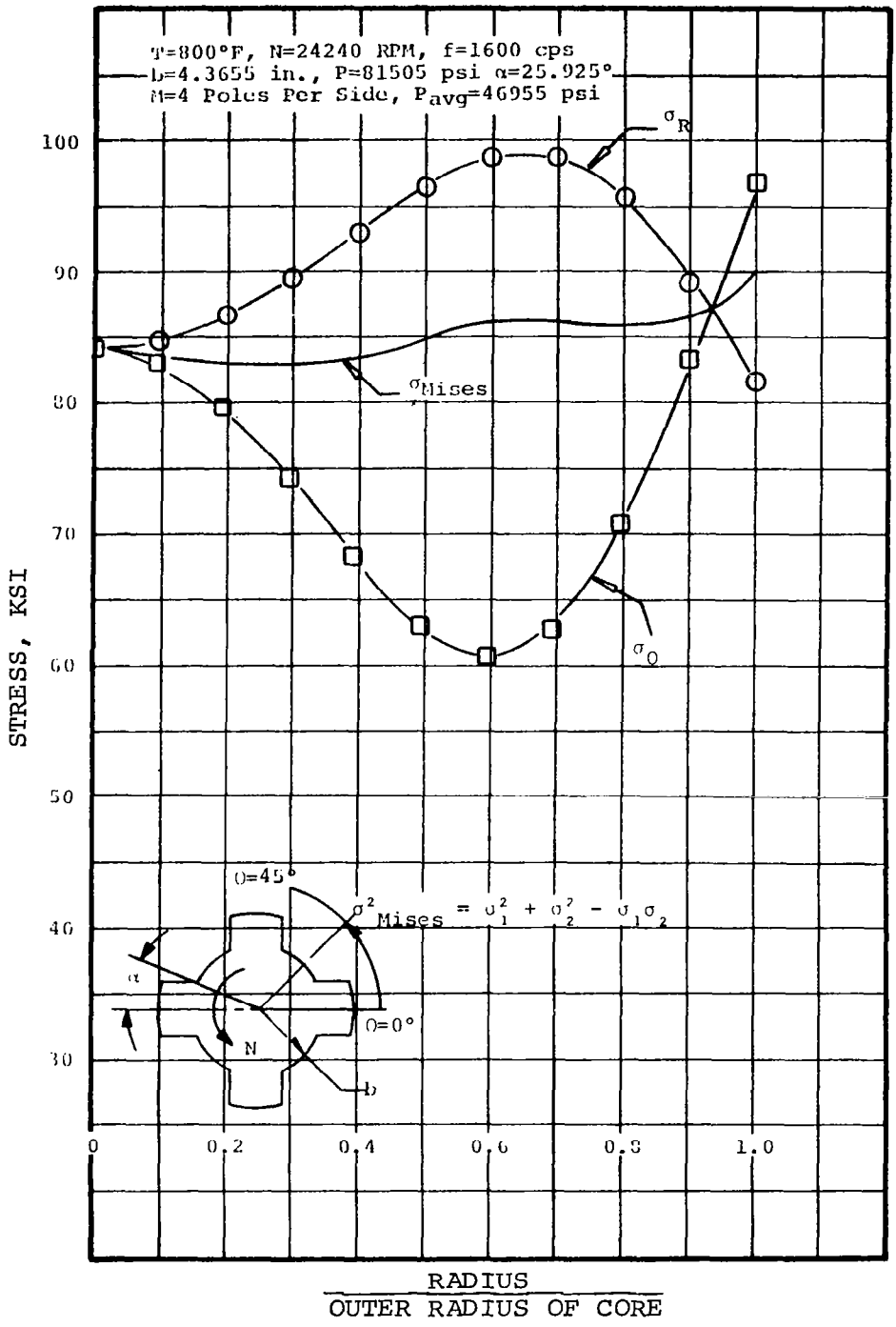

ROTOR STRESS AT θ = 0 DEG, 800°F COOLANT, 24,000 RPM

FIGURE 22

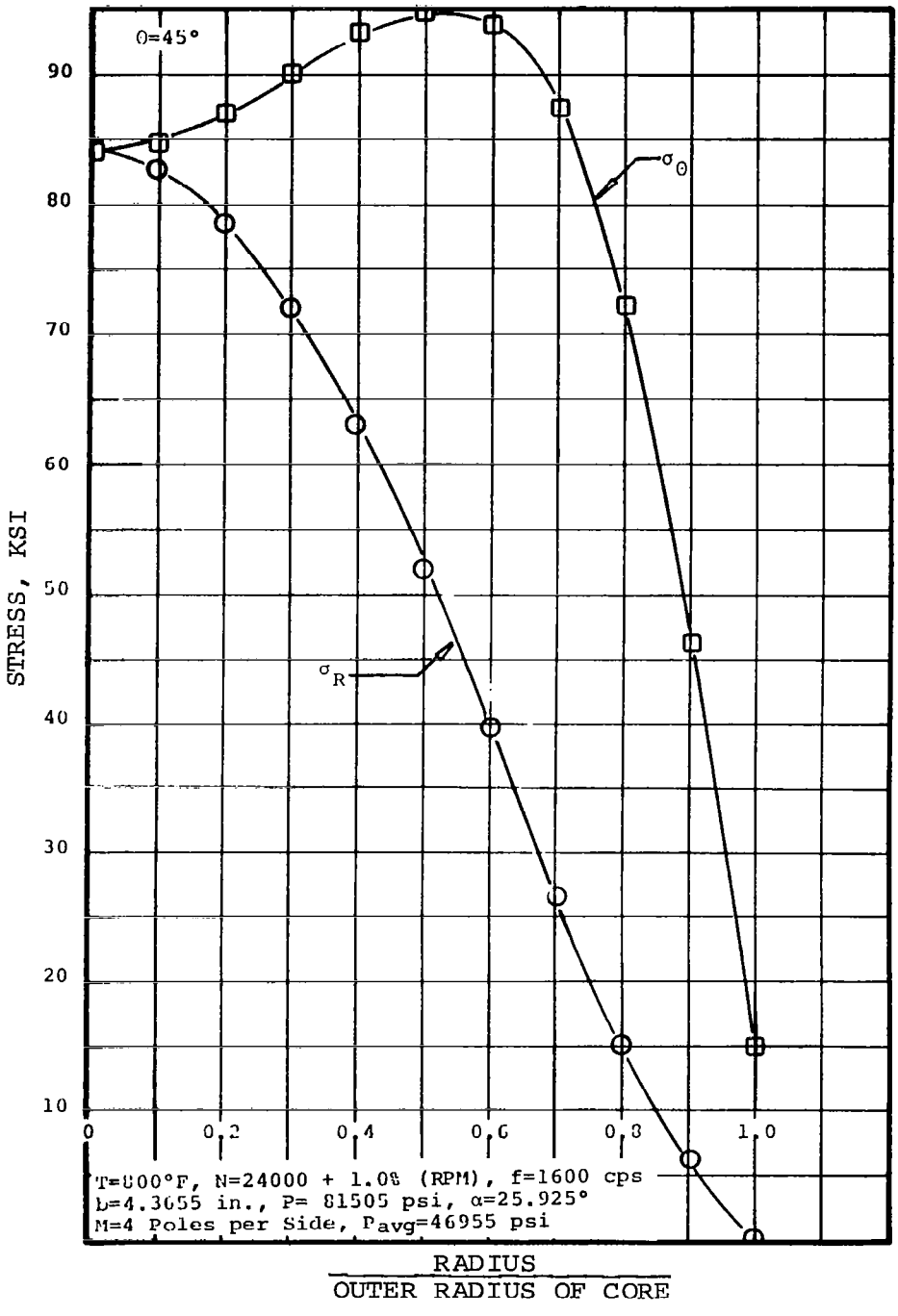

ROTOR STRESS AT θ = 45 DEG, 800°F COOLANT, 24,000 RPM

FIGURE 23

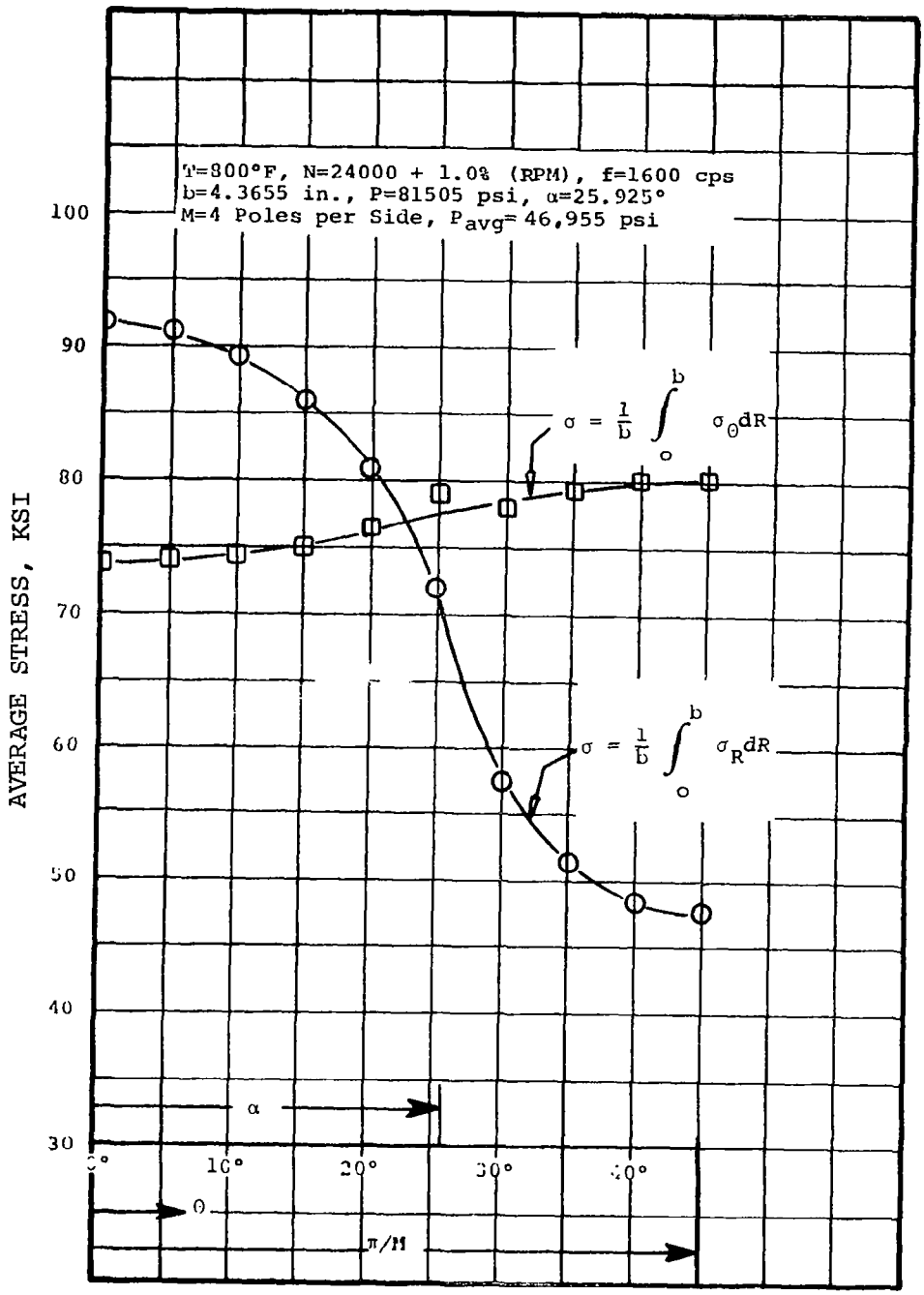

ROTOR STRESS (AVERAGE) AS A FUNCTION OF θ,
800°F COOLANT, 24,000 RPM

FIGURE 24

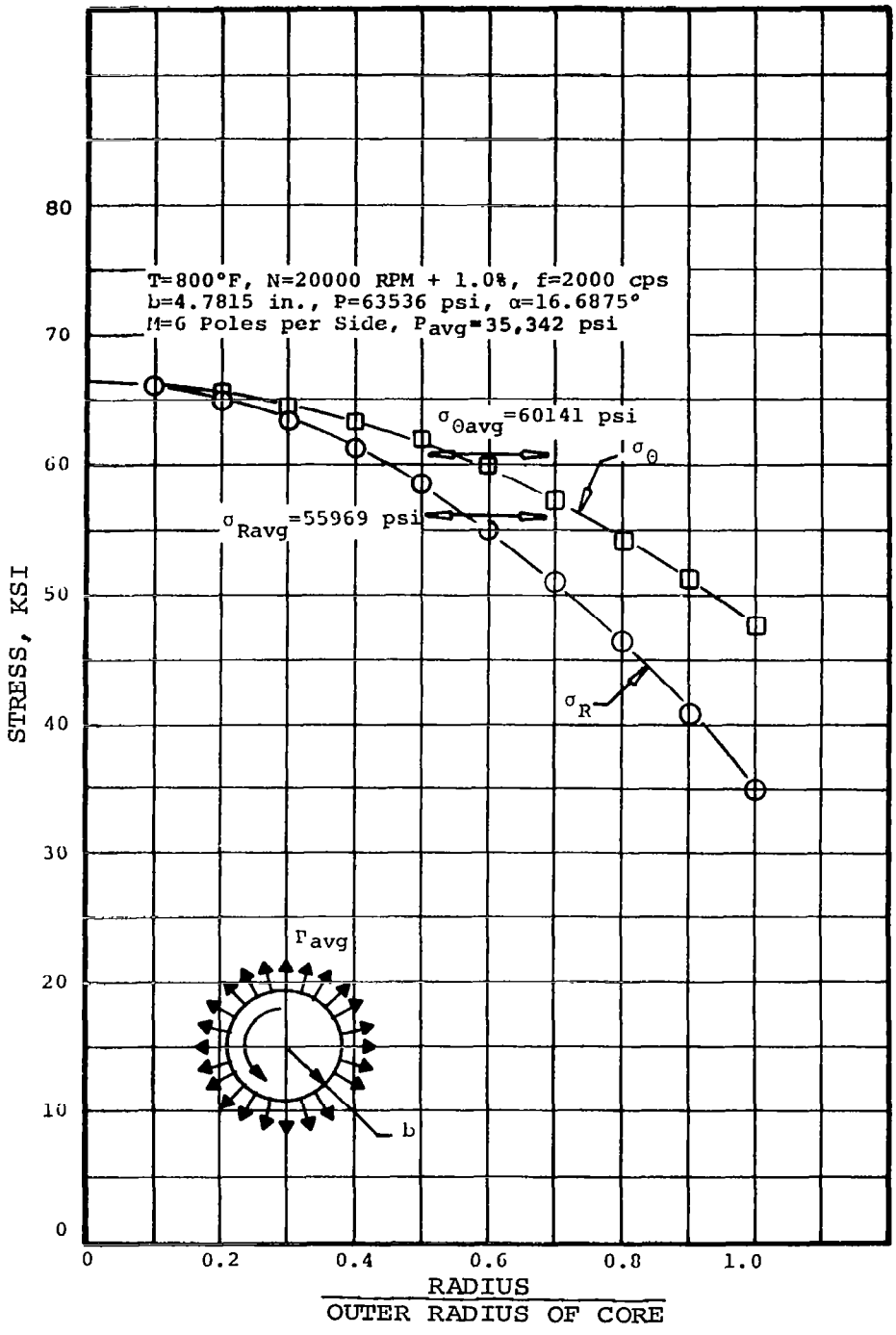

ROTOR STRESS AT UNIFORM LOAD,
800°F COOLANT, 20,000 RPM

FIGURE 25

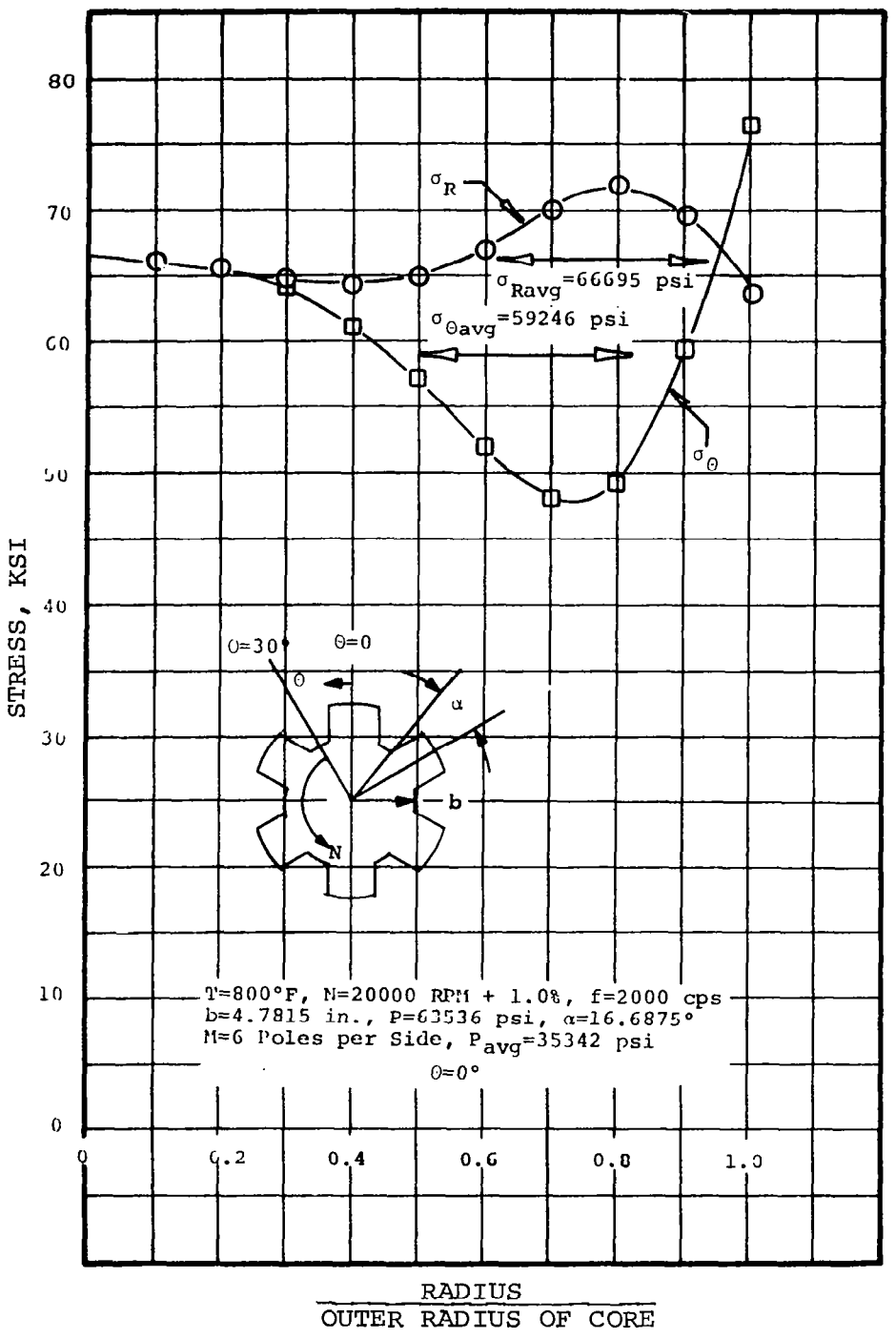

ROTOR STRESS AT θ = 0 DEG, 800°F COOLANT, 20,000 RPM

FIGURE 26

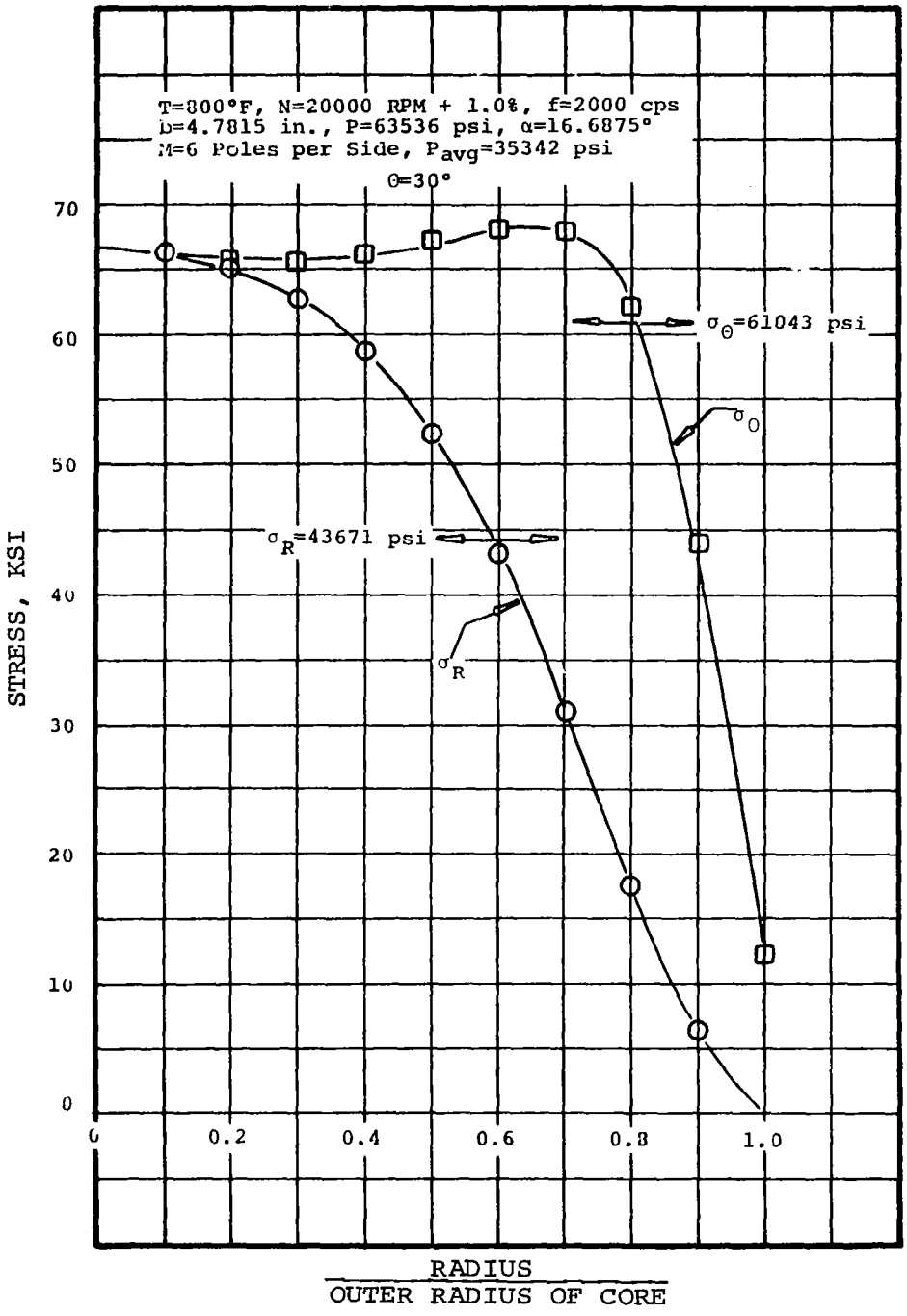

ROTOR STRESS AT θ = 30 DEG, 800°F COOLANT, 20,000 RPM

FIGURE 27

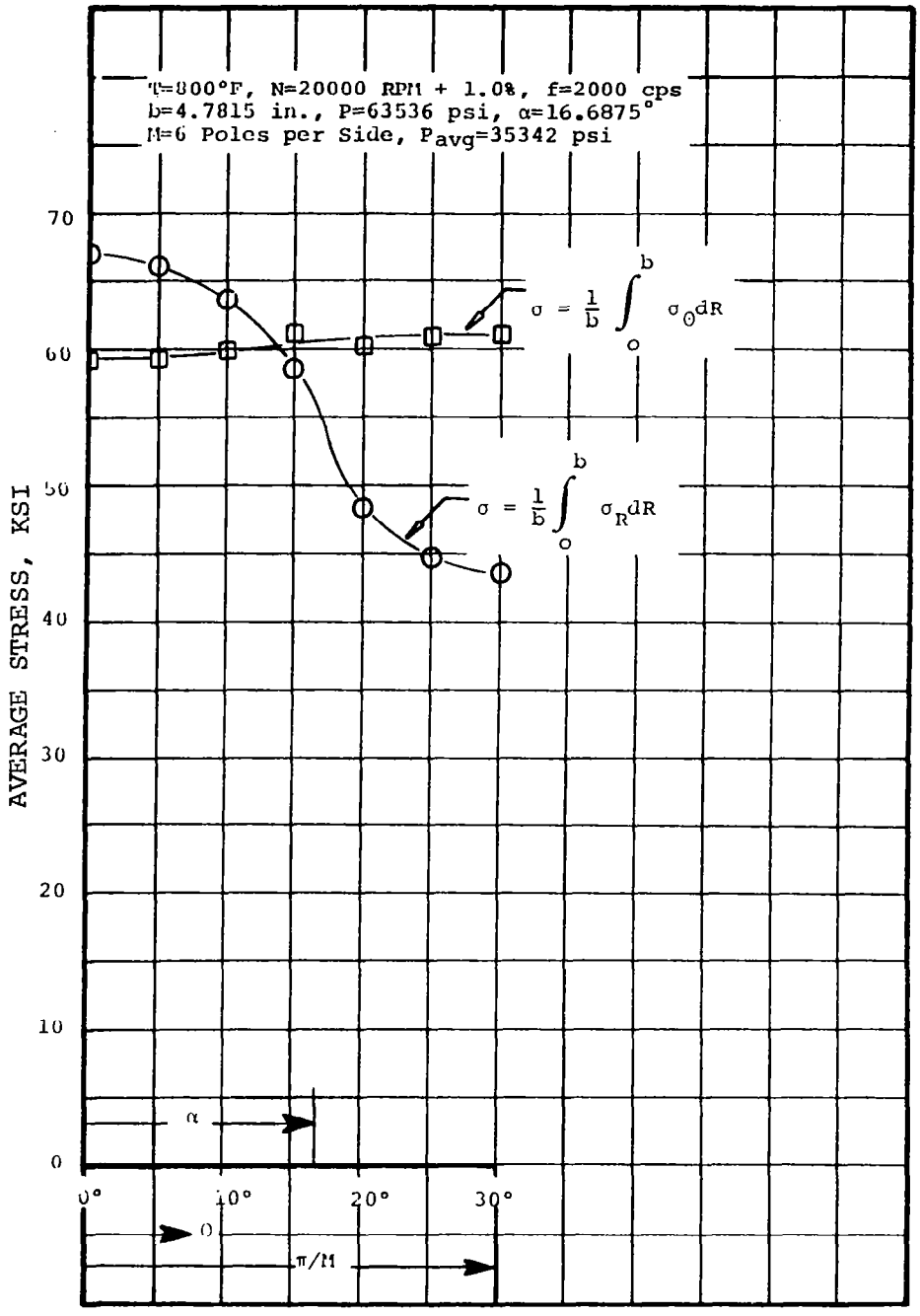

ROTOR STRESS (AVERAGE) AS A FUNCTION OF θ,
800°F COOLANT, 20,000 RPM

FIGURE 28

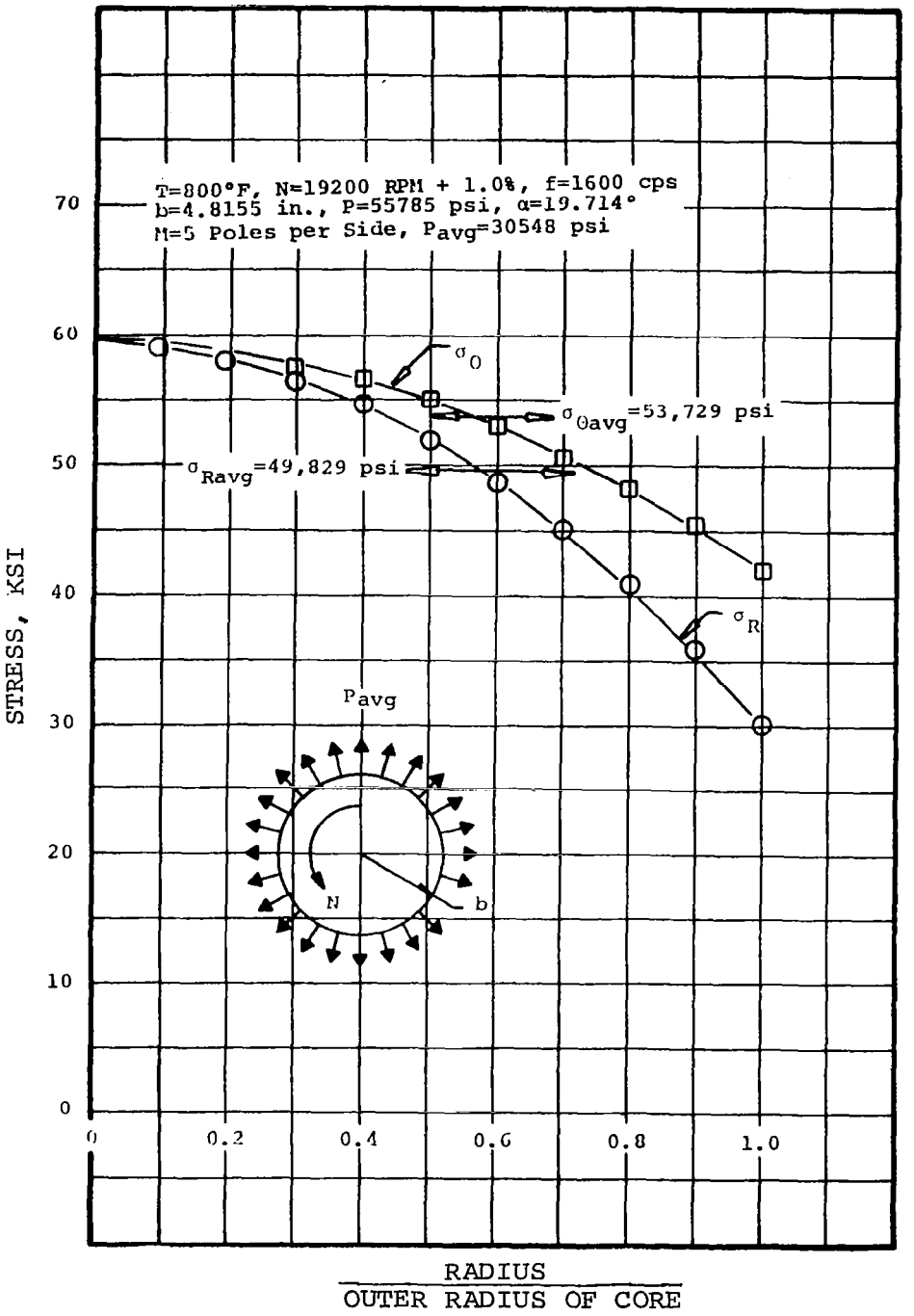

ROTOR STRESS AT UNIFORM LOAD,
800°F COOLANT, 19,200 RPM

FIGURE 29

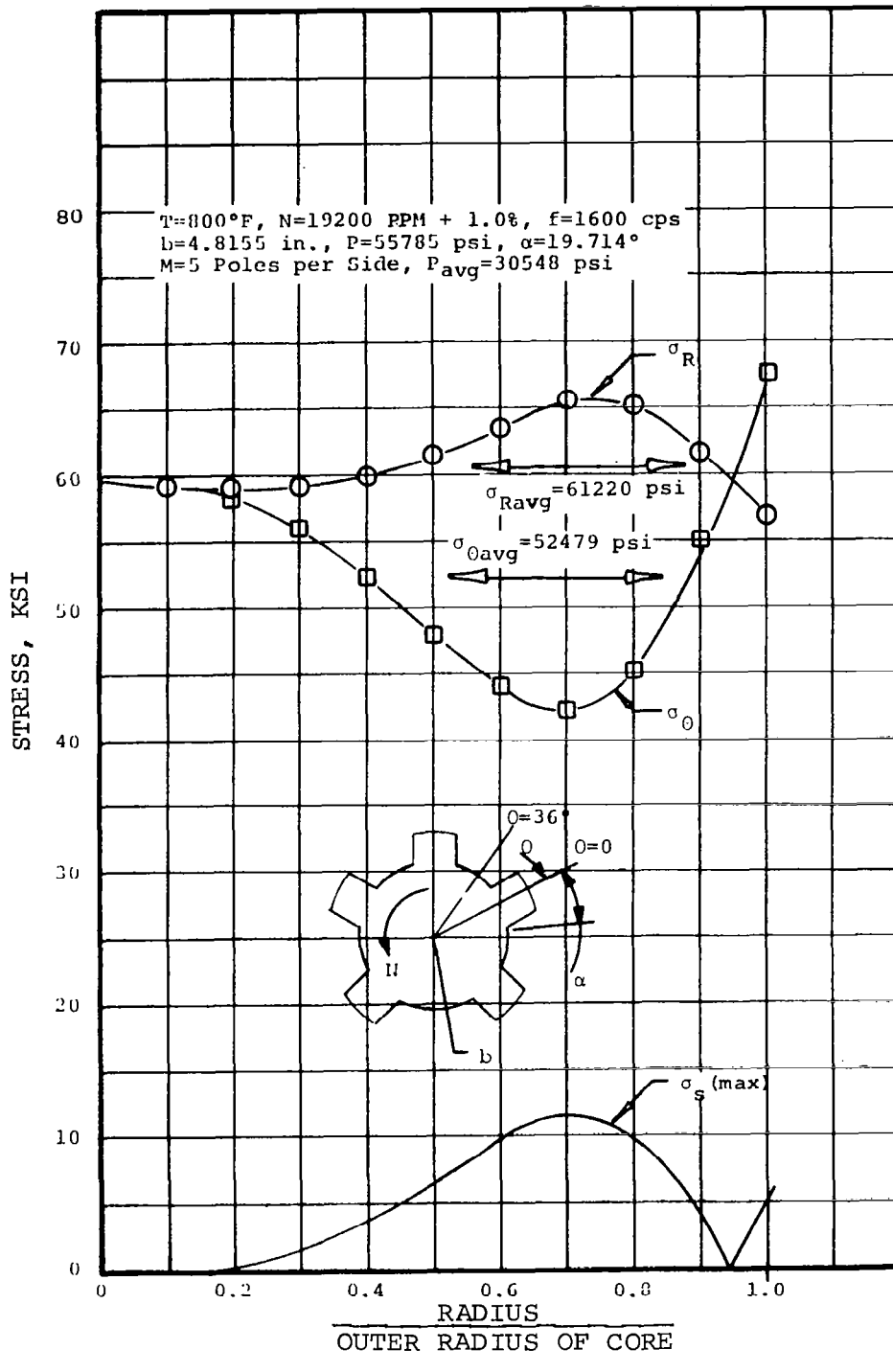

ROTOR STRESS AT θ = 0 DEG, 800°F COOLANT, 19,200 RPM

FIGURE 30

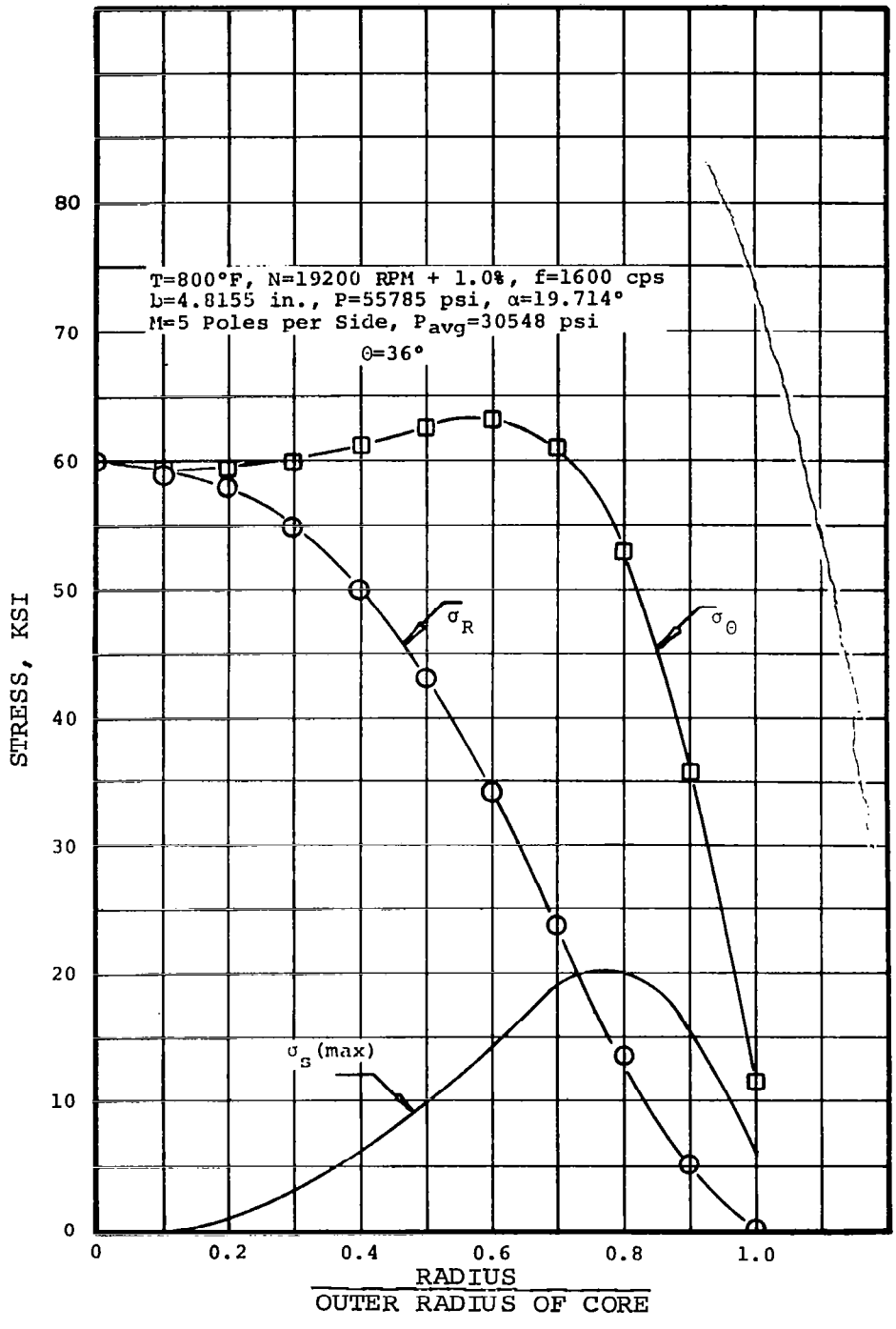

ROTOR STRESS AT θ = 36 DEG, 800°F COOLANT, 19,200 RPM

FIGURE 31

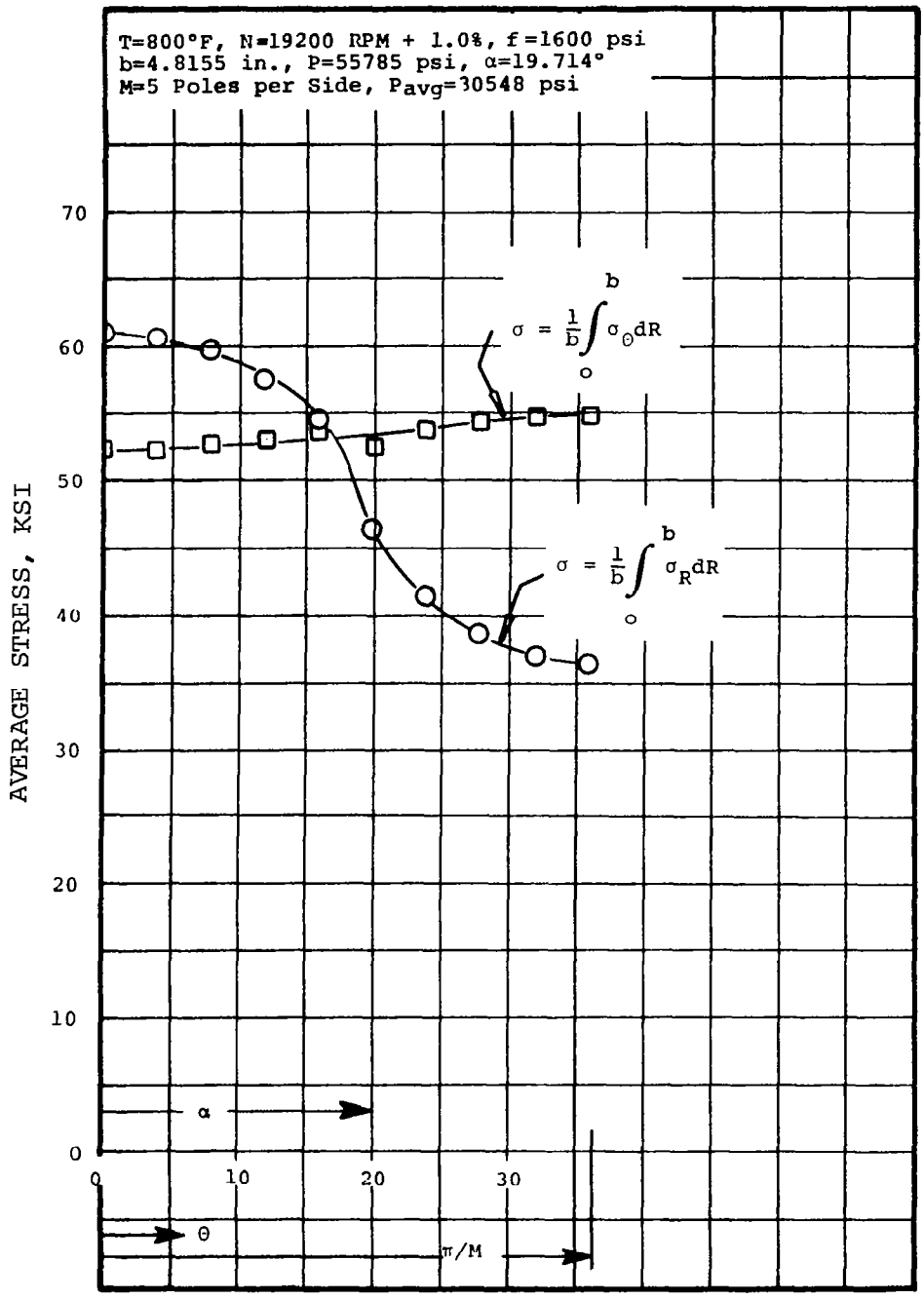

ROTOR STRESS (AVERAGE) AS A FUNCTION OF θ,
800°F COOLANT, 19,200 RPM

FIGURE 32

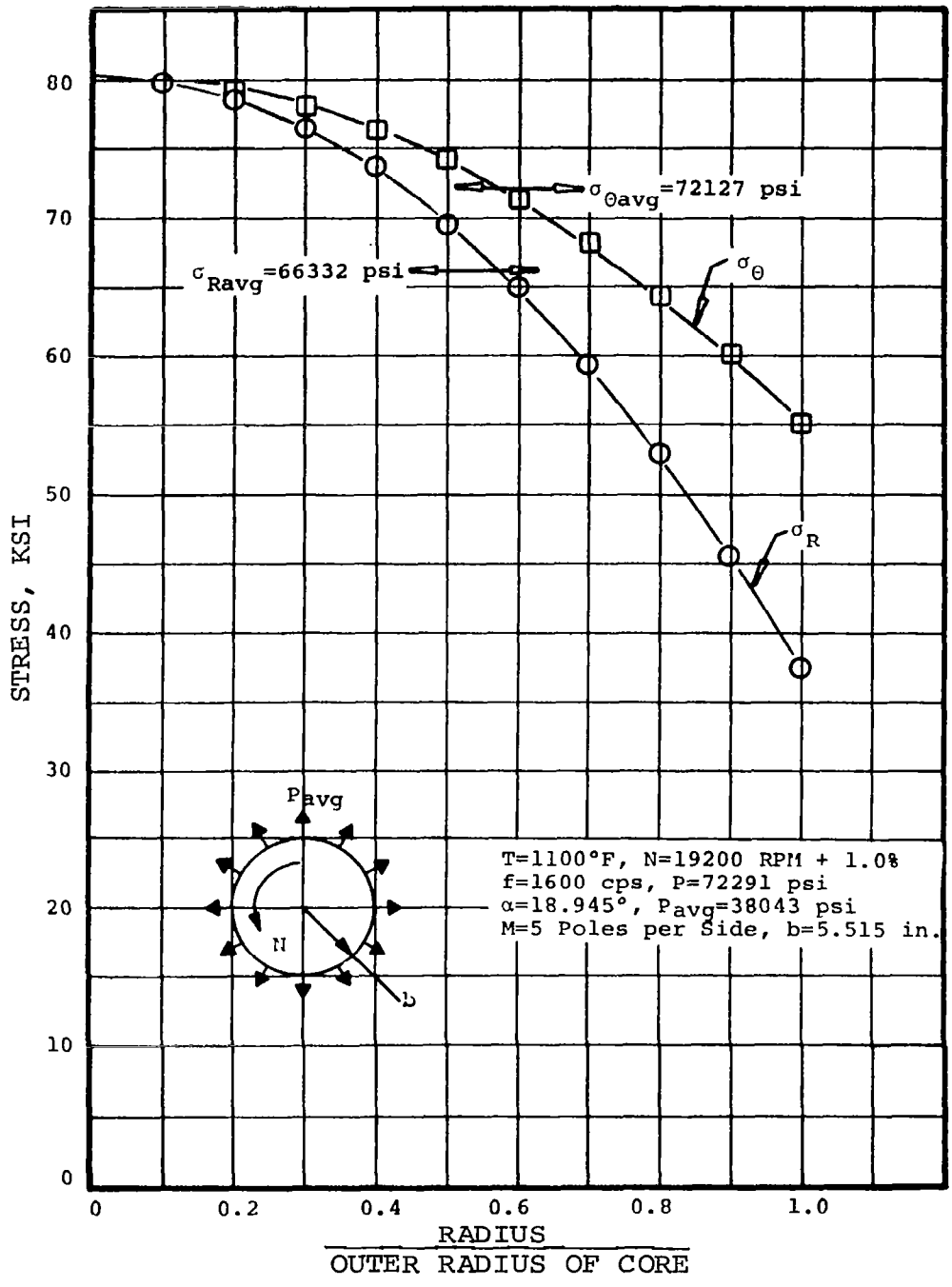

ROTOR STRESS AT UNIFORM LOAD,
1100°F COOLANT, 19,200 RPM

FIGURE 33

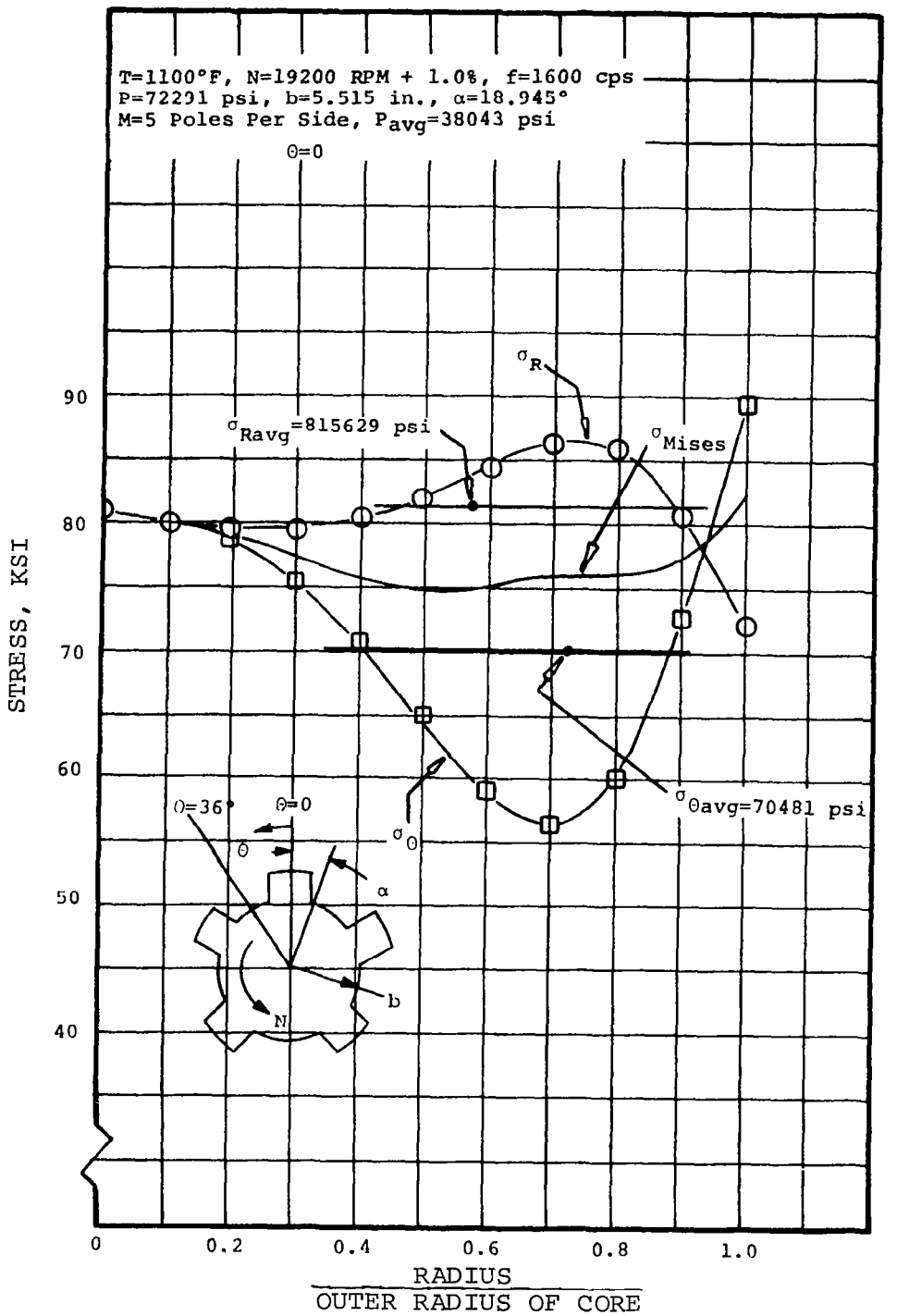

ROTOR STRESS AT θ = 0 DEG, 1100°F COOLANT, 19,200 RPM

FIGURE 34

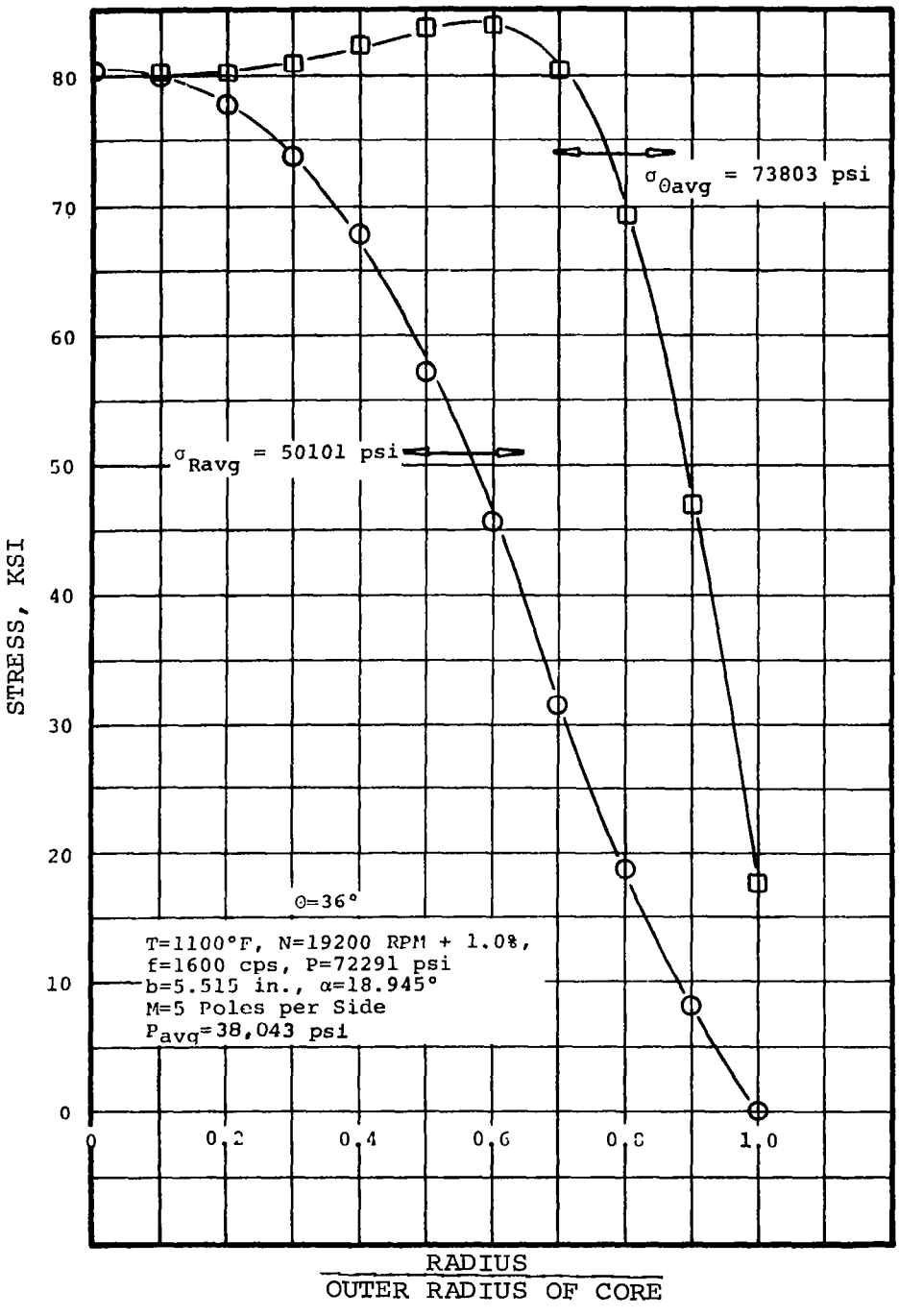

ROTOR STRESS AT θ = 36 DEG, 1100°F COOLANT, 19,200 RPM

FIGURE 35

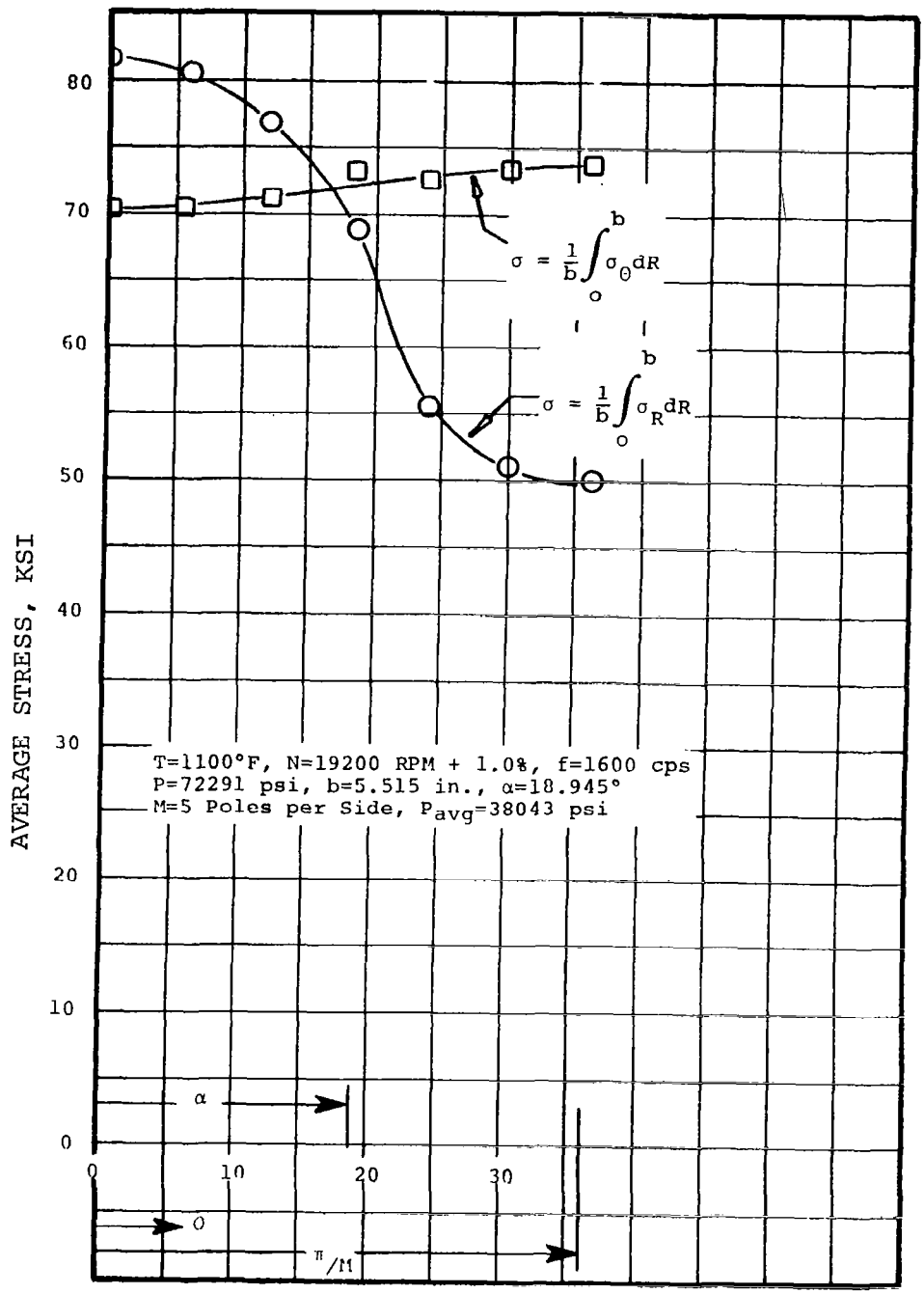

ROTOR STRESS (AVERAGE) AS A FUNCTION OF α,
1100°F COOLANT, 19,200 RPM

FIGURE 36

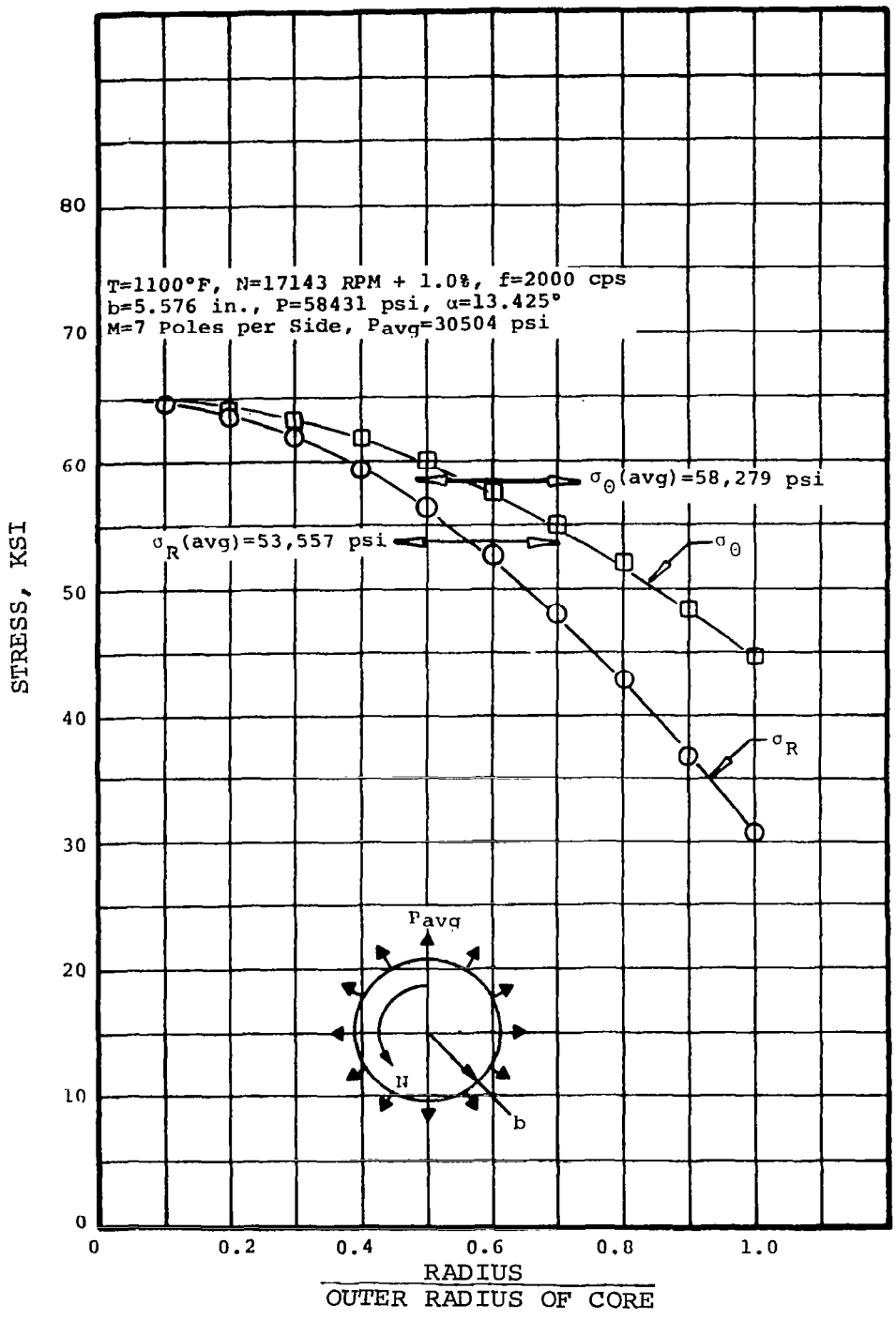

ROTOR STRESS AT UNIFORM LOAD,
1100°F COOLANT, 17,143 RPM

FIGURE 37

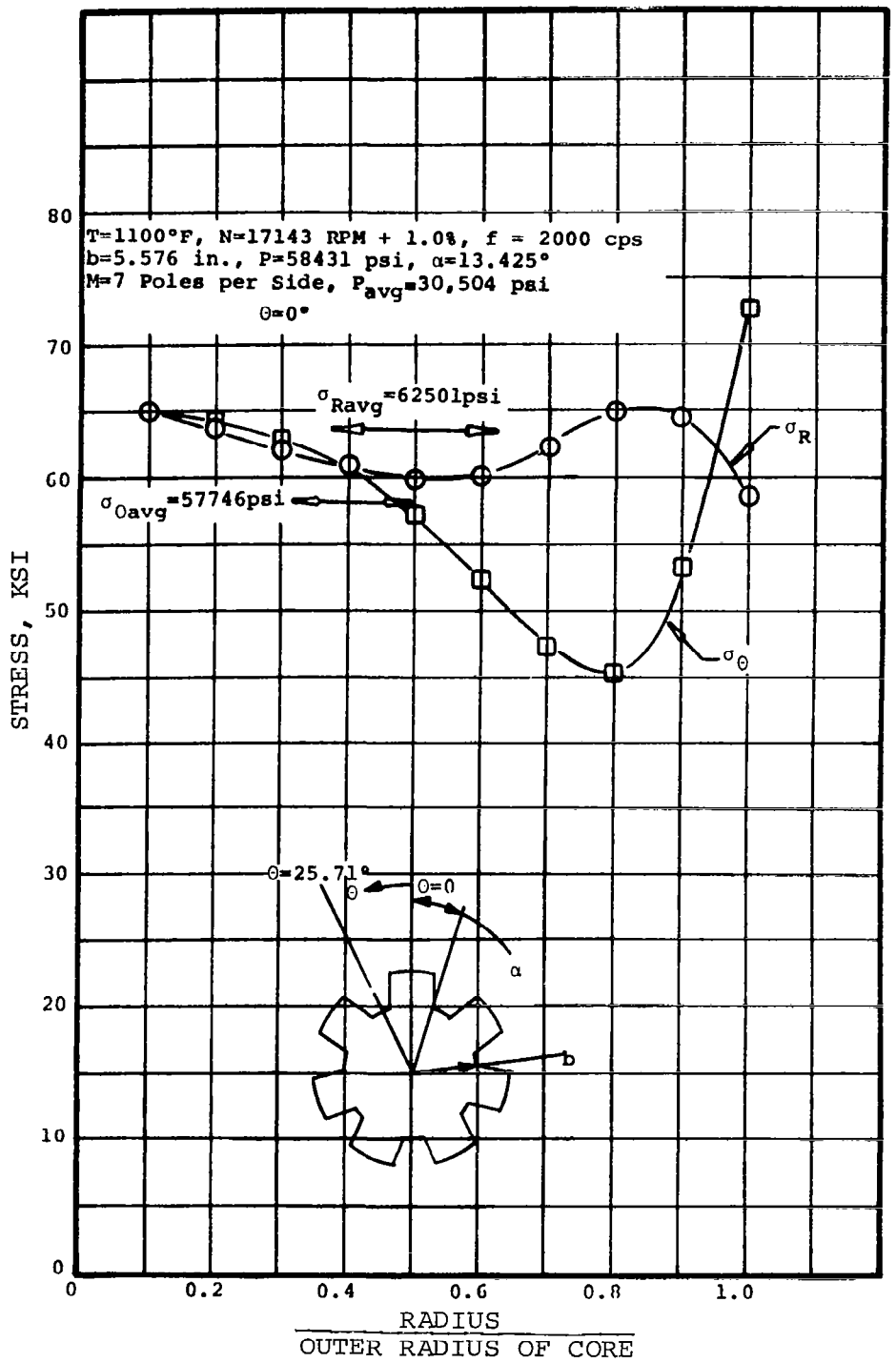

ROTOR STRESS AT θ = 0 DEG, 1100°F COOLANT, 17,143 RPM

FIGURE 38

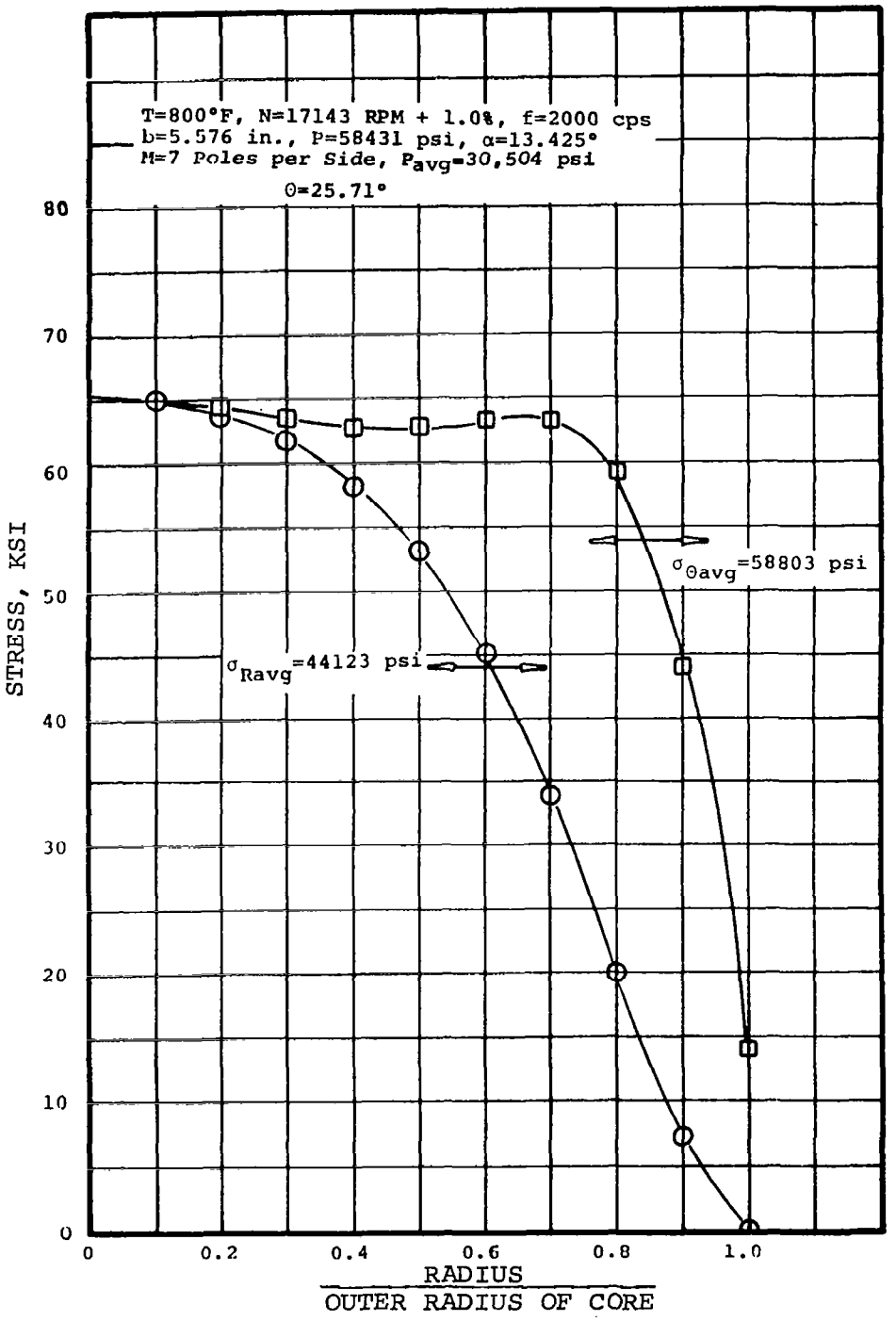

ROTOR STRESS AT θ = 25.71 DEG,
1100°F COOLANT, 17,143 RPM

FIGURE 39

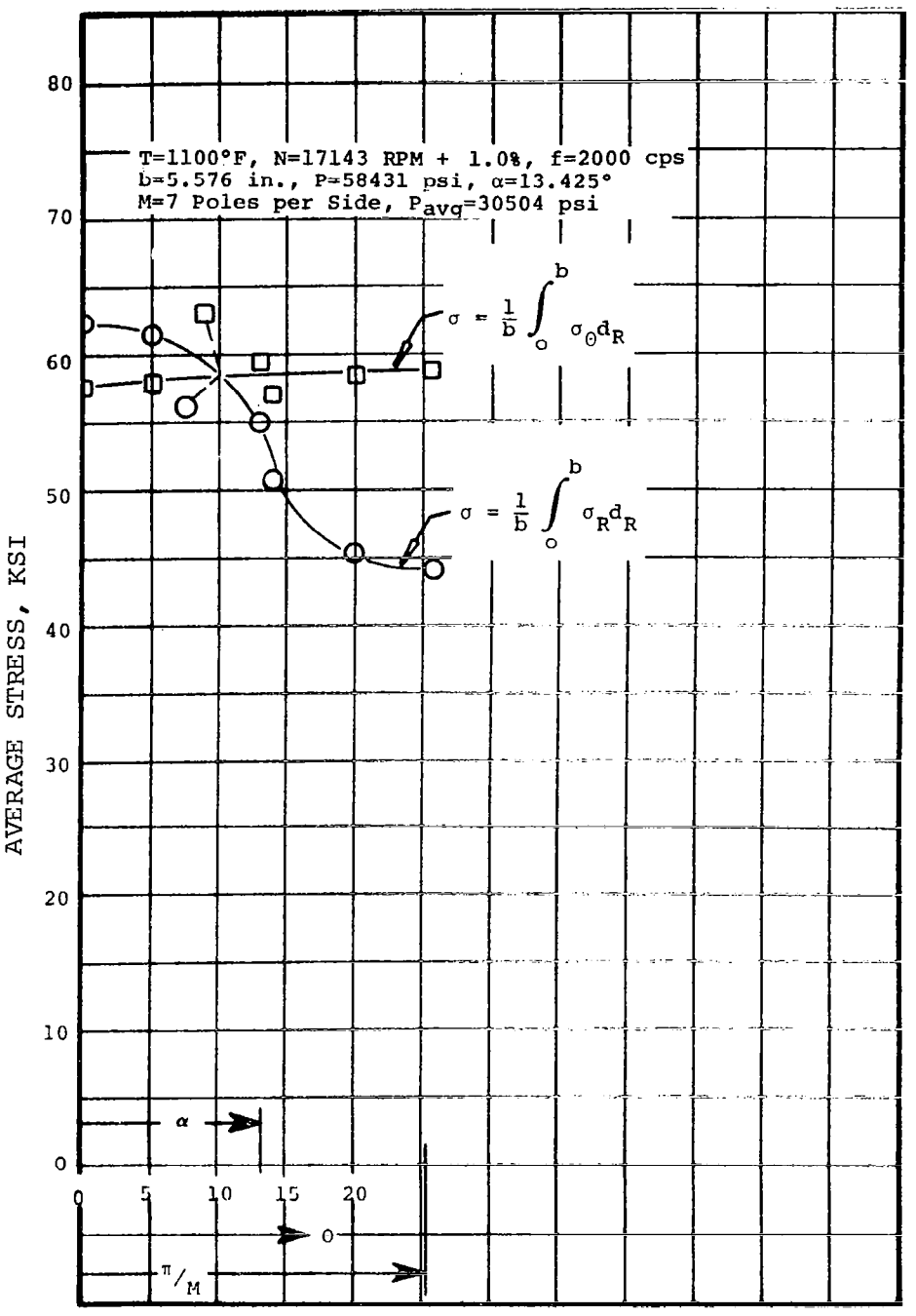

ROTOR STRESS (AVERAGE) AS A FUNCTION OF θ,
1100°F COOLANT, 17,143 RPM

FIGURE 40

(a) The stress within the rotors for the 800°F, 30,000-rpm alternator exceed the allowable stress for H-11 steel.

(b) The stress within the rotor for an 800°F, and speeds at or below 24,000-rpm alternator is within the allowable stress limit of H-11 steel.

(c) The stress within the rotor for a 1100°F, 19,200-rpm alternator exceeds the allowable stress for the precipitation-hardened, modified cobalt base alloy. The calculated stress intensity is approximately 83 percent of the average 0.2-percent offset strength of this material.

If one uses 72 percent of the average 0.2-percent offset strength as a limit, a material with a slightly higher yield strength would have to be developed for the application.

(d) The stress within the rotor for an 1100°F, and speed at or below 17,143-rpm alternator is within the allowable stress limit of the precipitation hardened, modified cobalt base alloy.

2.5 Organic Coolant Study

2.5.1 Introduction

The purpose of this study was to assist AiResearch in selection of organic lubricant(s)/coolant(s) and their temperatures which would be equally applicable to the organic lubricated turbine bearings and seals, the alternator bearings and seals, and the alternator coolant.

AiResearch suggested and Westinghouse concurred in the selection of the following organic fluids for the temperatures shown:

Fluid	Temperature, °F
Highly refined mineral oil	200
Highly refined mineral oil	400
Polyphenyl ether (5P4E)	600

An impractically large and technically unprofitable amount of analyses would have been required to perform the alternator design parametric screening studies discussed in Sections 2.2, 2.3 and 2.4 for each one of the organic fluids and temperatures listed above. Therefore, a single representative organic fluid and temperature was selected for the organic cooled/lubricated alternator design parametric screening studies. Highly refined mineral oil at 400°F was selected for this purpose in conjunction with AiResearch and NASA. It was believed that parametric alternator designs based on mineral oil at 400°F as the coolant/lubricant would best typify the characteristics of possible organic-cooled and lubricated designs because (1) 400°F is a "plateau" temperature for rotor material selection (Section 2.3), (2) it was expected that there would only be slight differences between the higher organic temperature designs and the 800°F potassium designs, and (3) 400°F was conveniently the mid-point in the organic fluid temperature range. However, to ensure a fair comparison and to provide a broader comparison between organic and potassium cooled/lubricated designs, a selected design from the 400°F parametric screening study was investigated using the other organic fluids and temperatures listed previously. The object of this limited coolant temperature excursion study was to obtain rough alternator performance data, particularly efficiency and weight, to compare to corresponding performance data of the potassium cooled and lubricated alternator designs. This study is the subject of the next section.

There are several considerations in the selection of an organic coolant/lubricant for the KTA alternator. Generally, these considerations include high temperature capabilities (particularly stability), nuclear radiation resistance, lubrication properties, heat-transfer capabilities, vapor pressure, and any specific problems associated with shaft seals - vapor shaft seals between the rotor cavity and liquid shaft seals between the potassium working fluid and the organic bearing lubricant in the turbine. Most of these considerations apply to both the turbine and the alternator. However, the following discussion will be limited to organic fluid selection considerations unique to the alternator. These two considerations are heat transfer (or cooling capabilities) and vapor pressure of the organic fluids.

A generalized approach was taken for the analysis of the cooling capabilities whereby the various film temperature drops were determined for a typical KTA alternator. The assumptions of the analysis were as follows:

(a) Rating = 550 kw_e
(b) Efficiency = 91 percent
(c) Total losses = 54 kw
(d) 90% of losses occur in stator = 48.5 kw
(e) Bulk fluid temperature rise through stator = 50°F
(f) Cooling configuration = 60 tubes through frame
3/16 OD by 0.032-in. thick
Single pass, straight through
tube wall 0.020 in. from frame ID

Analysis of this particular configuration results in a potassium film drop of about 1.0°F within the tubes. Thus, the film drops calculated for the various organic fluids may be normalized relative to the potassium coolant for rapid comparison.

The summary results of the analysis are presented in Table 38 for the fluids considered. The mean temperatures shown were selected to bracket the range of likely use temperatures. The property data was obtained for supplier data sheets.

Table 38 shows that a much higher flow rate would have to be used for mineral oil at 200°F than for the other organics. The fluids which appear to be the most attractive with respect to cooling capability are the two polyphenal ethers, 5P4E and 4P3E.

A weighted film temperature drop was used in the alternator parametric screening studies as previously discussed in Section 2.1. This was to permit the alternator temperature calculations to be made independently of any one particular organic fluid. The film temperature drops chosen were based on the analysis and data of Table 38 and are summarized below.

Mean Coolant Temperature, °F	Weighted Film Temperature Drop, T, °F
200	105
400	35
600	26
800	25

The vapor pressure limits the operating fluid temperature in the alternator. This is because the high vapor pressures of the organic fluids at the higher temperatures can impose intolerable rotor windage losses on the rotor cooling system. Consistent with the self-imposed limit of 1-kw windage loss in the rotor cavity (Section 2.1), the emphasis on selection of a fluid must be directed toward one with a low vapor pressure.

An analysis of the windage losses must be made for the various fluids considered to determine what pressure is low enough (or too

TABLE 38

ORGANIC FLUID COOLING CHARACTERISTICS

	Mean Temp., °F	Specific Heat, Btu/16°F	Required Mass Flow, lb/sec	Density, lb/in.^{3}	Viscosity, lb sec/in.^{2}	Thermal Cond., Btu/hr-ft-°F	Reynolds Number	Prandtl Number	Nus Numl
Potassium (reference fluid)	800	0.182	5.05	0.0269	0.2915×10^{-7}	22.65	77100	0.0039	6.
5P4E	600	0.529	1.74	0.0351	1.2×10^{-7}	0.0613	6430	17.3	79.
Polyphenol Ether (Monsanto OS-124)	800	0.593	1.55	0.0318	0.66×10^{-7}	0.0553	10410	11.8	100.
4P3E (Meta) Polyphenol Ether	400	0.465	1.98	0.0377	2.0×10^{-7}	0.0765	4400	20.3	63.
	600	0.530	1.74	0.0346	0.9×10^{-7}	0.075	8600	10.6	82.
Highly Refined Mineral Oil MLO-7277 (Humble 3158)	200	0.521	1.77	0.0303	12.0×10^{-7}	0.075	665	139.5	18.
	400	0.613	1.50	0.0277	1.9×10^{-7}	0.0665	3510	29.3	54.

[1]For Potassium: $N_{Nu} = 0.652(Pc)^4$ - Lubarsky & Kaufman Equation

For Re > 2300, Organic: $N_{Nu} = 0.023(Re)^{0.8}(Pr)^{0.4}$ - Dittus & Boelter Equation

For Re > 2300, Organic: $N_{Nu} = 1.86(Re)^{1/3}(Pr)^{1/3}(D/L)^{1/3}(u/u_s)^{0.14}$ - Sieder & Tate Equatio

$(D/L)^{1/3} = 0.20$ and u_s is based on $Ts = T_{fluid} - 50°F$

high) to achieve acceptable levels of windage losses. As a result, a quantitative comparison was made to illustrate which fluids might be best as well as the problems associated with them.

Various vapor data gathered on the organic fluids is shown on Table 39. The data is incomplete because of the general lack of its availability. The missing data could not be obtained from the original suppliers because vapor viscosity properties are not generally measured by the manufacturers. As a result, kinetic theory of gas relations were employed to calculate the vapor viscosity. That is[10]

$$\eta = 1/3 \; \delta \; \bar{c} l$$

where

δ = density

$\bar{c}$ = mean velocity of molecule

l = length of mean-free path of molecule between molecular collisions

The viscosities calculated are shown in Table 39. The molecular weights used were derived from the basic chemical formulae for the two fluids; that is, $C_{17}\ H_{36}$ for mineral oil and the five-ring structure shown below for 5P4E.

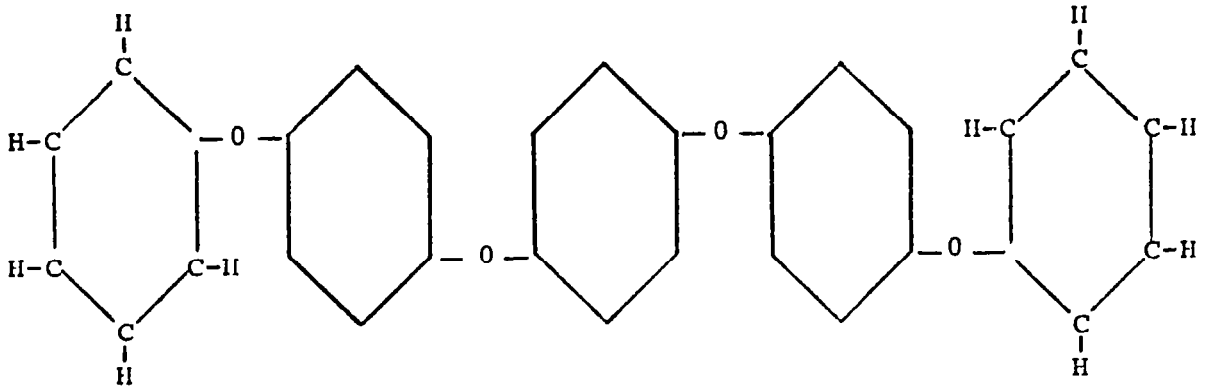

TABLE 39

ORGANIC FLUIDS, VAPOR DATA COMPARISON

Fluid	Temp., °F	Saturated Vapor Pressure, mm Hg	Va
Potassium (reference fluid)	600	0.58	0.
	800	8.8	0.
	1100	124.	0.
5P4E (Monsanto OS-124)	400	0.093	0.
	600	5.1	
	800	98.3	
4P3E (Meta)	400	0.304	
	600	25.4	
Highly Refined Mineral Oil (Humble 3158)	200	0.0023 (a)	
	400	1.91	0.

(a) Extrapolated Data
(b) Calculated, based on molecular weight = 446
(c) Calculated, based on molecular weight = 240

Any analysis of the effects of the various vapor pressures on windage should be viewed as a comparative first approximation, since windage losses are a function of rotor speed and geometry as well as fluid properties. Also, with molecular pump shaft seals and rotor cavity scavenge system, the vapor pressure in the rotor cavity can be reduced to superheated pressures. This has the effect of reducing the windage losses to tolerable levels even though they may be intolerably high for saturated vapor. Of course, this latter statement is predicated on the condition of being able to place enough pumping capacity into the shaft seal configuration. This is usually not possible for potassium vapor pressures much over 10 mm Hg, and the same probably holds true for organic vapors.

Typical windage losses were calculated for mineral oil vapor, and it was estimated that they could be kept less than 1 kw for vapor pressures as high as 0.005 psia. Assuming for purposes of comparison that the other organic fluids would result in losses similar to those for mineral oil, a relationship between maximum allowable vapor pressure and corresponding limiting temperature can be established. This relationship is shown in Table 40 below.

TABLE 40

SATURATED VAPOR TEMPERATURE
(P_{sat} = 0.005 psia = 0.258 mm Hg)

5P4E - Monsanto OS-124	455°F
4P3E - Shell ET 378	390°F
Monsanto MCS 210	380°F
Mineral Oil - Humble 3158	340°F

As seen by the data of Table 40, the fluid which has the lowest vapor pressure or maximum limiting temperature is the 5P4E. However, its maximum limiting temperature is still well below the desired 600°

to 800°F that would be needed if the oil were to be considered a competitive replacement for potassium.

The overall conclusion is that for organic coolant and lubrication alternator rotor, bearing, and shaft seal temperature, levels of 400°F have to be used instead of 600°F or higher, regardless of the thermal capabilities of the fluid, because of windage loss considerations.

The final selection of the fluid to be used is somewhat flexible from the standpoint of the alternator alone; either the mineral oil or the polyphenyl ethers should work. Thus, the choice of which of these must be left to other criteria such as thermal stability or nuclear radiation resistance.

Over the course of 3 to 5 years of alternator life, organic fluids will progressively degrade due to thermal effects and exposure to nuclear radiation. In general, fluid degradation will result in three types of physical change:

(a) Production of volatile decomposition products
(b) Changes in bulk viscosity of the fluid
(c) Formation and precipitation of oil-insoluble sludges

Changes in bulk viscosity will almost always be in the direction of an increase in viscosity, thus causing increased power losses in the bearings.

A large number of investigators have found that the effective fluid life at high temperatures can be increased many fold when oxidation effects are minimized by protection with an inert gas blanket in a closed system. Resistance of oils to radiation damage is also improved by a factor of at least 2 when air is excluded.

Super-refined petroleum oils are primarily straight-chain saturated hydrocarbons. Heat with or without pressure will produce cracking of the hydrocarbon chain. Increased pressure increases the amount of cracking. The products are one molecule of a saturated hydrocarbon and one molecule of an unsaturated hydrocarbon. The number of carbon atoms in each of two products will vary but the total of the two must equal the parent molecule. After several original molecules have broken, there will be a selection of unsaturated molecules of varied chain length available.

For example, a 12 carbon chain will split into molecules containing from one to eleven carbon atoms. The unsaturated hydrocarbon products are reactive and will tend to combine, producing chains of a wide variety of lengths. Thus, two long unsaturated fractions of perhaps 11 carbons would produce a new 22 carbon molecule. This new long molecule may be broken again at another location in the chain to produce additional active fragments. This sequence of reactions produces very short molecules down to the single carbon, saturated structure methane, and chains up to several times as long as the original. The small structures will have high vapor pressure and low viscosity. The heavy products will display high viscosity or will exist as a gummy solid.

The percentage of the various molecular weight products will be dependent upon the previously mentioned environmental factors. Operation at 200°F with low radiation flux and no oxygen or active metal catalyst will not produce any significant cracking. Operation at 400°F will produce some breakdown of the oil as described above. Accurate prediction quantities and molecular weights of the products is not possible since all environmental parameters are not known quantitatively. The weight percent distribution of the aging products of a typical oil may be estimated to be as high as the following:

Approximate Composition	Weight, %	Nature	Sp. Gr. at 77°F
Methane and Hydrogen	0.2	Dissolved gas	Up to 0.4
C_2 to C_8	0.3	Dissolved gas and light oil	0.4 to 0.7
C_9 to C_{20} (Original chain range)	97.5	Useful oil	0.7 to 0.8
C_{20} to C_{60}	2.0	Hard oils and gums	0.8 to 1.5

The original particle size of the high molecular weight gums will be very small but they tend to agglomerate. Pieces as large as several mils in diameter may be formed. These gums will tend to collect on metallic surfaces.

Polyphenyl ethers are cyclic molecules joined by oxygen atoms in an ether linkage. The cyclic or ring structure is much more resistant to heat and radiation than the straight chain petroleum molecules. The most significant change in performance characteristics is a reduction in fluid viscosity resulting from failure of the ether linkage. Typical specific gravity values at room temperature will be decreased by 800°F aging from 1.204 to perhaps 1.1. The 800°F values will decrease from 0.88 to about 0.8. Operation at 600°F will be much less severe but accurate estimation of fluid operating life is not feasible. Expectation of any long extended service life even at 600°F would be overly optimistic.

2.5.2 Organic Coolant Temperature Excursion Study

The objective of the organic coolant temperature excursion study was to determine if any specific design improvements could be attained

by operating at a coolant temperature other than 400°F. The coolant temperatures chosen for investigation were 200°, 400°, and 600°F.

The organic coolant-temperature excursion study results for the three coolant temperatures are presented in Table 41. The study was performed using the recommended frequency/speed/rotor material combination from the 400°F parametric studies. This combination was 1600 Hz, 24,000 rpm, and H-11 rotor material.

The temperature excursion had slight effects on generator design for constant frequency, speed, and rotor material. In general, generator weight increased slightly and generator efficiently decreased slightly with increasing coolant temperature. A 32,000-rpm generator design was made at the 200°F coolant temperature to determine any design advantages that might occur for the higher speed design. At this higher speed, the expected significant reduction in generator weight results; however, rotor stress slightly exceeded the established stress limit of the H-11 rotor material. The armature hot-spot temperature and rotor-radial temperature differences are larger because the required slot combination caused higher pole-face losses.

It was not considered necessary to evaluate a rotor material magnetically superior to H-11 at 200°F because of the results of the comparative evaluation made between Hiperco-27 alloy and H-11 in the 400°F parametric speed study and the results of the H-11, 32,000-rpm design discussed above. The 400°F parametric speed study showed that the amount the rotor diameter can be reduced to save weight and reduce stress at a given speed (24,000 rpm in the case of the 400°F speed studies) by using Hiperco-27, a superior magnetic material, is limited by stator design requirements. The same limitation applies to the 19,200-rpm designs. The design data presented in Table 48 Section 3 shows that the Hiperco-27, 19,200-rpm design (No. 3) is overstressed while the H-11 design (No. 4) is not. The allowable material stress

TABLE 41

ORGANIC COOLANT TEMPERATURE EXCURSION STUDY

Coolant	Average Coolant Temp., °F	Frequency, Hz	RPM	Elect. Weight, lb	Efficiency, %	Voltage Unbalance, %	Poles	Ar Hc Ten
Mineral Oil	200	1600	24,000	640	92.0	7.01	8	
Mineral Oil	200	1600	32,000	528	91.8	8.93	6	
Mineral Oil	400	1600	24,000	643	91.8	7.09	8	
Polyphenyl Ether	600	1600	24,000	684	91.8	7.67	8	

of Hiperco-27 at the 200°F coolant condition is only increased to approximately 57,000 from 55,000 psi. It is apparent from review of all the design data at 400°F that the stator size with 200°F coolant could not be reduced enough to permit reduction of rotor stress (by reducing rotor diameter) to much less than the 56,000-psi stress level of Design No. 3 without a significant penalty in efficiency. Thus the 200°F Hiperco-27 design would retain a marginal rotor design stress and only produce a weight saving over the H-11 design of slightly more than 15 lb, efficiencies remaining the same. Finally, since the 200°F, H-11 design is overstressed at 32,000 rpm, it is obvious that a 200°F Hiperco-27 rotor would be overstressed at 32,000 rpm.

The temperature excursion study plus the designs at 800° and 1100°F for potassium design provided data for an overall view of alternator weight and efficiency as a function of temperature. These data are plotted on Figure 41 and illustrate the increasing weight and decreasing efficiency trends that accompany increasing coolant temperature. The 1100°F efficiency is misrepresentatively high because the windage losses were excluded from the total electrical losses. Because these trends shown are contradictory to the decreasing weight of the cooling radiator as temperature increases, the system designer must evaluate the trade-off between the two (radiator versus alternator) to arrive at a coolant temperature giving their lowest combined weight.

2.6 Parametric Shaft Seal Studies

Analytical, parametric-type studies were performed to determine the performance of nonrubbing, screw-type seals for application in the KTA turbine and alternator. The results of these studies were used to compare the performance of the screw-type seals to other types, such as slinger, so that the type to be used in the KTA could be selected. As a result of this comparison, AiResearch selected the screw-type seals. The parametric performance data obtained in the study was then used to design the seals for the conceptual designs.

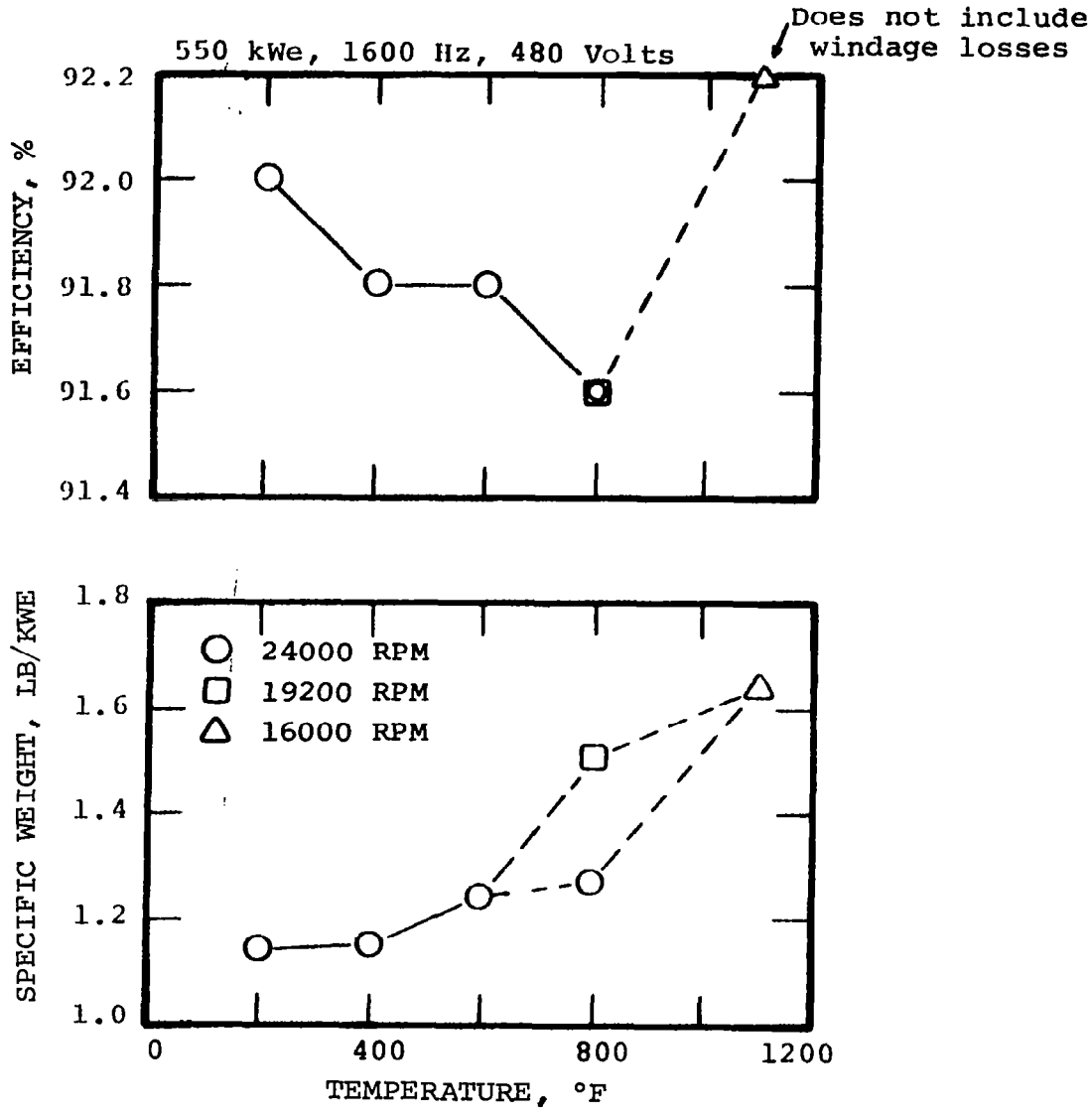

WEIGHT AND EFFICIENCY VERSUS COOLANT TEMPERATURE

FIGURE 41

These seals consist of two types: (1) hydrodynamic, nonrubbing, screw-type liquid shaft seals, called viscoseals, and (2) Holweck-type molecular pump vapor shaft seals. In the alternator, the viscoseal is used to seal the liquid-bearing lubricant in the bearing compartments from the rotor cavity. The Holweck vapor shaft seal is part of the rotor scavenging system and is used to reduce the pressure (and density) of the bearing lubricant vapor in the rotor cavity to minimize windage losses.

Separate studies were performed for the viscoseal and for the Holweck pump vapor shaft seal. These studies are the subject of the following sections.

2.6.1 Viscoseal Parametric Study

Viscoseal liquid shaft seal parametric studies were performed for 800° and 1100°F potassium, 400°F highly refined mineral oil, and 800°F polyphenyl ether. The basis for the study is summarized in Table 42. Performance results are summarized in Tables 43 and 44. For a more detailed discussion of the study, see Appendix B of this report.

2.6.2 Holweck Pump Vapor Shaft Seal Parametric Studies

The Holweck pump vapor shaft seal parametric studies were performed in two steps:

(a) Determination of the best thread configuration for three different stub shaft diameters based on an assumed constant fluid state. The constant fluid state was 800°F saturated potassium vapor corresponding to the fluid state at the low pressure side of the viscoseal. This analysis was applicable to the organic fluids being considered because they have vapor pressures of approximately the same order of magnitude in the 400° to 600°F range.

TABLE 42

VISCOSEAL PARAMETRIC STUDY PARAMETER RANGE

FLUIDS AND TEMPERATURES - Potassium at 800°, 1100°F, Highly Refined Mineral Oil at 400°F, Polyphenyl Ether (5P4E) at 800°F
SEAL DIAMETERS - 2.0, 3.0, and 4.0 in.
SEAL SPEEDS (ALTERNATOR DESIGN SPEEDS) - 16,000 to 32,000 rpm
MAXIMUM PRESSURE DIFFERENTIAL - 25 psi (Potassium) - 50 psi (Organics)
RADIAL CLEARANCE - 0.3 percent of seal diameter
DOUBLE HELICAL GROOVE THREAD GEOMETRY

TABLE 43

VISCOSEAL PARAMETRIC STUDY LENGTH OF SEALS

Design Speed, rpm	Seal Length, In.					
	400°F Mineral Oil			800°F Potassium		
	Seal Diameter, in.			Seal Diameter, in.		
	2.0	3.0	4.0	2.0	3.0	4.0
19,200	2.2	1.5	1.12	2.56	1.68	1.26
24,000	1.41	0.95	0.71	1.60	1.07	0.8

ΔP = 25 psi

- o Complete sealing of liquids at 50 percent of the alternator design speed.
- o Wetted length of seal at 50 percent speed equals 60 percent of the overall length of the seal. The remaining 40 percent of the seal length is required for dams at the ends of the threads and for scavenge of liquid which may break away from the interface.

TABLE 44

VISCOSEAL PARAMETRIC STUDY POWER CONSUMPTION

Speed, rpm	Power, w					
	400°F Mineral Oil			800°F Potassium		
	Seal Diameter, in.			Seal Diameter, in.		
	2.0	3.0	4.0	2.0	3.0	4.0
19,200	280	660	1235	140	335	615
24,000	320	750	1390	160	380	770

ΔP = 25 psi

(b) Determination of the performance of the selected thread configurations from Step a with and without multiple stages. Performance was determined for 800° and 1100°F potassium and for 400°F mineral oil.

The basis and the results of the first step of the study is summarized in Table 45.

The results of the second step of the study is summarized in Table 46. The entire study is discussed more thoroughly and in more detail in Appendix C.

TABLE 45

HOLWECK PUMP VAPOR SEAL PARAMETRIC STUDY PARAMETER RANGE

VAPORS AND TEMPERATURES - Saturated Potassium at 600° to 1100°F, 800°F specific

SPEEDS - 16,000, 20,000, 24,000, 32,000 rpm

CONFIGURATIONS - Stack over viscoseal and each other (nested)

Diameters, in.	3.5	4.5	5.5
Radial Cl., in.	0.006	0.009	0.012
Length, in.	1.75	2.25	2.75

OPTIMIZED THREADS - Based on 800°F Potassium Vapor, 24,000 ±8000 rpm

Two parallel threads on housing
Approximately 2-1/2-deg pitch angle
Root width to depth = 1.5
Root width to land width = 1.0
Root depth to clearance = 10 to 12.5

TABLE 46

HOLWECK PUMP STAGING AND WINDAGE POWER LOSS

Stages/Design	19,200 rpm, 800°F Potassium		19,200 rpm, 400°F Mineral Oil		24,000
	Rotor Cavity Pressure	Power Loss, w	Rotor Cavity Pressure	Power Loss, w	Rotor C Press
0 - Viscoseal	0.155[a]	2850	0.036[f]	5050	0.15
1 - 3.5-in. diameter	0.079[b]	1550	0.003[b]	420	0.06
2 - 4.5-in. diameter	0.040[c]	830	0.00003[c]	0	0.02
3 - 5.5-in. diameter	0.00465[d]	112			0.00
4 - 5.5-in. diameter	0.00005[e]	1			

a - Saturation pressure of potassium at 800°F
b - Rotor cavity pressure with a single-stage molecular pump
c - Rotor cavity pressure with a two-stage molecular pump
d - Rotor cavity pressure with a three-stage molecular pump
e - Rotor cavity pressure with a four-stage molecular pump
f - Saturation pressure of mineral oil at 400°F

3. ALTERNATOR BASE DESIGNS

With the completion of the parametric screening studies and as a result of design study review meetings with AiResearch, three alternator design coolant/speed/frequency configurations were selected for the Phase I preliminary alternator designs. These constituted the three Phase I base designs.

Preliminary realistic designs were needed during the Phase I design studies prior to the definition of the conceptual designs (which were to be the result of the Phase I studies). The base designs were needed to:

(a) Complete the alternator conceptual design studies using realistic configurations; this was to avoid doing nonessential academic analyses or an excessive number of analyses that would be required if all possible KTA alternator design configurations were considered. See Section 4.1 for explanation of these analyses.

(b) To permit AiResearch to carry out the bearing selection, bearing design, and rotor dynamic analyses at realistic conditions.

(c) To permit AiResearch to carry out the KTA integration and shaft bearing arrangement studies using realistic alternator configurations.

The base designs were selected from the groups of preferred configurations determined in the course of the parametric screening studies. These preferred configurations are summarized in Tables 47 and 48.

TABLE 47

SUMMARY OF 800° AND 1100°F ALTERNATOR DESIGNS

Coolant Temp., °F	800					1100			
Order of EM Design Preference	1	2	3	4	5	1	2	3	4
Speed, rpm	24,000	30,000	24,000	19,200	20,000	30,000	24,000	24,000	19,20
Frequency, Hz	1,600	2,000	2,000	1,600	2,000	2,000	1,600	2,000	1,60
No. of Poles	8	8	10	10	12	8	8	10	1
Weight, lb	701	566	676	844	761	622	770	749	93
Efficiency, %	91.6	90.4	90.6	91.7	91.0	92.4	92.7	92.3	92.
Conductors per Slot	2	2	2	2	4	2	2	2	
Voltage Unbalance, %	7.78	8.32	7.32	6.77	5.78	8.16	7.68	7.07	6.5
Rotor Radial ΔT, °F	95[1]	106	50	45	383	231[3]	242	107	9
Stator Hot Spot, °F	1189	1203	1157	1161	1148	1438	1434	1413	141
Rotor Weight, lb	274	214	275	353	336	287	368	368	47
Rotor Material	H-11 R_C45					1BS1			
Allowable Stress, ksi	97[2]					71			
Stress Type	0.5% Creep					Yield			
Max. Von Mises Stress Under Pole, ksi	90.2	127	89	62.8	70.6				8
Safety Factor	1.075	0.764	>1.0	1.545	1.372	<1.0	<1.0	<1.0	0.86
Order of Overall Preference	3	Not Acceptable	4	1	2	Not Acceptable			

[1] Values less than approximately 150°F indicate that the rotor can be of a one-piece, slotted-pole c coolant passages extending into the pole.
[2] Yield stress 99,000 psi.
[3] Values less than approximately 200°F indicate that the rotor can be of a one-piece, slotted-pole c coolant passages extending into the pole.

TABLE 48

SUMMARY OF 400°F ALTERNATOR DESIGNS

Coolant Temp., °F	← 400					
Order of EM Design Preference	1	2	3	4	5	6
Speed, rpm	24,000	24,000	19,200	19,200	30,000	32,000
Frequency, Hz	1,600	1,600	1,600	1,600	2,000	1,600
No. of Poles	8	8	10	10	8	6
Weight, lb	643	626	762	777	505	533
Efficiency, %	91.8	91.6	91.7	91.7	90.7	91.0
Conductors per Slot	2	2	2	2	2	2
Voltage Unbalance, %	7.09	7.97	6.42	6.23	7.58	9.00
Rotor Radial ΔT, °F	95*	39	26	44	107	356
Stator Hot Spot, °F	943	928	853	862	975	1108
Rotor Weight, lb	235	207	290	305	182	180
Rotor Material	H-11	Hiperco 27	Hiperco 27	H-11	H-11	H-11
Allowable Stress, ksi	118	55.5	55.5	118	118	118
Stress Type	← Yield					
Max. Von Mises Stress Under Pole, ksi	84.7		56.0		119.0	139.5
Safety Factor	1.395	<1.0	0.991	<1.0	0.990	0.845
Order of Overall Preference	1	Not Acceptable	Marginal	2	Marginal	Not Acceptable

*Values less than approximately 550°F for H-11 or 400°F for Hiperco 27 indicates that a one-pi
construction configuration without coolant passages directed up into the poles might be possi
This does not mean that rotor coolant passages can be eliminated from the rotor entirely. Wi
organic-coolant passage arrangement, the design of 400°F organic-coolant passage will be cons
difficult than potassium coolant design because of problems introduced by use of organic cool

Table 47 contains a summary of the alternator designs for coolant temperatures of 800° and 1100°F. In the first column, the order of electromagnetic preference is stated. The data substantiating these preferences for 800° and 1100°F coolant temperature is discussed in the previous section on parametric screening. Shown also in the table are the rotor material, the allowable stress, and the type of limiting stress for each design. The most crucial stress occurs under the rotor pole and is a biaxial stress that is related to the uniaxial material stress properties by the equivalent (or Von Mises) stress at the center of the base of the pole. This equivalent stress is shown in Table 47 along with a safety factor defined as the ratio of allowable to Von Mises stress. A rotor design is unacceptable when this safety factor drops below unity. Shown in the last column of the table is the order of overall preference among the alternator designs for both 800° and 1100°F coolant temperatures.

At a coolant temperature of 800°F, there is no acceptable configuration at 30,000 rpm or above. The 19,200-rpm configuration is preferred over the 20,000 because the latter requires four conductors per slot as previously discussed. Both 24,000-rpm designs are acceptable in third and fourth preference but are nearly stress limited. If the coolant temperature were reduced to 600°F, the 24,000-rpm, 1600-Hz design would become the first preference both from a standpoint of electrical design and stress.

At a coolant temperature of 1100°F only two configurations are acceptable on the basis of pole center plane stress; namely, the 17,143- and the 16,000-rpm configurations. Both of these configurations require four conductors per slot with all the attendant undesirable features previously described.

As pointed out above in the 400°F coolant studies, four speed studies were required to consider both candidate rotor materials, i.e., Hiperco-27 and premium quality H-11 at frequencies of 1600 and 2000 Hz. As seen in Table 48, the results show that the preferred combination of speed, frequency and rotor material for the 400°F coolant temperature (based on generator electromagnetic design considerations and minimum system weight with an assumed system specific weight of 100 lb/kw) is 24,000 rpm at a frequency of 1600 Hz for either H-11 or Hiperco-27 rotor alloy. The first alternate choice is 19,200 rpm at a frequency of 1600 Hz with either a Hiperco-27 or H-11 rotor material. The Hiperco-27 generator design is slightly lighter (15 lb) but does not have as large of stress safety factor as does the H-11 design. The second alternate choice is 30,000-rpm, 2000-Hz, H-11 rotor material and the third alternate choice is 32,000-rpm, 1600-Hz, H-11 rotor material. The 30,000-rpm, 2000-Hz, Hiperco-27 rotor material design is obviously overstressed and, therefore, was excluded from electrical-mechanical design preference consideration. The 16,000-, 17,143-, and 20,000-rpm designs have the less desirable four conductors per slot.

The Base Designs were selected as a result of a combined NASA/AiResearch/Westinghouse meeting at which the various alternative parametric designs were reviewed. The first design selected was for the 800°F potassium coolant and was the 19,200-rpm/1600-Hz design. This design had a speed compatible with the desired turbine speed, had the desired two conductors per slot configuration, and resulted in conservatively low rotor stress.

The second base design selected was for an organic fluid cooled/lubricated alternator. The parametric design with the highest order of preference was the 24,000-rpm, 1600-Hz, H-11 rotor design as shown in Table 48. However, 24,000 rpm was an unacceptable speed for the organic lubricated turbine; therefore, the parametric alternator design of next highest preference - the 19,200-rpm, 1600-Hz, H-11 rotor design - was selected.

The choice of the third base design was more difficult because there appeared to be no good designs at the 1100°F potassium coolant condition. The main problem was lack of a good rotor material for service at the 1100°F rotor coolant condition. After considering such alternatives as a design with 1100°F potassium or NaK-cooled stator and a lower temperature (600° to 800°F) for the rotor coolant, AiResearch and NASA jointly elected to eliminate the 1100°F coolant condition. This was primarily because of long term development problems associated with (a) obtaining a good rotor material for 1100°F potassium rotor coolant and (b) design of a satisfactory rotor cavity scavenging system (since Holweck pump vapor seals are not effective for 1100°F bearing and rotor coolant condition) to reduce windage losses to an acceptable level. (See Section 2.6.2 and Appendix C, Holweck Pump Vapor Seal Parametric Design Study.) Instead, the second alternate (third order of preference) 800°F potassium-cooled, 24,000-rpm, 1600-Hz, H-11 rotor material parametric design in Table 47 was selected. This design speed offered advantages to the potassium lubricated turbine design, and although it was recognized that the design might be marginal in rotor creep, it was anticipated that with design refinements in succeeding KTA phases, the design could be improved. This offered immediate potential benefits to the KTA component as opposed to long term benefit to the overall system designer offered by the 1100°F coolant condition.

Possible intermediate temperatures between 800° and 1100°F were not considered as discussed in Section 2.3.

The three base design conditions selected are summarized in Table 49 and are hereafter identified as Design No. 1, 2, or 3.

TABLE 49

BASE DESIGN IDENTIFICATION

No. 1	800°F Coolant, Alkali Metal (NaK or K) 19,200 rpm 1600 Hz 480 v (L-N)
No. 2	400°F Coolant, Highly Refined Mineral Oil 19,200 rpm 1600 Hz 480 v (L-N)
No. 3	800°F Coolant, Nak or K 24,000 rpm 1600 Hz 480 v (L-N)

The detail design aspects of these three designs are discussed in the following section on conceptual designs.

4. CONCEPTUAL DESIGN ANALYSES

4.1 Introduction

There are certain aspects of the computer design analyses used in the parametric screening studies which, for the sake of either expediency or design flexibility, are first approximations. They may be used as first approximations because they have secondary influence on optimizing the basic electromagnetic design. The main areas concerned and the rationale for their being first approximations are summarized below:

(a) Rotor Stress - First approximation determines the average tangential stress in the core and the pole root radial stress to indicate magnitude of stress levels. Final stress calculations are dependent upon cooling configuration, stress concentrations and thermal gradients; these items are subject to too many influences to permit practical application to generalized computer design program.

(b) Rotor Cooling Configuration and Temperature - First approximation determines preselected point temperatures based on three alternative cooling configurations and recommends which is best, based on maximum allowable pole tip temperature and coolant temperature. Final design selection and analyses subject to external and nonprogrammed influences (e.g., fabrication requirements) that require separate consideration.

(c) Pole Face Losses - Program size limitations require the generator design program use a first approximation of a more elaborate program that calculates pole face losses in detail.

(d) Windage Losses - First approximation uses input data that does not recognize loss reductions possible with "super-heating" the vapor nor does it account for anything more than estimated geometry influences. It is a simple matter to calculate these losses separately once electromagnetic design and shaft seal designs are determined.

(e) Stator Cooling Configuration and Temperature - Because of program size limits, first approximation uses coarse nodal grid to determine temperature distributions based on a fixed heat-sink design. Final temperatures must be recalculated on finer nodal grid once actual cooling configuration is selected.

(f) Stator (Structural) Stresses - Too many influences to permit programming into a generalized design program of practical size.

It is the purpose of the present section, Conceptual Design Analyses, to present these separate studies and the results derived from them with one exception; that is, the rotor stress results already presented in Section 2.4. The discussions are segregated into two areas, Rotor Studies and Stator Studies.

4.2 Rotor Studies

The basic purposes of the rotor studies were to examine the alternatives available for reducing the rotor losses (windage and pole-face), to evaluate the type of cooling configurations that may be required or are best suited to the design and losses, and to make recommendations for the final conceptual design. The goal was to determine the electromagnetic configuration giving sufficiently low losses to minimize the cooling configuration complexities. Both the

electromagnetic and cooling configurations were to be consistent with achieving a highly reliable design requiring the least development.

4.2.1 Rotor Cooling Concepts

The basic design philosophy associated with the KTA alternator rotor cooling was to minimize the losses so that, for a given coolant temperature and maximum allowable pole tip temperature, the concepts required would be consistent with least complex configurations having inherently high reliability. One of the least complex configurations is a solid rotor with the stub shaft surface area in the bearing cavity acting as the heat-sink. A slightly more reliable configuration that is almost as simple is a central coolant hole bored through the center of the rotor. The latter is a more effective cooling configuration that can be easily simulated with an accurate analytical design model. It does not require separate rotor flow; it can use bearing flow and will pump at its own desired coolant flow rate by taking rotational energy from the rotor. Rotor reliability is enhanced by the central coolant hole because the center of the rotor, where inclusions could occur, is removed; this hole is needed to obtain uniform hardness in the core during heat treatment.

Other possible rotor coolant path configurations that are more complex include (1) individual, parallel paths (small coolant holes) through the core and/or poles, (2) radial conducting rods in the core and/or poles, and (3) heat pipe configurations. The individual, parallel coolant holes are a very effective cooling sink but suffer from fabrication complexities required to plug the ends of the drilled passages. They also suffer from operating reliability due to centrifuging of solids in the outer passages. The design must accommodate these solids as they accumulate. The radial conducting rods add fabrication complexities but do not add much to cooling effectivness[16]. The heat pipe concept, as presented in the originally proposed KTA alternator, is a very effective cooling concept but is inconsistent

with the "ease of development" design philosophy, especially in light of the fact that a very effective cooling configuration was not needed in the KTA alternator. The radial conduction rods and heat pipe concepts were not analyzed in the KTA alternator.

The analyses were done on typical KTA configurations - Base Designs No. 1 and 2, Section 3 - and the results were normalized to degrees Fahrenheit temperature drop per unit loss in watts. The temperature drop was that in going from the pole tips to the rotor coolant. A summary of the normalized gradients is presented in Table 50 for each of the cooling configurations considered. With these normalized temperature gradients, it was possible to compare the multitude of watts loss, coolant temperature, and limiting temperature combinations of the studies and draw conclusions on applicability.

4.2.2 Pole Face Loss Minimization Studies

The designer of the alternator must cope with the problem of reducing the rotor pole face losses that are produced by the time dependent component of induction in the face of the poles. There are two sources of induction from the stator which are time dependent relative to a reference point in the rotor pole. The first source is produced by the teeth and slots in the armature. At one instant, a point on the pole face is under a tooth where the flux density is a maximum and at the next instant of time this point is under a slot where the flux density is a minimum. This varying flux produces EMFs which, in turn, produce eddy-current losses. The varying flux also produces minor hysteresis loops within the pole face, causing a further loss of energy. The second source of time-dependent induction results from harmonic MMFs associated with the armature windings.

Certain internal design variables can be varied to reduce the pole face losses. Those which have a significant influence on the losses are the radial gap, the ratio of the width of the slot opening

TABLE 50

ROTOR COOLING CONCEPTS SUMMARY

Configuration	Coolant, °F	°F/w	Maximum Allowable Pole Face Limit* Losses for 900°F Tip Temperature, w
Stub shaft	800°-Potassium	---	---
	400°-Mineral Oil	1.13	442
Central hole	800°-Potassium	0.181	553
	400°-Mineral Oil	0.210	2380
Parallel Passages through core	800°-Potassium	0.0627	1600
	400°-Mineral Oil	0.0801	6250
Parallel Passages extending into pole bodies	800°-Potassium	0.0181	5530
	400°-Mineral Oil	---	---

*Neglects windage losses and heat carry over to or from the stator components.

to the tooth pitch*, pole pitch, and the direct axis synchronous reactance of the machine. Most of these were evaluated as part of the internal variables parametric screening studies. In general, the parameters can be varied to reduce the amplitude of flux density variations on the surface of the pole face.

However, performance penalties can be incurred in the overall design when these parameters are optimized only from the standpoint of pole face losses. One is, therefore, obliged to consider other means which will also reduce the pole face losses.

It is generally true that the materials which offer the best high temperature/strength properties for a rotor have inferior magnetic properties from the standpoint of the reduction of pole face losses. For example, the pole face losses in NIVCO alloys will be two- to three-fold greater than the losses in H-11 steel, which are approximately eight- to ten-fold greater than the losses in a CUBEX magnetic alloy. In some cases, the superior creep strength property offered by a rotor material is offset by the additional heat and temperature rise produced by the higher pole face losses.

The most promising solution to this dilemma is to use a pole material which offers excellent properties for the reduction of losses in conjunction with a core material that offers the required creep strength for the highly stressed portion of the rotor. A material of much lower creep strength can be used on the pole tips since the stress is small near the surface of the pole face. In addition, the creep strain may be allowed to approach 1 to 1.5 percent since the length of the pole piece will be small, whereas a creep strain of 0.5 percent for other parts of the rotor could be considered excessive,

*Special slot configurations to reduce pole face losses are presently a standard part of the inductor alternator design at Westinghouse Aerospace Electrical Division.

since this amount of strain can cause a large change of the radial gap in the alternator.

Further reduction of pole face losses can be obtained with laminated pole tips. Eddy-current losses can be decreased approximately two-fold due to the increase of effective resistance offered by laminations when compared with the effective resistance of grooved pole faces. Grooving the pole face increases the effective resistance of the eddy-current path approximately two to three-fold, which can decrease the pole face losses approximately 40 percent when compared with a solid pole face.

Only one of these three techniques was considered for reduction of pole face losses during the parametric screening studies. This technique consisted of slotting the pole faces with grooves at right angles to the rotor longitudinal centerline. The grooves were 0.006-in. wide by 0.10-in. deep at a slot pitch of about 30 grooves/in. With the grooves, the resistance of the eddy-current path was increased by a factor of 3.8 when compared with the resistance of a solid pole face. Unfortunately, the H-11 material, which offers superior dc magnetic and strength properties for the rotor, has a very low magnetic permeability when it is subjected to a time-varying induction. Pole-face losses are primarily a function of $(\rho\mu)^{-1/2}$, where ρ equals the effective resistivity along the eddy-current path and μ equals the effective permeability of the material when a time-varying induction is imposed upon the steady induction. A comparison of the properties of interest for H-11 steel to a steel which offers superior properties is given in Tables 51 and 52.

It can be noted from the tables that the resistivity of the two materials are about the same magnitude. However, a comparison of the effective permeability of the material shows that the silicon steel is a much better material from the standpoint of pole-face losses. For example, if one considers the 800°F, 19,200-rpm base design, the

TABLE 51

RESISTIVITY
(microhms-cm)

Property	H-11 Steel	Nongrain-oriented 4-1/4% Silicon Steel
Bulk material	78.7	108
Effective resistivity of slotted poles	304	416
Effective resistivity of laminated pole piece, 0.010-in. sheet x 0.25 depth	566	778

TABLE 52

EFFECTIVE PERMEABILITY
(cgs)

Steady Induction = 8.75 kG		
Amplitude of Time Varying Induction on Surface of Pole Face, G	H-11 Steel	Nongrain-oriented 4-1/4% Silicon Steel
0	1.8	350
130	7.1	520
182	8.1	580
242	9.0	642
394	11.0	739
578	12.8	803
802	14.7	885

amplitude of the time-varying induction due to stator teeth is approximately 182 gauss, which means that the effective permeability of the silicon steel would be 71.5 times greater than the effective permeability for H-11 steel. If we also consider a laminated, silicon steel pole tip construction in place of a grooved H-11 steel pole face, the relative pole-face losses become approximately equal to

$$\frac{\text{Loss (laminated Silicon steel)}}{\text{Loss (grooves H-11 steel)}} = \left(\frac{304}{778}\,\frac{8.1}{580}\right)^{1/2} = \frac{1}{13.53} = 0.0739$$

For the example above, the pole face loss due to flux ripple produced by the stator teeth can be reduced by a factor of about 13.5 by using the silicon steel in a laminated construction.

The several techniques for reducing pole face losses that were investigated are summarized for each of the alternator base designs in Table 53. The techniques investigated included (1) grooved pole tips of H-11 steel, (2) laminated pole tip of 4 1/4 percent silicon steel, and (3) laminated pole tip of 3 1/4 percent silicon, grain-oriented steel. The losses for each of these designs was compared with the losses associated with a solid pole tip of H-11 steel. In general, the pole-face losses with a solid pole tip were approximately 1.5 times greater than the losses associated with grooved pole tips and approximately 23 to 37 times greater than the losses associated with a laminated pole tip construction.

The use of a laminated pole tip construction greatly simplifies the required rotor cooling system. In order to indicate the cooling features required for each of the designs, the temperature drop required to conduct the losses through the body of the pole and from the pole face to a central passage on the axis of rotation is given in the table. With the pole face limited to a maximum hot-spot temperature of 950° and with 800°F coolant, the following conclusions can be made:

TABLE 53

POLE FACE LOSS REDUCTION STUDY

Reference Design Speed, rpm Coolant Temp., °F	No. 1 19,200 800	No. 2 19,200 400	No. 3 24,000 800	Pole Tip Configuration
Estimated Losses, Excluding Pole Face Losses, kw	49.4	48.8	49.9	
Efficiency, Excluding Pole Face Losses, 550.00-kw output, %	91.8	91.8	91.8	
Pole Face Losses per Unit Area, w/in.^{2}	18.5	17.4	40.6	Solid pole tips of H-11 steel
Pole Face Losses, kw	2.71	2.28	4.89	
Efficiency, including pole face losses, %	91.3	91.5	90.9	
Temperature drop required to conduct losses from pole faces and into rotor core, °F	170	160	363	
Temperature drop required to conduct losses from pole faces to a central passage 1/2 in. dia, °F	490	480	952	
Pole Face Losses Per Unit Area, w/in.^{2}	11.9	11.2	26.0	Grooved pole tips, 0.006 in. wide by 0.10 in. deep with 29.4 grooves/in.
Pole Face Losses, kw	1.74	1.46	3.14	
Efficiency, including pole face losses, %	91.5	91.6	91.2	
Temperature drop required to conduct losses from pole faces and into rotor core, °F	109	103	233	
Temperature drop required to conduct losses from pole faces to a central passage 1/2 in. dia, °F	315	308	611	
Pole Face Losses per Unit Area, w/in.^{2}	0.814	0.770	1.712	Laminated pole tips, 4.25% silicon steel, nongrain-oriented, depth of laminations = 0.5 in. thickness = 0.010 in.
Pole Face Losses, kw	0.119	0.101	0.206	
Efficiency, including pole face losses, %	91.7	91.8	91.6	
Temperature drop required to conduct losses from pole faces and into rotor core, °F	7.4	7.1	15.3	
Temperature drop required to conduct losses from pole faces to a central passage 1/2 in. dia, °F	21.5	21.3	40.2	
Pole Face Losses per Unit Area, w/in.^{2}	0.518	0.490	1.086	Laminated pole tips, 3.25% silicon steel, grain-oriented, depth of laminations = 0.5 in. thickness = 0.010 in.
Pole Face Losses, kw	0.076	0.064	0.131	
Efficiency, including pole face losses, %	91.7	91.8	91.7	
Temperature drop required to conduct losses from pole faces and into rotor core, °F	4.8	4.5	9.7	
Temperature drop required to conduct losses from pole faces to a central passage 1/2 in. dia, °F	13.7	13.5	25.5	

(a) A solid pole face of H-11 steel will require coolant passage within the body of each pole.

(b) A grooved pole face of H-11 steel will require a coolant passage through the rotor core near the base of each pole.

(c) A rotor with a laminated pole tip construction can be cooled by using a central passage on the axis of the rotor.*

(d) A detail study of the rotor cooling scheme for very low losses may demonstrate that it will be possible to cool the rotor through the shaft extensions, thereby eliminating the need for any coolant passages within the rotor.*

In addition, Table 53 shows improvements in efficiency obtained by using laminated pole tips. Although the actual improvements in efficiency are small, these differences may have more important significance when evaluated in terms of system weight penalty.

The concept proposed for the laminated pole tips is shown on Figure 42. The laminations are assembled into bundles by a stitch-weld through several layers. Steel shim spacers, about 0.002 in. thick, act as interlaminar insulation between the SiFe laminations. They are recessed below the depth of penetration of the time-varying flux (about 0.10 in.). The thickness of bundle is determined by the penetration capabilities of the weld used, e.g., electron beam welder. The height is about 3/8 in. and changes with each bundle. The steps shown on the H-11 pole provide beam clearance for the bonding of each lamination bundle to the pole. Assuming a pole length of 3 in. and

*Based on negligible windage losses.

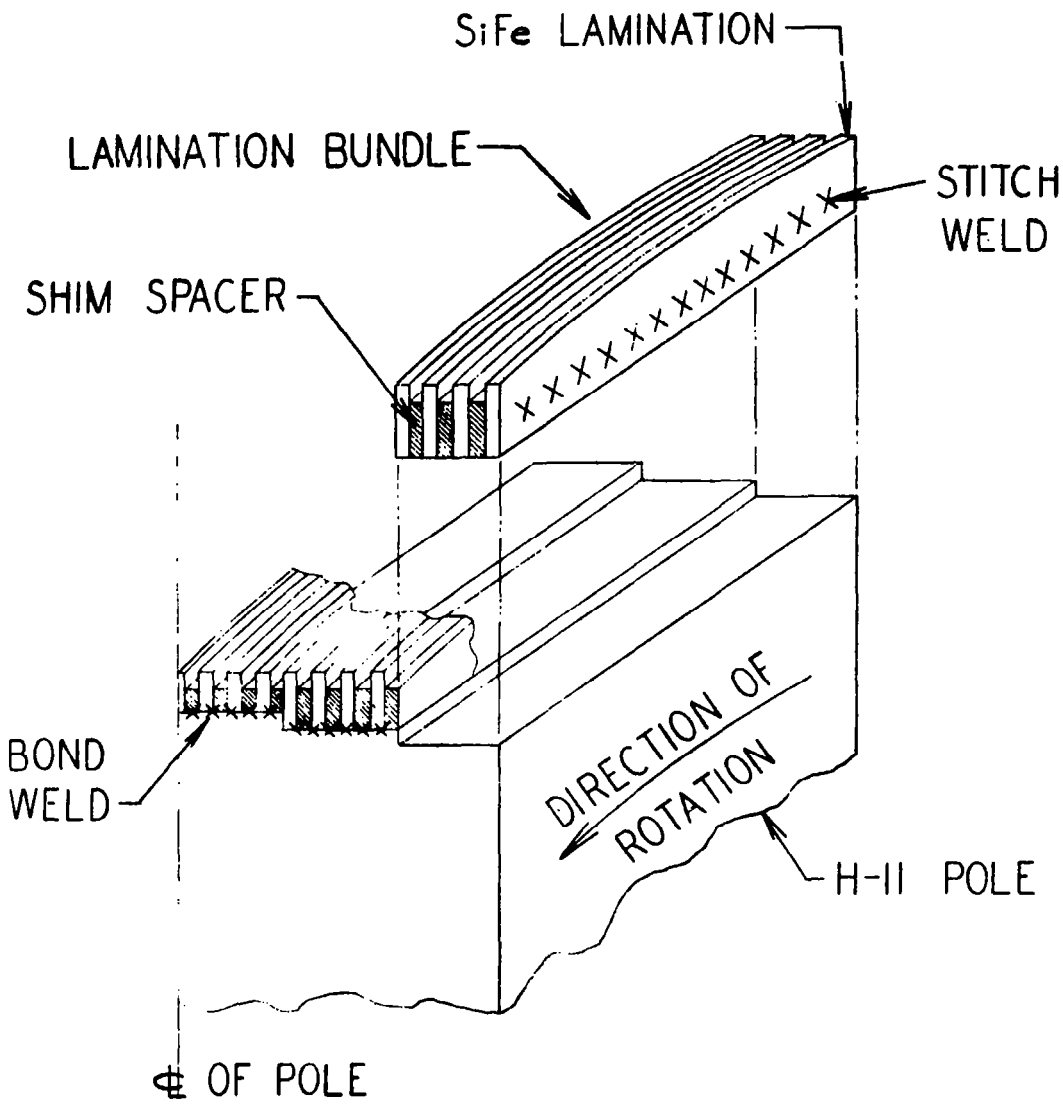

LAMINATED POLE CONCEPT

FIGURE 42

an electron beam (E.B.) weld penetration of 3/4 in., only one step would be needed if the top step were started on the centerline shown. For a 4-in.-pole length and 1/2-in.-beam penetration, three steps would be needed.

4.2.3 Windage Loss Calculations

As previously stated in Section 2.1, a self-imposed limit was placed on the windage losses that could be permitted in the rotor cavity. This was to maintain uncomplicated rotor cooling configurations, thereby improving reliability, not to improve alternator efficiency (even though some modest gains can be achieved as a result). Initially, the limit imposed was 1 kw based on past experience with the SNAP-50/SPUR alternator and the realization that the 800°F minimum potassium coolant temperature would make it more difficult to minimize windage losses. As the study progressed, however, it became apparent that a limit of a few hundred watts was much more desirable and just as feasible (based on windage loss minimization studies and the Holweck pump vapor seal studies). Therefore, this latter reduced limit became the goal of the conceptual design studies. The assumption was used that the windage losses end up in the rotor-cooling circuit. This is conservative to the rotor-cooling design since, in reality, most of the losses manifest themselves as heat on the colder stationary walls of the rotor cavity.

As part of the studies and in parallel with other related studies[11], it became apparent that the calculation procedures derived by Smith[4] in the past were inappropriate to the KTA design conditions. As a result, an improved calculation procedure was derived (Appendix A), and it is upon this procedure, plus the original experimental data[5] of Smith, that the windage losses were based.

A survey of the several windage power loss experiments performed by Smith was made, and a limited amount of data was found on a rotor configuration similar to rotor designs under investigation. A comparison of the test rotor and the designs of interest is given in Table 54. In general, the physical variations between the test rotor and the designs under investigation are small. The fact that the test model had more poles and a nonsmooth stator bore means that the data from this model should be conservative from the standpoint of similarity when it is applied to the other designs.

The experimental data from the model rotor configuration is graphically illustrated in Figure 43. This data was plotted in accordance with functional Eq. (6) in Appendix A. The data consisted of 16 points and is represented by the small circles shown on the figure. The ranges of the independent dimensionless parameters represented by this small amount of quantitative data are:

$$0.134 \leq M \leq 0.364$$

$$0.12 \times 10^6 \leq \frac{\rho R a^*}{\mu} \leq 2.205 \times 10^6$$

$$1.71 \times 10^4 \leq \frac{\rho R^2 \omega}{\mu} \leq 80.3 \times 10^4$$

Unfortunately, the range of these independent parameters did not provide a graphic solution of the problem for the rotor designs under investigation. The corresponding values of these parameters for the KTA alternator designs are given in Table 55.

The Mach numbers for the KTA designs are much higher than the Mach numbers associated with the experimental model. Similarly, the magnitudes of the dimensionless parameter, $\rho a^* R/\mu$, are lower than the range experienced with the test model. Therefore, it was necessary to extrapolate the parametric form of the graphic solution offered by the data from the model to gain some knowledge of the windage

TABLE 54

COMPARISON OF DESIGNS AND TEST MODEL

	Design No. 1 19,200/800°F	Design No. 2 19,200/400°F	Design No. 3 24,000/800°F	Test Rotor
Rotor Diameter, in.	15.553	14.934	14.676	7.87
Core Diameter / Rotor Diameter	0.619	0.608	0.595	0.619
Axial Length of Pole / Rotor Diameter	0.288	0.279	0.268	0.288
Arc Length of Poles Per Side / Circumference of Rotor	0.345	0.335	0.332	0.329
Length of Rotor Core / Rotor Diameter	0.786	0.789	0.769	0.921
Radial Clearance Per Side / Rotor Diameter	0.0032	0.0032	0.0032	0.00318
Number of Poles	10	10	8	16
Condition of Stator Bore	Smooth	Smooth	Smooth	*

*72 slots with the wedges 0.005 in. below the stator bore.

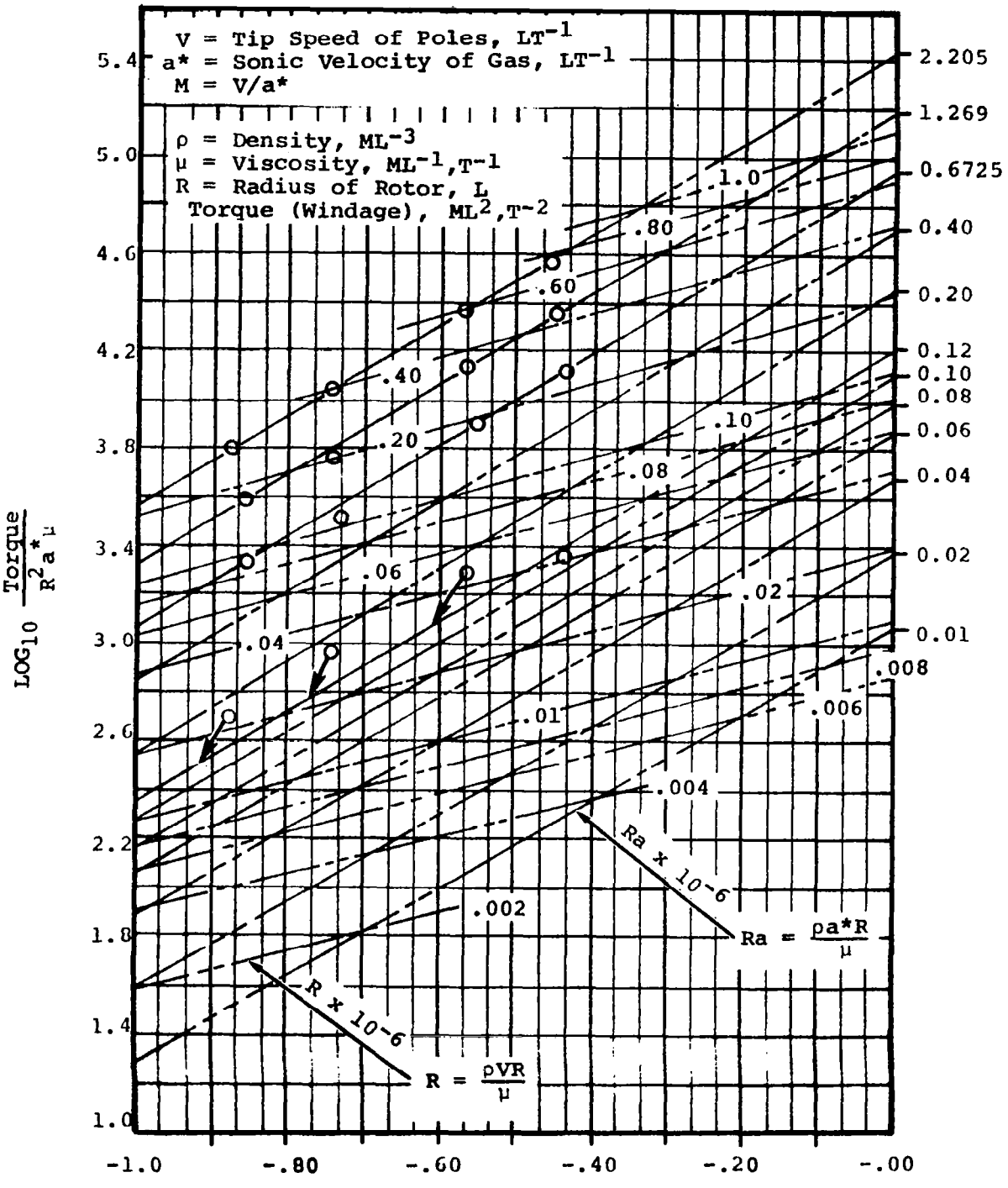

WINDAGE LOSS PARAMETERS

FIGURE 43

TABLE 55

RANGE OF DIMENSIONLESS PARAMETERS FOR ROTOR CONFIGURATION UNDER INVESTIGA

	Design No. 1	Design No. 2	Design No. 3	Vapor Seal Confic
Fluid	K	Mineral Oil	K	
Rotor Speed, rpm	19,200	19,200	24,000	
Fluid Temp., °F	800	400	800	
Sonic Velocity of Gas, a*, fps	1575	860	1575	
$M = R\omega/a^*$	0.826	1.453	0.974	
$\rho Ra^*/\mu$	2.96×10^4	8.30×10^4	2.78×10^4	For saturated vapor rotor cavity
$\rho R^2\omega/\mu$	2.44×10^4	12.0×10^4	2.62×10^4	
$\rho Ra^*/\mu$	1.51×10^4	0.69×10^4	1.11×10^4	Rotor cavity pressu single stage Holwe
$\rho R^2\omega/\mu$	1.25×10^4	1.0×10^4	1.05×10^4	Diameter of pumps = Length = 1.75 in.
$\rho Ra^*/\mu$	0.715×10^4	<1	0.377×10^4	Rotor cavity pressu one additional sta
$\rho R^2\omega/\mu$	0.631×10^4	<1	0.356×10^4	Holweck pumps Diameter of second s Length of second sta
$\rho Ra^*/\mu$	0.899×10^3		<1	Rotor cavity pressu three stage Holwe
$\rho R^2\omega/\mu$	0.741×10^3		<1	Diameter of third st Length of third stag

(a) Based on molecular weight = 240

power loss in the KTA designs. These extrapolations were performed using a logarithmic plot of the experimental values shown in Figure 43. The extrapolations to lower values of $\rho a^* R/\mu$ were based on the condition, first, that the dimensionless windage torque parameter is an exponential function of $\rho a^* R/\mu$ and, second, that the windage power loss is zero when the density of the fluid is zero. The extrapolations to higher values of Mach numbers were made by using a straight line extension of the lines on Figure 43.

It is very likely that this kind of extrapolation would not produce accurate data in the high Mach number range because the aerodynamic drag on a pole is strongly dependent on the Mach number when this parameter is greater than 0.35[13]. For example, the data from Reference 13 show that the drag coefficients on cylinders increase by 70 percent when the Mach number is increased from 0.35 to 1.0. Thus, it would be reasonable to assume that the windage loss obtained from Figure 43 must be increased 50 to 70 percent when the Mach number approaches 1.0.

Windage power losses for the KTA alternator designs for various rotor cavity pressures were calculated using the graphical solution presented in the Figure. These losses were increased by 50 percent to compensate for errors which may have been introduced by extrapolating the limited amount of quantitative data. The power losses are given in Table 56 for the three base designs.

The windage power losses are generally excessive when the rotor is operated within a cavity filled with a vapor at a pressure equal to the saturation pressure of the bearing lubricants. A complex cooling scheme would be required to maintain an acceptable pole tip temperature if a considerable portion of the windage power loss were transferred to the poles. Coolant passages within the main body of the poles would be required with an 800°F coolant (saturated potassium) temperature. A reduction of the rotor cavity pressure is required to

TABLE 56

WINDAGE POWER LOSS

Design No. 1 19,200 rpm, 800°F Potassium		Design No. 2 19,200 rpm, 400°F Mineral Oil		Design No. 3 24,000 rpm, 800°F Potassium	
Rotor Cavity Pressure, psia	Power Loss, w	Rotor Cavity Pressure, psia	Power Loss, w	Rotor Cavity Pressure, psia	Power Loss, w
0.155 (a)	2850	0.036 (f)	5050	0.155 (i)	4270
0.100	1900	0.02	2800	0.10	2800
0.079 (b)	1550	0.01	1420	0.062 (j)	1750
0.060	1210	0.006	850	0.04	1190
0.040 (c)	830	0.003 (g)	420	0.021 (k)	650
0.020	450	0.001	140	0.01	320
0.010	244	0.0006	84	0.006	200
0.008	200	0.0003	42	0.003	103
0.006	154	0.0001	14	0.001	37
0.00465 (d)	122	0.0006	8	0.0006	23
0.004	108	0.0003	5	0.0003 (l)	12
0.002	58	0.00003 (h)	0+		
0.001	31.5				
0.00028	10				
0.00005 (e)	<1				

(a) Saturation pressure of potassium at 800°F

(b) Rotor cavity pressure with a single-stage molecular pump

(c) Rotor cavity pressure with a two-stage molecular pump

(d) Rotor cavity pressure with a three-stage molecular pump

(e) Rotor cavity pressure with a four-stage molecular pump

(f) Saturation pressure of mineral oil at 400°F

(g) Rotor cavity pressure with a single-stage molecular pump

(h) Rotor cavity pressure with two-stage molecular pump

(i) Saturation pressure of potassium at 800°F

(j) Rotor cavity pressure with a single-stage molecular pump

(k) Rotor cavity pressure with a two-stage molecular pump

(l) Rotor cavity pressure with a three-stage molecular pump

reduce the windage power loss to a magnitude that will allow the use of a simple rotor cooling scheme. A cooling scheme with a central passage can be used with an 800°F coolant if the windage power is reduced to 130 w or less.

With the 400°F organic coolant, a cooling scheme with a central passage can be used if the windage power loss is reduced to 1500 w or less; with additional reduction of the windage power loss it would be possible to cool the rotor through the shaft extensions. A preliminary examination of this cooling scheme indicates that a temperature drop of 1.13°F/w of heat input into the rotor pole faces would exist between the pole face and the viscoseal on the shaft extension. Thus, if the total heat input into the pole face from windage, eddy-currents, and convection from the stator bore seal can be limited to approximately 400 w, a pole face temperature of approximately 850°F could be maintained with a 400°F coolant within the viscoseals.

The pressure head developed within Holweck type molecular vacuum pumps between the liquid seals and the rotor cavity was evaluated as part of the screw-type shaft seal parametric studies. The reductions of rotor cavity pressure that can be obtained by staging these pumps are given in Table 56. It became apparent from this evaluation that only a few stages of pumps would be required to reduce the rotor cavity pressure to a magnitude which will allow the use of a simple rotor cooling scheme.

The rotor cavity pressures for the organic coolant in the table are based on the assumption that volatile products from the decomposition of the organic coolant will not accumulate within the rotor cavity. If this happened, the rotor cavity would have to be vented to space to prevent excessive power losses. The opinion is that decomposition of the oil in the seals is very likely to occur; therefore, it must be recommended that the organic cooled/lubricated

alternator be vented to space. Furthermore, with the rotor cavity vented to space, operation at pole tip peripheral velocities greater than the sonic velocity of the oil vapor, the effects of which are not completely known, are no longer of concern. In the case of a vented rotor cavity, provisions would have to be made to prevent a direct "line-of-sight" from the vapor seal outlet to the bore seal to prevent possible carbonous products (which are good electrical conductors) from depositing on the bore seal.

So far, the discussion of reducing windage losses has centered around the effects of reduced vapor pressure, because that is where the most significant reductions are achieved. Another method is to use baffling to break up the turbulence around the poles. Three such methods are illustrated in Figure 44. All three concepts require nonmagnetic material that has a high electrical resistance, and all three suffer from mounting problems--the stationary baffles, because they must be of ceramic material and be close to the rotor wall; the rotating baffles, because they cannot be ceramic material in order to have sufficient mechanical strength.

While it is unknown precisely how much each of the configurations may reduce windage, some limited data by Smith[5] indicates that they could reduce losses to one-third of those for an open rotor pole configuration. Because of the minimal gains that can be achieved by baffling (compared to the more dramatic reductions achieved by reduced vapor pressure) and of the attendant mounting complexities, it must be recommended that baffling not be used in the KTA alternator.

4.2.4 Rotor Study Summary

Based on the analyses of the rotor cooling concepts, the pole-face losses, and the windage losses, it was possible to arrive at conclusions on which configurations or combinations thereof would be

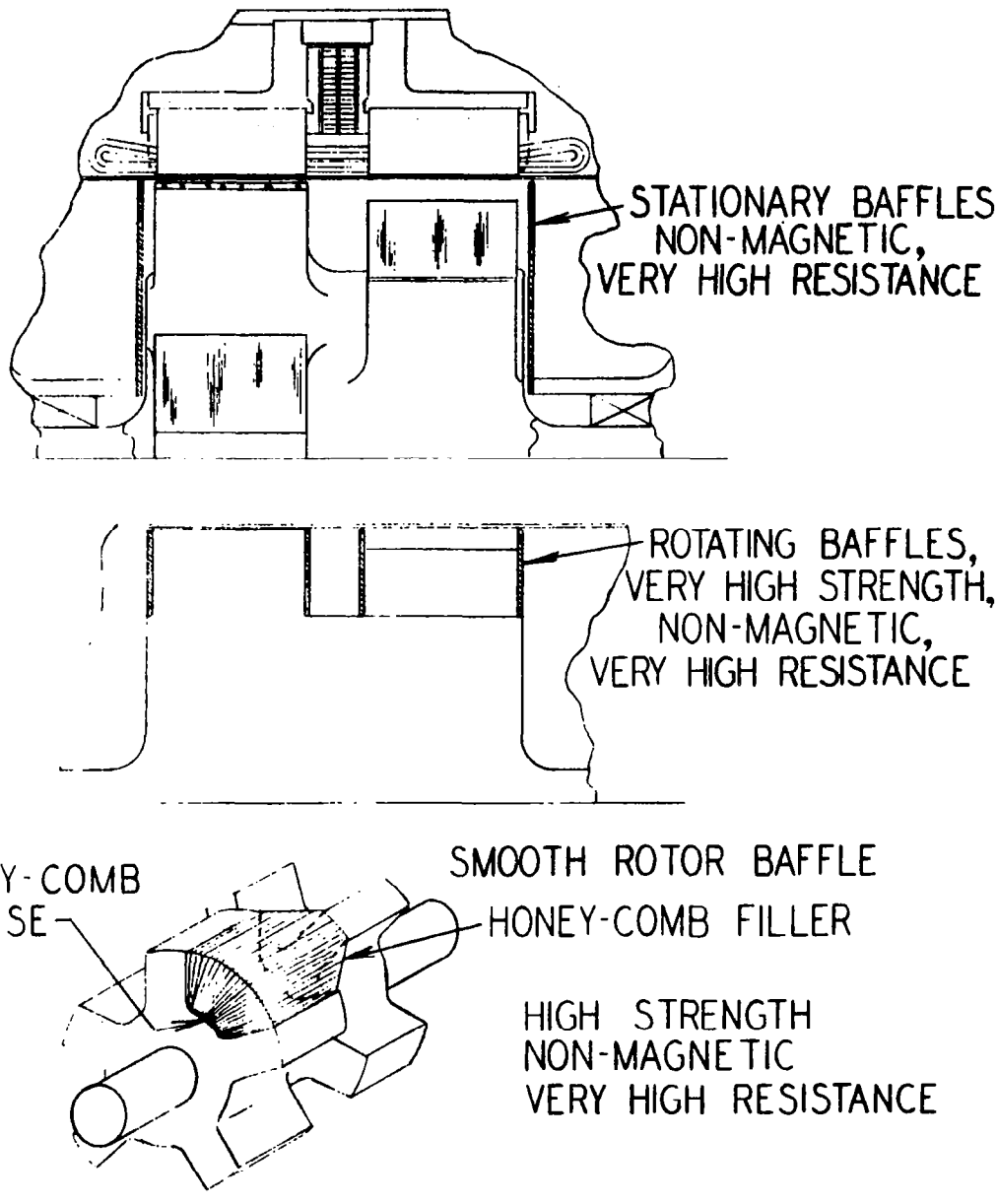

WINDAGE BAFFLE CONCEPTS

FIGURE 44

applicable to the various KTA requirements. These conclusions are consolidated into Tables 57 through 60. Summary comments relative to the applicability, advantages and disadvantages are included in the tables.

Table 60 gives a general ordering to the preferred configurations. For instance, the top combination would be laminated pole faces with a central cooling hole and provisions for lowering the vapor pressure in the rotor cavity. Note however, that particular circumstances can influence the mix of configurations comprising the top choice. For example, if the electromagnetic design is directed toward making pole-face losses sufficiently low to permit a slotted pole configuration, the top combination might be slotted poles on pole body with central coolant hole and provision for low vapor pressure in the rotor cavity.

In summary, the listing of Table 60 can be considered as a general guide but the peculiarities of the particular design must be the final guide to selecting the best configuration mix. The mix selected for the three base designs are tabulated in Table 61.

The configuration for designs No. 1 and 3 appears to be the most suited to the KTA alternator concept except for one aspect, the laminated pole faces. Being relatively uncommon and sensitive to fabrication anomalies, the laminated pole faces may be contrary to high reliability and ease of development requirements. Future studies will evaluate this configuration further, relative to either reducing the losses and heat load or conceiving a relatively simple, reliable laminated pole configuration.

TABLE 57

ROTOR COOLING CONFIGURATION SUMMARY

USUALLY ONE OF TWO CHOICES

(1) High Losses, Complex Cooling Configuration
(2) Low Losses, Simple Cooling Configuration

CONFIGURATION	COOLANT	°F/W	REMARKS
Stub Shaft	800°-K	---	Impossible with 800°F coo
	400°-Mineral Oil	1.13	Feasible with low losses
Central Hole	800°-K[1]	0.181	Feasible with low losses
	800°-K[2]	0.194	Feasible with low losses
	400°-Mineral Oil	0.210	Feasible with moderate lo
Parallel Passages Through Core	800°-K[1]	0.0627	Feasible with moderate lo
	800°-K[2]	0.0741	requires manifolds with volume for storage of h that centrifuge out of
	400°-Mineral Oil	0.0801	Not feasible due to centr heavy materials
Passage in Body Poles	800°-K	0.0181	Requires extra passage fo heavy materials that ce of K
	400°-Mineral Oil	---	Not feasible

[1] 19,200 rpm
[2] 24,000 rpm

TABLE 58

ROTOR POLE FACE LOSSES SUMMARY

Based on calculation procedures developed by Westinghouse for tooth ripple losses; load losses are based on calculation procedures developed by Berello

	Losses, kw	Design	Remarks
Laminated Pole Tip	0.12	Typical	A Rotor cooling scheme is simple A 0.4% increase in efficiency D Integrity of a laminated construction has not been defined
Slotted Iron Piece	0.19	Typical	A 0.4% increase in efficiency A Rotor cooling scheme is simple D Integrity of weld has not been defined D Complex slotting required
Slotted Pole	1.74 1.46 3.14	19,200, 800° 19,200, 400° 24,000, 800°	A 0.2% increase in efficiency D Coolant passages near the base of poles D Complex slotting and drilling required
Plain Poles	2.71 2.28 4.89	19,200, 800° 19,200, 400° 24,000, 800°	A Pole faces easy to fabricate D Excessive pole face losses D Complex cooling scheme into poles

A = Advantage
D = Disadvantage

TABLE 59

ROTOR WINDAGE POWER LOSS SUMMARY

Calculated values based on model theory and data from a similar rotor

Lower Mach numbers and higher Reynold numbers
Considerable extrapolation of model data
Margin for error in KTA is necessary
Minimize by lower density or baffling

		Losses, kw	Remarks
Saturated Pressure in Rotor Cavity	K-800°F 0.155 psia	2.85 (1) 4.27 (2)	D Decreases efficiency by 0.5% D Complex cooling scheme A Simple vapor seals
	Mineral Oil-400°F 0.036 psia	5.05	A Simple vapor seal A Complex cooling scheme D Bore seal become a conductor
Lower Press	K-800°F 0.004 psia	0.108 (1) 0.133 (2)	A Simple cooling scheme A Increase in efficiency D Scavenge system required
	Mineral Oil-400°F 0.0003 psia	0.005	A Simple cooling scheme D Vapor pump required D Bore seal would become a conductor
Vent to Space	K-800°F	0	A Simple cooling scheme D Complex vapor pumps required
	Mineral Oil-400°F	0	A Bore seal would not become conductive D Complex vapor pumps required (0.00005-psia forepressure on vent required)
Baffling (stationary)		1/3 of above values	A Vapor seal requirements are diminished D Baffling must be ceramic material

(1) 19,200 rpm
(2) 24,000 rpm

TABLE 60

ROTOR DESIGN STUDIES

Preferencial Order of Rotor Configuration Alternatives
Laminated Poles
Slotted Poles on Iron Piece
Slotted Poles on Pole Body
Unslotted Poles
Low Vapor Pressure
Vent to Space
Saturated Vapor with Baffling
Saturated Vapor
Central Cooling Hole
Cooling Through Stub Shafts
Coolant into Core
Coolant into Poles Also
Expect exceptions in each case depending on particular circumstances

TABLE 61

ROTOR DESIGN DETAILS SUMMARY

Design No. 1	Laminated Pole Face Losses	= 0.076 kw
	Windage Loss with 0.0004 psia Cavity Pressure	= 0.108 kw
19,200 rpm	Stator Heat Load	= 0.220 kw
1600 Hz		0.404 kw
800°F	Central Hole - Pole Tip Temp., 875°F	
	- Creep Strain, 0.12%	
Design No. 2	Laminated Pole Face Losses	= 0.064 kw
	Vented to Space	no losses
19,200 rpm	Stator Heat Load	= 0.100 kw
1600 Hz		0.164 kw
400°F	Coolant through Stub Shafts -	
	Pole Tip Temp., 580°F	
	Creep Strain, <0.1%	
Design No. 3	Laminated Pole Face Losses	= 0.131 kw
	Windage Loss with 0.0003 psia Cavity Pressure	= 0.012 kw
24,000 rpm	Stator Heat Load	= 0.144 kw
1600 Hz		0.387 kw
800°F	Central Hole - Pole Tip Temp., 875°F	
	- Creep Strain, 0.52%	

4.3 Stator Studies

The basic purposes of the Stator Studies were to (1) examine the alternative cooling configurations that would result in minimal hot spots consistent with ease of development (or fabrication) and reliability, and (2) define the structural configurations that would result in allowable stresses consistent with minimum weight, reliability, and ease of development. The structural studies were limited to those areas critical to the conceptual definitions: namely, the bore seal end member configurations and stator magnetic frame and punching stack shrink-assembly fits. Structural studies of the mounting frame and end bells were deferred to Phase II studies as they were not critical to the conceptual designs of Phase I. As a result, the frame and end-bell configurations shown later in Section 5.1 are heavy, boiler-plate configurations derived from "artists-concepts" rather than engineering studies.

The reasoning behind these separate stator studies evolves from past design experiences on the first SNAP-50/SPUR alternator. Near "equal-time" was given to the various analyses that covered the whole spectrum of the design. This was to evolve the first conceptual design[14, 15]. Later, after the conceptual designs had been "frozen" and hardware development was proceeding[16] it was determined that, had more emphasis been initially placed on certain critical analyses, the stator design could have been made more reliable and easier to fabricate. To avoid repetition of this in the KTA alternator conceptual designs, the separate stator studies below were executed.

4.3.1 Stator Cooling Concepts

The purpose of the study was to determine a basic stator cooling configuration that provides minimum operating temperatures without incurring electrical or mechanical design compromises. The study was

performed with the use of a three-dimensional heat transfer digital computer program that finds the transient and/or steady-state temperature distribution of an irregular body[17]. The body is described by an analytical model made up of a nodal grid that simulates the physical configuration of the body and can accommodate changes in material properties going from one location (node) to another. The program considers the heat transfer mechanisms of (1) conduction between internal (nodes) points, (2) conduction between internal and surface points, (3) radiation between surface points, and (4) radiation, free-convection and forced-convection between surface and boundary points. The boundary points represent the fixed boundary conditions. The program also considers internal heat generation as a function of space and time and boundary temperatures that may vary as a function of time. For purposes of carrying out the study, a typical generator design was initially selected from the generator parametric screening studies. Later, after Base Designs had been selected, the studies were based on the three selected designs. All temperature distributions in the conceptual design studies were based on the 550-kw_e operating condition.

The initial studies were based on the following conditions and considerations:

(a) Liquid metal as coolant at average temperatures of 800° and 1100°F

(b) All losses rejected to the coolant and to the end-bells and housing, when radiation from the armature end turns was considered

(c) An effective slot conductance (of the ac conductor and slot liner) of 0.2 w/in.^{2}-°C in directions perpendicular to current flow in the conductor. The 0.2 w/in.^{2}-°C

corresponds to a slot conductance that might be expected with a space vacuum ambient in the stator[11]

(d) Maximum allowable hot-spot temperature of 1300°F

Evaluation of the following stator cooling configurations was made during the study.

(a) Axial cooling tubes every 3 deg on the outside of the stack connected to a manifold around the field coil. This configuration is a very effective cooling sink but is complex and expensive and requires as many as 500 weld joints.

(b) Axial cooling tubes every 15 deg on the outside of the stack and around the field coil. This is like number (a) above but with fewer tubes to reduce the quantity of weld joints.

(c) Circumferential cooling manifold on the outside of the stator frame. This is to "fuse" the axial tube configurations above into one continuous duct, thereby lessening the weld joints and fabrication.

(d) Circumferential cooling manifold on the outside of the stator frame with a separate cooling manifold around the field coil. This is like (c) above but with added cooling to minimize field coil temperatures.

(e) Same as (d) above with cooling fins nestled between the ac windings in the gap between the stacks and on the end turns. Heat-transfer to these fins from the windings is by radiation only. This is to increase the

area of material around the windings, thereby presenting more cooling sink surface area to the heat flux attempting to cross from the windings to the coolant. This is to reduce the winding temperatures.

These cooling configurations are presented schematically in Figures 45 through 55. Additional known (commercial) configurations which place the coolant either in the slots with the wire, in the wire itself, or in the punchings around the slots were not analyzed, as the problems in fabrication for high-temperature alkali metal operation are inconsistent with the desire for ease of development.

As seen on the figures, an axisymmetric section was used for the analytical model that generally extended for one-half slot pitch plus one-half tooth pitch. Net heat exchange between the rotor and stator was neglected in these initial studies so rotor nodal points are not shown.

Temperature distributions for the above cooling configurations were determined for various combinations of 800° and 1100°F average coolant temperature, with and without end-turn radiation being included as a heat path. The temperatures resulting from these combinations are summarized in Table 62 with the respective maximum stator temperatures. The complete temperature distributions are presented in Figures 46 through 55.

Temperature distributions were also made for cooling configuration "e" (Figure 55) with effective slot conductances of 0.4 and 0.6 $w/in.^2$-°C to determine the effects of any improvements (undefined) that might be possible with an increase in the thermal conductance between the conductor and the slot liner. This was because, on the 1100°F-coolant designs, the heat was not being carried out of the

CONFIGURATION "a" & "b"

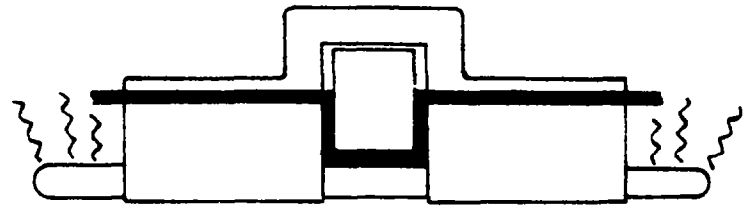

COOLANT TUBES THRU FRAME AND AROUND FIELD COIL

CONFIGURATION "c"

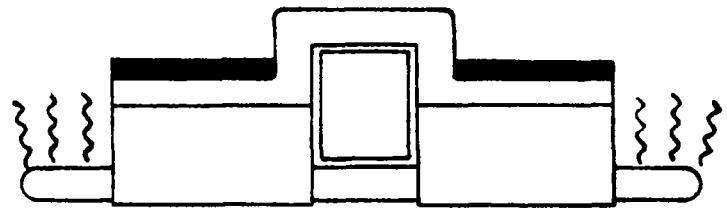

MANIFOLD ON FRAME O.D.

CONFIGURATION "d"

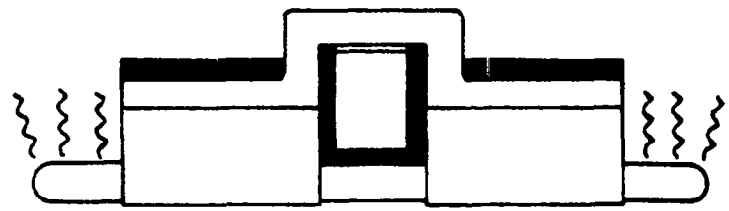

MANIFOLD ON FRAME O.D. AND AROUND FIELD COIL

CONFIGURATION "e"

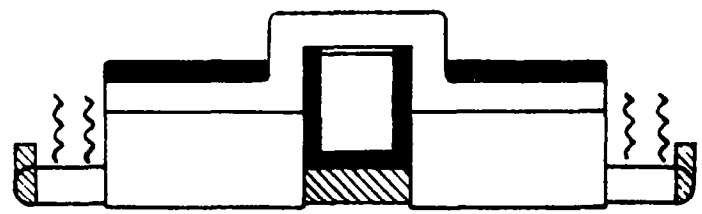

MANIFOLD ON FRAME O.D. AND AROUND FIELD COIL WITH RADIATION S AND ON ENDS OF WINDINGS

STATOR COOLING CONCEPTS

FIGURE 45

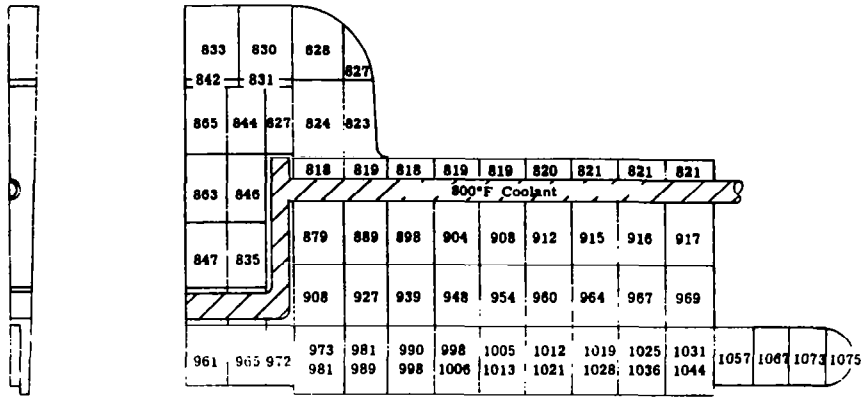

STATOR COOLING SCREENING STUDY, TEMPERATURE DISTRIBUTION (°F)
COOLING TUBES EVERY 3 DEG, 800°F COOLANT, END TURN RADIATION

FIGURE 46

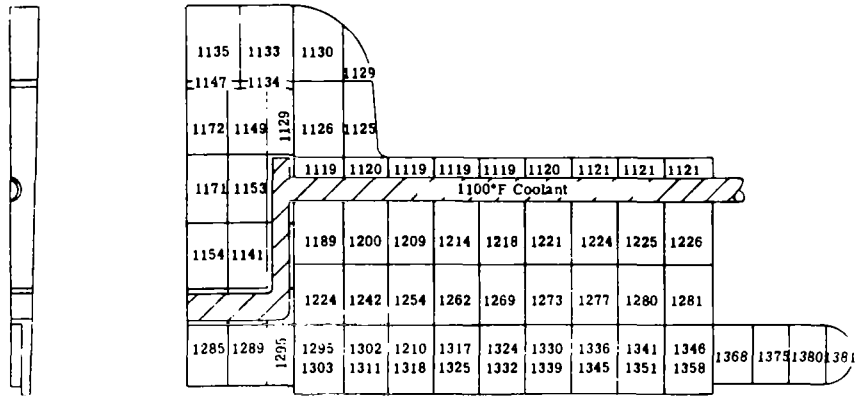

STATOR COOLING SCREENING STUDY, TEMPERATURE DISTRIBUTION (°F)
COOLING TUBES EVERY 3 DEG, 1100°F COOLANT, END TURN RADIATION

FIGURE 47

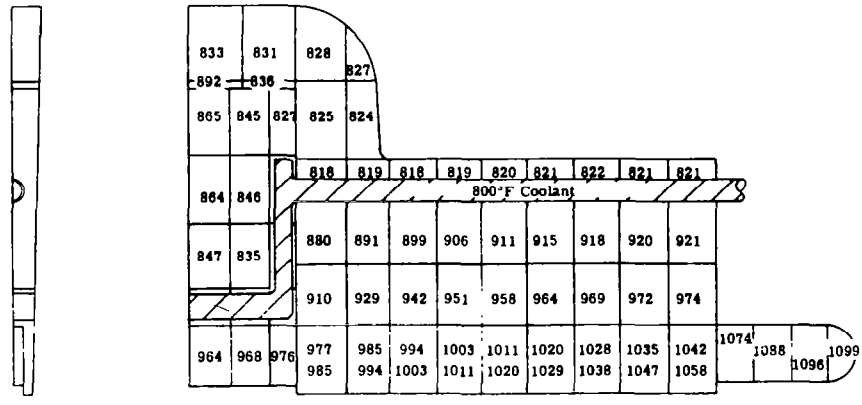

STATOR COOLING SCREENING STUDY, TEMPERATURE DISTRIBUTION (°F)
COOLING TUBES EVERY 3 DEG, 800°F COOLANT, NO END TURN RADIATION

FIGURE 48

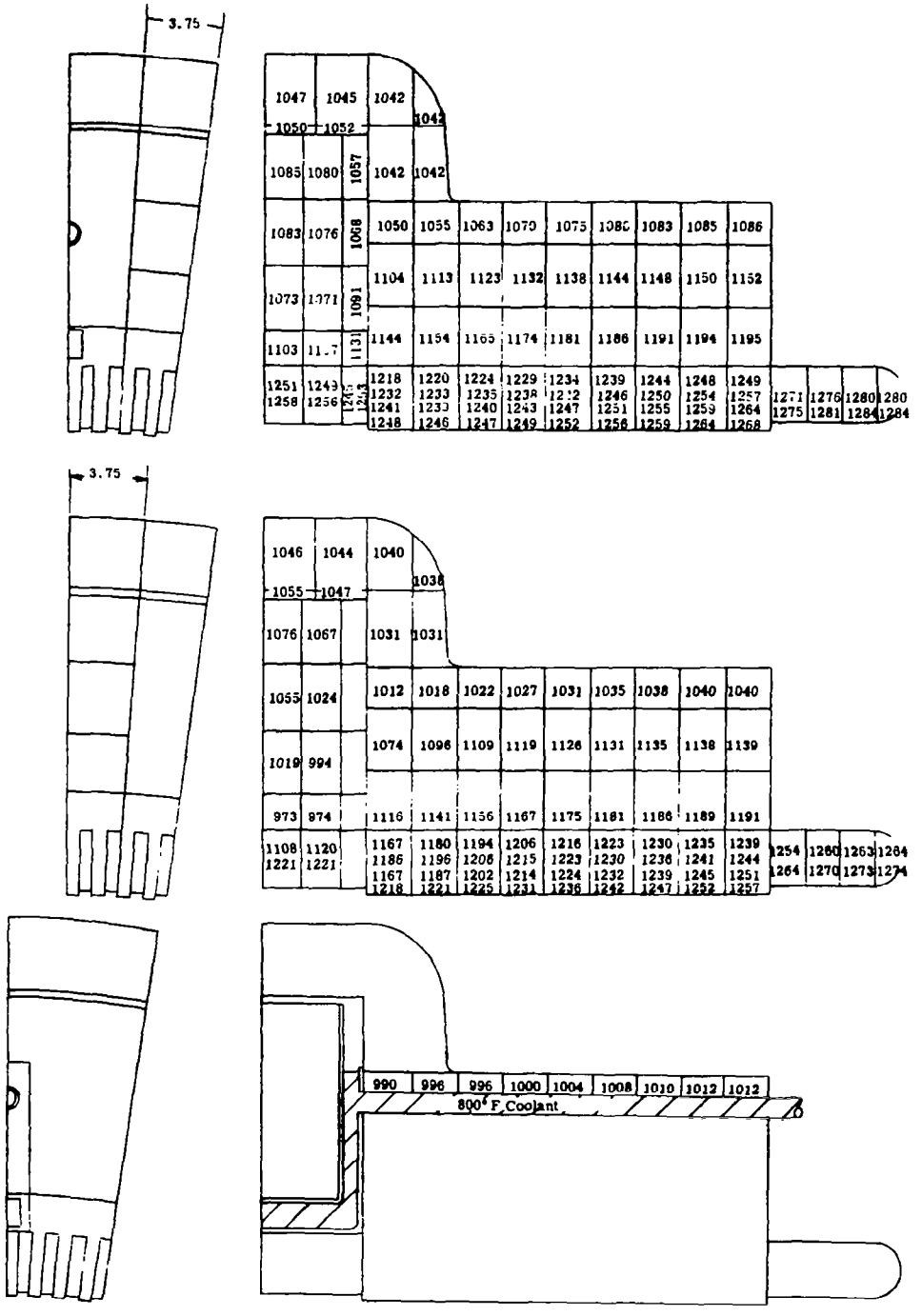

STATOR COOLING SCREENING STUDY, TEMPERATURE DISTRIBUTION (°F) COOLING TUBES EVERY 15 DEG, 800°F COOLANT, END TURN RADIATION

FIGURE 49

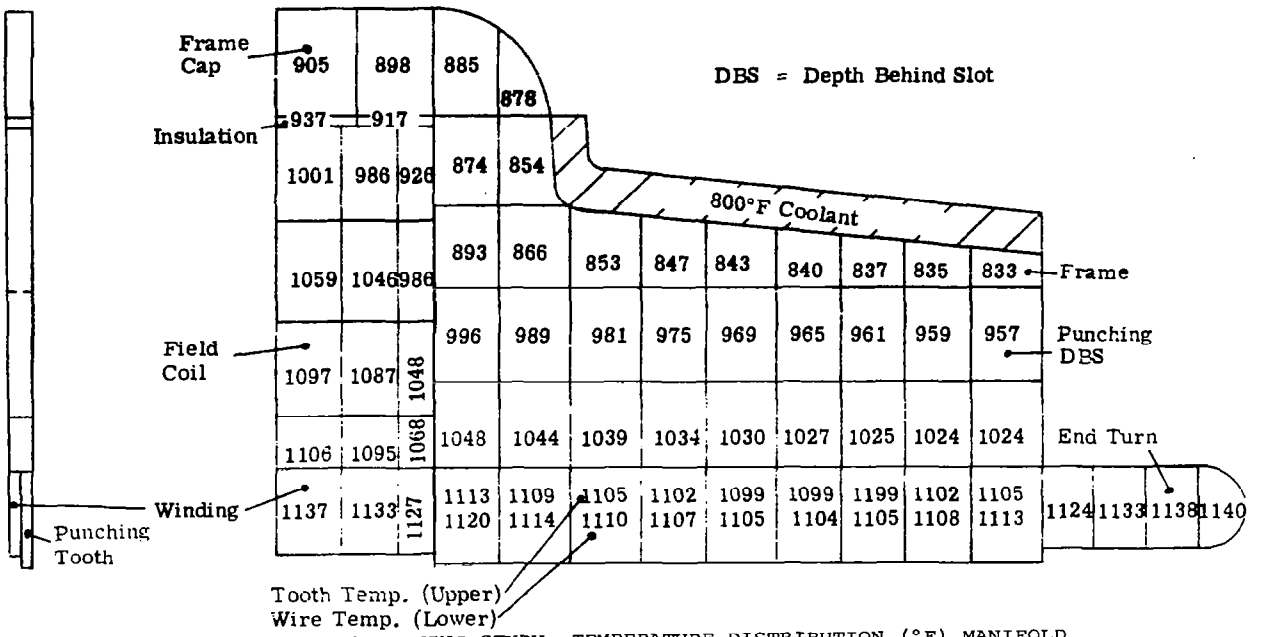

STATOR COOLING SCREENING STUDY, TEMPERATURE DISTRIBUTION (°F) MANIFOLD COOLING, 800°F COOLANT, END TURN RADIATION

FIGURE 50

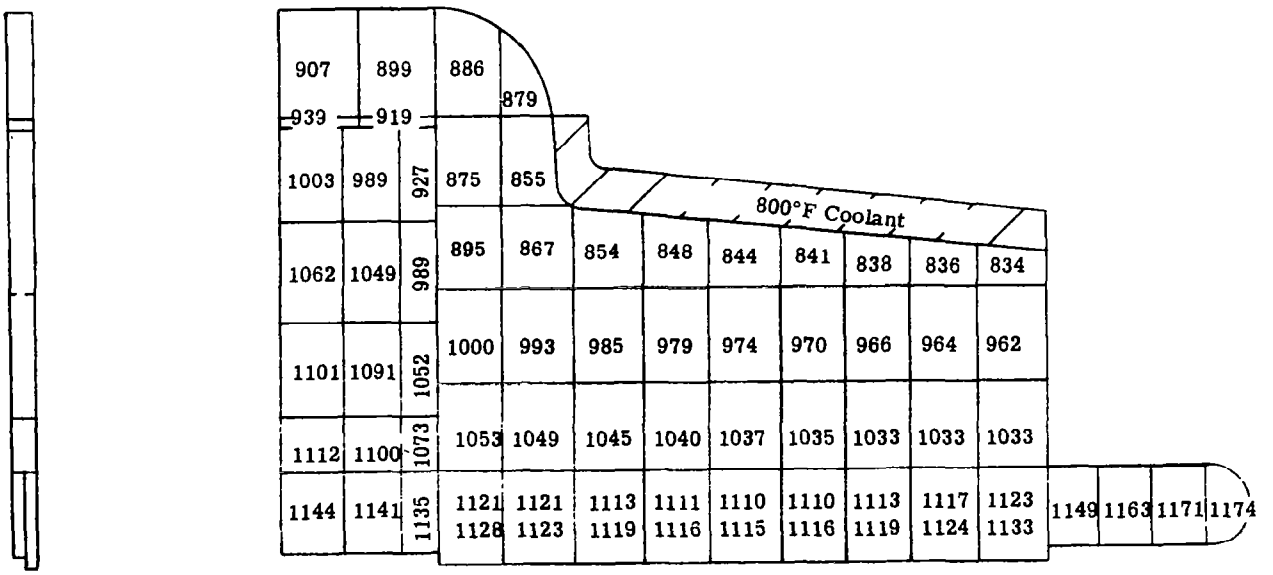

STATOR COOLING SCREENING STUDY, TEMPERATURE DISTRIBUTION (°F) MANIFOLD COOLING, 800°F COOLANT, NO END TURN RADIATION

FIGURE 51

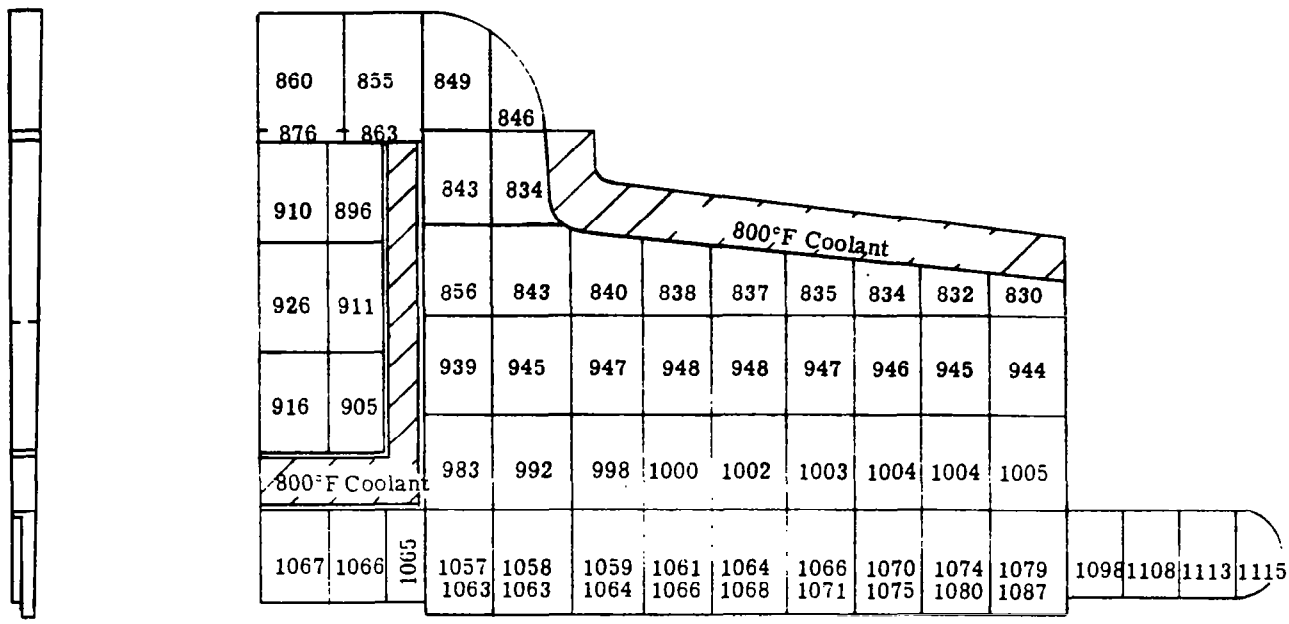

STATOR COOLING SCREENING STUDY, TEMPERATURE DISTRIBUTION (°F) MANIFOLD AND FIELD COIL COOLING, 800°F COOLANT, END TURN RADIATION

FIGURE 52

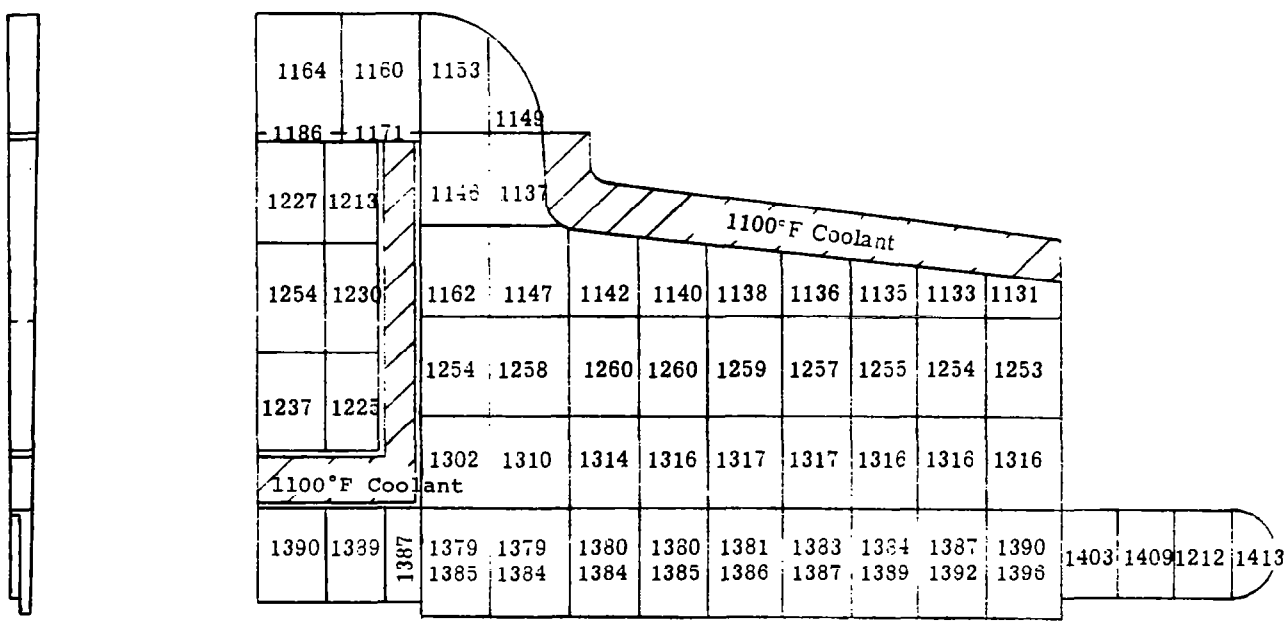

STATOR COOLING SCREENING STUDY, TEMPERATURE DISTRIBUTION (°F) MANIFOLD AND FIELD COIL COOLING, 1100°F COOLANT, END TURN RADIATION

FIGURE 53

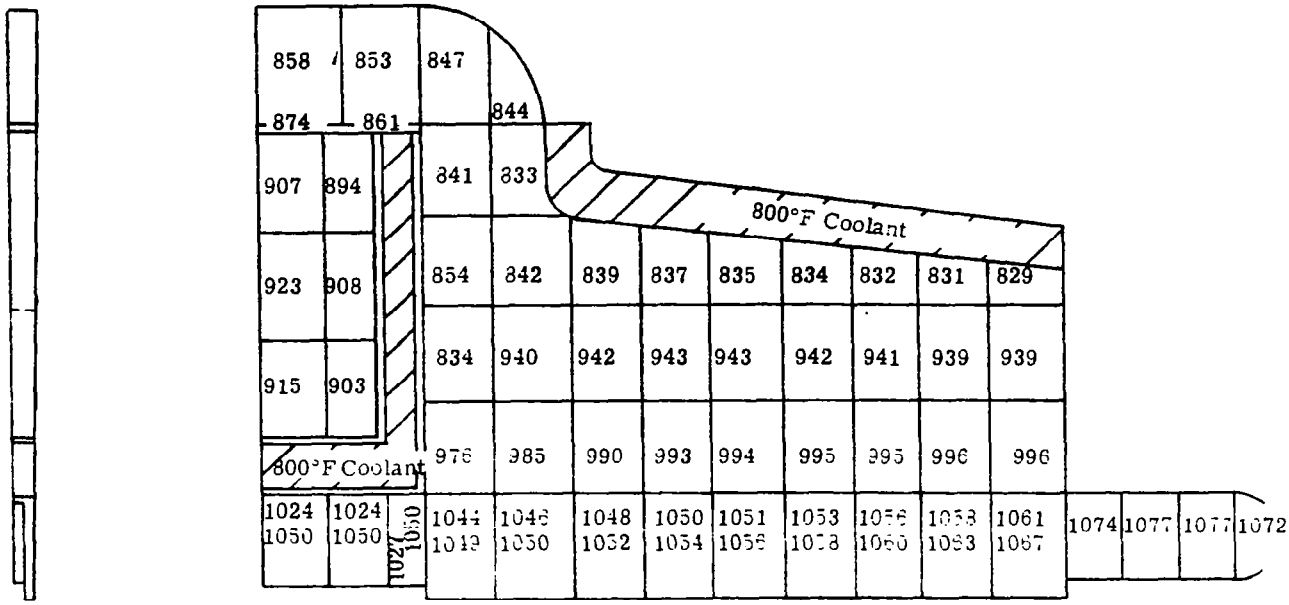

STATOR COOLING SCREENING STUDY, TEMPERATURE DISTRIBUTION (°F) MANIFOLD AND FIELD COIL COOLING WITH AC WINDING COOLING FINS, 800°F COOLANT, END TURN RADIATION

FIGURE 54

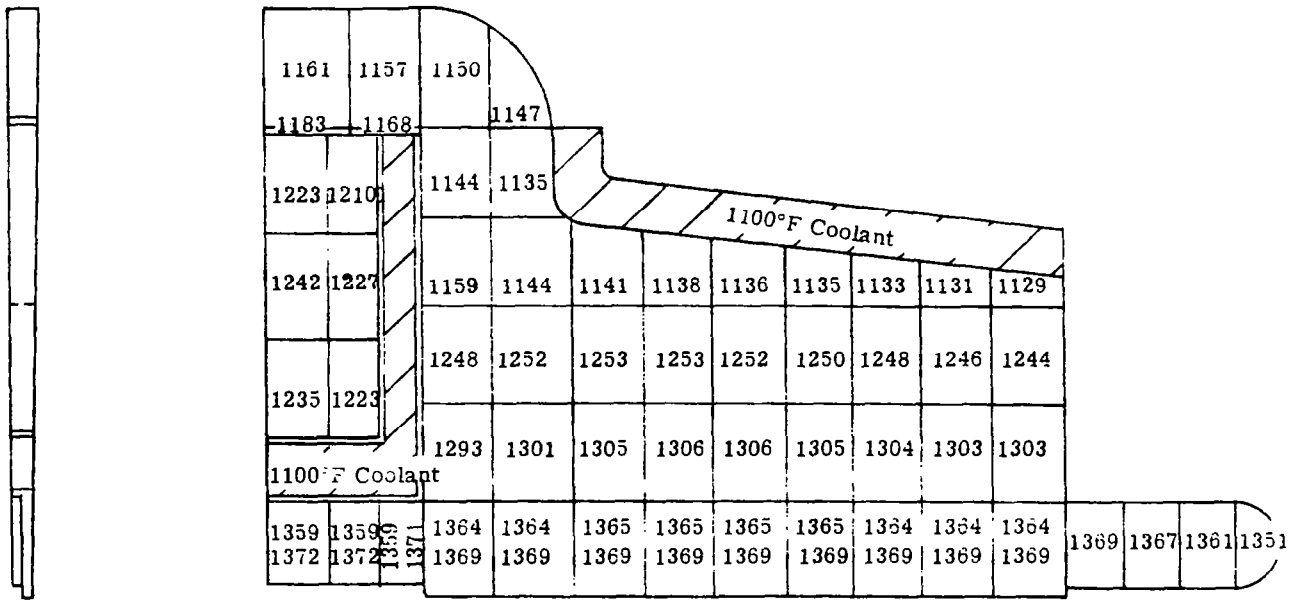

STATOR COOLING SCREENING STUDY, TEMPERATURE DISTRIBUTION (°F) MANIFOLD AND FIELD COIL COOLING WITH AC WINDING COOLING FINS, 1100°F COOLANT, END TURN RADIATION

FIGURE 55

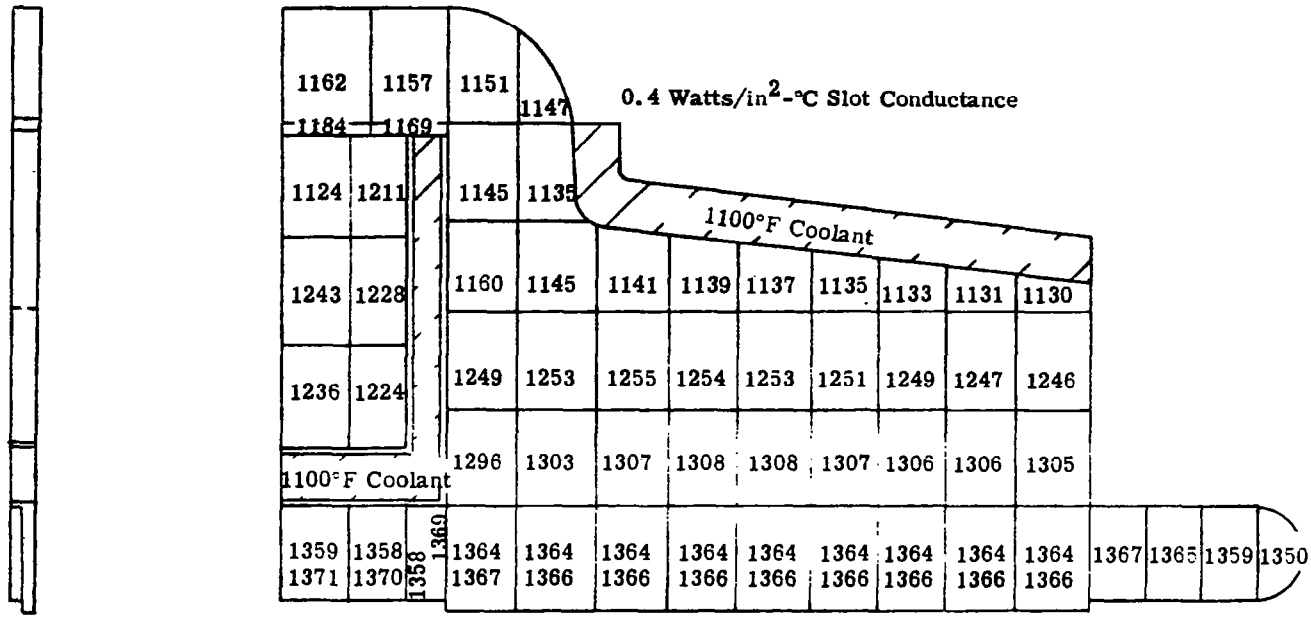

STATOR COOLING SCREENING STUDY, TEMPERATURE DISTRIBUTION (°F) MANIFOLD AND FIELD COIL COOLING WITH AC WINDING COOLING FINS, 1100°F COOLANT, END TURN RADIATION -0.4 W/IN.^{2}°C SLOT CONDUCTANCE

FIGURE 56

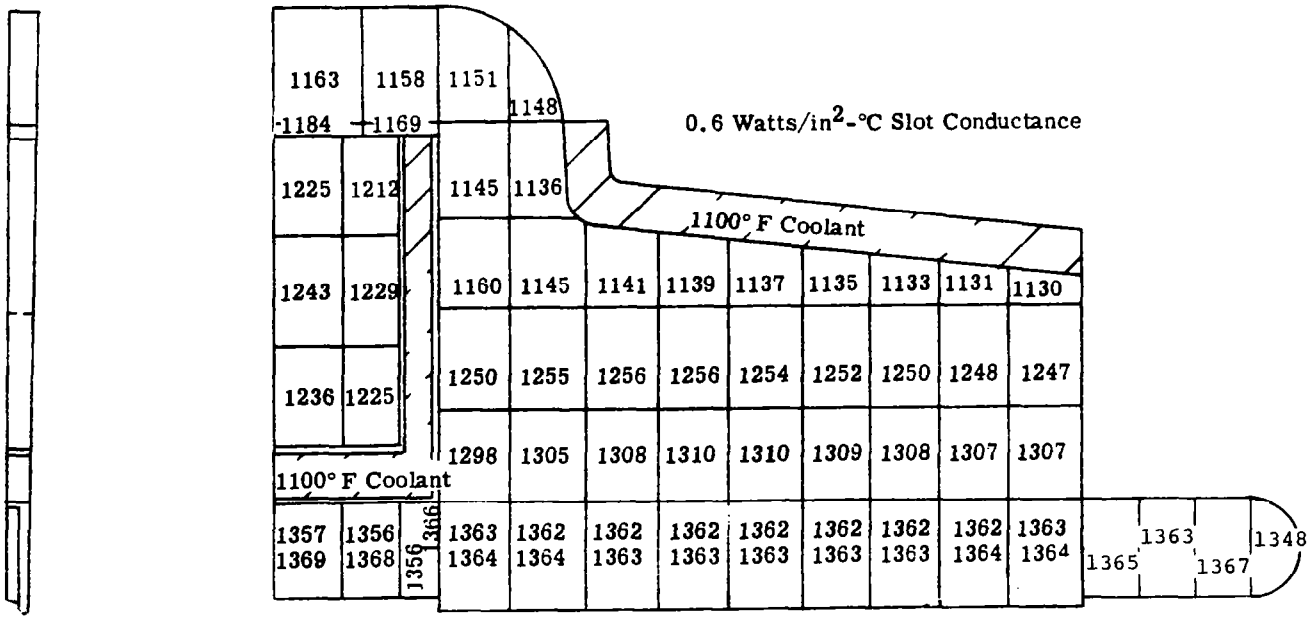

STATOR COOLING SCREENING STUDY, TEMPERATURE DISTRIBUTION (°F) MANIFOLD AND FIELD COIL COOLING WITH AC WINDING COOLING FINS, 1100°F COOLANT, END TURN RADIATION -0.6 W/IN.^{2}°C SLOT CONDUCTANCE

FIGURE 57

TABLE 62

STATOR COOLING SCREENING STUDY,
MAXIMUM STATOR TEMPERATURES

Cooling Configuration	With End-Turn Radiation	
	800°F	1100°F
Cooling Tubes Every 3 Deg	1075	1381
Cooling Tubes Every 15 Deg	1284	--
Manifold Cooling	1140	--
Manifold and Field Coil Cooling	1115	1413
Manifold and Field Coil Cooling with ac Winding Cooling Fins	1077	1372
Manifold and Field Coil Cooling with ac Winding Cooling Fins - 0.4 w/in.^{2}°C Slot Conductance	—	1371
Manifold and Field Coil Cooling with ac Winding Cooling Fins - 0.6 w/in.^{2}°C Slot Conductance	—	1369

wire as quickly or as well as desired. These results, presented in Table 62 (also Figures 56 and 57) show only negligible reductions of the winding temperatures. It would appear then that the effective (analytical) slot thermal conductivity used (in directions perpendicular to current flow) is sufficiently low and, therefore, any physical schemes to increase it over 0.2 w/in.^{2}-°C do not greatly effect the conductor temperatures. Because of this, it would be well to note at this time from where the 0.2 w/in.^{2}-°C effective slot conductance is derived.

In a physical configuration, the contacts between the wire and slot liner and punching side are subject to wide variations and irregularities. The effect is that it is impossible to establish an analytical model that describes what might or could be present. The safe approach to this analytically, then, is to be ultraconservative. This was done on the SNAP-50/SPUR Alternator[16] and the result was a prediction for a required cooling configuration similar to the Configuration a of the present studies. In later analytical studies[2] in which most of the possible variations and irregularities were examined in a parametric comparison, the ultraconservative approach was shown to be unrealistic to the average worst-case. In these studies, it was shown that on the average the effective slot conductance may be about 0.4 ±0.2 instead of 0.04 w/in.^{2}-°C for the ultraconservative case.[16] Thus, a more realistic (yet conservative) value to use for a design would be 0.2 w/in.^{2}-°C. Proof of whether this rationale is valid or not must wait until an alternator is built and thermally tested.

For the 1100°F coolant stators and for slot conductances that approach maximum expected levels with end-turn radiation, the maximum stator temperatures remained in excess of the maximum allowable 1300°F for the basic configurations of Figures 46 to 55. As a result, it became apparent that alternate methods for cooling the

1100°F stator were required. A reduction of the stator losses and the length of the thermal path to the coolant are two desirable methods for reducing these stator temperatures. Based on recent experimental results on AEC Contract AT(04-3)-679[1,11], evaluation of these two methods appeared to be appropriate. A temperature distribution was made for the approximate expected reductions of stack DBS length and stator losses to determine the magnitude of expected temperature reductions. The resulting temperature distribution, presented in Figure 58, reveals a maximum temperature reduction in the conductor of 119°F and a maximum stator temperature of 1272°F. These temperatures, though not completely accurate since actual reductions of stator size and losses were not available at the time, are an indication of what could be expected.

Results of the stator cooling parametric study also revealed the desirability of direct cooling of the field coil in the stator cooling configuration. The actual final selection of the particular field coil cooling configuration for conceptual design analysis will be based on cooling ability and ease of fabrication consistent with the schematic configuration above.

In summary, the 800°F nominal cooling configuration that gave reasonably low hot-spot temperatures consistent with ease of fabrication was a circumferential manifold on the stator frame with cooling fins nestled in the ac windings between the stacks. These fins are in conjunction with a separate cooling manifold around the field coil. This is the d Configuration examined with a portion of the radiation cooling fins extracted from the e Configuration.

For 1100°F nominal coolant, the electromagnetic design of the alternator would have to be altered specifically to reduce the winding hot spot. This is because the temperatures were well over the 1300°F limit even with cooling Configurations such as b or c

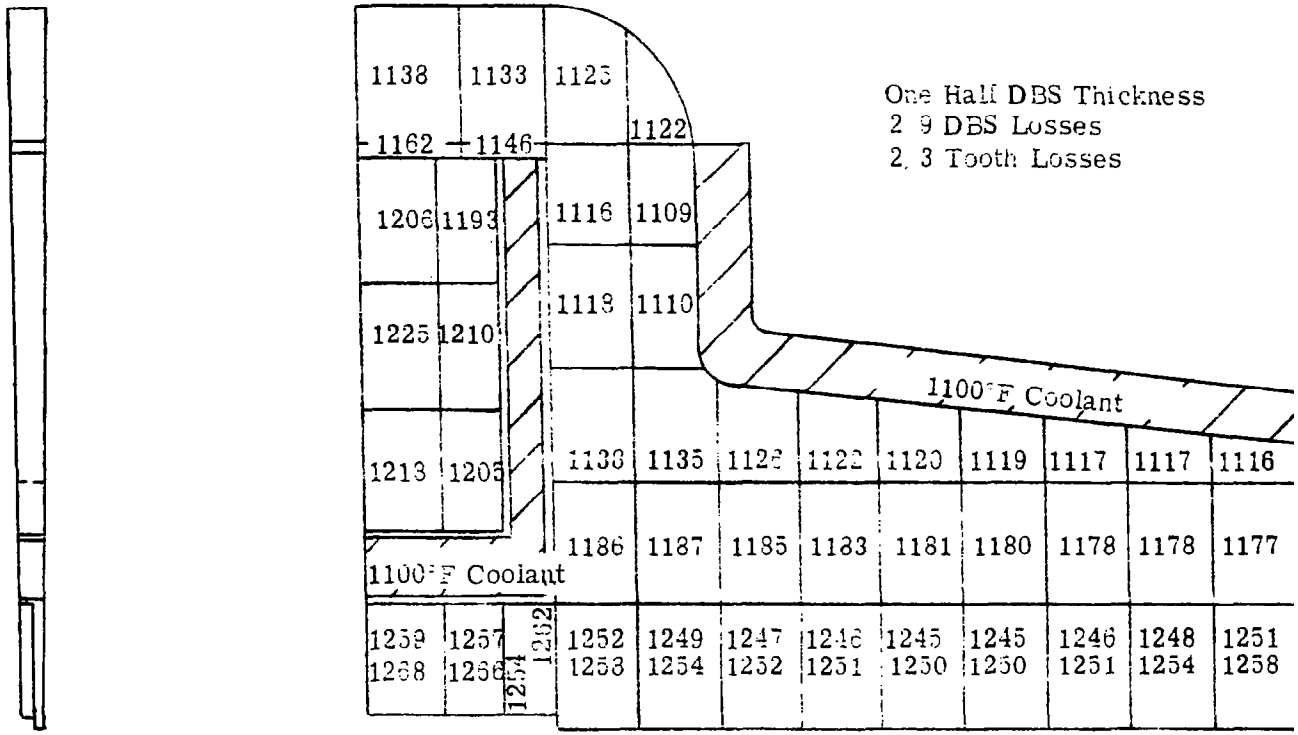

STATOR COOLING SCREENING STUDY, TEMPERATURE DISTRIBUTION (°F)
MANIFOLD AND FIELD COIL COOLING WITH AC WINDING COOLING FINS,
1100°F COOLANT, END TURN RADIATION

FIGURE 58

which make maximum use of cooling sinks. It does not appear possible to add sufficiently more cooling configurations to the present electromagnetic design configurations without sacrificing ease of development.

4.3.2 Bore Seal End Member

The KTA design requires that liquid potassium or an organic fluid be the lubricant for the alternator. A technology for shaft seals has been acquired whereby it is anticipated that the leakage rate from the bearings can be maintained at an acceptable level. However, these seals cannot eliminate the presence of a vapor within the rotor cavity, even when the cavity is vented to the vacuum of space. At the low pressure of space, the mean free path between molecular collisions would be large (compared with a saturated or superheated vapor in a non-vented cavity), but 3- to 5-year operations with free diffusion of the molecules from an organic fluid will not significantly decrease the severity of the problems from those associated with potassium since the stator temperatures will still be in the 1000°F range. Contact of organic vapors with the hot stator components will cause a build-up of conductive deposits with time.

Protection of the stator from potassium vapor or the vapor associated with an organic fluid requires a bore-seal in the form of a thin-wall tube in the radial gap of the alternator. A thin-wall ceramic tube has been judged best suited to provide a good combination of resistance to attack by alkali metal and electric resistivity high enough to limit eddy-current losses to low values. The ceramic tube in the gap between the stator and rotor poles must be bonded to metal end members for sealing to the alternator frame in order to provide a sealed stator enclosure. In the event that both the stator and rotor would be vented to space, the seal would not necessarily be hermetic nor of a high purity alumina. In that case, a term "bore-barrier" might be used to describe the ceramic tube and end members.

In the discussion following, the more common term "bore seal" will be used to imply the presence of either a bore seal or a bore barrier, the choice being entirely dependent upon the cavity venting specification yet to be made.

The concept of designing an alternator without the bore seal was evaluated relative to the expected limitations or requirements that would be imposed on the design. Using technology and experience derived from actual tests[20], the summary of Table 63 was prepared. The limitations concern materials, voltage, and electromagnetic effects. While it is recognized from the table that potassium-resistant materials are available and impose no restrictions, the deleterious effects of the voltage limitations and electromagnetic effects are sufficient cause for ruling out designs without a bore seal or bore carrier in the radial gap.

Long-time testing in potassium vapor has demonstrated assemblies of a 99.8 percent pure alumina (CE998) and the refractory alloy of 99Cb-1Zr joined by the 75Zr-19Cb-6Be braze alloy (or other active-metal brazes) to be resistant to potassium vapor at 900°F for more than 10,000 hours[18]. The higher strength tantalum base refractory alloy (T-111, 90Ta-8W-2Hf) has displayed good brazing characteristics and the potential for being very resistant to alkali metal vapor[19]. High purity low silica beryllia, although lower in strength than alumina, has adequate resistance to potassium for operation up to 1300°F. Assemblies may be brazed using the 60Zr-25V-15Cb braze alloy. BeO material is not, however, available at this time in thin tube sections larger than 6 in. in diameter.

TABLE 63

CONSIDERATIONS IN DESIGN WITHOUT A BORE SEAL

Material Limitations

(a) Organic - Insulation system must withstand carbon deposits on hot-spot e vented to space. Applicable materials, limiting temperatures, and undes qualities are summarized below:

Conductor Insulation:	Anadur	< 1300°F (is porou
	Teflon	< 600°F (low radia
	ML (H film)	< 400°F
Slot Liner:	Alumina (99.5%)	< 1400°F
	Teflon	< 600°F
	ML-Glass	< 400°F
	MICA	< 800°F (poor in v
Conductor:	Copper	< 900°F
	Clad silver	< 1400°F
Stator Magnetic Material:	Hiperco-27	
	CUBEX	

(b) Potassium - Requires potassium resistant system. Materials and limitin temperatures given below:

Conductor Insulation:	Plasma arc sprayed alumina
Slot Liner:	Alumina (99.5%) Beryllia (99.8%)
Conductor:	Nickel clad silver
Stator Magnetic Material:	Hiperco-27 < 1400°F
	CUBEX < 1100°F

Voltage Limitations, Reference 20

(a) For saturated potassium vapor, voltage must be < 125 vac at 1600 Hz

(b) For superheated potassium vapor, voltage must be < 180 vac at 1600 Hz

Potassium Vapor Effects in Electric and Magnetic Fields, Reference 20

(a) Ionization causes extensive erosion of magnetic material and ceramics

(b) Ceramic surfaces above 450°F become coated with a conductive film of pot

(c) Odd energy transfer phenomena that result in conductor destruction and e meter reading.

Because the technology required for the bore seal is relatively new and has not been carried to operational status for the sizes needed in the KTA alternator, the opportunity exists for coordinating the configuration design from the standpoint of both mechanical and metallurgical considerations. Past designs[16] suffered somewhat from a lack of such coordination. As a result, the designs contained both mechanical and metallurgical compromises that did little to enhance the reliability of this very critical component in the alternator.

In those past designs, it was initially believed the most critical design area was the ceramic-to-metal joint between the tube and end member. Consequently, the majority of the design and development effort was concentrated in that area[18]. Later detailed stress analyses identified an equally critical aspect, excessive stress in the end member between the ceramic-to-metal joint and the stator frame[16]. At the time, because hardware fabrication was proceeding, resolution of the problem was attempted by modifying the design and thickening the metal end member from 0.017 to 0.030 in. Neither approach met with significant success since the thicker metal did not reduce stresses enough, and it did detract from the successful development of the joint. Completely new and different design approaches were examined, but before little more than promising approaches were identified, the development project was terminated. The purpose of the present study is to continue evaluation of these promising concepts and select the one most suited to the KTA alternator.

The dilemma faced by the designer in selecting the best configuration is the result of two contrary requirements. The first is that the end member must be flexible (thin) to accommodate the differential thermal expansions between the ceramic tube and the metal frame. The second is that the metal end member must be rigid (thick) enough to

support any pressure differential between the rotor and stator cavity.* The solution to the dilemma is to find the proper balance between the two requirements.

The importance of this second requirement was not fully realized until large size bore seal designs were attempted, causing the previously discussed problems of Reference 16. Prior experience with small bore seals (up to 6-in. diameter) had given no indication of a pressure limitation or problem. As a check on the validity of the conclusions drawn on the dilemma, several of these small bore seals were stress-analyzed in detail. All showed low stress except one where calculated stresses were greater than yield strengths but less than ultimate strength. Visual examination of that particular bore seal revealed that its metal end members had indeed undergone a permanent, plastic deformation without catastrophic failure.

One of the least complicated approaches (from the standpoint of ease of development and minimum weight) to solving the two requirement dilemmas is to design the end member so that the thermal expansion strains are counteracted by the pressure differential strains. The net strains and stresses are thereby minimized. The procedure of the study was to evaluate several configurations believed to contain features for doing this. Likewise, because transition pieces would be needed in going from the refractory alloy end-members on the bore seal to the frame, bimetallic configurations for these pieces were included in the study. The transition pieces are needed to provide a nonrefractory alloy section to weld to the generator frame on final assembly.

*Even if the alternator is designed for near-equal pressures in the rotor and stator cavity, "abnormal" situations can be foreseen where a pressure differential could exist. As the metal end member must survive these abnormal situations, the off-design requirements take on equal importance in selection of a design.

The comprehensive stress analyses carried out on the bore seal end-members to select the conceptual designs were based on the following:

(a) The maximum pressure differential across the bore seal and end members shall not exceed 20 psi in either direction. Internal pressurization shall be only at room temperature, external at all temperatures listed below.

(b) The temperatures of the bore seal and end-members shall be room temperature (uniform), soaking temperature (uniform), operating temperature (gradients) and the transients between them. Soaking temperature is assumed to be at least 1100°F.

The stress analysis was conducted with the use of a computer program that calculates stress and displacements of elastic axisymmetrical open and closed shells. This computer program was previously written and verified at another division in the Westinghouse Electric Corporation. The analysis is made by setting up a number of points (stations) along the meridional profile of the shell. At each of these points, input is furnished to describe the flexibility of the shell and the external loading. The program is based on a Myklestad-type finite difference solution set up in matrix form. The analysis takes into account the effects considered in Love's first approximation and also includes the effect of shear deflection. At the conclusion of the calculation, the stress and deformations of the shell are printed out for each of these same points.

The basic bore seal design used in the analyses consists of a thin-walled, high-purity alumina (or beryllia) cylinder brazed to refractory metal end members. The seal is completed by bonding of

the end member to the alternator housing through transition pieces. This analysis of the end member stresses was based on the following assumptions relative to the basic design.

(a) The metallic end members are 0.017 in. thick. This thickness was selected from previous studies[18] and is based on commercial experience with thin gauge metal components in producing vacuum-tight joints in brazed ceramic-refractory metal assemblies.

(b) The bore seal diameter is 15.5 in. This value is the approximate diameter of the bore seals of the conceptual designs.

(c) The relative axial expansion of the bore seal is 0.014 in. to be compensated for at one end of the bore seal only. In other words, one end of the bore seal is fixed, relative to the end bell on that end.

This value was selected based on previous studies[16] as approximating relative expansion for the conceptual design configurations. Temperature distributions from which expansions could be calculated had not been determined at the time of these studies.

Stresses were determined for a variety of end-member configurations having expansion compensating features for the 20-psi pressure differential simulating stator pressurization, 1100°F constant soak-temperature, and 0.014-in. axial displacement. These configurations included bellows, large curved members, and short conical members; all three were in both the inward and outward directions. Butt and sandwich type metals to ceramic joints (Figure 59) were investigated with no stress advantage evident of one over the other. Results of

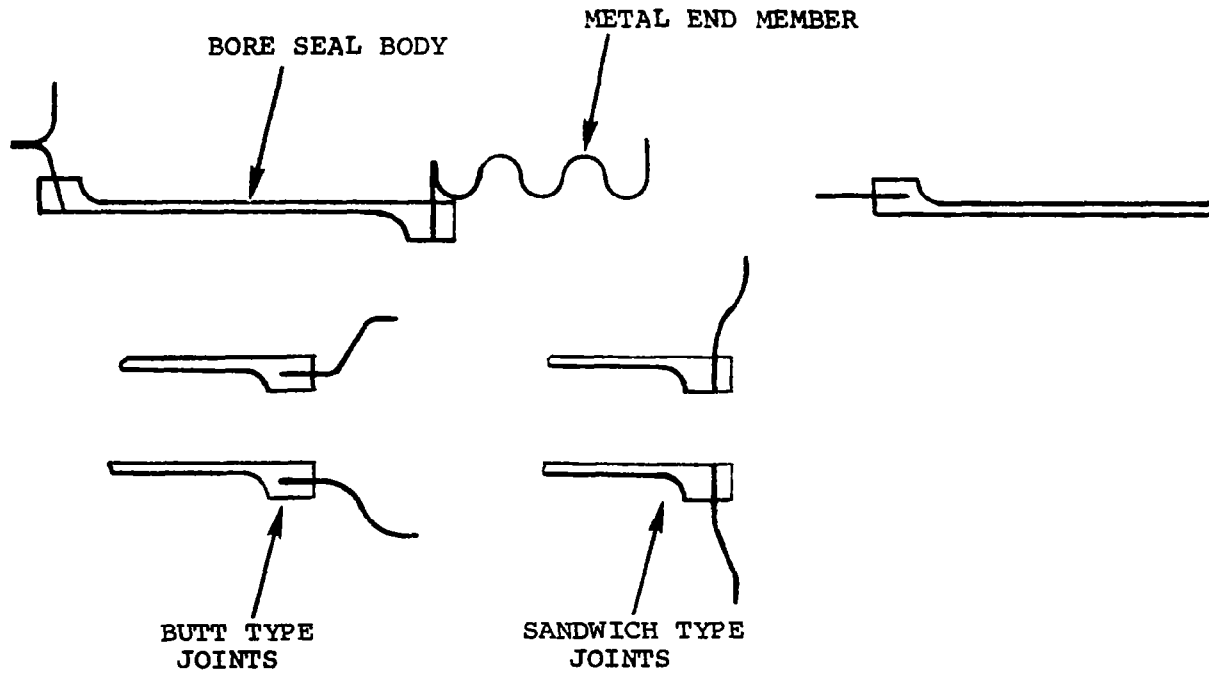

TYPICAL BORE SEAL DESIGN CONCEPTS

FIGURE 59

the stress calculations, summarized in Table 64, show that the simple, straightforward short configurations are the lowest stressed. However, even then, the end-member stresses were in excess of a self-imposed limit of 15,000 psi.

Due to the "compensating" configurations not resulting in low stresses and because of the desirability of providing and maintaining accurate alignment of the bore seal in the radial gap, it became necessary to consider a different configuration that provided more positive mechanical support for the bore seal and end-members while maintaining flexibility. The configuration concept (for the fixed-end) consists of a ring fixture which is custom-mated with the ceramic on the bore seal and fits snugly against the unpressurized side of the metal end-member. The snug fit is important to provide the thin end-member support. A curvic-coupling (radial-tooth) type arrangement accommodates radial thermal expansion differences and supports the axial loading required to keep the fixture pressed against the end member. This concept is illustrated on the left-hand view of Figure 60.

On the opposite end of the bore seal (axial expansion compansating end), a similar support fixture arrangement is used. In order to accommodate both radial and axial differential expansion between the seal and stator frame, two separate support fixtures (with curvic-type couplings) are used. One fixture provides radial support for the bellows-type metal end-member, and the other supports the ceramic bore seal ends that carry the axial loading. Besides providing support to reduce the stress in a fairly flexible arrangement, the use of this bore seal support arrangement will allow an increase in the thickness of the ceramic bore seal, because the radial teeth and positive support points provide accurate alignment of the bore seal relative to the stator. In their absence, the bore seal could conceivably

TABLE 64

KTA BORE SEAL END-MEMBER STUDY (DRIVE END)

No.	Configuration	Maximum Stress, psi	Location
1	Trial run to test program input		
2	Semitoroidal, to inside - 1-in. rad	604,472	E.M. - B.S. Jt.
3	1 cycle over lap bellows, to inside - 0.5-in. rad	3,847,084	E.M. - B.S. Jt.
4	1 cycle over lap bellows, to outside - 0.5-in. rad	260,978	E.M. - B.S. Jt.
5	2 - quarter toroids, back-to-back, to inside - 1-in. rad	105,225	E.M. - B.S. Jt.
6	2 - quarter toroids, back-to-back, to outside - 1-in. rad	48,169	E.M. - End Bell Jt.
7	2 - quarter toroids, butt reverse together, to inside - 1-in. rad	71,227	E.M. - End Bell Jt.
8	2 - quarter toroids, butt reverse together, with straight section between to inside - 1-in. rad	88,551	E.M. - End Bell Jt.
9	2 - quarter toroids, butt reverse together, to outside - 1-in. rad	133,239	E.M. - B.S. Jt.
10	30° conical section, to inside - 1.5 in. lg., 0.5-in. rad bends	52,907	E.M. - B.S. Jt.
11	15° conical section, to inside - 1.5 in. lg., 0.5-in. rad bends	70,597	E.M. - B.S. Jt.
12	45° conical section, to inside - 1.5 in. lg., 0.5-in. rad bends	524,283	E.M. - End Bell Jt.
13	30° conical section, to inside - 1 in. lg., 0.5-in. rad bends	30,863	E.M. - B.S. Jt.
14	30° conical section, to inside - 0.5 in. lg., 0.5-in. rad bends	28,891	E.M. - B.S. Jt.
15	30° conical section, to inside - 0.5 in. lg., 0.5- and 0.1-in. bends	233,427	E.M. - End Bell Jt.
16	30° conical section, to inside - 0.5 in. lg., 0.5-in. rad bends	89,842	E.M. - End Bell Jt.
17	30° conical section, to inside - 0.5 in. lg., 0.1-in. rad bends	61,116	E.M. - End Bell Jt.
18	3/4 cycle deep bellows section - 1 in. deep, 0.25-in. rad bend	473,274	In Bend
19	15° conical section, to outside - 0.5 in. lg. midsect., 0.5-in. rad bends	49,280	E.M. - End Bell Jt.
20	15° conical section, to outside - 1 in. lg. midsect., 0.5-in. rad bends	100,350	E.M. - End Bell Jt.
21	15° conical section, to outside - 0.25 in. lg. midsect., 0.5-in. rad bends	37,315	E.M. - End Bell Jt.
22	15° conical section, to outside - 0.0-in. lg. midsect., 0.5-in. rad bends	65,171	E.M. - B.S. Jt.
23	Quarter toroid, to inside - 1-in. rad	86,245	E.M. - End Bell Jt.
24	30° conical section, to outside - 0.5-in. rad bends, 0.5 in. lg. midsect.	43,238	E.M. - End Bell Jt.
25	30° conical section, to outside - 0.5-in. rad bends, 0.5 in. lg. midsect.	85,484	E.M. - End Bell Jt.
26	2 - quarter toroids butt together (reverse), to inside - 1-in. rad bends	524,644	E.M. - B.S. Jt.
27	30° conical sect., to outside - 0.5-in. rad bends, 0.5 in. lg. midsect.	70,605	E.M. - End Bell Jt.
28	45° conical sect., to outside - 0.5-in. rad bends, 0.5 in. lg. midsect.	80,173	E.M. - End Bell Jt.
29	30° conical sect., to inside - 0.5-in. rad bends, 0.5 in. lg. midsect.	76,993	E.M. - End Bell Jt.
30	30° conical sect., to inside - 0.5-in. rad bends, 0.75 in. lg. midsect.	111,354	E.M. - End Bell Jt.
31	15° conical sect., to outside - 1-in. rad bends, 0.0 in. lg. midsect.	37,258	E.M. - End Bell Jt.

Nomenclature:

 ≡ butt-type joint, outward and inward, respectively

 ≡ sandwich-type joint, outward and inward, respectively

E.M. - B.S. Jt.* = stress occurs in end member at bore seal joint (not in joint itself but just outside)

E.M. - End Bell Jt.* = stress occurs in end member at joint where it attached to the end bell

*NOTE: Because of stress concentrations, the maximum stresses nearly always occurred at one of these two locations.

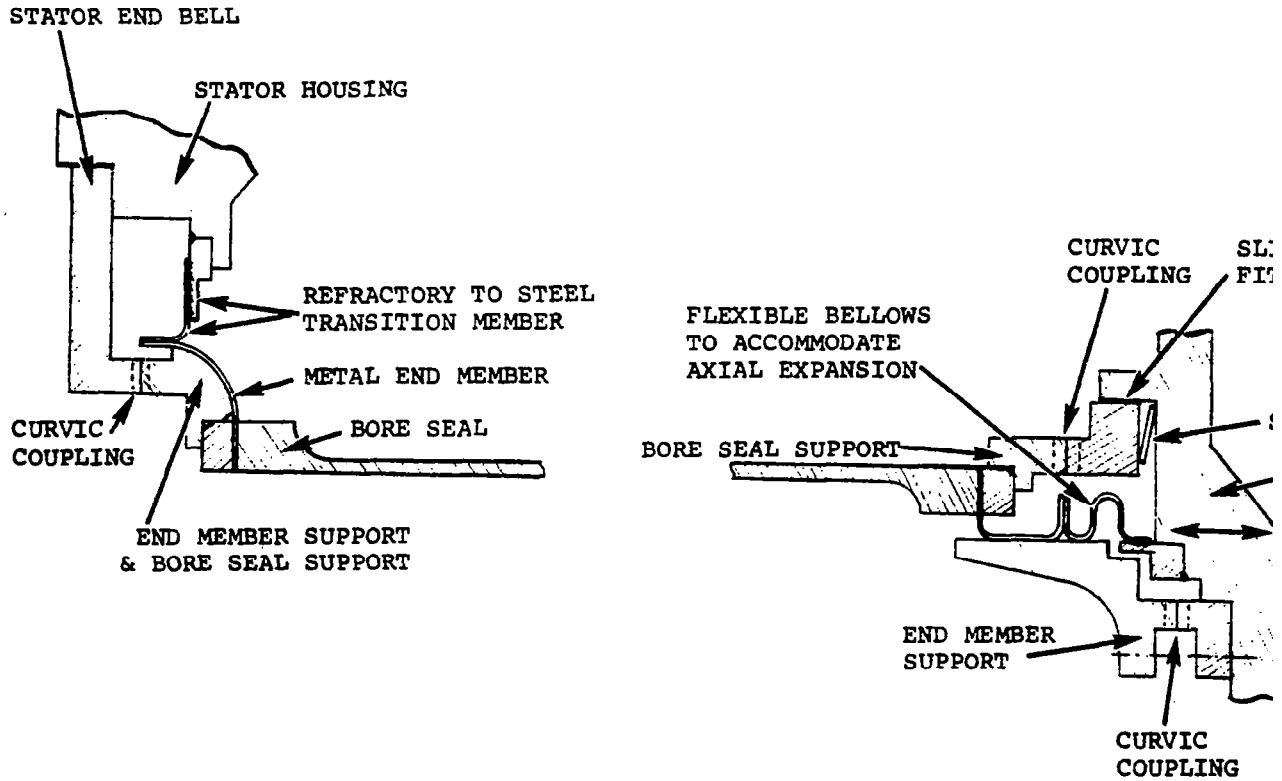

PROPOSED BORE SEAL END MEMBER CONFIGURATIONS

FIGURE 60

become cocked*, and more assembly tolerance build-up allowances would have to be allowed in the air gap.

As the concepts illustrated on Figure 60 were conceived late in Phase I studies and as it was felt additional refinements could be conceived with continued study in Phase II, detailed stress analyses were not conducted on the configuration. The reader is referred to Volume III of this report for the latest configuration and resulting stresses.

*The bore seal is assembled in a loose fit in the bore at room temperature, and due to differential (radial) thermal expansion, becomes even more loose at operating temperatures.

5. CONCEPTUAL DESIGNS

There were three conceptual designs made from the three Base Designs discussed in Section 3. Recall that the three base designs were selected from elimination and optimization screening studies. The base designs were then subjected to further detailed analysis to seek more refined designs. These latter designs constitute the Conceptual Designs.

5.1 Conceptual Design Layouts

Because the basic design features of the three conceptual designs are similar in many respects, one discussion will be given for the three. Differences between the three will be identified. The three layouts are illustrated on Figures 61 through 63.

The significant features of the alternator electrical designs are found in the rotor and stator configurations. The remaining components that make up the complete generators are considered work-horse parts relative to the electrical designs and were not optimized in the Phase I studies except the rotating shaft seal and stub shaft configurations.

The stators are hermetically sealed to permit operation without subjecting the stator components to corrosion damage by either air or moisture external to the generator or by potassium vapor of the rotor cavity. The bore seal in the radial gaps between the rotors and stators is high purity aluminum oxide. The stator magnetic frames consist of the iron-cobalt magnetic alloy, Hiperco-27. Electrical conductors are of Inconel-clad silver and insulated with Anadur (glass fibers). The rotor is composed of solid forgings of high-strength H-11 steel. Electrical power is taken out of the generators through bus rings and terminals located on the anti-drive ends.

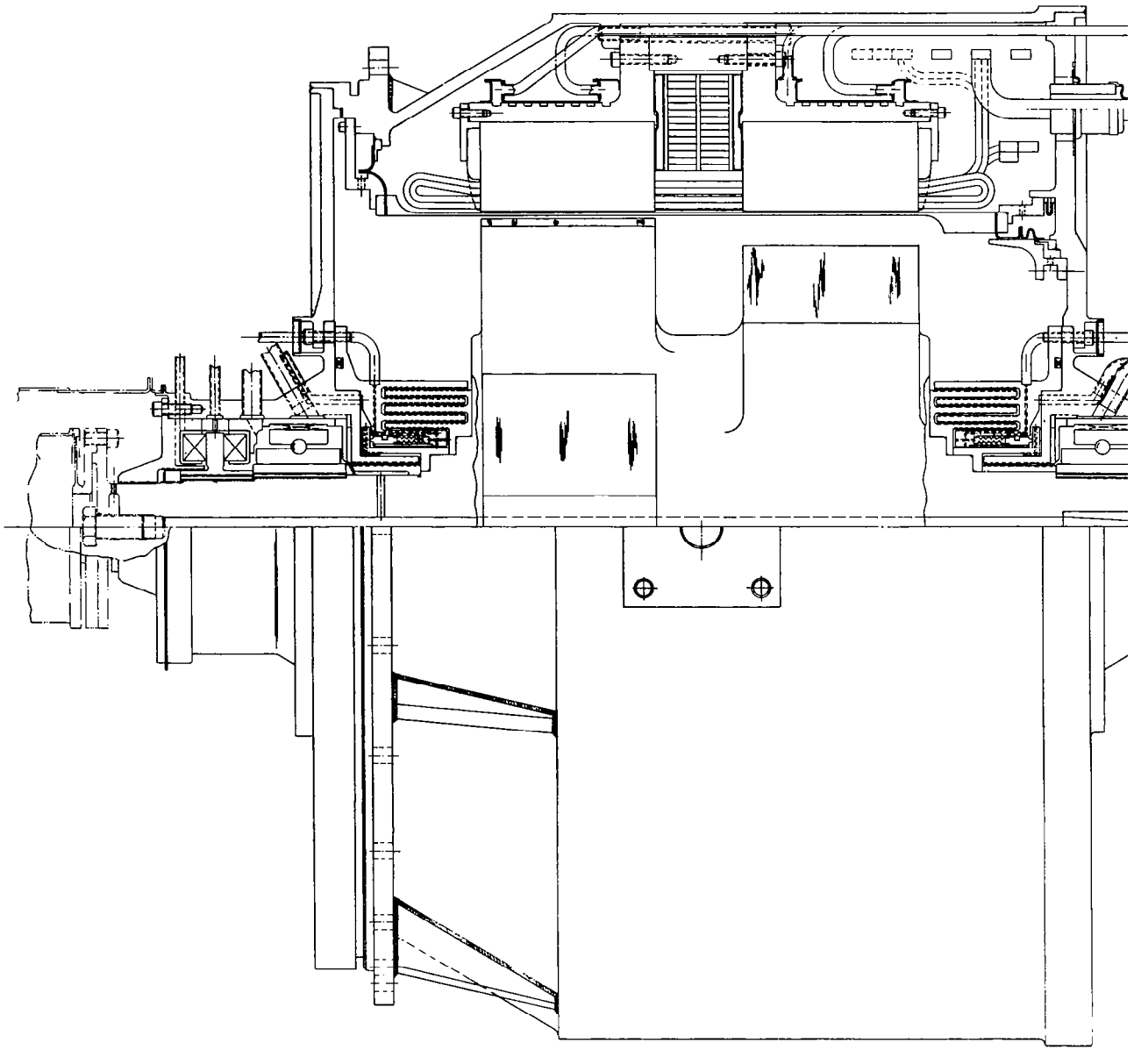

CONCEPTUAL DESIGN LAYOUT, 19,200 RPM, 800°F COOLANT

FIGURE 61

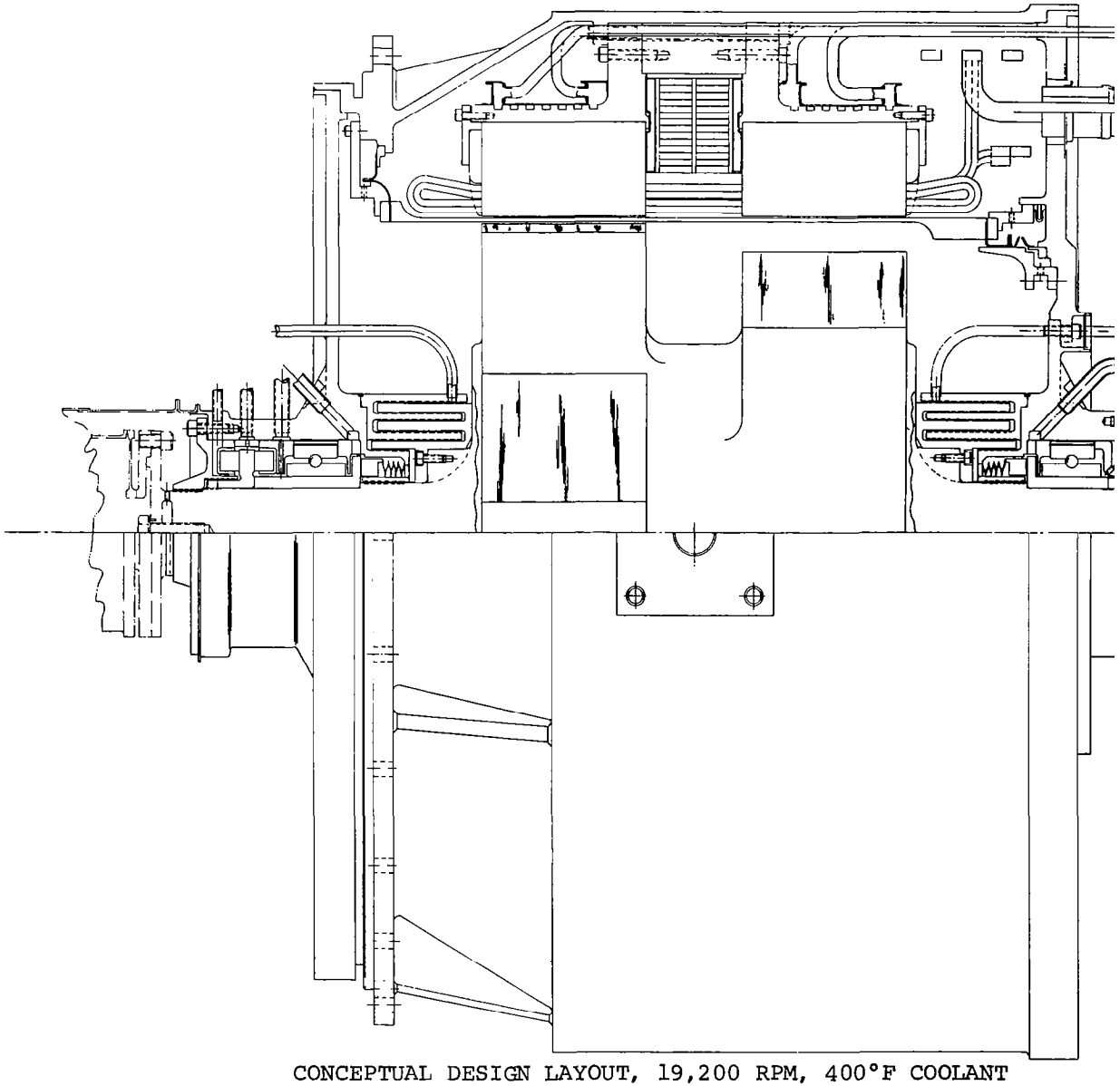

CONCEPTUAL DESIGN LAYOUT, 19,200 RPM, 400°F COOLANT

FIGURE 62

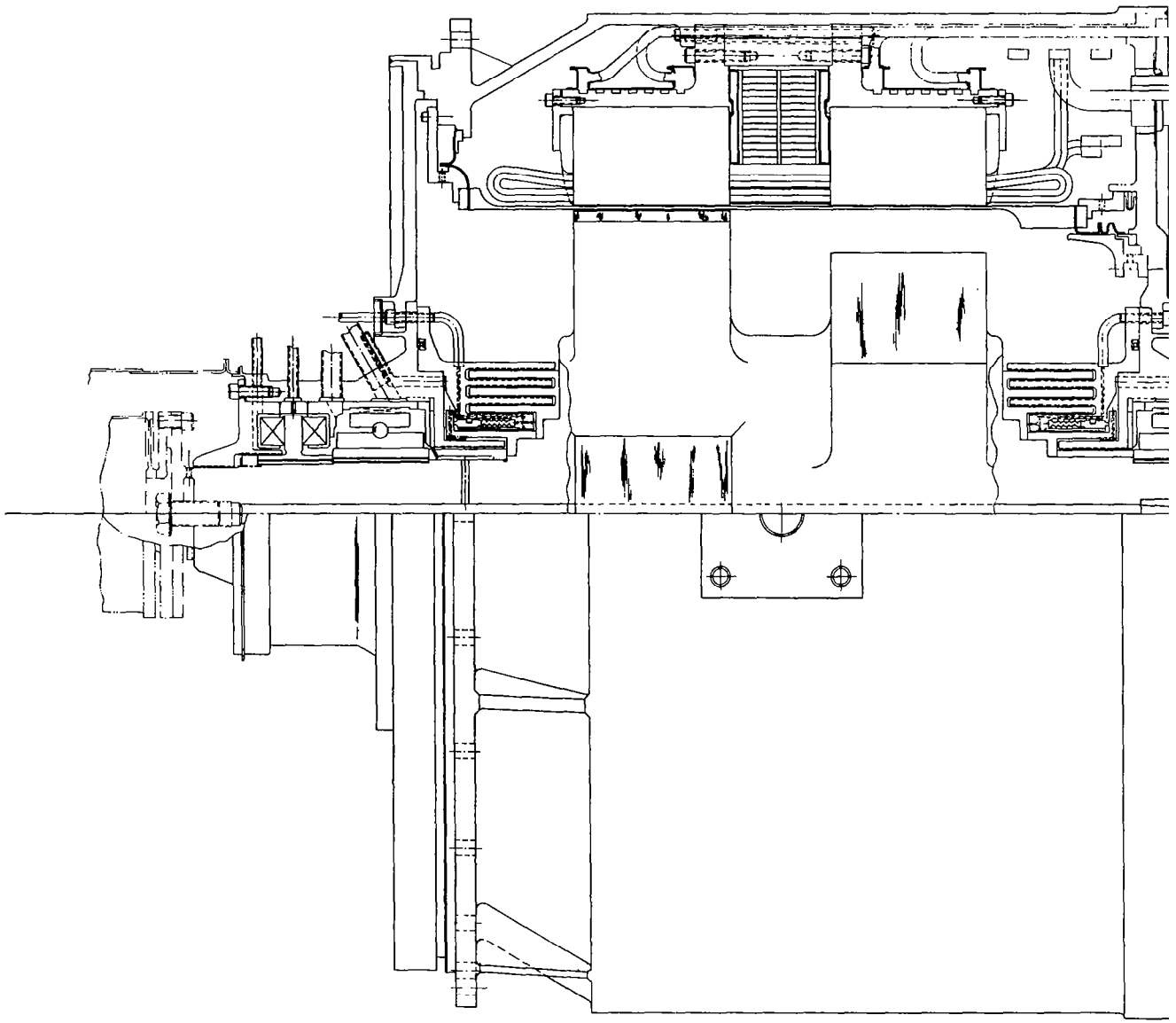

CONCEPTUAL DESIGN LAYOUT, 24,000 RPM, 800°F COOLAN'

FIGURE 63

Stator coolant enters and leaves through toroidal-shaped manifolds located on the stator frame outside diameter. The manifolds are bonded directly to the stator frame.

Rotor coolant enters the antidrive end and discharges out the drive end with the drive-end bearing lubricant. A special rotor-cavity scavenge system is included as part of each rotor flow circuit. The one exception to this is the 400°F coolant organic design where cooling is through the stub shafts. None goes through the rotor as discussed in Section 4.2; the pole tips are laminated to minimize losses. Features of the rotor pole tip design are discussed fully in Section 4.2.

Pivoted-pad journal bearings support the rotors. The bearing lubricant is separated from the rotor cavities by noncontact viscosity screw-pump seals (viscoseals). The rotor cavities are further isolated by molecular vacuum pumps between the viscoseals and rotor cavity. Some further comments on the seal designs are warranted at this time because two alternative sealing arrangements are being proposed for the oil cooled/lubricated alternator with rotor cavity vented to space.

The flow of lubricant from the alternator bearing compartments is prevented by using noncontacting, pressure-generating, screw seals. An inherent problem with this type of seal is that no sealing can be provided at zero or very low speed. To overcome this problem, it is necessary to incorporate some sort of contact seal with lift-off provisions.

A combined version of a contact seal and a noncontacting, pressure-generating seal arrangement proposed by Westinghouse for the potassium-lubricated and the oil-lubricated designs is shown in Figure 64. This sketch is for the antidrive end of the alternator,

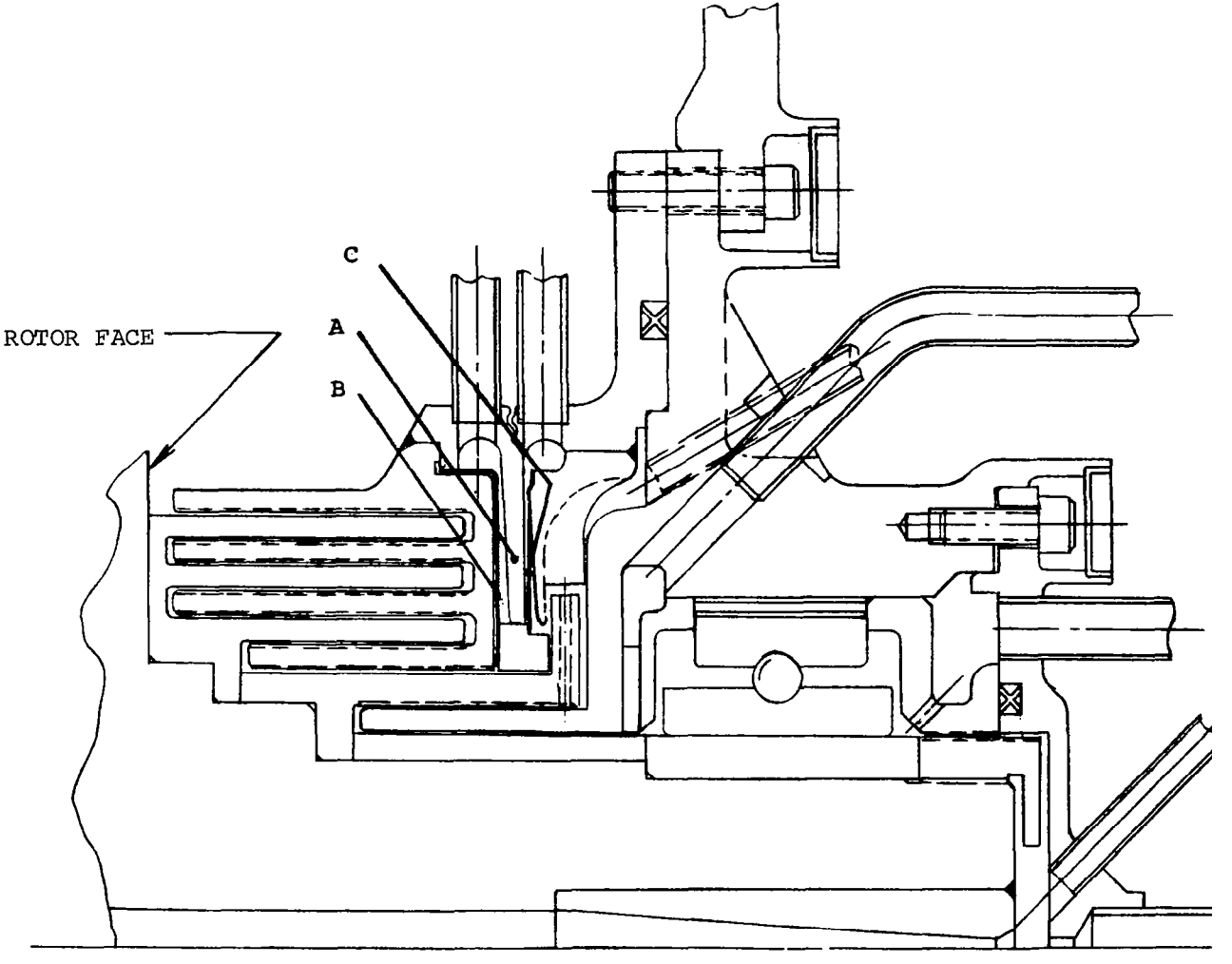

BEARING AND SEAL ARRANGEMENT INCORPORATING
HYDROSTATIC LIFT-OFF SEAL

FIGURE 64

but the "mirror image" of the seal arrangement is used on the drive end. The sealing arrangement incorporates a hydrostatic lift-off contact seal. The contact seal consists of a pressure divider, (A), between two diaphragms, (B) and (C), which move the nosepiece. The ON and OFF positions of the nosepiece are maintained hydrostatically by venting one of the chambers to a high-pressure source and the opposite chamber to low-pressure source of the working fluid. Leakage between the two chambers is minimized by using a close-clearance seal between the pressure divider and the nosepiece. The nosepiece will be in the ON position only when the bearings compartments are flooded with liquid and when the shaft speed is 3000 rpm or less. At 3000 rpm, the sliding velocity of the seal will be approximately 52 ft/sec, which is well within operating limits for this type of seal for several start-ups and shutdowns.

Sealing of liquid from the bearing compartments into the vapor seals and rotor cavity after the initial acceleration of the rotor can be easily achieved with this combination of seals. At 50-percent operating speed of the alternator, only 60-percent engagement of the first stages of the screw seals is required to generate a back pressure of 24 psia which means that 40 percent of the primary seals will be available to scavenge any liquid which may break away from the interface.

The hydrostatic lift-off contact seal shown in Figures 61 and 63 utilizes a double-bellows arrangement instead of the two-diaphragm arrangement described above. The design utilizing the diaphragms is the preferred design, and the double bellows arrangment is an alternate. The diaphragm arrangement is not shown in these two because it was evolved after completion of the conceptual design layouts.

Another solution is to incorporate a face contact seal which has a hydrodynamic lift-off feature. This type of seal has been under investigation and development at the NASA Lewis Research Center.

A version of a contact seal with a hydrodynamic lift-off feature applied to the alternator is shown in Figure 65. The seal configuration consists of a rotating seal seat, (A), and a nosepiece, (B). The nosepiece has a series of spiral grooves which pump the liquid downward, a conventional contact seal dam, and a series of spiral grooves which pump the liquid outward. The sliding dam on the nosepiece is forced against the seal seat by a spring force when the rotor is not rotating and during the initial acceleration. The action of the spiral grooves pumps the liquid inward at start-up and generates a hydrodynamic force which separates the sliding surfaces. It is postulated that the pressure gradient generated by the spiral grooves which pump the liquid inward will more than offset the pressure gradient due to the centrifugal force on the liquid.

An essential part of the hydrodynamic, lift-off seal arrangement is the bellows, (C), which provides a seal between the high- and low-pressure regions. This bellows allows the nosepiece to follow the seal seat when the rotor moves axially and also permits the required relative motion between the nosepiece and the seat.

It is very likely that drops of liquid from the interface will migrate toward the center. Therefore, a short length screw seal, (D), shall be used to back-up the spiral groove seal.

The NASA-type, hydrodynamic lift-off seal was specified by AiResearch for application in the KTA designs for the vented-to-space oil lubricated turbine and alternator. Therefore, this type of contact seal was shown in the conceptual layout of the oil cooled/lubricated alternator (Figure 62). However, it is believed by

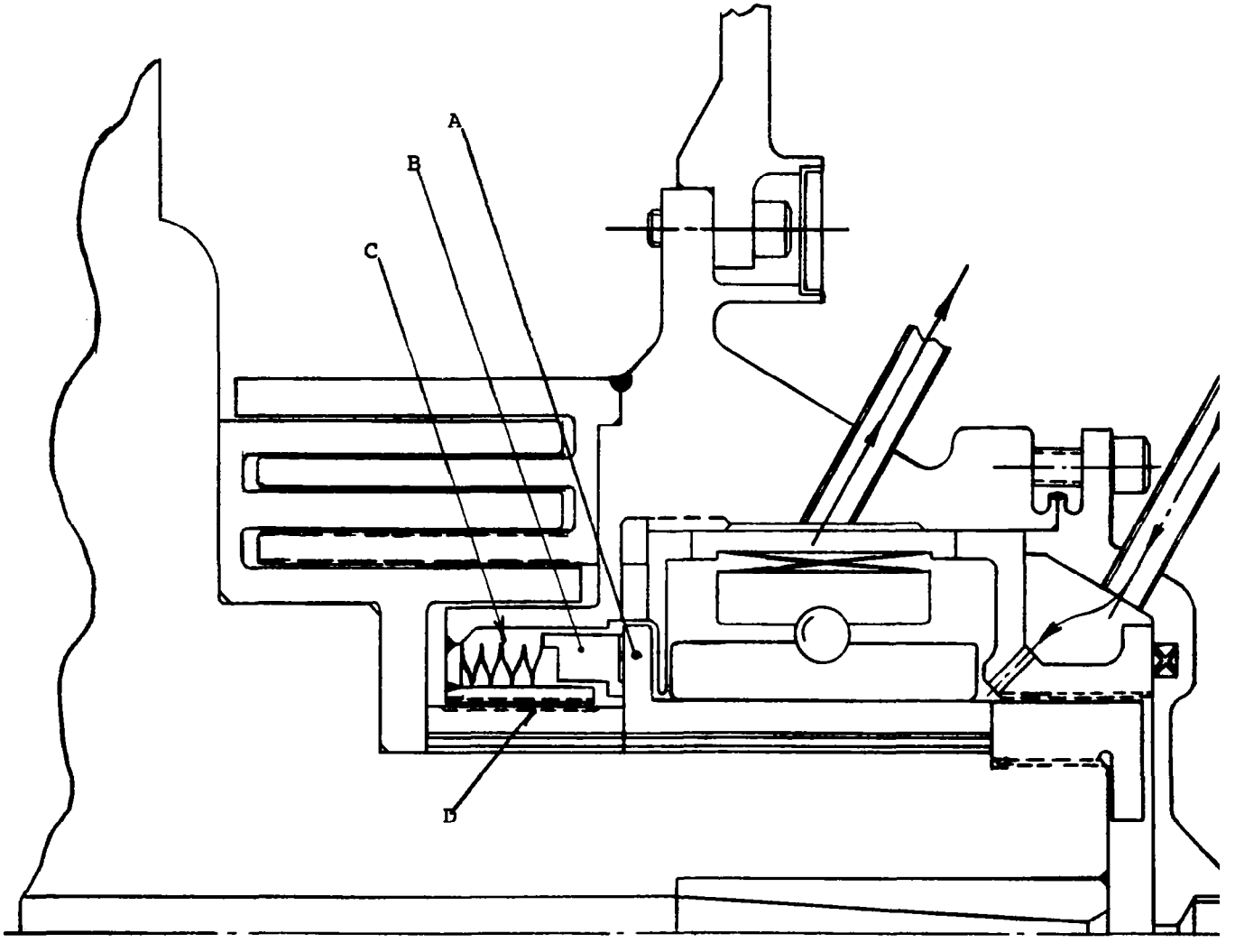

BEARING AND SEAL ARRANGEMENT INCORPORATING
HYDRODYNAMIC LIFT-OFF SEAL

FIGURE 65

Westinghouse that the NASA-type, hydrodynamic lift-off face seal should not be considered as the primary, unquestionable choice for several reasons, primarily because the seal has not been fully developed. In particular, the performance has not been demonstrated under the more strenuous design conditions applicable to the KTA. Its final selection should first be left to further development and demonstration of satisfactory performance in all respects under design conditions applicable to the KTA. The conclusions above are based upon the summary list of advantages and disadvantages of the two types of face seal concepts presented in Table 65.

On the illustrations, a drive-end shaft seal-to-space is not shown. All that is required is a low-leakage barrier or seal to separate the generator bearings from the turbine bearings. The two bearing cavities would be connected by a hermetic shroud. The actual turbine and alternator frames would be connected by a cold-frame fixture.

The outer mounting flanges, which double as the hermetic shrouds for the alternators, act as the support structure. The full weight of each generator is carried through two center-of-gravity mounting pads, one on each side at the horizontal centerline.

One of the features of the generators is the disassembly capability. Breaking the bolted joint on the antidrive end bell and the top weld joint on the drive end bell is all that is required to permit removal of the stator assembly intact, complete with bore seal, terminals, and cooling ducts. This feature is included to permit, if necessary, complete separation of the potassium-exposed rotor cavity from the stator cavity prior to breaking any of the hermetic (potassium-exposed) seals separating them.

TABLE 65

COMPARISON OF HYDROSTATIC AND HYDRODYNAMIC FACE SEALS

Hydrodynamic Lift-Off Seal	Hydrostatic Lift-Off Seal
Advantages	Advantages
1. Functions as a contact seal at very low speeds and as a non-contacting, pressure-generating seal after hydrodynamic forces generate a gap between the seal seat and nosepiece above some minimum speed; therefore, the seal is self-acting and does not require any external equipment for control of the nosepiece.	1. Sliding contract surfaces are only used for sealing during start-up and shutdown.
2. Start-up and shutdown can be easily accomplished without leakage of bearing lubricant into the vapor seals or rotor cavity.	2. Hydrodynamic forces and those generated by the motion of the rotor are not present after the seal is in the lift-off position. Thus, fatigue failure of the flexible parts is not a critical design problem.
Disadvantages	3. The sliding contact surfaces only have to follow the seal seat during start-up and shutdown. Thus, critical speeds and shaft deflection will not be a design problem for these seals.
1. The stability of the seal can only be postulated since little, if any, experimental data exists on this arrangement of spiral grooves at KTA-design conditions.	Disadvantage
2. The force balance upon the nosepiece depends upon a bellows-type seal on the pressurized side of the seal. A failure of the seal will produce a pressure-loaded nosepiece and rubbing contact.	1. External equipment is required to operate and control the position of the nosepiece.
3. The force balance upon the nosepiece depends upon the hydrodynamic forces produced by the spiral grooves, and any wear patterns on the seal seat or nosepiece which effect the parts can cause rubbing contact.	
4. Is an integral part of the complete seal system; therefore, this seal must be designed for long life with high reliability regardless of the fact that it only serves a critical function during start-up and shutdown. Critical speeds and shaft deflection must be considered in the design.	

The required number of field coil ampere-turns may be obtained by either a large number of low-current turns or a few large-current turns. The choice is dependent on a number of factors such as voltage regulator exciter (VRE) requirements, heat-transfer, material availability, fabrication requirements, etc. A design using a large number of turns is easiest to fabricate but difficult to cool. The latter reason led to the choice of a few straps rolled one on top of the other. The number of turns will be dependent upon the VRE requirements but is presently estimated at about 50. Heat is carried out of the straps on each side where thermal contact is made with the cooling ducts. Center spacers between the straps separate the two bundles. Dimensional fabrication tolerance build-up is accomplished by forcing the two bundles outward onto the cooling ducts by the use of the center spacers. Interlaminar electrical insulation separates the strap layers.

The stator punchings are 0.004-in-thick Hiperco-27 magnetic alloy, have a semiclosed slot to reduce pole face losses, and are assembled into an unwelded stack to reduce iron losses. A 0.0004-in.-thick layer(s) (total) of plasma arc sprayed alumina constitutes the interlaminar insulation. The block of materials shown on the ends of the stacks are to hold and align the unwelded stacks and to prevent the 0.004-in.-thick teeth from flaring. The BeO ceramic heat-sink between the stacks (over the armature wires, beneath the field coil ID) acts as a spacer to serve the same function between the stacks. The punching diameter is about 20 in. for the three designs which is about 5 in. over the allowable width for rolling 0.004-in.-thick Hiperco-27 on a regular commercial basis; thus, special rolling will be required for procurement of the material.

There are four to six bus rings on the antidrive end of each generator; three are for line connections, and one to three are for neutral connections to the phases. The parallel phase groups of the

armature are connected to each bus-ring in such a manner that bus ring copper losses are held to a minimum which, in turn, permit the rings to be cooled by radiation to the stator cavity walls. The maximum bus ring temperature can be expected to be less than 1000°F with an 800°F sink-temperature on the end-bell wall. The one to three neutrals are shown depending on the final design requirements.

There is one terminal per bus-ring located so that each carries not more than 2000 amp full-load current. Because of the temperatures brought on by the high current densities and the limited space available, standard terminal feed-throughs cannot be used. Special terminal studs are required.

The conductors through the terminal feed-throughs are sized to have sufficient cross-sectional area to permit them to be self-cooled by radiation and/or natural convection. They are nickel-plated and black-oxide-coated to obtain an emmissivity of at least 0.4 on the outer surface. Radiation cooling alone limits the conductor temperature to less than 1000°F at full-load current in an 800°F ambient.

One of the more vital components in the generator is the ceramic bore seal which separates the rotor cavity from the stator cavity. This separation is necessary because the stator components are incompatible with the potassium vapor in the rotor cavity. Since the bore seal is in a continuing state of development, the bore seal design for the conceptual design generators was not finalized; each design must be treated individually when complete operating/fabrication conditions are specified or known. The configuration shown is that previously discussed in Section 4.3.

The bore seal proposed for 800°F coolant generators is a 99.8 percent pure alumina cylinder with Cb-1Zr refractory alloy metal end-members. Since the bore seal will most likely be hermetically joined

to nonrefractory material in the generator, the use of refractory end members requires that an equally sound transition joint also be provided. Seal-weld joints are made during final assembly by electron-beam or TIG welding. The various states of these bore seal concepts are summarized in Appendix A of Reference 2.

In addition to alleviating the bore seal end-member design problems, the proposed bore seal end-member configuration permits more accurate control of the alignment of the bore seal in the radial gap. The net effect of this is that less radial gap is required for assembly tolerances and then (1) the gap may be decreased, (2) the rotor may be allowed to creep more, or (3) the bore seal may be thickened.

The thicknesses required for the alternator bore seals were determined to be greater than the minimum thicknesses that could be fabricated. In other words, the minimum permissible bore seal thickness is greater than the possible minimum; therefore, fabrication development problems should be reduced somewhat so far as bore seal thickness goes. Because the brazing alloy in the joints might be one of the active-metal alloys containing beryllium (Reference 2, Appendix A), there may be a limit to the size of the bore seal that can be brazed with presently available brazing facilities. The reader is referred to Reference 18 for a more detail discussion of these design considerations.

One of the unique features of the alternators is the rotor cavity scavenge system. This system acts to clear the rotor cavity of liquid during start-up and keep it clear during operation. It is designed as an integral part of the generator shaft seal system and works automatically without external controls. Tests which demonstrated and verified the performance of the system were completed and are reported in detail in Appendix D of Reference 16.

The bearings furnished by AiResearch are pivoted-pad hydrodynamic journal bearings that use a spherical pivot to accommodate angular misalignment. See Section 3.0 of Volume I for the bearing discussion.

The vapor shaft seals are in the form of molecular vacuum pumps*. The liquid seals prevent liquid from escaping the bearing cavity whenever the seal pumping head becomes greater than the pressure between the bearing cavity and the rotor cavity. At that condition, there is established within the liquid seal, a liquid-to-saturated vapor interface through which only vapors can leak. These saturated vapors are prevented from entering the rotor cavity by the molecular pump vapor seals. The vapor seals accomplish this by pumping the rotor cavity down to a lower pressure so that the vapors must be super-heated at the temperature conditions found in the rotor cavity. Thus, any wet vapors from the liquid seal interface eventually passing into the rotor cavity will have become dry in the process. The performance of the vapor seals is illustrated in Figures 66 and 67. The analytical details of the molecular pump vapor seals are given in Appendix C.

A second more beneficial effect is derived from the reduced rotor cavity pressure achieved by the vapor seals; the windage losses are reduced as discussed in Section 4.2.

5.2 Conceptual Design Performance Data

The electrical performance data for the three conceptual designs is presented in Table 66. The efficiency is about 93 percent for all three designs at both the 450- and 550-kw_e rating. The efficiency includes the windage friction losses but does not include the bearing

*A molecular vacuum pump operates on the same principle as a diffusion pump except that the momentum is imparted to the molecules by a rotating cylinder rather than by a fluid. The configuration is that of a smooth shaft (or cylinder) running in a close-fitting (e.g., two to three times the bearing clearance), helical-threaded housing.

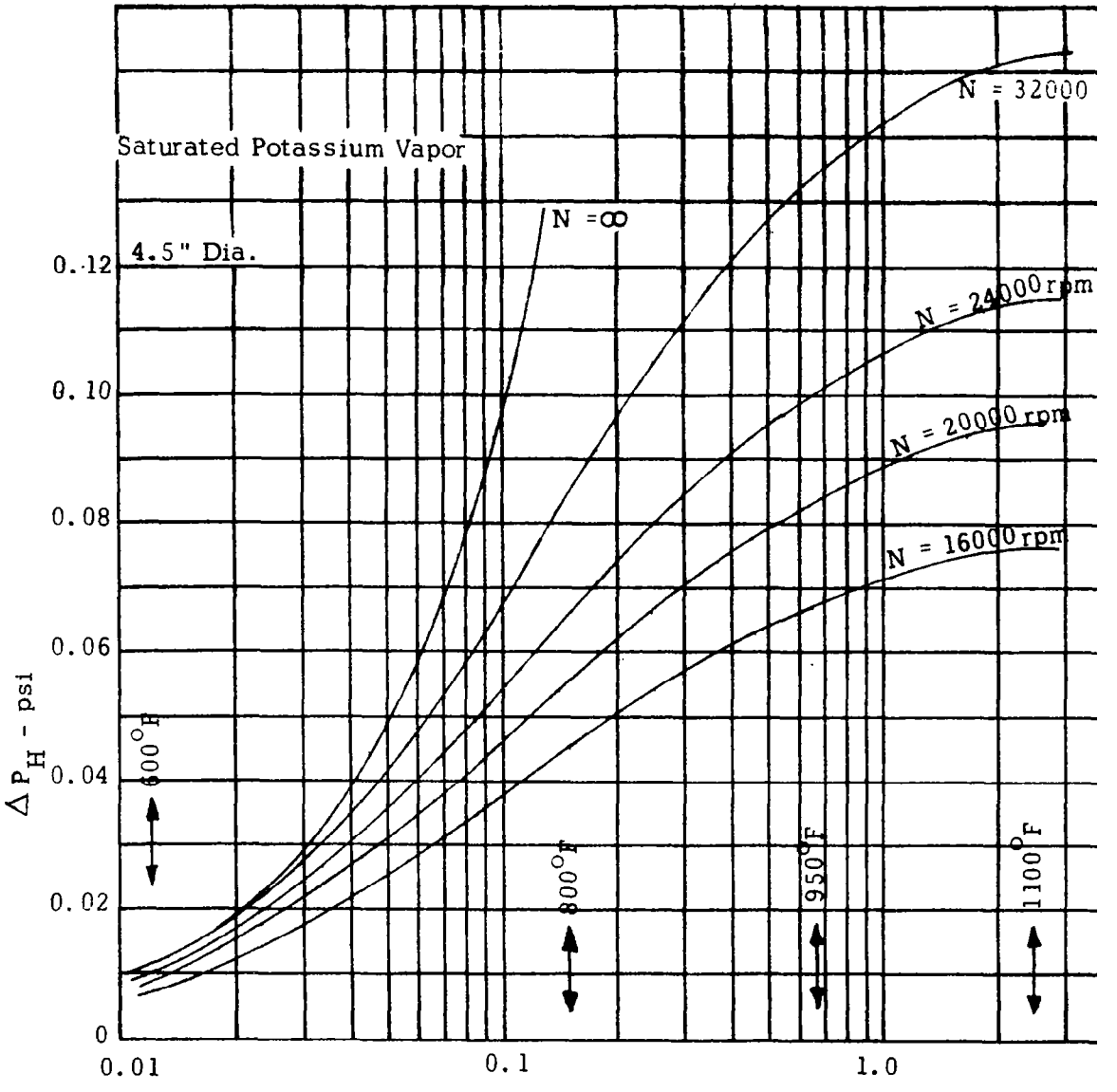

HOLWECK PUMP VAPOR SEAL TYPICAL PERFORMANCE

FIGURE 66

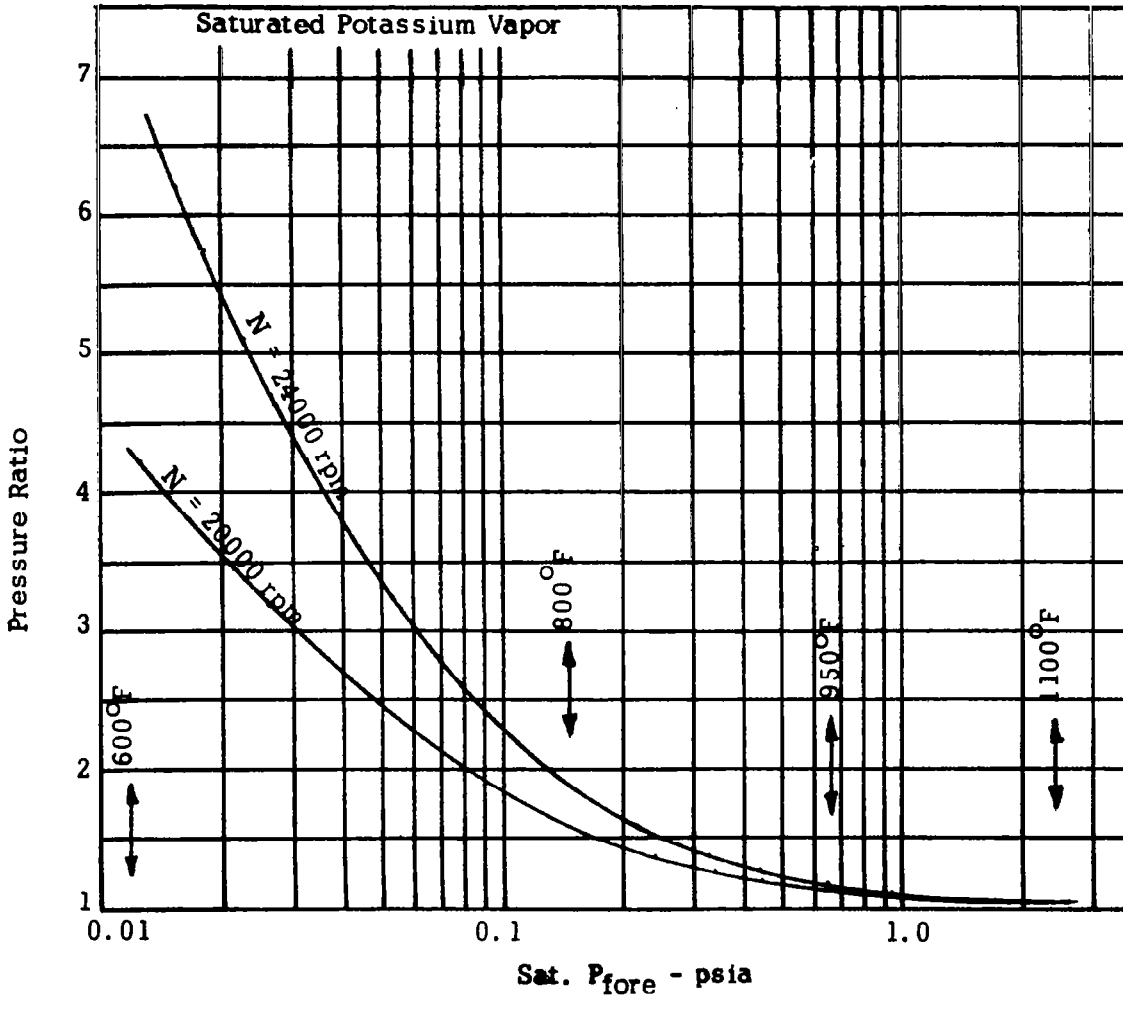

HOLWECK PUMP VAPOR SEAL TYPICAL PERFORMANCE

FIGURE 67

TABLE 66

ELECTRICAL PERFORMANCE OF CONCEPTUAL DESIGNS

	No. 1		No. 2		No. 3	
	450kw$_e$	550 kw$_e$	450kw$_e$	550 kw$_e$	450kw$_e$	550 kw$_e$
Speed, rpm	19200		19200		24000	
Frequency, Hz	1600		1600		1600	
Poles	10		10		8	
Coolant Temperature, °F	800		400		800	
Coolant/Lubricant	NaK & K		Mineral Oil		NaK & K	
Total Stator Losses, kw	35.06	44.45	37.59	46.15	32.85	41.91
Stator Iron Losses, kw	23.35	25.19	27.66	30.16	21.63	23.37
Armature Copper Losses, kw	8.72	14.78	7.72	12.68	8.25	14.09
Field Copper Losses, kw	2.99	4.47	2.21	3.31	2.97	4.45
Total Rotor Losses, kw	0.17	0.19	0.05	0.06	0.11	0.14
Pole Face Losses, kw	0.06	0.08	0.05	0.06	0.10	0.13
Windage Losses, kw	0.11	0.11	0.001	0.001*	0.01	0.01
Efficiency, %	92.70	92.50	92.28	92.25	93.18	93.00
Weights						
Electrical, lbs		837		777		701
Rotor (Without Stub Shafts), lb		352		304		274
Stator, lb		485		473		527
Total Weight (Exclusive of Bearings, Housings, Stub Shafts)		1200		1100		1000

*For cavity vented to space, windage is infinitesimal.

and seal friction losses. Likewise, the weights shown exclude the weights of the bearings, shaft seals, stub shafts, and bearing housings.

The difference between the total weights and the electrical weights given is deduced from the end-bells, frame housing, bus-rings, and terminals. The weights of these components were not minimized and are somewhat heavy as a result. They were left in a conceptual form for Phase I and will be minimized in Phase II.

The performance of the rotor design is presented in detail in Section 4.2 and will not be repeated here. The only additional consideration not previously covered is the overspeed capability of the various designs. It was determined the 19,200 rpm, 800°F rotor designs could operate for about 1 year at 20-percent overspeed. This is summarized in Table 67. The 24,000-rpm, 800°F-coolant case cannot operate over any period of time at 20-percent overspeed without excessive creep. The maximum stresses exceed the guidelines set forth at the start of the study (e.g., 72-percent yield strength), but they do not exceed the actual property data limitations. Thus, even if the 24,000-rpm rotor survived the initial short overspeed surge, it would still not survive for long. Note however, that plastic yielding may deform the rotor so that, even though the rotor may not have failed catastrophically, it must be considered failed and unsuitable for 3 to 5 years of normal life. The 400°F, 19,200-rpm design can run at 20-percent overspeed indefinitely.

The temperature distribution of the stator conceptual designs was based on the designs and studies of Section 4.3. The conceptual design stator cooling configuration selected from the parametric study consists of a circumferential manifold on the stator frame with cooling fins between the ac windings in the area between the stacks. Separate manifolds are included on the sides of the field coil.

TABLE 67

OVERSPEED

19,200 rpm, 800°F rotor

0.12% creep in 3 years at design speed

0.3 % creep in 5 years at design speed

0.6 % creep in 3 years at 20% overspeed

Conclude: Could operate at 20% overspeed for about 1 year.

TABLE 68

MAXIMUM TEMPERATURES OF CONCEPTUAL DESIGNS

	°F		
CONCEPTUAL DESIGNS	1	2	3
450 kw, 0.2 Slot Conductance	1024	724	1048
550 kw, 0.2 Slot conductance	1106	815	1144
550 kw, 0.1 Slot Conductance*	1112	-	-
550 kw, 0.05 Slot Conductance*	1119	-	-
550 kw, 0.01 Slot Conductance*	1162	-	-
550 kw, 0.002 Slot Conductance*	1276	-	-
550 kw, 0.2 Slot Conductance, 3Ø Short Circuit	1168	-	-
550 kw, 0.2 Slot conductance, Rotor Heating from Stator Included	1078	-	1111

*Reference Figure 81

Temperature distributions were made for the above cooling configurations as shown in Table 68 and Figures 68 through 80. The temperatures determined from the studies are highlighted in Table 69. Details of these studies follow.

The temperature distributions determined for the three conceptual designs at normal operating conditions of design power output (450 kw_e) and maximum continuous load rating (550 kw_e) with slot conductance of 0.2 $w/in.^2°C$ are shown on Figures 68 and 69 and Figures 76 through 79.

Temperature distributions presented in Figures 70 through 73 were prepared to determine the minimum slot conductance that does not result in excessive stator temperatures. These resulting maximum stator temperatures plotted against slot conductance are shown in Figure 81 from which the minimum slot conductance of 0.04 $w/in.^2°C$ was determined. This value of slot conductance is within the range of values that can be expected for the proposed slot configuration. These temperature distributions were determined for normal operating conditions at maximum continuous load rating (550 kw_e) of the Number 1 generator conceptual design.

Figure 74 presents the temperature distribution for 5 sec of three-phase short-circuit condition after steady-state conditions of normal operation at 550-kw_e load rating with 0.2 $w/in.^2°C$ slot conductance for No. 1 design. These data show a 62°F increase in the maximum stator temperature to 1168°F and indicate that for the lower coolant temperatures (400° and 800°F), the generator will meet the requirement of remaining operational after undergoing a three-phase short-circuit condition for 5 sec. Three-phase short-circuit condition temperature distributions were not prepared for No. 2 and 3 designs due to lack of time. In all of the above temperature distributions, all stator losses were rejected to the stator coolant by conduction and convection and to the end bells and housing by radiation from the end turns.

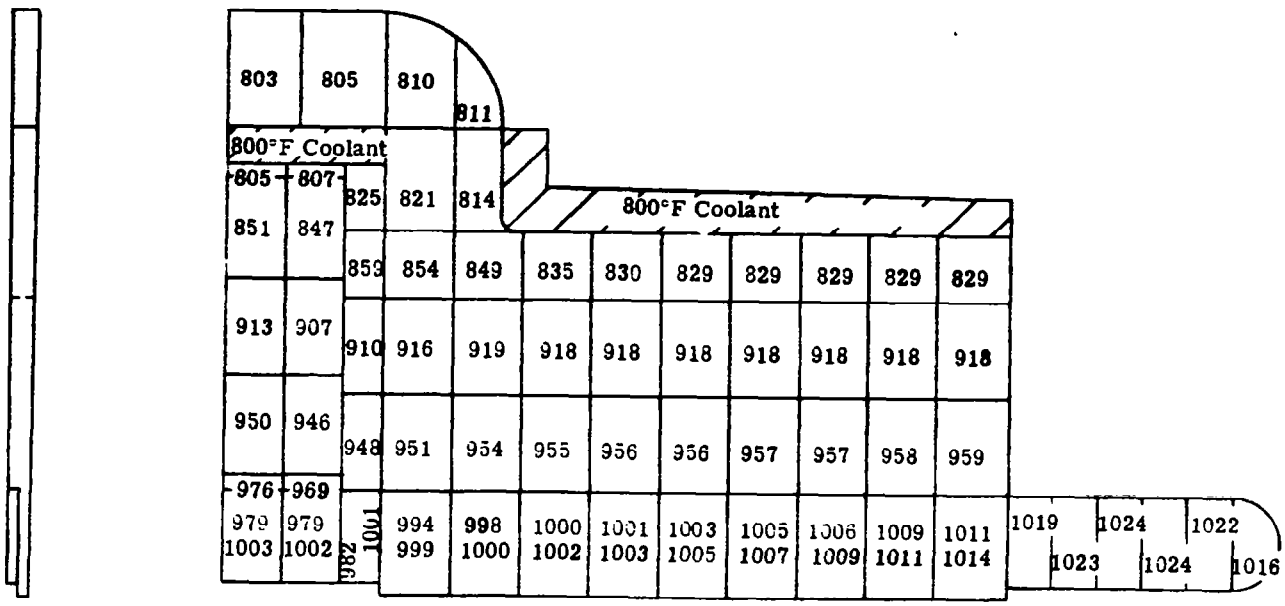

NUMBER 1 DESIGN STATOR TEMPERATURE DISTRIBUTION (°F)
450-KW_E RATING, 0.2 W/IN.^{2}°C SLOT CONDUCTANCE

FIGURE 68

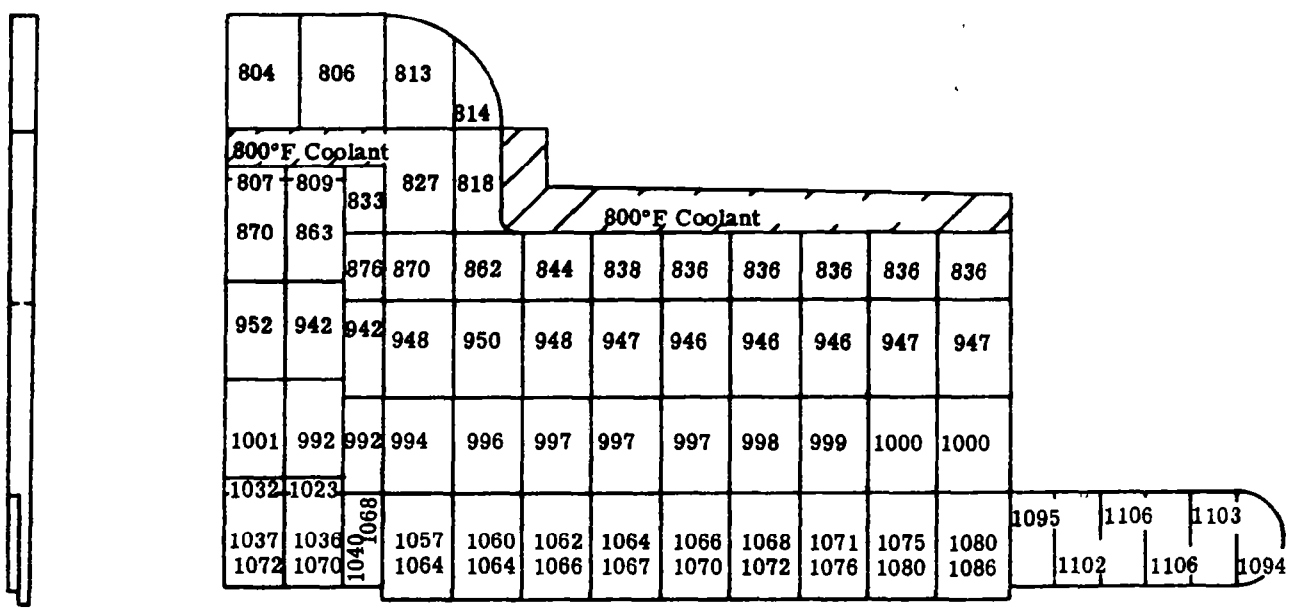

NUMBER 1 DESIGN STATOR TEMPERATURE DISTRIBUTION (°F)
550-KW_E RATING, 0.2 W/IN.^{2}°C SLOT CONDUCTANCE

FIGURE 69

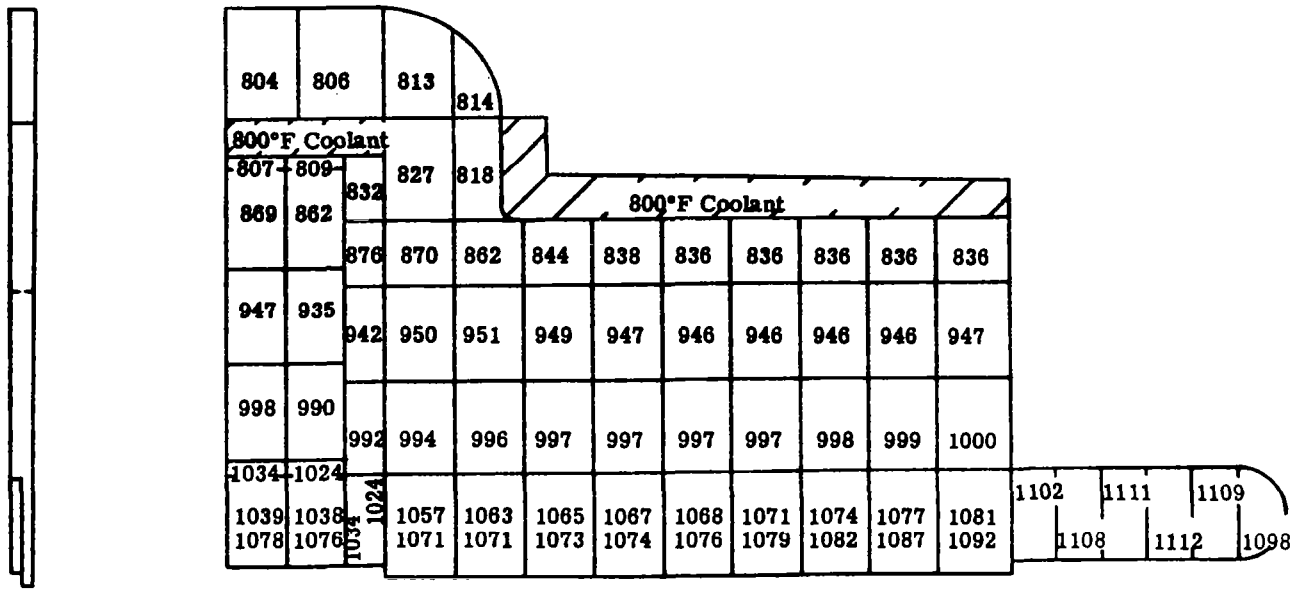

NUMBER 1 DESIGN STATOR TEMPERATURE DISTRIBUTION (°F)
550-KW_E RATING, 0.1 W/IN.^{2}°C SLOT CONDUCTANCE

FIGURE 70

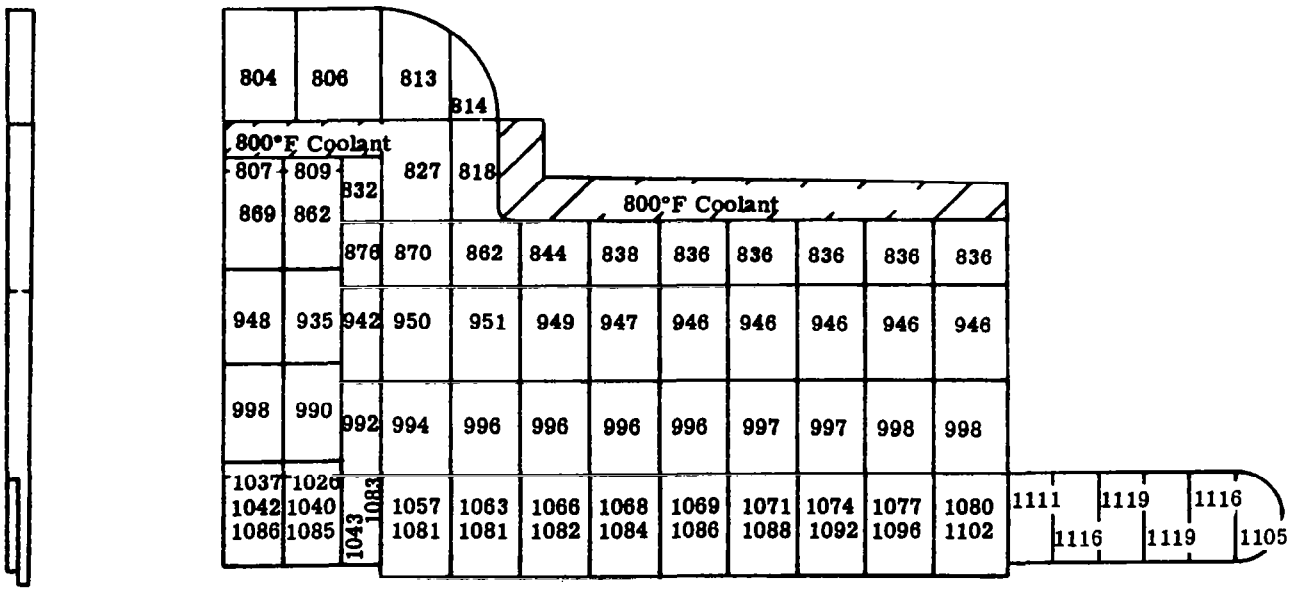

NUMBER 1 DESIGN STATOR TEMPERATURE DISTRIBUTION (°F)
550-KW_E RATING, 0.05 W/IN.^{2}°C SLOT CONDUCTANCE

FIGURE 71

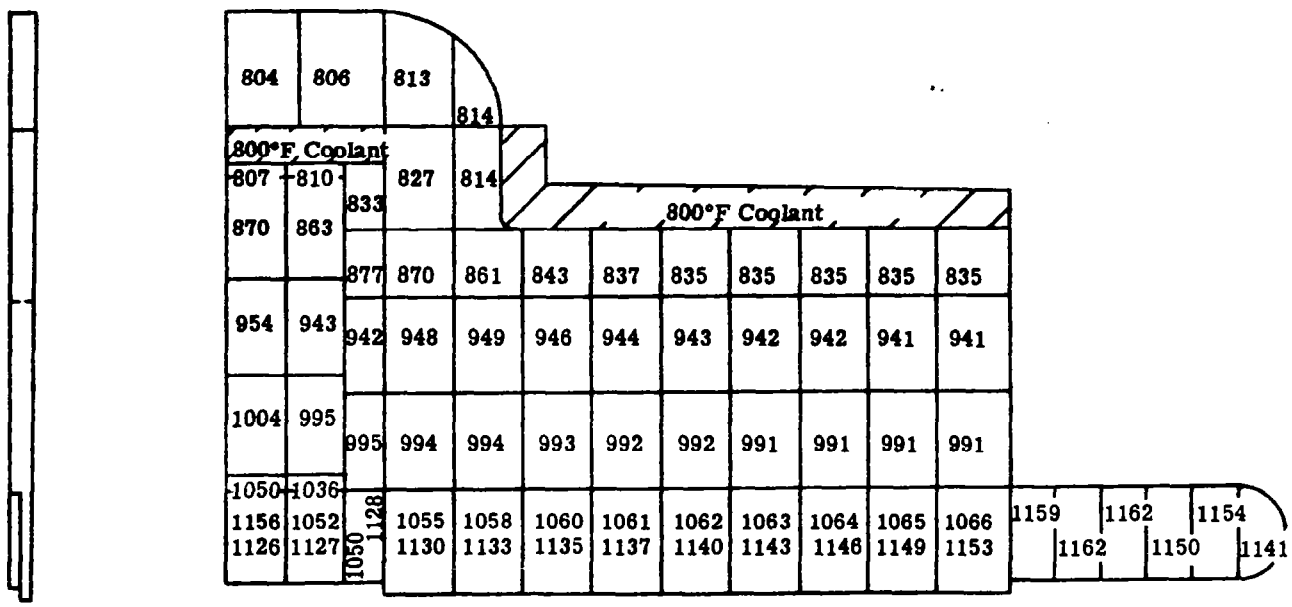

NUMBER 1 DESIGN STATOR TEMPERATURE DISTRIBUTION (°F)
550-KW_E RATING, 0.01 W/IN.^{2}°C SLOT CONDUCTANCE

FIGURE 72

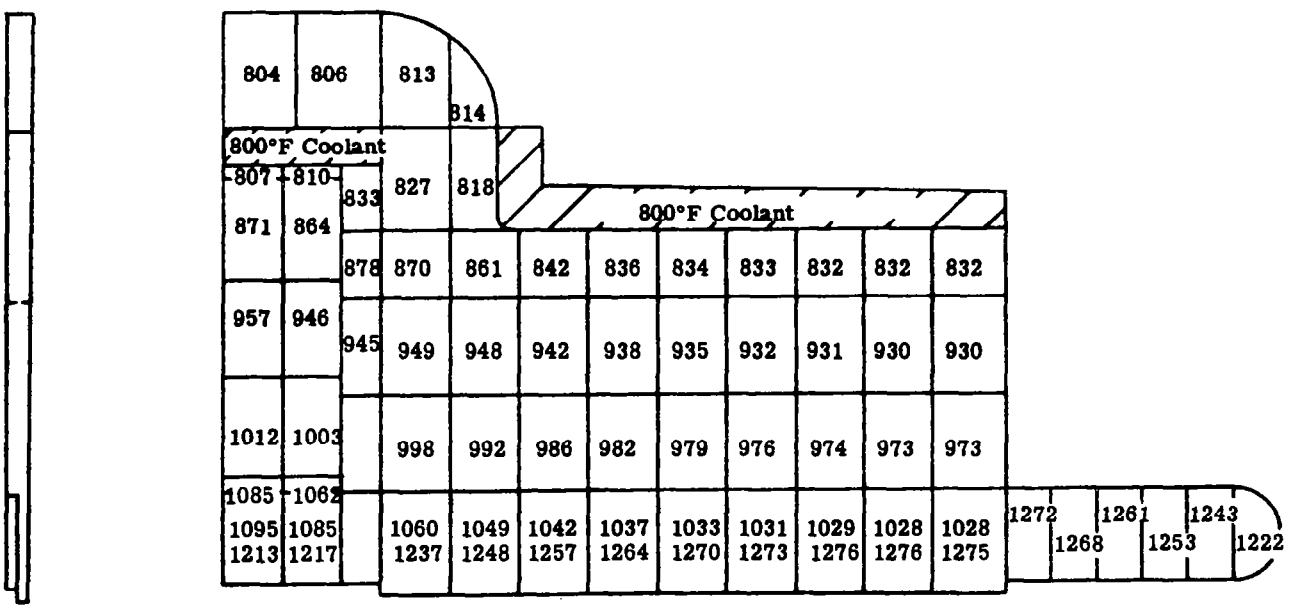

NUMBER 1 DESIGN STATOR TEMPERATURE DISTRIBUTION (°F)
550-KW_E RATING, 0.002 W/IN.^{2}°C SLOT CONDUCTANCE

FIGURE 73

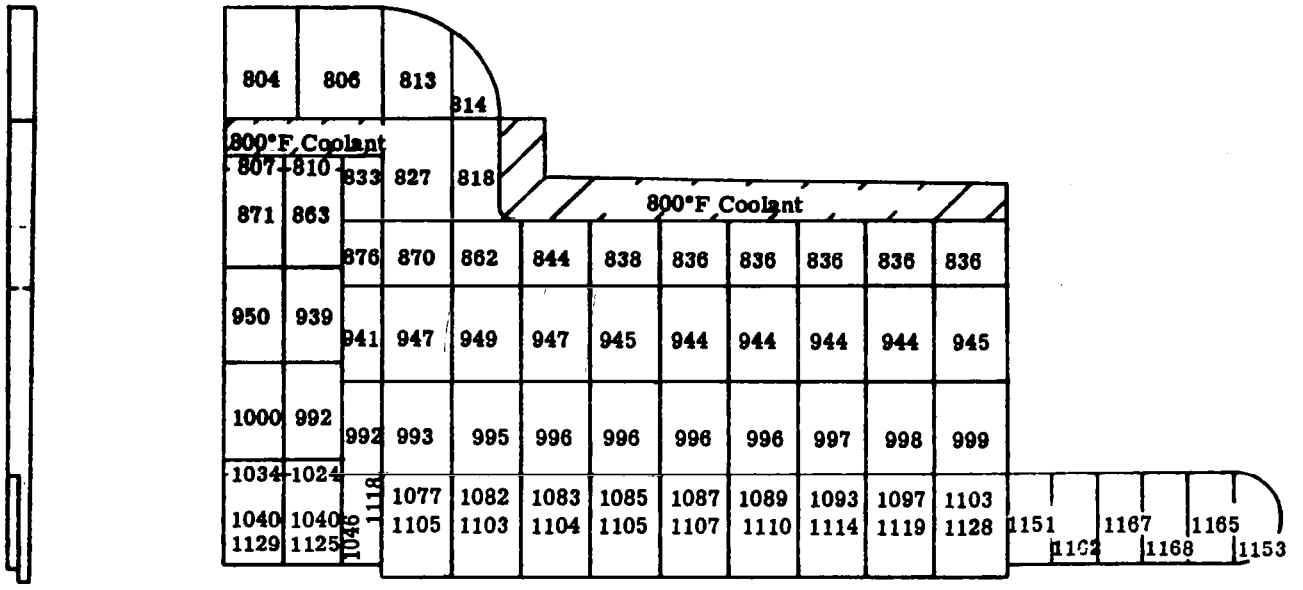

NUMBER 1 DESIGN STATOR TEMPERATURE DISTRIBUTION (°F) 550-KW_E RATING, 0.2 W/IN.^{2}°C SLOT CONDUCTANCE, FIVE SECONDS OF THREE-PHASE SHORT-CIRCUIT

FIGURE 74

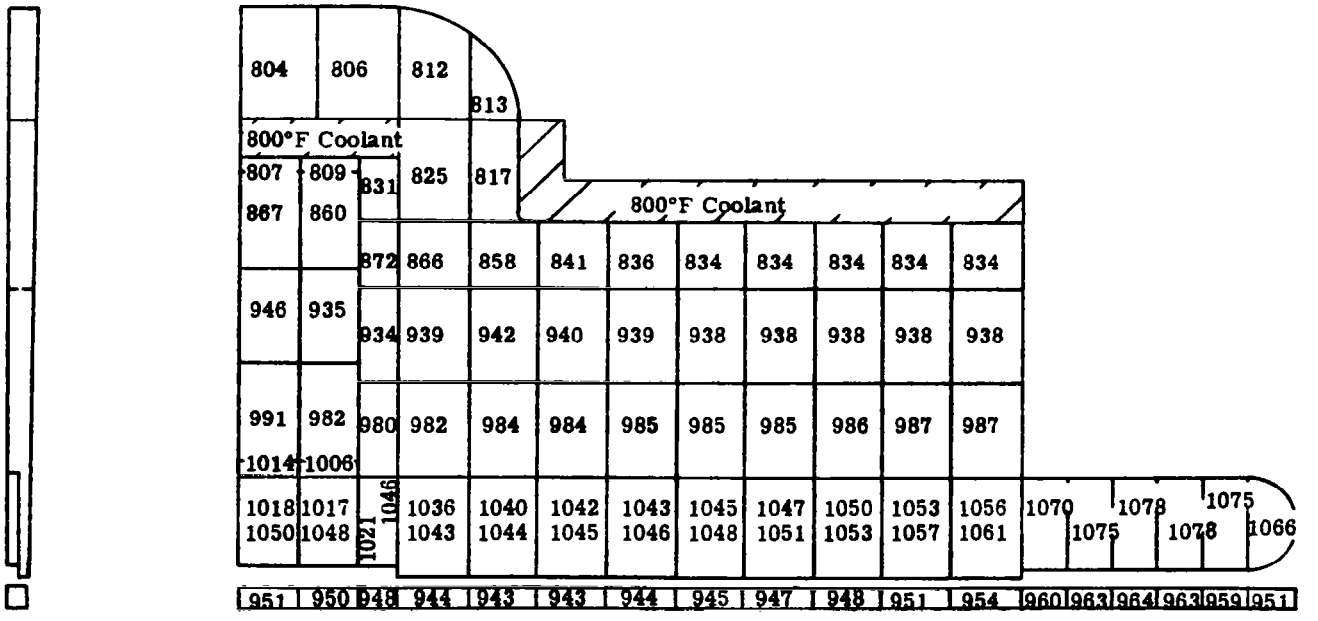

NUMBER 1 DESIGN STATOR TEMPERATURE DISTRIBUTION (°F) 550-KW_E RATING, 0.2 W/IN.^{2}°C SLOT CONDUCTANCE WITH ROTOR HEATING FROM STATOR

FIGURE 75

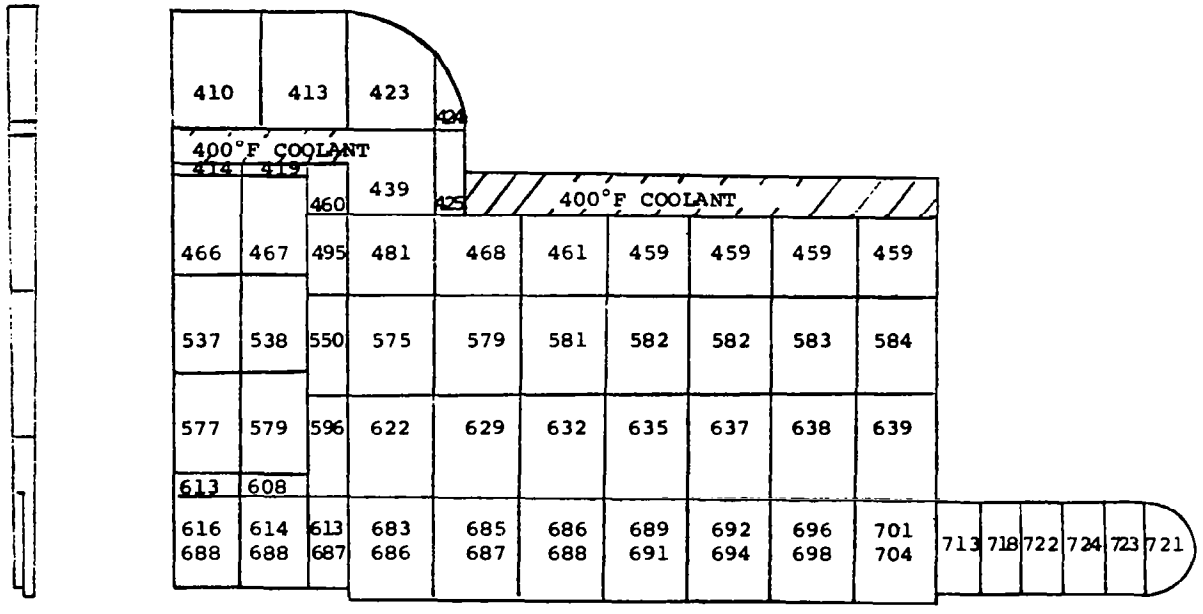

NUMBER 2 DESIGN STATOR TEMPERATURE DISTRIBUTION (°F)
450-KW_E RATING, 0.2 W/IN.^{2}°C SLOT CONDUCTANCE

FIGURE 76

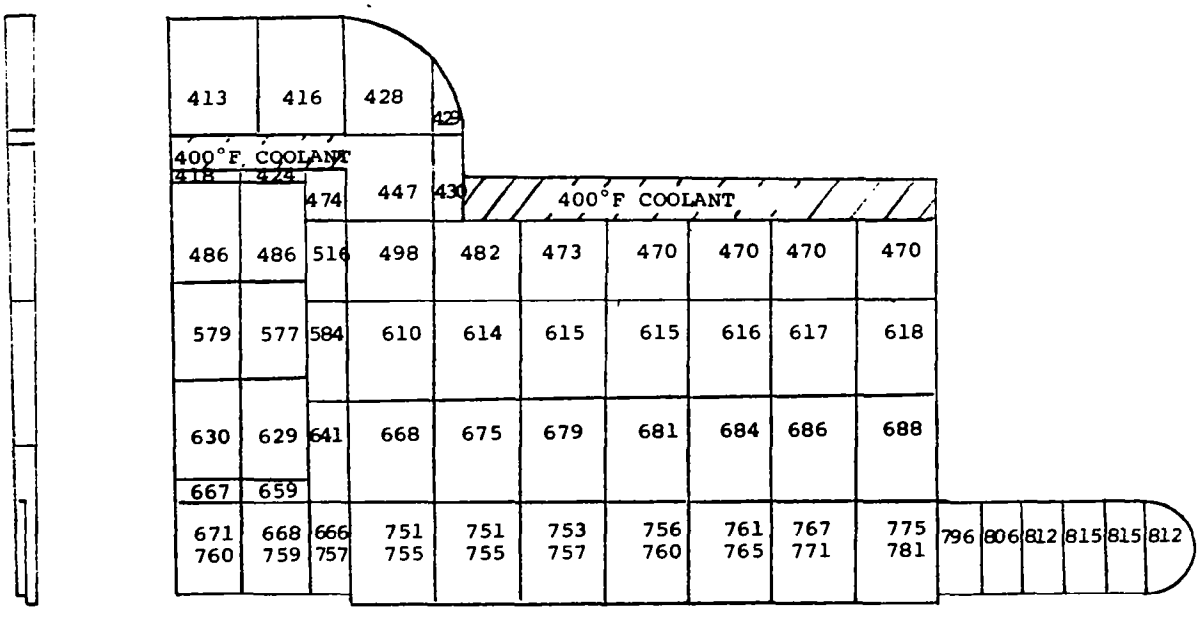

NUMBER 2 DESIGN STATOR TEMPERATURE DISTRIBUTION (°F)
550-KW_E RATING 0.2 W/IN.^{2}°C SLOT CONDUCTANCE

FIGURE 77

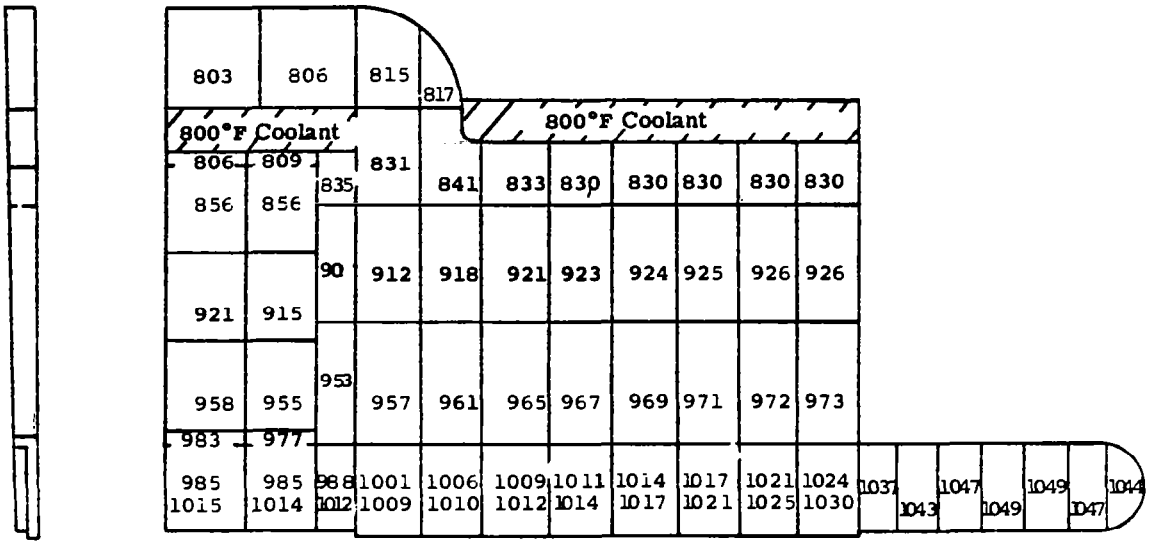

NUMBER 3 DESIGN STATOR TEMPERATURE DISTRIBUTION (°F)
450-KW_E RATING, 0.2 W/IN.^{2}°C SLOT CONDUCTANCE

FIGURE 78

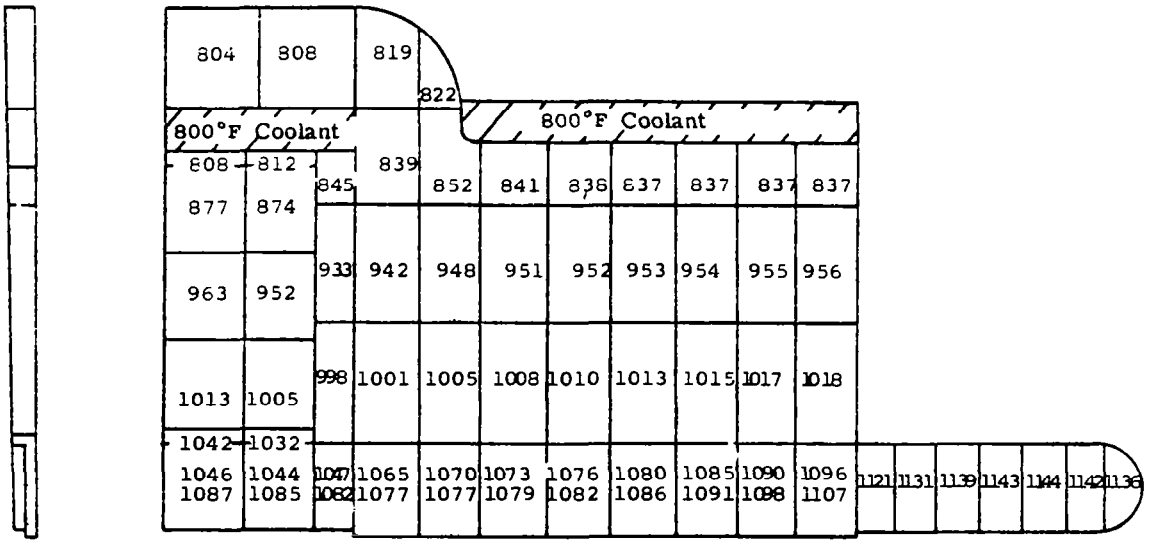

NUMBER 3 DESIGN STATOR TEMPERATURE DISTRIBUTION (°F)
550-KW_E RATING, 0.2 W/IN.^{2}°C SLOT CONDUCTANCE

FIGURE 79

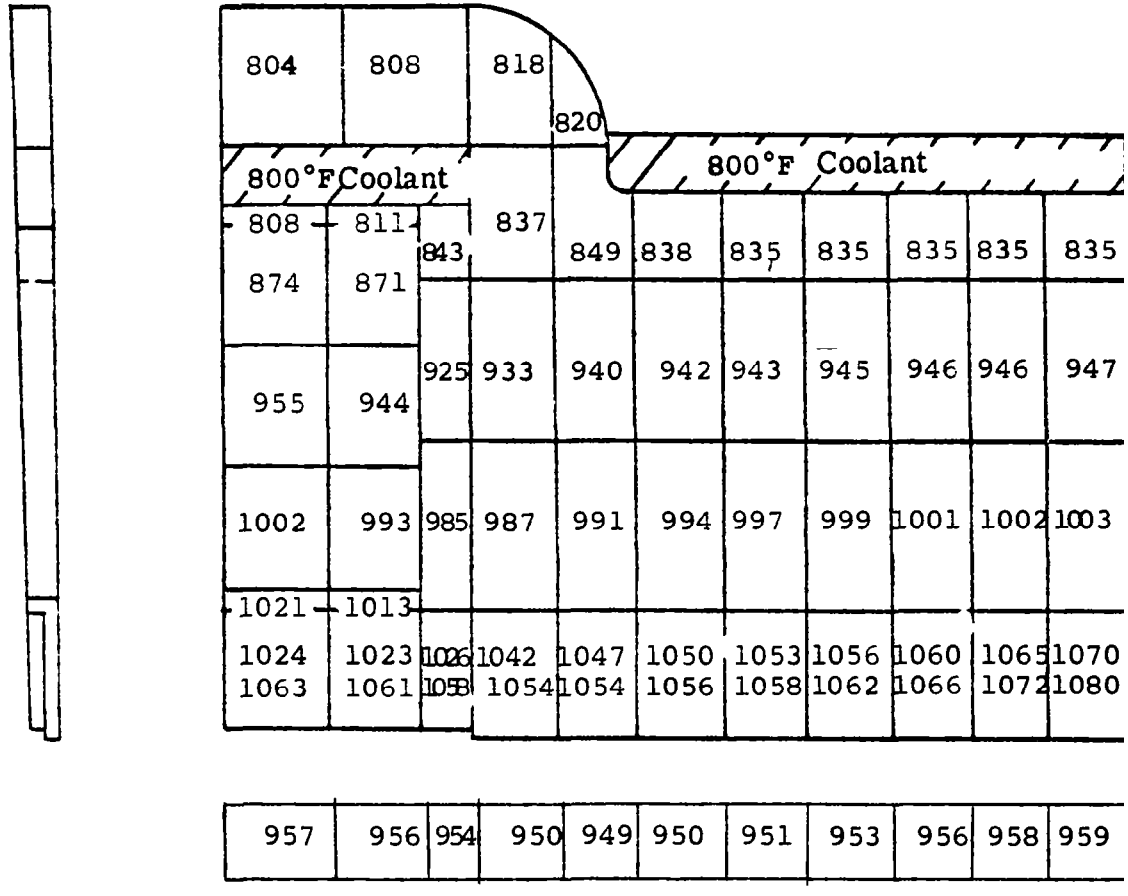

NUMBER 3 DESIGN STATOR TEMPERATURE DISTRIBUTION (°F) 550 RATING, 0.2 W/IN.^{2}°C SLOT CONDUCTANCE WITH ROTOR HEATING FROM STATOR

FIGURE 80

TABLE 69

STATOR COOLING SUMMARY

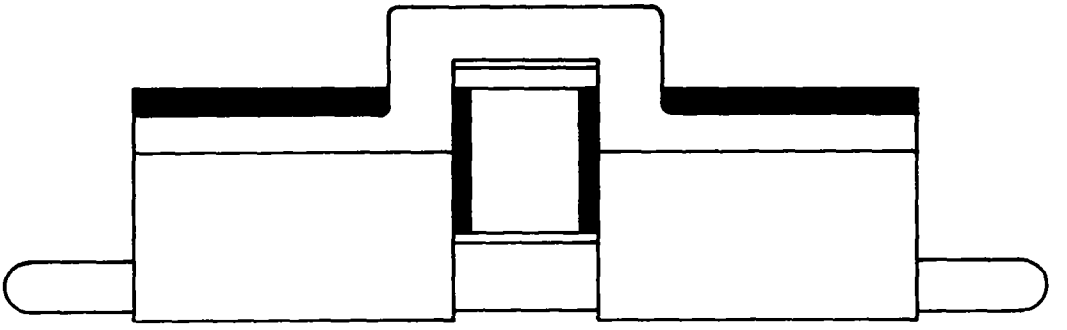

Maximum Temperature, °F	No. 1		No. 2		No. 3	
	450 kw	550 kw	450 kw	550 kw	450 kw	550 kw
AC End Turns	1024	1106	724	815		1144
AC Center	1003	1072	688	760		1087
Bore Seal		964				
Stator Tooth	1011	1080	701	775		1096
DBS	959	1000	639	688		1018
Frame	854	870	481	498		852
Field Coil	950	1001	579	630		1013
Sink Temperature, °F	800		400		800	

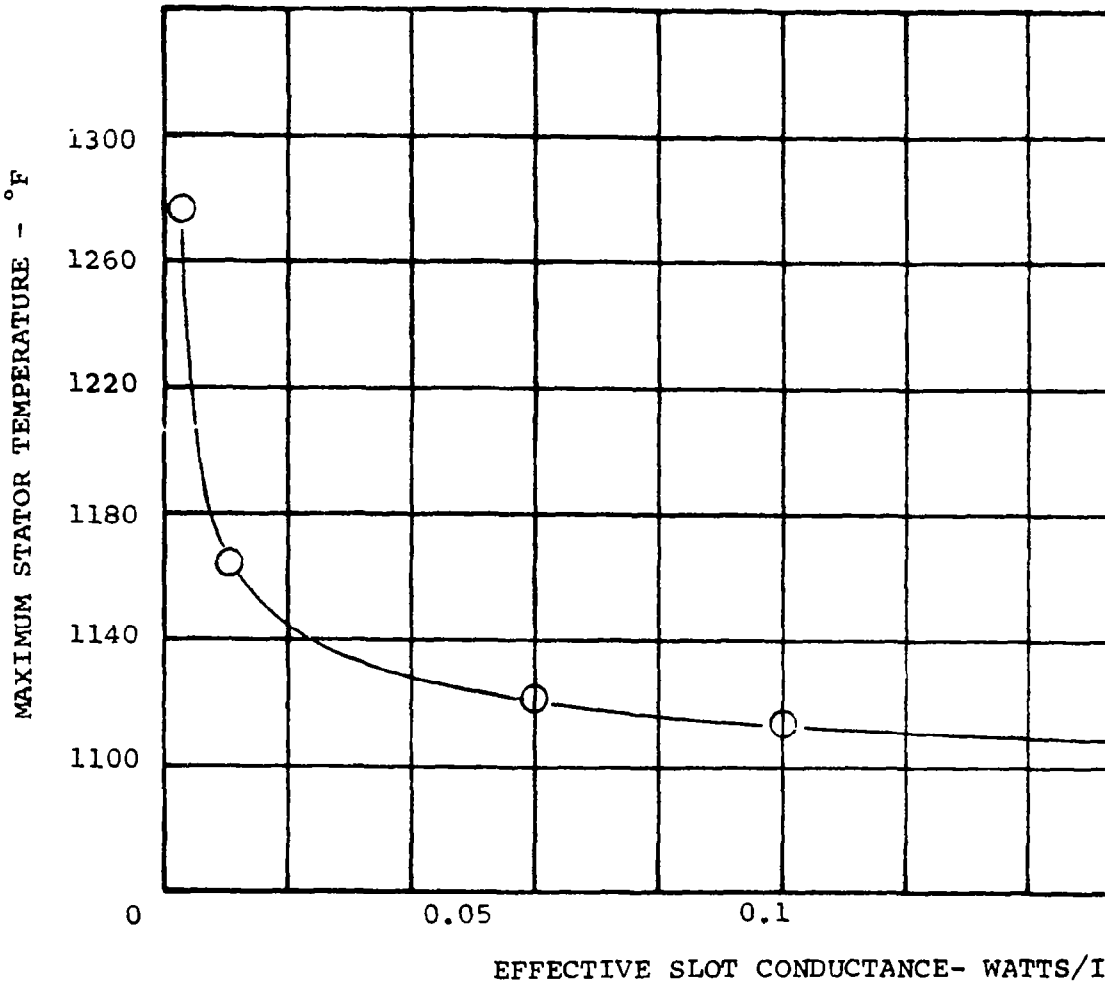

STATOR MAXIMUM TEMPERATURE VERSUS SLOT CONDUC

FIGURE 81

An evaluation of stator temperatures and cooling for conceptual designs 1 and 3 was conducted, taking into consideration heat transfer to the rotor in addition to cooling, as described above. The resulting temperature distributions are presented in Figures 75 and 80. The addition of heat transfer to the rotor results in a reduction of the stator maximum temperature by 28° to 1078°F for design No. 1 and by 33° to 1111°F for design No. 3. The stator losses rejected to the rotor were 2750 w (6.2 percent of stator losses) and 3080 w (17.3 percent of stator losses) for conceptual designs 1 and 3, respectively. Heat transfer to the rotor was by radiation from the armature windings and stator teeth to the bore seal and by radiation and forced convection from the bore seal to the rotor with the temperature of the rotor being held constant.

A temperature distribution with heat transfer to the rotor for conceptual design 2 was not determined due to lack of time and appropriate property data on oil vapor from which to determine the heat-transfer coefficient.

Investigation of field coil configuration was conducted with seven designs of both horizontal and vertical strap wound arrangements. Field coil cooling for the horizontal strap configurations was provided by two methods: (1) a central duct dividing the coil into two halves, and (2) by ducts on both sides of the coil. Cooling for the vertical strap configurations was by a duct on the OD of the coil. Based on both electrical and mechanical considerations, the field coil and cooling configuration selected consisted of two horizontal counterwound strap coils separated by ceramic insulation with cooling ducts on the outside of each coil. They are electrically isolated from the coil by ceramic. This arrangement allows both coil leads to be located at the coil OD with the common connection at the ID of the coil. The cooling ducts on the coil sides provide a short direct thermal path for each turn to the coolant and additional cooling for the stack and

and ac windings between the stacks. This field coil cooling configuration differs from that used in determining the temperature distributions for the conceptual designs. This is due to the fact that the final cooling configuration was selected after the majority of the temperature distributions had been prepared using a preliminary selected cooling arrangement. Time limitations did not allow recalculating temperature distributions with the new field coil cooling configuration. For comparison, however, a temperature distribution of the No. 1 design was prepared with this new field coil cooling method for the 550-kw_e rating and is presented in Figure 82. Comparing these temperatures with those of Figure 69 shows substantial reductions in temperatures of the field coil and the ac windings between stacks and a 32°F reduction in stator hot-spot temperature.

The basic stator cooling configuration, consisting of a circumferential coolant manifold on the stator frame with coolant ducts on the sides of the field coil, was finalized during Phase II of this program.

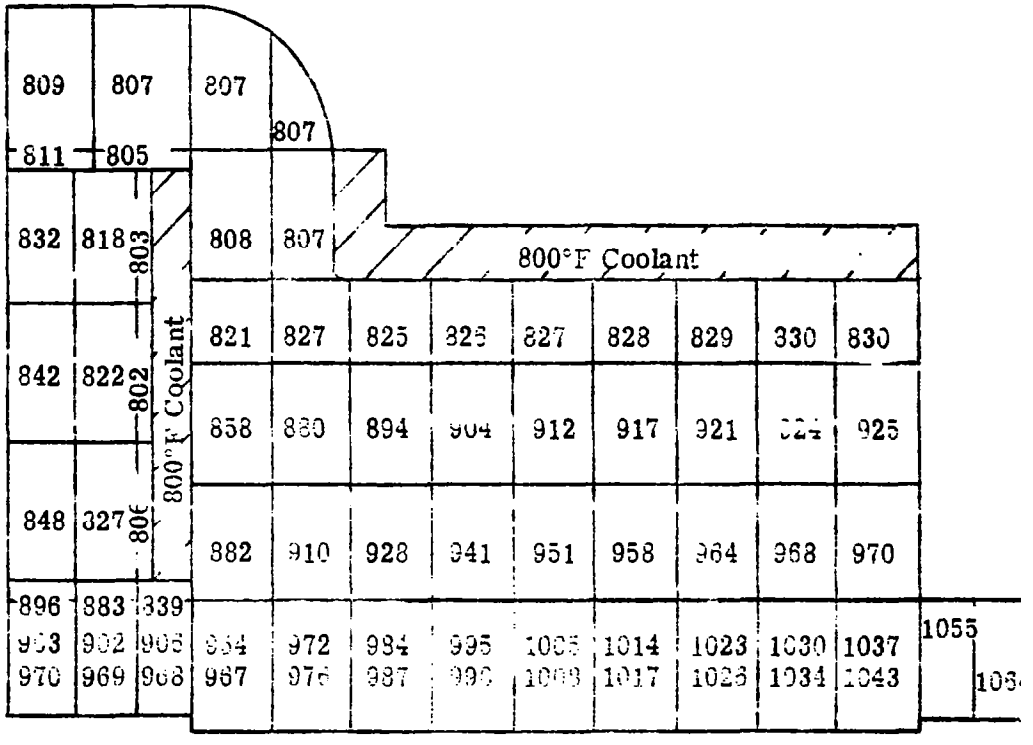

NUMBER 1 DESIGN STATOR TEMPERATURE DISTRIBUTION (°F) 550-kw_e RATING, 0.2 W/IN.^{2}°C SLOT CONDUCTANCE WITH FIELD COIL SIDE COOLING FINS

FIGURE 82

6. MISCELLANEOUS STUDIES

Separate studies, not directly related to deriving the conceptual designs, were carried out to provide additional data on operation and performance. These studies considered motoring start-up performance, magnetic force unbalances between the rotor and stator, and reliability engineering evaluations. The motoring start-up study was done for purposes of identifying the inherent motoring capabilities up to 120 percent of design speed and any steps that might be taken to improve the motoring performance.

The magnetic unbalance forces were calculated for maximum force conditions. The reliability engineering studies were concerned with (1) statistical evaluations of critical materials and properties and (2) a Failure Mode, Effect, and Criticality Analysis.

6.1 Motoring*

The inductor alternator is inherently a good salient pole synchronous motor, and variable speed operation can be achieved by variable supply frequency methods. Unfortunately the synchronous motor is not self-starting, and the absence of rotor windings or squirrel-cage type conductors precludes the normal induction motor starting methods. The special considerations are discussed below.

6.1.1 Induction Performance

6.1.1.1 Eddy-Current Torque

Considering the rotor at standstill with balanced three-phase currents flowing in the armature windings, a rotating field will be

*The motoring performance analyses were originally carried out in Phase I but were later updated in Phase II. The updated analyses are included in this volume because they were not specific tasks of Phase II. They are for the 660-kva design of Phase II.

produced. The rotating flux will "cut" the surfaces of the rotor poles and will be alternating in the pole bodies and rotor core. The flux cutting the pole surfaces will induce voltages axially across the poles causing current to flow through the rotor material. The greater part of this current will flow in a small portion of the rotor surface (skin effect) and will follow various paths along and around the rotor.

Tne effect of the induced currents is to produce a magnetic field tending to oppose that which originally produced the currents and consequently a force is set up between the rotor material and the rotating armature field. This force produces rotor torque as in a normal induction motor.

The calculation of the induced voltage presents no problem, but the calculation of the electrical resistance of the current paths can only be made by approximating the complex current paths to rather simplified patterns. The major current paths are as shown in Figure 83. Currents will also flow circumferentially across the pole faces due to the approximate sinusoidal distribution of flux across the pole face. Other currents will flow between poles on the same end of the machine. The prediction of the current paths at the ends of the rotor is virtually impossible with any accuracy due to the skin effect, corner effects, and stray field effects.

The effective rotor resistance has been calculated for the estimated major current paths--this resistance varies with frequency (due to skin effect) and pole surface configuration. Associated with this resistance is an effective rotor surface inductance which is dependent on the current paths and surface current magnitude. Due to the irregular "solid-body" rotor configuration, no attempt can be made to approximate this effective inductance with any degree of accuracy, and consequently it has to be neglected with probable large calculation error on the eddy-current torque. Eddy-current torque can be estimated

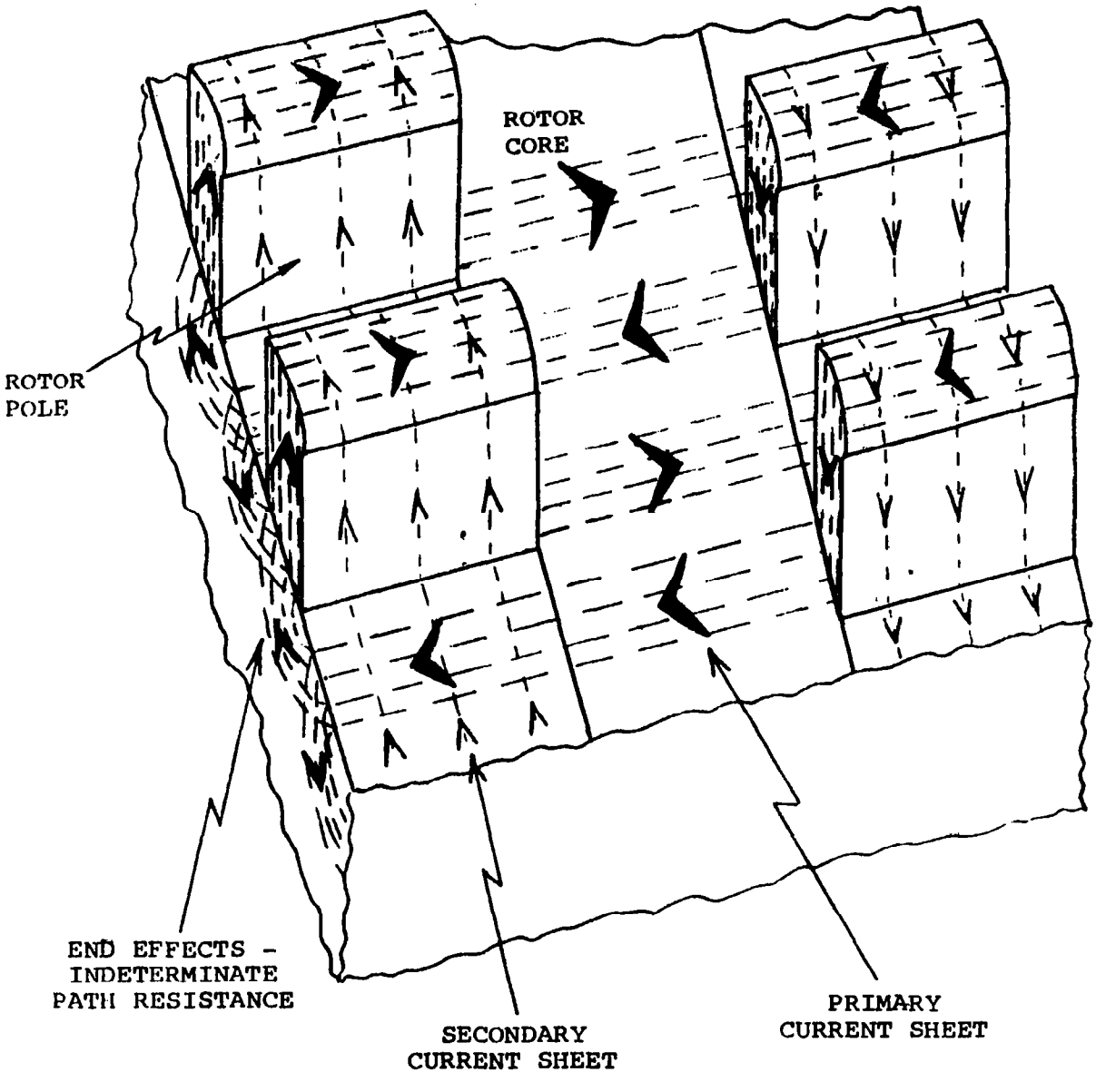

PLANAR SURFACE MODEL OF ROTOR SECTION
SHOWING ESTIMATED EDDY-CURRENT PATHS

FIGURE 83

from the calculated rotor resistance--the limit on torque is set by armature tooth saturation with the following estimated output torques for 60-Hz input.

	Torque Out, ft-lb	Phase V, v	Phase I, a	Total Pin, kw
Laminated Pole	5.8	25.5	328	11.8
Slotted Pole	51.	26.8	338	12.0

The above figures are at standstill, and torque decreases rapidly with speed.

6.1.1.2 Induced Current Torque

The alternating flux flowing through the poles and rotor core can be utilized to induce voltage in conducting loops attached to the poles as shown in Figure 84.

The induced voltage maximum value is determined by saturation of the armature teeth. The resistance of the conducting loop can be found from assumed dimensions. The inductance of the loop must be considered by taking the entire rotor/stator/frame flux path, and a good estimation can be made by utilizing the no-load saturation curve of the alternator. Typical values of resistance and inductive reactance of such a loop are:

$R = 1.3 \times 10^{-6}$ ohms $\qquad XL = 9.27 \times 10^{-4}$ ohms

An approximate value of starting torque for such a configuration at 60 Hz is 62.8 ft-lb. This is in addition to the rotor eddy-current torque. Inspection of the previous values of R and XL reveal that the resistance of the loop is almost negligible compared to its reactance, and consequently the loop may be constructed of almost any material

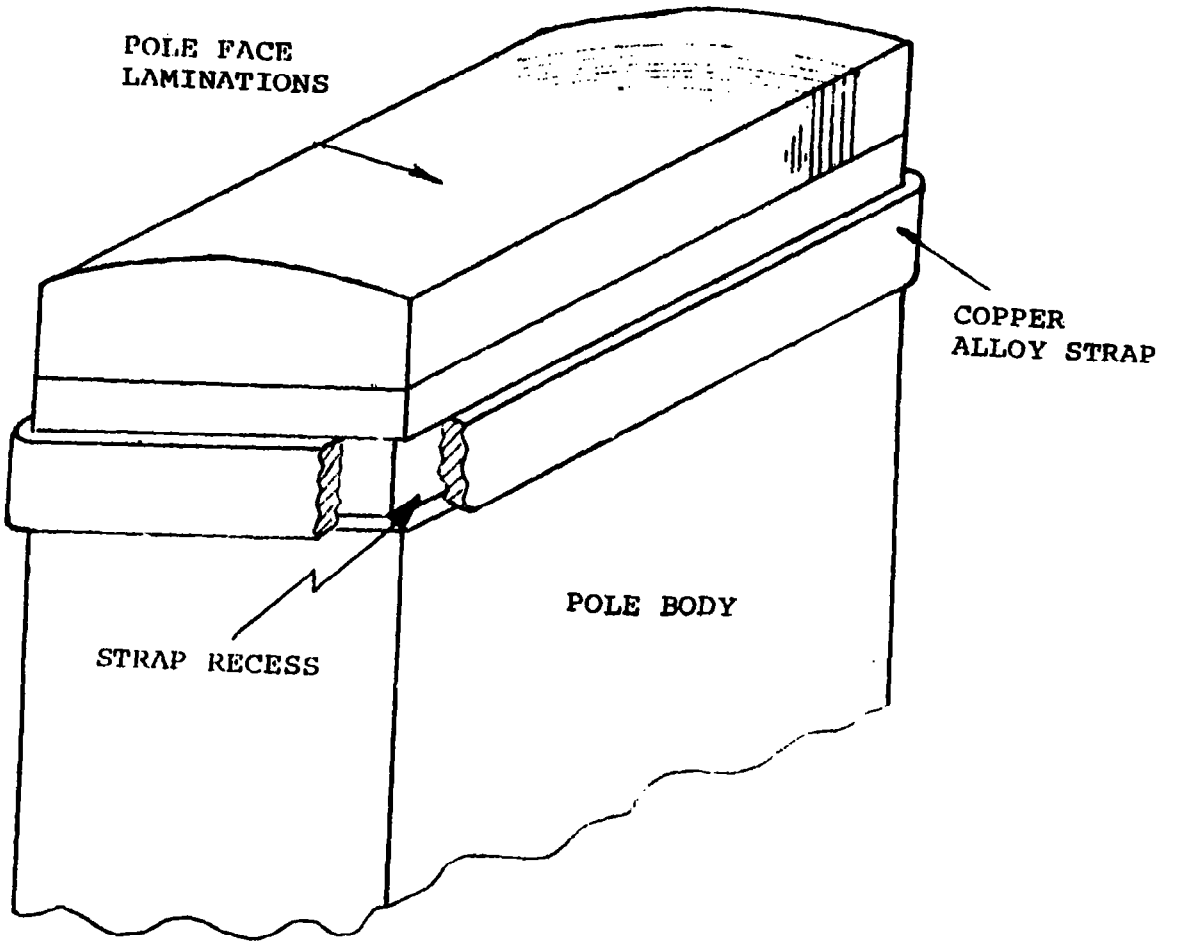

CONSTRUCTION OF CONDUCTING LOOPS
AROUND THE POLE BODY

FIGURE 84

(such as H-11 steel). This consideration brings to light the existence of such "loops" as being part of the pole body and rotor core, and hence, a contribution to starting torque is to be realized. The calculation of this torque is rendered almost impractical due to the undefined loop dimensions and nonlinear embraced flux for different loops under consideration. It is, therefore, concluded that the addition of extra conducting loops would have virtually no effect upon the resulting output torque and that the torque contribution of the existing material loops would be greater than that calculated for the conducting loops.

Additional damper bars in the pole faces were not analyzed because of their detrimental effects on pole face losses during normal operation as an alternator and because it seemed little, if any, additional gains could be achieved with them.

6.1.1.3 Hysteresis Torque

The alternating flux flowing throughout the rotor material will cause major hysteresis loops to be executed with a corresponding hysteresis loss. The magnitude of this loss is a function of material hysteresis loss constant and material volume. The material volume is known accurately but little data is available for hysteresis loss (as distinguished from core loss) for H-11 at 60 Hz. If hysteresis loss is approximately 10 w/lb at the induction under consideration, approximately 34 ft-lb of hysteresis torque would be available. This torque is constant for a given induction and is independent of slip speed and applied frequency.

6.1.1.4 Total Resultant Torque

The above three torques will act together, and the resultant torque will be the sum of these three. The following figures give

maximum and minimum estimated torque values, as derived above, for the cases of slotted and laminated pole faces at 60-Hz frequency.

Torque Component	Variation with Slip and Frequency	Estimated Torque (S=1), ft-lb	
		Maximum	Minimum
Laminated Pole Faces			
Eddy-Current Torque	$S^{1/2}f^{-3/2}$	6	4
Induced Current Torque	S	200	60
Hysteresis Torque	None	300	30
TOTALS		506	94
Slotted Pole Faces			
Eddy-Current Torque	$S^{1/2}f^{-3/2}$	60	40
Induced Current Torque	S	200	60
Hysteresis Torque	None	300	30
TOTALS		560	130

The calculations of the above torques were made independently, and the resultant output power of the combined torques may represent such a loading on the armature that excitation to these power levels is impractical, especially with the estimated maximum torques. Due to the effects of saturation and armature loading, it is impractical to try to calculate required input power, etc., as the rotor effective resistance is such an indeterminate quantity and calculation errors would render the results meaningless. The only practical methods of calculating motoring torque accurately are to either perform lengthy calculation procedures or to perform practical tests on an actual alternator.

A secondary conclusion reached during this motoring evaluation was that little motoring improvement could be obtained with slotted

over laminated pole faces. As a result, the choice of laminated pole tips over slotted is still dependent on pole face losses and cooling configuration design limitations.

6.1.1.5 Acceleration Characteristics

The induction starting capability of the alternator is required to achieve a run-up time of approximately 1 sec between 0 and 400 rpm. Based on a friction breakaway and running torque of approximately 14 ft-lb over this speed range and an inertia of the rotor and turbine of 20.8 lb-in.-sec^2, it is estimated that a torque of 200 ft-lb at starting (and decreasing with slip as $S^{1/2}$) will be required to achieve 1 sec run-up. This required torque lies between the estimated maximum and minimum induction torques and may or may not be achieved. Based on the minimum estimated torque of 94 ft-lb (laminated rotor poles), a run-up time to 400 rpm of approximately 3 sec is calculated. For the slotted poles, this time would be approximately 2 sec. For the maximum estimated torques of 506 and 560 ft-lb, run-up times of less than 0.5 sec are calculated.

Review of the findings with past motoring performance data indicates the starting torque may be about 60 percent of the rated alternator input torque. This places the probable torque at the low side of the estimates (i.e., near 100 ft-lb) which means the time to 400 rpm should be closer to the 3 sec maximum than the 1-sec minimum. Breakaway torque requirements should be minimized by a strong pulsating (vibration) torque. This will enhance meeting the 3-sec time.

6.1.2 Synchronous Performance

Due to the decreasing relationship of torque with speed and frequency during induction starting, it is desirable to utilize the inherent synchronous motoring performance of the alternator at the

lowest possible speed. It is suggested that synchronization be performed when the alternator speed is approximately 400 rpm.

6.1.2.1 Method of Achieving Synchronism

As soon as the rotor speed reaches approximately 400 rpm (representing a synchronous frequency of 33 Hz), the supply frequency should be steadily reduced to some value less than 33 Hz, the actual frequency being determined by the rotor speed, which will slowly decrease due to friction torque. As soon as the applied frequency is equal to or less than the synchronous frequency at that rotor speed, synchronization will be automatically effected by the reluctance torque of the machine.

Once synchronization has occurred, reluctance torque will be constant, tending to accelerate the rotor, provided that the "load angle" is non-zero. If excitation is applied to the field coil at this point, generated torque will be produced, tending to accelerate the rotor. However, both of these torque components will disappear if the load angle becomes zero. In order to produce rotor acceleration, the armature frequency must be increased steadily, whereupon the rotor will accelerate to maintain synchronism.

6.1.2.2 Synchronous Acceleration

During acceleration, armature and field excitation may be varied at will to provide the best combination of torque, current, and power factor. The acceleration is purely dependent on the rate of change of armature applied frequency which has a maximum value consistent with maintained synchronism and is such that an acceleration of up to 1200 rpm/sec may be obtained. It is suggested that an acceleration of less than half of this value be obtained to avoid the disastrous effects of loss of synchronism (e.g., severe armature overload currents and bearing shock). Power supply requirements during

synchronous motoring depend on the required run-up time. In order to maintain rated armature current, the voltage/frequency ratio must be almost constant (Figure 85); consequently, the power requirement for this condition will increase steadily to a maximum at full speed. If a limited power supply is to be used, the rate of change of frequency must be reduced to compensate for the reduction in maximum torque to avoid loss of synchronism. The power supply should be capable of programmed frequency and voltage variation with very close frequency regulation.

If 400 rpm is reached within 2 sec, synchronization is affected within 1 sec more, and the alternator is accelerated at 1200 rpm/sec, the times to reach 40-percent design speed, rated-speed, and 120-percent speed are approximately 9, 19, and 21 sec, respectively. If 600 rpm/sec synchronous acceleration is used, the times increase to approximately 15, 35, and 40 sec.

6.2 Magnetic Unbalance Forces

In an electromagnetic generator, a magnetic radial force can result if the rotating member is made eccentric to the stator. The magnitude of the radial force is dependent upon the degree of eccentricity between the rotor and stator and the level of field excitation. The magnetic force on the rotor will be present regardless of the conditions of gravity.

When a magnetic field exists in the space between two magnetized forces, there exists a force equal to:

$$F = \frac{B^2 A}{72.13} \text{ lb} \qquad (1)$$

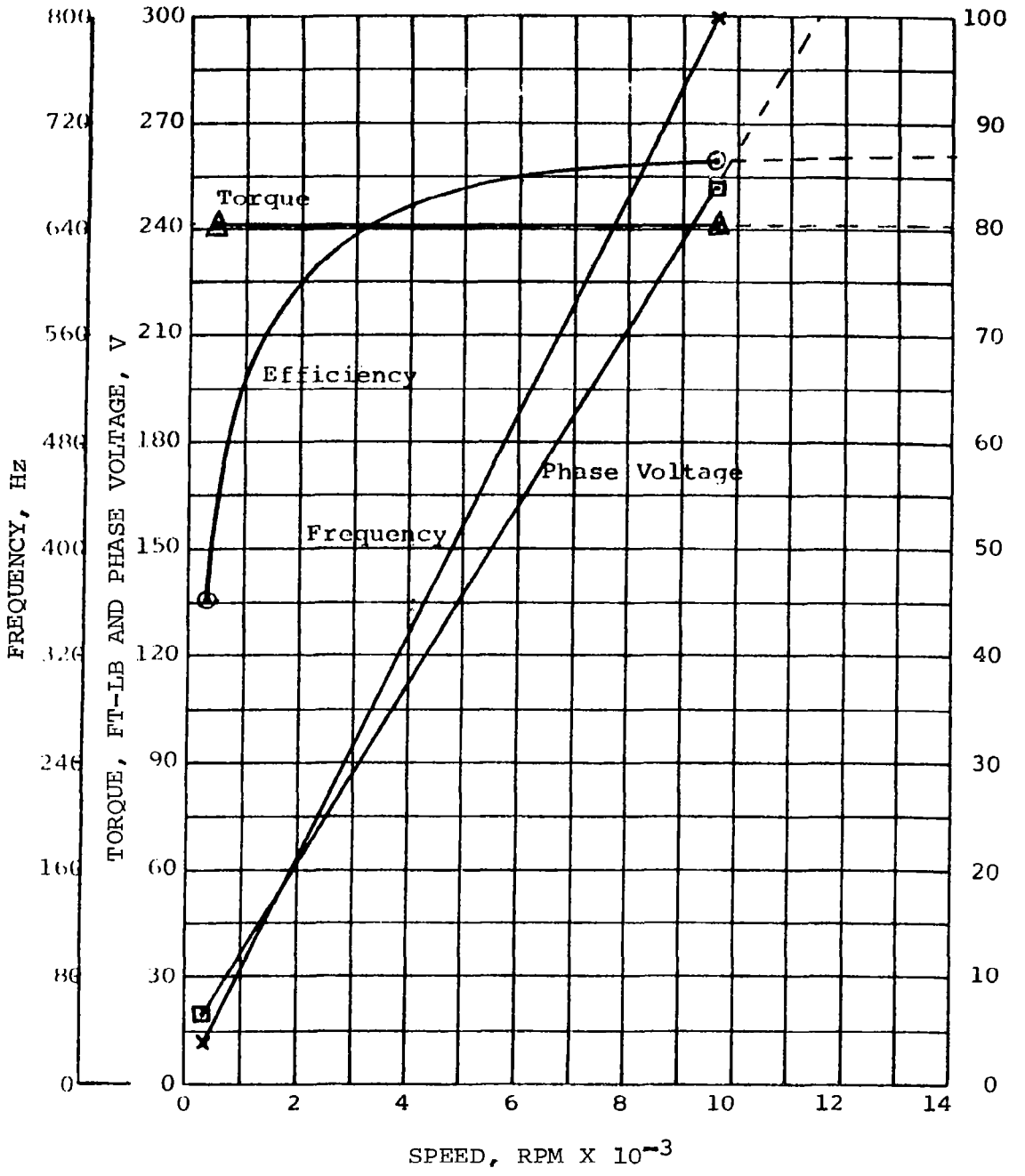

SYNCHRONOUS MOTOR PERFORMANCE UNITY P.F.

FIGURE 85

where

B = flux density in kilolines/in.^{2}

A = cross sectional area of the gap in square inches

The amount of energy per unit volume (i.e., energy density) in a given space is identical with pressure or force per unit surface area when the surface is taken at right angles to the direction in which the pressure can act to move a substance. Whenever there is an immediately available supply of energy, a mechanical force is in evidence. The energy stored in a magnetic field is

$$E = \frac{B^2}{72.13}(r) \quad \frac{\text{in.-lb}}{\text{in.}^3} \tag{2}$$

where

r = relative permeability

For a field density of 8.49 kl/in.^{2} in space where r = 1, there exists an energy density of 1.0 in.-lb/in.^{3} or 1.0 lb/in.^{2}. Hence, the pressure tending to move the two bodies together will be equal to 1.0 lb for each square inch of cross section of the gap. Therefore, the force equals the energy density E times the cross sectional area A. In air or free space where the relative permeability r is unity, the product of E times A results in Eq. (1) above.

Past studies[11] have shown that the magnetic unbalance force at zero speed, no-load excitation*, is both a maximum and a linear function of the eccentricity between the rotor and stator. Because of this, the unbalanced forces were calculated for 0.010 in. eccentricity

*Approximately, depending on the saturation characteristics of the design.

at the maximum force conditions and the results were then fed into the bearing design considerations. This simplified approach without feedback from the bearing designs or minimization of forces is possible only because the forces calculated for this worst-case are still too small to influence the bearing design. As a result, only the absolute maximum values are of interest and the actual operating values are of academic value only.

When the rotor is rotated, certain events take place which act to reduce the magnetic force unbalance on the rotor. Assume a given flux density exists at a fixed point on the face of a bottom pole. When the rotor is turned so that the reference pole takes the position of the upper pole, the flux density at the reference point is reduced due to the increased reluctance of the magnetic path. Further rotation of the rotor will return the reference point to its initial position and the flux density to its original values. Under rotation, the reference point on the pole face sees a periodically varying flux density. The variation generates a voltage in the rotor poles, and therefore, electric currents will flow according to the impedance of the conductance paths. The MMF of these eddy-currents act to oppose the alternating magnetic field which caused them. Since the alternating field represents the difference in field magnitude responsible for the magnetic force unbalance on the rotor, the currents act to reduce the force. The flow of the currents will, of course, create additional rotor losses. If the armature winding has several parallel paths, the difference in the magnitude of the magnetic field will cause currents to circulate in the windings. These currents also act to reduce the magnetic force unbalance.

The impedance of the electric circuits in which these currents flow is composed of both resistance and inductive reactance. Inductive reactance is directly proportional to frequency, and therefore, at low rotor speeds, the magnitude of the opposing currents will be determined mostly by the resistance. At higher rotor speeds, the

inductive reactance increases, and the magnitude of the currents will depend increasingly on the value of this reactance. The induced voltage, like the inductive reactance, is directly proportional to rotor speed. The ratio of induced voltage to inductive reactance represents reactive current. As rotor speed is increased, the force opposing currents approach this ratio which is a constant. The rotor speed at which the opposing currents closely approximate the limiting value is dependent upon the ratio of resistance to inductance of the electric circuits.

The forces for the three base designs were determined for static conditions using the analysis techniques presented in Reference 11. The maximum forces were found to occur at about 70 percent of rated excitation and are given in Table 70. Since eccentricities will only be of the order of 1 to 2 mils, the maximum expected unbalanced forces should only be 30 to 60 lb total.

TABLE 70

MAGNETIC UNBALANCED FORCES

Design No.	Maximum Force, lb/in.
1	32.3×10^{-3}
2	26.7×10^{-3}
3	27.6×10^{-3}

6.3 Reliability Engineering

The reliability engineering studies were concerned with two basic areas: (1) statistical evaluations of critical materials/properties to relate to reliability predictions on the alternator design and (2) a Failure Mode, Effect, and Criticality Analysis (FME & CA). The

FME & CA carried out was preliminary in nature and concerned itself with a typical design from Phase I. The final FME & CA was carried out on the Phase II design and is reported in Volume III.

The statistical studies concerned themselves with H-11 rotor material only. It was originally hoped that all candidate materials could be included in the studies, but the lack of useful data or the relative need compared to cost of analyzing them precluded all but the H-11 steel. This conclusion was reached as a result of (1) itemizing candidate materials, probable temperatures and properties to be analyzed, (2) collecting all possibly useful data on each of the materials, and (3) reviewing the lists and data with experts – both mathematical and materials – who would carry out the proposed study. Lack of useful data required the majority of the materials be dropped from further statistical considerations. The expense involved in analyzing the remainder relative to the need-to-know precluded all but the H-11 steel. The statistical analysis of the H-11 steel is discussed in the next subsection. It is interesting to note that even for the H-11 steel, analysis of the creep strengths were not carried out. This is because of a lack of useful, consistent data with which to do a meaningful study.

6.3.1 Statistical Analysis of Tensile-Test Data on H-11 Steel Bars

The purpose of the statistical study was to analyze tensile-test data to determine lower limits for three tensile properties which appear in design calculations. For each property, the corresponding lower limit is supposed to be a value which one can safely assume will nearly always be exceeded. The statistical formulation of this problem is to find a lower limit so that there is a confidence γ that a proportion P (or more) of the population exceeds the limit. The "safely" of the previous sentence corresponds to γ and the "nearly always" to P. A typical choice of values would be $\gamma = 0.95$ and $P = 0.99$. The resulting limit is called a tolerance limit.

Tensile specimens from three heats of steel were previously tested[6] and for each test data set, the properties of concern were:

(a) Modulus of elasticity, psi

(b) Ultimate tensile strength, psi

(c) Offset yield strength, psi

In addition, the specimens were heat-treated to various levels of hardness and tested at various temperatures. The test temperatures represent possible temperatures of the expected environment for the device; the various hardness values represent the expected hardness gradient through the device. The purpose of the analysis was to provide lower tolerance limits which are specific to various values of temperature and hardness.

Table 71 is a list of the data on which the analysis was based. Each heat was analyzed separately. This consisted of fitting an equation involving hardness and temperature to each tensile property. The "best" equation for each property was found by first fitting a full second-degree polynomial in two variables (temperature and hardness) and then seeing if any terms could be omitted without significantly diminishing the predicting ability of the equation. The fitting referred to previously was carried out by least-squares. To illustrate the equations that were used let Y stand for any tensile property, let H stand for hardness and let T stand for temperature. Then the full second-degree polynomial is given by

$$Y = \beta_O + \beta_H H + \beta_T + \beta_{HH} H^2 + \beta_{TT} T^2 + \beta_{HT} HT$$

TABLE 71

H-11 PROPERTY DATA

Mod. of Elas., 10^6 psi	Ult. Tens. Strength, psi	Offset Yld. Strength, psi	Hardness Rockwell C	Test Temp., °F	Ref Spec. No.
		Heat H-10283-K2[6]			
26.10	201,195	151,394	48	800	23T
25.79	191,446	159,878	48	800	24T
26.97	158,475	121,364	44.5	900	25T
27.55	163,306	118,448	44.5	900	26T
24.95	177,645	134,731	47.5	900	27T
28.66	178,536	140,421	47.5	900	28T
20.74	167,677	116,162	48.0	1000	31T
20.30	173,653	117,764	48.5	1000	32T
26.53	210,632	164,493	50	800	33T
26.89	207,753	164,016	50.5	800	34T
25.19	196,819	146,123	51	900	35T
25.36	208,583	154,691	51	900	36T
24.39	170,974	131,730	51	1000	37T
22.41	174,950	136,680	51	1000	38T
		Heat D-14-K2[6]			
27.00	168,706	140,421	46	800	9X
26.94	170,500	137,410	46	800	10X
26.70	198,603	160,179	48	800	11X
27.97	203,610	164,995	48	800	12X
26.67	152,457	117,352	44	900	13X
27.58	170,061	132,382	44.5	900	14X
28.10	158,065	123,656	46	900	15X
26.51	188,064	147,944	46	900	16X
28.82	205,588	167,165	48.5	900	17X
27.21	182,547	146,940	48	900	18X
25.08	128,385	92,778	43.5	1000	19X
23.91	137,613	102,862	44	1000	20X
23.09	134,403	99,298	46	1000	21X
21.71	128,048	95,528	46	1000	22X
24.81	168,347	129,032	48	1000	23X
23.37	136,089	102,823	48	1000	24X
26.26	154,645	118,181	44	900	25X
28.28	163,672	127,246	44.5	800	7X
25.44	165,344	122,100	44.5	800	8X
		Heat H-9228-K2[6]			
27.08	177,419	138,105	44.5	800	16Z
27.68	177,533	138,415	44.5	800	17Z
29.07	215,725	174,395	48	800	18Z
28.27	194,584	155,466	47.5	800	19Z
27.26	165,497	125,376	44.5	900	20Z
29.01	163,672	124,750	44.5	900	21Z
26.91	175,025	139,919	48	900	22Z
25.79	188,565	144,433	48	900	23Z
23.44	141,129	100,806	44	1000	24Z
23.71	140,421	104,313	44.5	1000	25Z
25.83	142,137	103,333	48	1000	26Z
24.51	142,427	107,823	48	1000	27Z

where the βs are determined from the given Y, H, T, using the principle of least-squares. The estimated coefficients are given in Table 72. The equations represented by data of Table 72 are plotted on Figures 86, 87 and 88. These plots cover the values of temperature and hardness that are of interest. Since the data for heat H-10283-K2 include only one point in the region of interest, this heat was not plotted and was not considered further. Refer to the plot of modulus of elasticity for heat D-14-K2 (Figure 86). The ordinate is marked from 2.20 to 3.00. At the top of the plot the notation "at 7" means that the 2.20 is x 10^7. A similar notation is found on the abscissa so that the markings are actually 800, 850, 900, etc. The graph itself is "drawn" using the letter "C", and a careful examination will reveal some lack of smoothness. This is not an intentional feature of the graph but a result of the somewhat poor resolution of a computer printer when used as a plotter. Next consider the plot of ultimate tensile strength for heat D-14-K2 (Figure 87). Here two independent variables are being represented and the extra one, hardness, is held constant at three different values as explained in the note along the abscissa. Thus the "A" graph shows the relation between tensile strength and temperature when hardness is 44. Finally, to see the resolution problem at its worst, consider the plot of ultimate tensile strength for heat H-9228-K2 (Figure 88). The "A" graph is representing a straight line sloping from approximately 175,000 to 142,500 psi. Similarity is evident for the "B" and "C" graphs.

The final step in the analysis was to compute lower tolerance limits for the various tensile properties at selected values of hardness and temperature. The results of this work are presented in Tables 73 through 75. A description of the computation of the tolerance limits follows.

Suppose a linear regression analysis has been carried out (linear in the parameters, not necessarily in the independent variables), and a lower P (proportion) tolerance limit with confidence γ is desired

TABLE 72

STATISTICAL COEFFICIENTS

Coefficient	Heat		
	H-10283-K2	D-14-K2	H-9228-K2
Modules of Elasticity, psi			
β_O	-140,435,834	-103,847,757	-40,865,000
β_T	392,687.5	308,104.8	169,612.5
β_{TT}	-230.29	-180.60	-104.38
Ultimate Tensile Strength, psi			
β_O	-1,171,588	-1,302,844	-1,606,739
β_H	30,624.3	7,808.0	43,344.3
β_T	1,029.2	2,672.3	1,726.7
β_{TT}	---	-1.59	---
β_{HT}	-27.90	---	-42.83
Offset Yield Strength, psi			
β_O	630,169	-1,247,146	-1,481,860
β_H	-6,525.1	7,673.2	39,572.7
β_T	-793.2	2,474.3	1,543.7
β_{TT}	---	-1.48	---
β_{HT}	12.35	---	-38.62

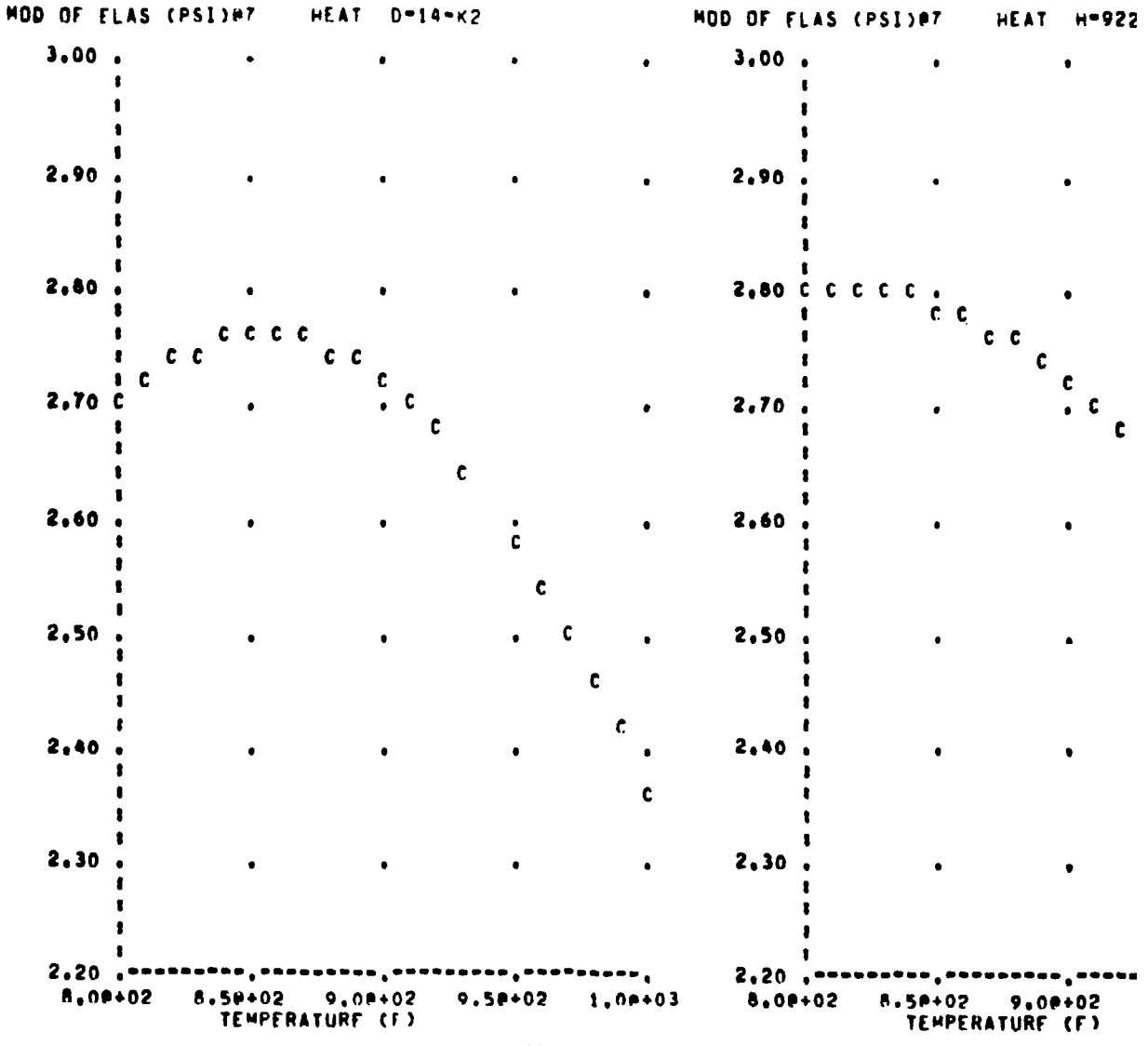

MODULUS OF ELASTICITY

FIGURE 86

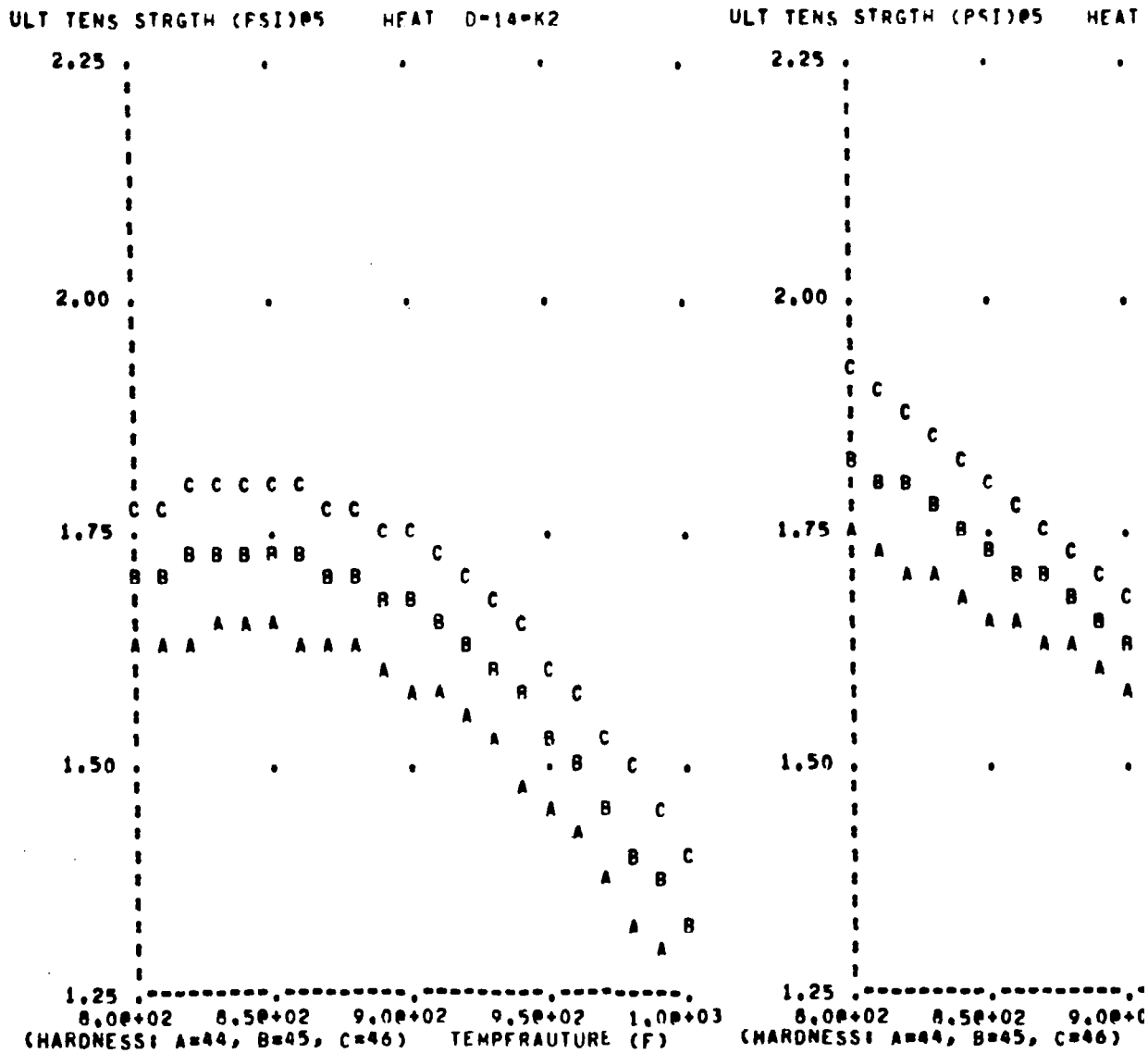

ULTIMATE TENSILE STRENGTH

FIGURE 87

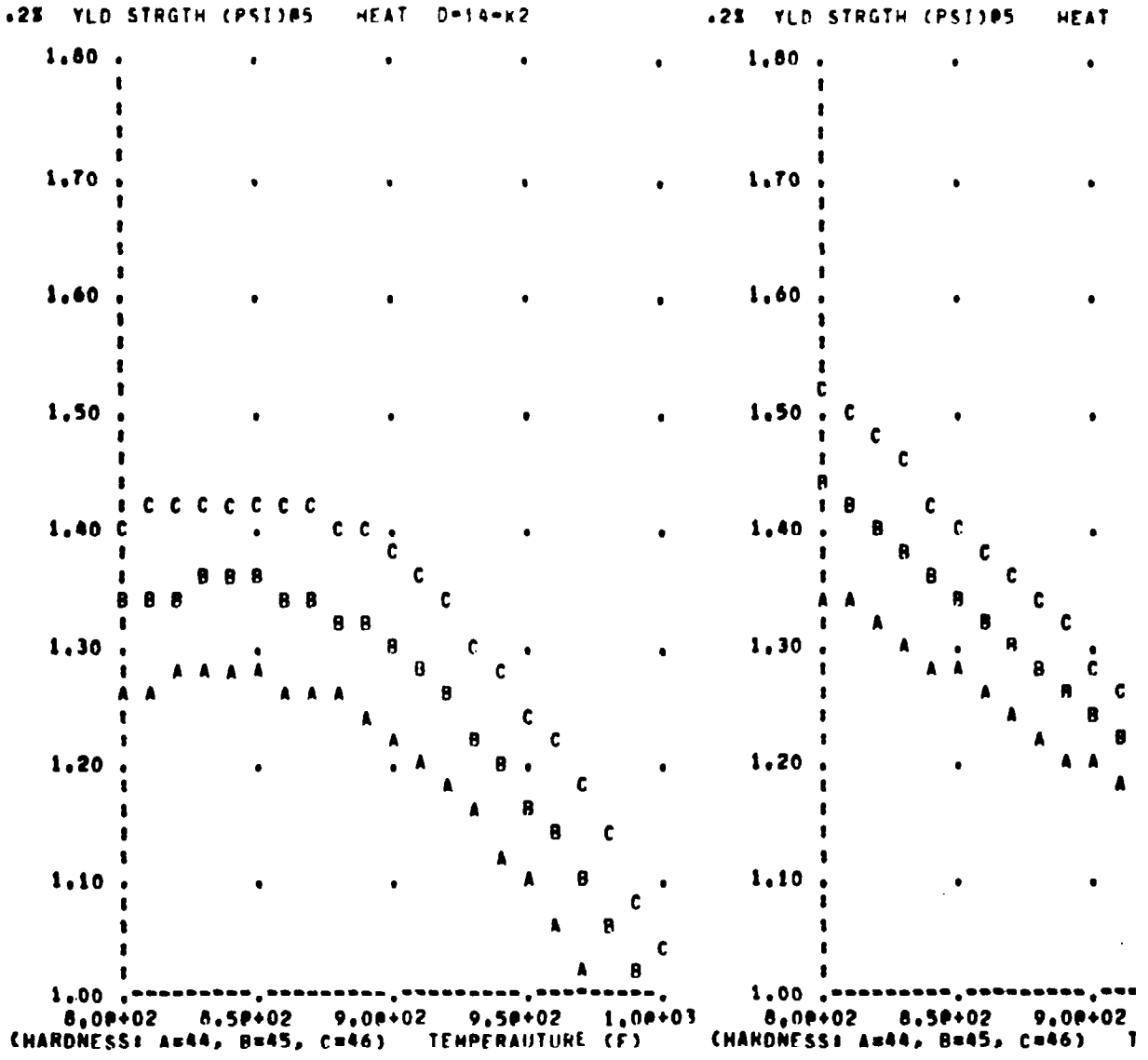

YIELD STRENGTH - 0.2 PERCENT

FIGURE 88

TABLE 73

MODULUS OF ELASTICITY TOLERANCE LIMITS

Heat D-14-K2	MODULUS OF ELASTICITY (psi)		
Temperature = 800			
Confidence Proportion	.90	.95	.99
0.90	24837468	24353007	23423164
0.95	24564781	24046226	23045531
0.99	23944308	23336511	22153135
Temperature = 900			
Confidence Proportion	.90	.95	.99
0.90	24985368	24498023	23563022
0.95	24624283	24201889	23194379
0.99	24127151	23513371	22319589
Temperature = 1000			
Confidence Proportion	.90	.95	.99
0.90	21444135	20959673	20029831
0.95	21171448	20652893	19652198
0.99	20550975	19943177	18659801
Heat H-9228-K2	MODULUS OF ELASTICITY (psi)		
Temperature = 800			
Confidence Proportion	.90	.95	.99
0.90	25590549	25071388	24069318
0.95	25183344	24602025	23473398
0.99	24109138	23336202	21822684
Temperature = 900			
Confidence Proportion	.90	.95	.99
0.90	24808049	24288888	23286818
0.95	24400844	23819595	22690898
0.99	23326638	22553702	21040184
Temperature = 1000			
Confidence Proportion	.90	.95	.99
0.90	21938049	21418888	20416818
0.95	21530844	20949595	19820828
0.99	20456638	19683702	18170184

Reference AFAPL-TR-66-127, Hardness = 44 - 46 R_C, Temperature = °F

TABLE 74

ULTIMATE TENSILE STRENGTH TOLERANCE LIMITS

Heat D-14-K2	Ultimate Tensile Strength (psi)		
Hardness = 44 Temperature = 800			
Proportion / Confidence	.90	.95	.99
0.90	137386	132480	123054
0.95	134112	128860	118712
0.99	126673	120496	108442
Hardness = 45 Temperature = 800			
Proportion / Confidence	.90	.95	.99
0.90	146126	141163	131631
0.95	143134	137807	127517
0.99	136270	129973	117698
Hardness = 46 Temperature = 800			
Proportion / Confidence	.90	.95	.99
0.90	154341	149349	139764
0.95	151472	146106	135747
0.99	144856	138499	126117
Hardness = 44 Temperature = 900			
Proportion / Confidence	.90	.95	.99
0.90	135134	130188	120687
0.95	132065	126761	116511
0.99	125044	118783	106571
Hardness = 45 Temperature = 900			
Proportion / Confidence	.90	.95	.99
0.90	143765	138761	129155
0.95	140944	135563	125174
0.99	134426	128044	115618
Hardness = 46 Temperature = 900			
Proportion / Confidence	.90	.95	.99
0.90	151806	146784	137145
0.95	149055	143649	133218
0.99	142679	136258	123766

Heat D-14-K2	Ultimate Tensile Strength		
Hardness = 44 Temperature = 1000			
Proportion / Confidence	.90	.95	
0.90	100021	95089	8
0.95	96830	91558	8
0.99	89560	83351	7
Hardness = 45 Temperature = 1000			
Proportion / Confidence	.90	.95	
0.90	108643	103669	9
0.95	105698	100357	9
0.99	98929	92610	8
Hardness = 46 Temperature = 1000			
Proportion / Confidence	.90	.95	
0.90	116707	111716	10
0.95	113841	108475	9
0.99	107229	100871	8

Reference AFAPL-TR-66-127, Hardness = R_c, Temperatu

TABLE 74 (Contd.)

ULTIMATE TENSIL STRENGTH TOLERANCE LIMITS

Heat H-9228-K2	Ultimate Tensile Strength (psi)		
Hardness = 44 Temperature = 800			
Proportion / Confidence	.90	.95	.99
0.90	157629	154615	148783
0.95	154424	151035	144426
0.99	145872	141241	132106
Hardness = 45 Temperature = 800			
Proportion / Confidence	.90	.95	.99
0.90	168193	165086	159078
0.95	165468	161948	155098
0.99	157978	153113	143565
Hardness = 46 Temperature = 800			
Proportion / Confidence	.90	.95	.99
0.90	177971	174803	168691
0.95	175468	171864	164874
0.99	168461	163450	153671
Hardness = 44 Temperature = 900			
Proportion / Confidence	.90	.95	.99
0.90	144013	140846	134736
0.95	141506	137904	130916
0.99	134491	129483	119708
Hardness = 45 Temperature = 900			
Proportion / Confidence	.90	.95	.99
0.90	149564	146312	140072
0.95	147293	143575	136414
0.99	140778	135579	125528
Hardness = 46 Temperature = 900			
Proportion / Confidence	.90	.95	.99
0.90	154701	151403	145097
0.95	152536	148755	141507
0.99	146238	140937	130753

Heat H-9228-K2	Ultimate Tensile Streng	
Hardness = 44 Temperature = 1000		
Proportion / Confidence	.90	.95
0.90	126436	123401
0.95	123357	119938
0.99	115087	110403
Hardness = 45 Temperature = 1000		
Proportion / Confidence	.90	.95
0.90	128182	125064
0.95	125500	121965
0.99	118107	113215
Hardness = 46 Temperature = 1000		
Proportion / Confidence	.90	.95
0.90	129258	126089
0.95	126756	123151
0.99	119750	114738

TABLE 75

YIELD STRENGTH TOLERANCE LIMITS

Heat D-14-K2	Offset Yield Strength (psi)		
Hardness = 44 Temperature = 800			
Confidence \ Proportion	.90	.95	.99
0.90	105079	100936	92976
0.95	102314	97879	89309
0.99	96032	90816	80636
Hardness = 45 Temperature = 800			
Confidence \ Proportion	.90	.95	.99
0.90	113539	109348	101298
0.95	111013	106514	97824
0.99	105216	99899	89532
Hardness = 46 Temperature = 800			
Confidence \ Proportion	.90	.95	.99
0.90	121556	117341	109246
0.95	119133	114602	105854
0.99	113546	108178	97721
Hardness = 44 Temperature = 900			
Confidence \ Proportion	.90	.95	.99
0.90	102198	98021	89997
0.95	99606	95127	86471
0.99	93677	88389	78077
Hardness = 45 Temperature = 900			
Confidence \ Proportion	.90	.95	.99
0.90	110566	106340	98228
0.95	108184	103639	94867
0.99	102680	97290	86796
Hardness = 46 Temperature = 900			
Confidence \ Proportion	.90	.95	.99
0.90	118436	114195	106055
0.95	116113	111548	102739
0.99	110728	105306	94757

Heat D-14-K2	Offset Yield Streng	
Hardness = 44 Temperature = 1000		
Confidence \ Proportion	.90	.95
0.90	68891	64734
0.95	66196	61744
0.99	60057	54813
Hardness = 45 Temperature = 1000		
Confidence \ Proportion	.90	.95
0.90	77251	73051
0.95	74765	70254
0.99	69048	63712
Hardness = 46 Temperature = 1000		
Confidence \ Proportion	.90	.95
0.90	85141	80926
0.95	82720	78189
0.99	77137	71768

Reference AFAPL-TR-66-127, Hardness = R_C, Temperat

TABLE 75 (Contd.)

YIELD STRENGTH TOLERANCE LIMITS

Heat H-9228-K2	Offset Yield Strength (psi)		
Hardness = 44 Temperature = 800			
Proportion / Confidence	.90	.95	.99
0.90	122020	119663	115102
0.95	119514	116863	111696
0.99	112826	109205	102061
Hardness = 45 Temperature = 800			
Proportion / Confidence	.90	.95	.99
0.90	131859	129429	124731
0.95	129728	126975	121619
0.99	123871	120066	112599
Hardness = 46 Temperature = 800			
Proportion / Confidence	.90	.95	.99
0.90	141084	138606	133826
0.95	139126	136308	130841
0.99	133646	129728	122080
Hardness = 44 Temperature = 900			
Proportion / Confidence	.90	.95	.99
0.90	108165	105688	100910
0.95	106205	103387	97923
0.99	100719	96802	89158
Hardness = 45 Temperature = 900			
Proportion / Confidence	.90	.95	.99
0.90	113571	111028	106148
0.95	111795	108888	103287
0.99	106700	102634	94775
Hardness = 46 Temperature = 900			
Proportion / Confidence	.90	.95	.99
0.90	118654	116074	111143
0.95	116961	114004	108335
0.99	112035	107890	99926

Heat H-9228-K2	Offset Yield St
Hardness = 44 Temperature = 1000	
Proportion / Confidence	.90 .95
0.90	91212 88839
0.95	88804 86131
0.99	82337 78674
Hardness = 45 Temperature = 1000	
Proportion / Confidence	.90 .95
0.90	93130 90692
0.95	91033 88269
0.99	85251 81426
Hardness = 46 Temperature = 1000	
Proportion / Confidence	.90 .95
0.90	94525 92047
0.95	92568 89749
0.99	87089 83170

for the true values η_0 of the dependent variable at a specified point $(X_{10}, X_{20}, \ldots, X_{k0})$ in the independent variables. The regression analysis will provide an estimate of η_0 such as Y_0, and an estimate of the underlying standard deviation, as s. The general form of the lower tolerance limit is given by

$$L = Y_0 - \frac{s\left[K_p + \left(K_p^2 - ab\right)^{1/2}\right]}{a}$$

where

$$a = 1 - K_\gamma^2/(2n) \qquad b = K_p^2 - K_\gamma^2/N^*$$

n = degrees of freedom for s

N^* = the effective number of observations

K_ε = the value of a standard normal variable which is exceeded with probability $1 - \varepsilon$

The effective number of observations, N^*, is defined by the property that the standard deviation of Y_0 is given by $s/\sqrt{N^*}$. If C denotes the inverse of the moment matrix used in the regression analysis and X_0 denotes the column vector with components $X_{10}, X_{20}, \ldots, X_{k0}$ then N^* is given by

$$N^* = \frac{1}{X_0} CX_0'$$

The preceding is taken from Wallis, W. A. (1951) "Tolerance intervals for linear regression", Second Berkeley Symp. Math. Statist, Prob. 43-41.

In Tables 73 through 75, lower tolerance limits are presented for various values of hardness, temperature, P, and γ, as indicated. All three tensile properties are represented for each of heats D-14-K2 and H-9228-K2.

The impact that the tolerance limits have on the present design is one of adding confidence to the screening and design selection processes. In general, it was found that at the nominal 45 R_C hardness and at 800°F, one could attach at least a 95-percent confidence level to 99 percent (proportion) of the material having strengths above the minimum yield strengths being used (72 percent of nominal 0.2-percent offset yield strength). It is not until 65 percent of the nominal yield strength is reached that a 99-percent proportion at 99-percent confidence level can be attached to the material samples. For the ultimate strength criteria (87 percent of ultimate at 20-percent overspeed), it was found that for the same hardness, temperature and confidence level, there may only be 90 percent of the material above the strengths being used in the design. This indicates that the designs are less reliable (stress-wise) than originally believed in the 20 percent overspeed condition. To reach the 99-percent proportion at a 99-percent confidence level, either the overspeed must be reduced (to about 10 percent) or the allowable 87 percent of ultimate being used must be reduced to 81 percent of ultimate.

Because only three heats were used, some penalty is paid in the small statistical sample. For instance, the above conclusions were drawn from results of the heat having the lowest stresses. With a larger number of heats, the confidence levels, etc., could possibly improve. Since the actual design stresses are generally lower than the above material stress criteria limits, confidence levels may be sufficiently high even for the small statistical sample used. Because of this, definition of any development test program required to prove the compatibility of the design stresses and material strengths can not be determined until the details of the final design are completely

known. This is because the application of the foregoing type of result is very much dictated by the details of a particular situation. In the present instance, only a very few alternators will ultimately be manufactured, and not much material is involved. Thus, when it comes time to build the alternator, it may be feasible to try several heats of steel and select one for use. This means, for example, that the worst one of the two heats investigated here could be used to obtain design values with the idea that later one can, by selection, obtain a heat at least as good. The point being raised is that we have only dealt with within-heat variability and our situation is such that we can do this. In other applications, however, it would be essential to take account of heat-to-heat variability. In such cases many more sample heats would be needed in the analysis.

6.3.2 Preliminary Fracture Toughness Considerations of H-11 Steel for Rotor Application

Although not a specific part of the reliability engineering studies, the fracture toughness in the presence of flaws of a generator rotor made from H-11 steel was considered, is considered inherently reliable, and is reported here. The analysis makes use of existing fracture toughness data. Recommendations for additional testing are also made.

The rotor material considered is H-11 steel having a room temperature yield strength of 200 ksi. Operating temperature range of the rotor is between 0° and 800°F. Due to the thickness of the rotor, plane strain conditions prevail throughout most of the rotor. At present K_{1C} fracture toughness values of H-11 steel under the above conditions have not been generated. Some data for H-11 steel has been presented in the literature. These results are for a higher strength level and a more restricted temperature range than of current interest. The existing data was examined and some first-order approximations of short-time K_{1C}'s for the strength level and temperatures of

interest were made. The term "short-time K_{1C} value" refers to values obtained by rapidly loading the test specimen to the fracture load. The K_{1C} or fracture toughness obtained under long-time creep exposure could differ appreciably from the short-time results. This point will be amplified later. The estimates are only intended to act as a starting point for preliminary considerations and should not take the place of actual tests.

The H-11 data to be examined is presented in Reference 21 and 22. Only that portion of the data which was considered valid by ASTM recommendations of 1964 (Reference 23) tabulated in Reference 24 and shown in Figures 89 and 90 will be considered. Since 1964, the ASTM criteria for validity of fracture toughness test results have been modified and, in general, made more restrictive (Reference 25). The present recommendations for plate specimens (bend specimens, etc.) require that

$$a \geq 2.5\left(\frac{K_{1C}}{\sigma_{ys}}\right)^2 \tag{1}$$

$$B \geq 2.5\left(\frac{K_{1C}}{\sigma_{ys}}\right)^2 \tag{2}$$

where a and B are the crack length and thickness of the test specimens. For notched round specimens, B has no meaning, and the corresponding recommended requirement is

$$D \geq 10\left(\frac{K_{1C}}{\sigma_{ys}}\right)^2 \tag{3}$$

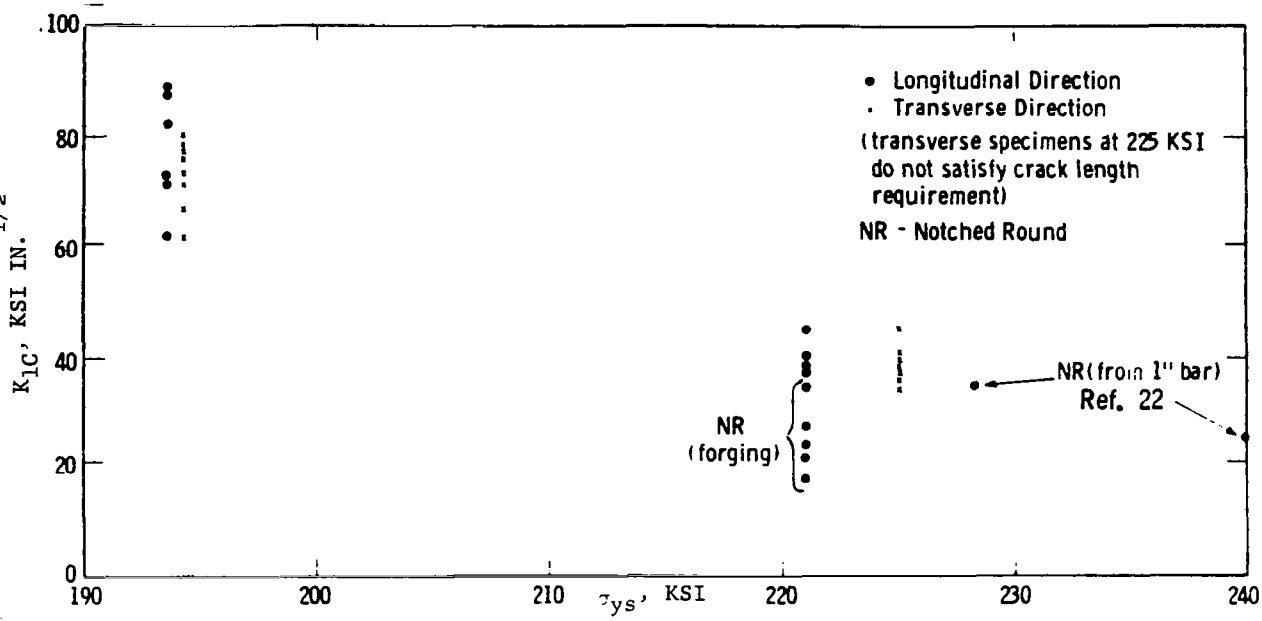

H-11 FRACTURE TOUGHNESS VERSUS YEILD STRENGTH

FIGURE 89

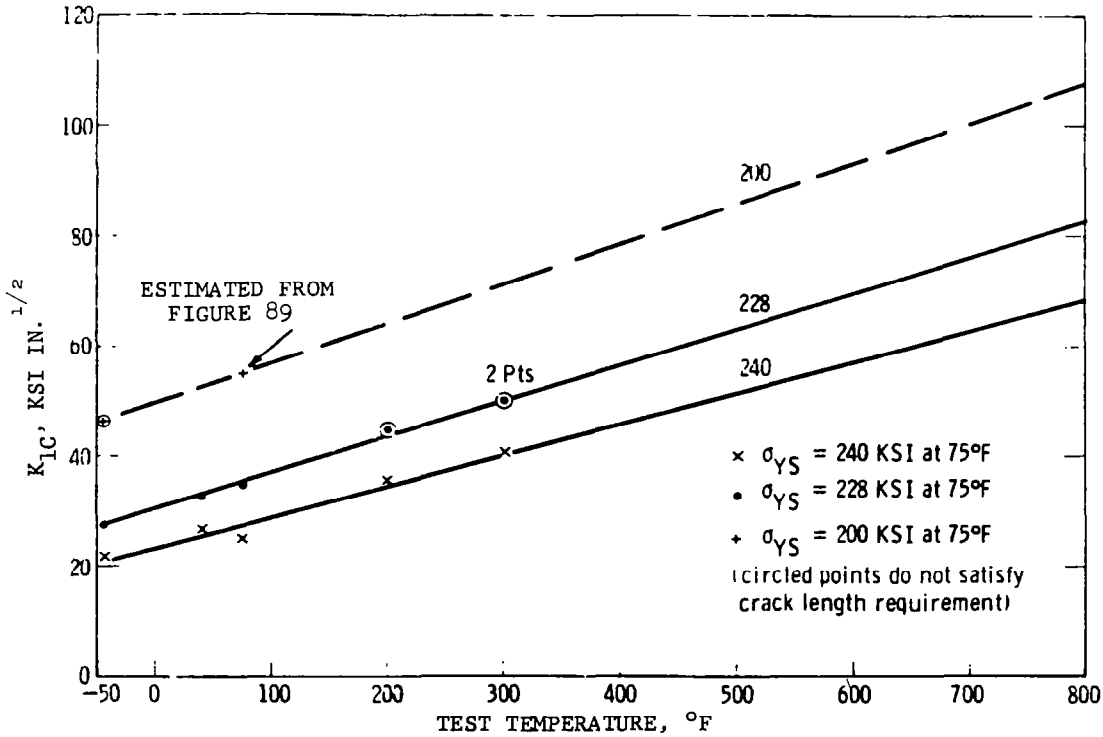

H-11 FRACTURE TOUGHNESS VERSUS TEMPERATURE

FIGURE 90

where D is the diameter at the unnotched section. For the notched round specimen, the crack length a now corresponds to the notch depth. All data points shown in Figures 89 and 90 satisfy the B or D requirement. Some of the data points shown do not satisfy the crack length requirements and are approximately designated. It is believed that the crack length requirement is not as crucial as the thickness or diameter requirement and, therefore, these points have not been eliminated.

The data presented in Figure 89 shows the effect of room temperature yield stress level on K_{1C}. The strength level was varied by changing from the tempering temperature. All but two specimens were machined from a 8.00-in. square forged-billet. The two indicated exceptions were machined from 1.0-in.-diameter bars. The specimens taken from the forged-billet should be more representative of the rotor condition than those machined from the bars. The data is mainly in the 195-, 200-, and 225-ksi yield stress ranges. The following comments on this data can be made.

(a) The notched round tests at the 220-ksi level have appreciable scatter and give lower values than the bend specimens for the same strength level.

(b) Specimen orientation does not appear to effect K_{1C} at room temperature for the particular forging considered.

(c) It is also reported in Reference 21 that for the strength levels considered in Figure 89, the position of the specimen in the forging had no significant effect on K_{1C}.

Due to the scatter shown in Figure 89, it is difficult to estimate a room temperature K_{1C} for the 200-ksi yield strength level of

interest. A conservative estimate can be made from a lower boundary of the data. Such an estimate would give a room temperature K_{1C} of 55 ksi $\sqrt{in.}$

From Figure 90, a very rough conservative estimate of the effect of temperature on K_{1C} of the 200-ksi level can be made. The data shown in this figure was obtained from specimens machined from 1.0-in.-diameter bars. Specimens machined from heavier sections would be more desirable. All specimens satisfy the unnotched diameter requirement, and all but the indicated points satisfy the crack length requirement. Data between -50° and 300°F is shown for room temperature strength levels of 228 and 240 ksi. A data point at -40°F is shown for what is believed to be a room temperature strength level of 200 ksi.

For many metals, the K_{1C} varies approximately linearly with temperature below T_o. The K_{1C}'s shown in Figure 90 for two different strength levels vary approximately linearly with temperature. Above the temperature T_o, the rate of increase of K_{1C} with temperature usually increases rapidly. With this point in mind, it can be stated that a linear extrapolation of the data shown in Figure 89 probably will be a conservative extrapolation. The linear extrapolation of the 228 and 240 levels are shown in Figure 90 as solid lines. The conservative estimate of K_{1C} variation for the 200 level could be obtained by either drawing a straight line between the -40°F value and the previously estimated room temperature value (55 ksi $\sqrt{in.}$) or by extrapolation of the 240 and 228 ksi strength level - K_{1C} lines shown in the figure. Both approximations give roughly the indicated dashed-line. This type of an extrapolation gives a K_{1C} of 110 ksi $\sqrt{in.}$ at 800°F for 200-ksi room temperature yield stress H-11 steel under short-time test conditions.

From the estimated values of K_{1C} obtained in the previous paragraphs, an indication of whether the principles of fracture mechanics

are applicable to the rotor for short-time fracture conditions can be obtained. Where it is applicable, critical flaw sizes can be estimated. For initial considerations, the simplest and most likely defect is a penny-shaped crack or flaw near the center of rotor. The relation between crack tip stress intensity, the uniform applied stress σ normal to the plane of the crack, and the radius a of crack is

$$K = \frac{2}{\sqrt{\pi}}\sqrt{a}\sigma \tag{4}$$

The critical crack size is then

$$a_{cr} = \frac{\pi}{4}\left(\frac{K_{1C}}{\sigma}\right)^2 \tag{5}$$

Linear elastic fracture mechanics is only applicable to the prediction of crack instability when the plastic zone at the crack tip at instability is small compared to the crack length. To be more qualitative, it can be stated that based on experimental data (Reference 25), fracture mechanics is applicable when

$$a_{cr} \geq a_m = 2.5\left(\frac{K_{1C}}{\sigma_{ys}}\right)^2 \tag{6}$$

where a_m indicates minimum crack size.

First room temperature conditions will be considered. The maximum tensile stress at the center of the rotor is approximately σ = 100 ksi. The estimated room temperature K_{1C} is 55 ksi $\sqrt{\text{in.}}$ and room temperature σ_{ys} is 200 ksi. From Eq. (5), a critical crack radius of a_{cr} = 0.24 in. is calculated. From Eq. (6), a_m = 0.189 in. Since $a_{cr} \geq a_m$, the applicability of fracture mechanics at this

temperature is valid. Therefore, if K_{1C} is approximately 55 ksi $\sqrt{in.}$, then a penny-shaped flaw of 0.24-in. radius is needed for fracture. For the size rotor under consideration, a flaw of this size should be detectable by nondestructive test methods.

The estimated short time K_{1C} at 800°F was 115 ksi $\sqrt{in.}$ The yield stress at this temperature is 125 ksi. Therefore, still maintaining σ = 100 ksi, the use of Eq. (5) and (6) results in a_{cr} = 1.04 in. and a_m = 2.12 in. From a rigorous point of view, these calculations would indicate that for short time considerations, plane strain fracture mechanics would not be applicable at this temperature ($a_{cr} < a_m$). An estimated flaw size of a_{cr} = 1.04 in. for a K_{1C} of 115 ksi $\sqrt{in.}$, and σ = 100 ksi probably is realistic and could be easily detected. Flaws of this size are very unlikely, however.

The calculations of the previous paragraphs show that for the estimated short-time K_{1C} values, the size of flaw at the rotor center needed for catastrophic failure are large enough so that nondestructive test methods will be able to detect them. The estimate of the K_{1C} temperature dependence, although intended to be conservative, was very approximate. Fracture mechanics tests of the H-11 at the yield strength of interest and over the temperature range of interest should be carried out to see if this preliminary conclusion is valid.

All estimates and calculations presented in this analysis are with respect to the effect of flaws on a short-time basis. The influence of long-time creep conditions on the reduction in ductility and subsequent reduction in fracture toughness in the presence of flaws has not been considered. There is very little data at present on the effect of creep on the fracture toughness of high-strength steels. In Reference 26, it is reported that a relatively high-strength material, AMS 6304, showed approximately 70-percent decrease in fracture toughness after creep exposure, when tested above the 250°F toughness-transition temperature. It is suggested that some testing be

undertaken to determine the reduction in toughness of H-11 caused by creep exposure. Note also, the effects of cyclic loading have not been considered, as the high-stress areas in the rotor will be subjected to a negligible amount of cycling.

6.3.3 Failure Mode, Effect, and Criticality Analysis

The FME & CA study was carried out for purposes of identifying and cataloging the various modes and effects of component failures down to and including subassembly levels wherever possible. The components and subassemblies were categorized by a reliability model that consisted of

(a) Rotor and rotor coolant

(b) Stator and stator coolant

(c) Bore seal assembly

(d) Field winding and insulation

(e) Armature winding and insulation combined and the inert hardware

The bearings and seals were not considered part of the reliability model. These are not part of the specific alternator electromagnetic design task at Westinghouse.

The specific configurations within the model were considered general in order to be applicable to all the base designs. The preliminary FME & CS was undertaken at a joint meeting of the materials, design, and reliability engineers most experienced in the KTA design philosophies. At this meeting, all known possible failure modes were identified, discussed, and tabulated, which, in addition to discovering

failure modes, provided guidance in choosing between alternate concepts in the alternator designs. The failure modes identified were correlated according to immediate or long-term effects on the system. The severity of the effects were categorized:

(a) Minor – no noticeable immediate or long-range effect

(b) Major – no noticeable immediate effect but definite long-range effect

(c) Critical – immediate and long-range effect

For the study, it was assumed the alternator was in an operating condition, and successful operation constituted the ability to produce useful power for the power system. The power system was defined as the KTA and its ability to produce power. The effect of the failure on the power system was evaluated from the standpoint of life, power output, overload, shorts, vibration, unbalance, overspeed capability, etc. The guiding philosophy in cataloging the failure modes was, "What must the power system do to respond to the various failure modes." Because the Phase I study was preliminary in nature, the probably causes of the failure modes were included in the FME & CS and the probability or likelihood of their occurrence was not included in the evaluations.

The tabulation of the preliminary FME & CS is presented in Table 76. In all, 47 major failure modes are catalogued.

TABLE 76

KTA ALTERNATOR PRELIMINARY FAILURE MODE, EFFECT AND CRITICALITY ANALYSIS

Probable Causes of Failure	Mode of Failure	Immediate Effect on Operation	Long-Range Effect on Operation	Severity
		ROTOR		
Particular reason not clearly identifiable	Pole slot or lamination short	Increased losses and tip temperature	Increased creep strain	Major
Due to magnetic pulses, electrical vibration windage	Individual pole lamination fatigues	Cuts bore seal	Stator shorts through open seal; excessive creep strain	Critical
Due to same as individual laminations	Pole laminations fatigue as unit	Breaks off into bore seal and stator	--	Critical
Due to nonuniform properties	Nonuniform creep rate or yield	Increased vibration, creep strain	Increased creep strain	Major
Due to loss of concentricity	Stub shaft rubs seals at base	Increased vibration	Wear or seizure	Critical
Due to increased vibration or poor/ changed properties	Stub shaft fatigue	Breaks off	--	Critical
Due to embrittling and high stress	Crack propagation in rotor core	Increased strain	Rotor disintegrates	Critical
All due to mass transfer	Mass transfer, stress corrosion and galvanic corrosion	Added solids into coolant	Increased stress strain and possible loss of rotor	Major
Due to corona and $\overline{U} \times \overline{B}$ in plasma	MHD and plasma erosion on poles	Reduce output	Loss of pole tip or bore seal	Major

TABLE 76 (Contd.)

Probable Causes of Failure	Mode of Failure	Immediate Effect on Operation	Long-Range Effect on Operation	Severity
		ROTOR (Contd.)		
Due to flexibility of mounting configuration	Windage baffle or support fatigues	Rubs on rotor	Increased vibration	Minor
Baffle coats with potassium or carbon	Windage baffle shorts with conductive film	Increased losses	Increased rotor creep strain	Major
Due to fit or bearing wear	Minor loss of concentricity	Increased vibration	Additional creep strain	Major
Due to loss of bearing	Major loss of concentricity	Rub and/or loss of rotation	--	Critical
Embrittlement, creep resistivity, permeability	Material property change	Change in power output	Excessive creep or yield	Major
		ROTOR COOLANT		
Due to solids accumulation on system malfunction	Flow blockage (decreased or stopped	Increased rotor temperature or vibration	Excessive creep or yield	Critical to major
In coolant passage	Leak in weld	Increased cavity pressure and windage	Liquid erosion	Critical
Due to high fluid pressures	Excessive stress corrosion effects	Added solids into coolant	Excessive stress, strain or loss of rotor	Major to critical
Due to system malfunction	Excessive coolant temperature	Possible plastic yield or rupture	Excessive creep or yield	Critical to major

TABLE 76 (Contd.)

Probable Causes of Failure	Mode of Failure	Immediate Effect on Operation	Long-Range Effect on Operation	Severity
		ROTOR COOLANT (Contd.)		
Due to seal failure or vent plugging	Loss of cavity vacuum control	Increased cavity pressure and windage	Excessive rotor creep	Major
		BORE SEAL ASSEMBLY		
Due to fatigue in joint, tube, bellows or end member; stress corrosion, mass transfer or plasma erosion, instability of braze alloy	Loss of hermetic seal	Allows rub or increased vibration	Stator shorts	Critical
Due to potassium or carbon coating	Seal ID shorts with conductive film	Increased losses	Increased rotor creep strain	Major
Due to stack or broken stator parts	Fretting wear	Short-out stack teeth	Loss of hermetic seal	Critical to major
Due to abnormal electrical operation	Abnormal temperature excursion	Excessive thermal stress	Loss of hermetic seal	Critical to major
		STATOR AND STATOR COOLANT		
Due to fatigue stress corrosion mass transfer	Leak in cooling duct	Stator shorts increased stator cavity pressure to induced corona	--	Critical
Due to solids accumulation or system malfunction	Flow blockage decreased or stopped	Excessive temperatures and losses	Accelerate insulation deterioration	Major

TABLE 76 (Contd.)

Probable Causes of Failure	Mode of Failure	Immediate Effect on Operation	Long-Range Effect on Operation	Severity	E Po
		STATOR AND STATOR COOLANT (Contd.)			
Due to bond or contact pressure loss	Duct separating from frame	Excessive temperatures and losses	Accelerate insulation deterioration	Major	Sh
Due to mechanical or electrical fatigue	Stack clamps fatigue	Separation of stack, loss of power	Fretting wear on bore seal	Critical	Nc
Due to system malfunction	Excessive coolant temperature	Excessive losses, loosen stack fits	Accelerated deterioration or increased vibration	Major	Sh
Due to loose stack fit, fretting wear or shorting	Loss of interlaminar insulation	Increased losses and excessive temperatures	Accelerated deterioration	Major	Sh
Due to mechanical or electrical vibration	Fatigue of teeth	Breaks off, flux unbalance	Decrease output wears through bore seal	Major to critical	Sh
	Short-circuit effects on stack	Turn stacks in frames	Increase pressure and wear on insulation	Major	Sh
		WINDINGS AND INSULATION			
Wire expands in slot and tries to straighten end turns	Short-circuit operation	Cracks slot liners or end turn insulation or wedges Straightens wires to bus rings	Accelerated insulation deterioration	Major to minor	Sh
Due to mechanical and electrical vibration	Slot cell insulation fatigue	Loss of slot liner or wedgers, increased temperatures	Stator shorts	Major	Re

TABLE 76 (Contd.)

Probable Causes of Failure	Mode of Failure	Immediate Effect on Operation	Long-Range Effect on Operation	Severity
		WINDINGS AND INSULATION (Contd.)		
Due to mechanical and electrical vibration	Anadur frets away	Loosening of windings, increased temperatures	Accelerated insulation deterioration	Major
Due to handling abuse, electrical stress, poor manufacturing	Cladding breaks	Silver migrates out of wire	Shorts insulation or opens wire	Major to critical
Due to plating or cladding breaks or chemical reaction	Joint cladding instability	Loss of solid bond	Silver migration	Major to critical
Due to mechanical or electrical failure	A/C opens	Reduction in output, phase unbalance	--	Major to critical
Due to mechanical or electrical failure	F/C opens	Loss of output over speeds	--	Critical
Due to system malfunction	Excessive coolant temperatures	Increased losses, bus rings and wires sag	Accelerated deterioration, possible short	Major
Due to mechanical and electrical vibration	Bus rings and leads fatigue	Open circuits	--	Major
Due to vibration	Terminal cracks or breaks	Loss of hermetic seal, shorts out	--	Critical
Due to vibration	Heat shorts fatigue	Excessive temperatures and losses	Accelerates insulation deterioration	Major

TABLE 76 (Contd.)

Probable Causes of Failure	Mode of Failure	Immediate Effect on Operation	Long-Range Effect on Operation	Severity	Eff Powe
			INERT HARDWARE		
Due to joint failure or fatigue crack	Loss of rotor cavity hermetic seal	Lower cavity pressure, less windage	Loss of potassium	Major	Shor
Due to system malfunction	Excessive coolant temperature	Thermal stress and distortions	Excessive creep loosens fits; loses concentricity	Major to critical	Shor lo
Due to excessive vibration	Fatigue of housings, endbells, etc.	Increase vibration	Loss of potassium	Major	Shor
Due to evaporation of coating	Reduction of emissivity on stator ID	Excessive armature temperatures increase losses	Accelerate insulation deterioration	Major	Shor
Due to vibration	Mounting flange loosens	Increased vibration, loss of concentricity	Accelerated fatigue and breaking-up	Major	Shor lo

7. CONCLUSIONS AND RECOMMENDATIONS

The detail conclusions and recommendations are presented in the preceding discussions. The following will be limited to major highlights to give an overall view of the results.

It is recommended that two designs be considered for Phase II; they are the designs at either 19,200 or 24,000 rpm. Both are at 1600 Hz, 480 v, and 800°F or less potassium coolant. The 19,200-rpm case was the primary choice over the 24,000-rpm design, based on the Phase I requirements. However, with a stress-minimized design and some relaxation in the long-term overspeed requirement, the 24,000-rpm case could be made the more attractive of the two. It is already the most attractive from the electromagnetic design point of view. The coolant temperature choice could be 800°F, but for H-11 reliability considerations should be 600° to 700°F. No apparent benefits appear in going to higher or lower temperatures than the 600° to 800°F range. Higher temperatures require different rotor materials that limit the KTA speed to 16,000 rpm. This lower speed penalizes the KTA and system. The lower temperatures with organic coolants do not offer significant reduction in design complexity nor do they allow speeds over 24,000 rpm, the maximum allowed for the potassium coolant. Besides the system weight and coolant life penalties with the lower coolant temperature, the complexities of potassium-to-organic turbine shaft seals preclude any recommendations for organic fluids in the KTA alternator.

The recommended temperature of 600° to 800°F is tied to the choice of rotor material. The studies indicated H-11 steel at 45 R_C is the best choice at temperatures as low as 200°F. Above 800°F, magnetic materials are available for rotors but their strength capabilities penalize the KTA by limiting speeds. Magnetic properties of the materials evaluated appear adequate. As a guide to future materials development, the following statement can be made based on the present findings. "If a rotor material could be developed which had 1100°F

magnetic and strength properties similar to those for H-11 at 800°F, then an 1100°F KTA alternator could be developed as easily and be as attractive as one for 800°F coolant." The stator designs and materials used are not limited until about the 1100°F-temperature range so any higher temperatures are keyed upon the rotor material limitations.

In the stator design, it was determined that the same basic materials and concepts would be either desirable or adequate for 400°F designs, 800°F designs or 1100°F designs. Only slight material changes would be made between the three temperatures. The low-temperature designs could use some standard low-temperature materials, but because of the concept to design at high power density, the insulation and wire materials must still be capable of 800°F hot spots. The 1100°F designs would use slightly higher temperature wire and insulation materials and be supported better to prevent excessive creep or sagging of the Hiperco-27. Neither of these changes have any significance to the design concepts. Designs at all three temperatures make maximum use of direct radiation off the wire end turns and cooling ducts in direct contact with the stator frame and field coil to have sufficient cooling in a space vacuum ambient.

Regardless of whether both or either cavities (rotor and stator) are vented to space or whether potassium or organic coolant is used, a ceramic bore barrier or seal is required in the radial gap between the rotor and stator. The fabrication of the ceramic (99.8 percent alumina) body for 800°F or below coolant is within present technology. At 1100°F, beryllia ceramic is required, and this material will require development to fabricate the large size bodies required. The ceramic-to-metal joints and the metal end member design and fabrication will require the most development for any temperature or material choice, once a design is finalized and fabrication starts. Venting the rotor cavity to space would obviate the need for a hermetic bore seal and a simpler bore barrier concept would suffice. This would introduce

the need for potassium shaft seals-to-space. Of the two – bore seals or shaft seals-to-space – the hermetic bore seal approach appears more appropriate to the KTA requirements.

8. REFERENCES

1. Topical Report, Parametric Study of Inductor Alternators, U.S. Atomic Energy Commission Research & Development Report SAN 679-6, February 1968. Prepared by Westinghouse Electric Corporation, Aerospace Electrical Division, Lima, Ohio.

2. Final Report, Design Study for Electrical Component Technology for 0.25 to 10.0 Megawatt Space Power Systems, U.S. Atomic Energy Commission Research & Development Report SAN 679-8, February 1968. Prepared by Westinghouse Electric Corporation, Aerospace Electrical Division, Lima, Ohio.

3. Evaluation of Pole Face Losses for the 467 KVA SNAP-50/SPUR Generator, USAF Systems Command, Report No. AFAPL-TR-66-143, January 1967. Prepared by Westinghouse Electric Corporation, Aerospace Electrical Division, Lima, Ohio.

4. Smith, O. G., "Windage Power Losses in Inductor Type Aerospace Electric Generators", M.S. M.E. Thesis, University of Pittsburgh, Pittsburgh, Pennsylvania, 1962.

5. Smith, O. G., "Windage Power Losses in Aerospace Generators", Westinghouse Electric Corporation, Aerospace Electrical Division, Lima, Ohio. Report No. RP71310, December 1961.

6. AC Generator Rotor Materials Topical Report, USAF Systems Command Report AFAPL-TR-66-127, January 1967. Prepared by Westinghouse Electric Corporation, Aerospace Electrical Division, Lima, Ohio.

7. Magnetic Materials Topical Report, NASA Lewis Research Center Report, NASA-CR-54091, September 1964. Prepared by Westinghouse Electric Corporation, Aerospace Electrical Division, Lima, Ohio.

8. High Temperature Magnetic Materials, Westinghouse Electric Corporation, Aerospace Electrical Division, Lima, Ohio. Report No. WAED 67.34E, October 1967, Prepared on "Contract for Development and Evaluating Magnetic and Electrical Materials Capable of Operating in the Temperature Range from 800° to 1600°F". Contract No. NAS 3-6465.

9. Work on Contract NAS 5-1234 was reported in six volumes: Vol. I, II, III, and IV as Westinghouse Electric Corporation, Aerospace Electrical Division, Lima, Ohio, Report No. D-709533, December 1962. Volume IV numbered NASA-CR-50861.

One volume as Westinghouse Aerospace Electrical Division Report No. WAED 63.11E, December 1963.

One volume, unnumbered, by Westinghouse Aerospace Electrical Division on 250- and 500-kw designs on an extension of NAS 5-1234.

10. Gladstone, S., "Textbook of Physical Chemistry", 2nd Ed., 13th Printing, D. Van Nordstrand Co., Princeton, New Jersey, p. 280.

11. Topical Report, Experimental Verification, U.S. Atomic Energy Commission Research & Development Report SAN 679-7, February 1968. Prepared by Westinghouse Electric Corporation, Aerospace Electrical Division, Lima, Ohio.

12. Electrical Conductor and Electrical Insulation Materials Topical Report, NASA Lewis Research Center Report, NASA-CR-54092, October 1964. Prepared by Westinghouse Electric Corporation, Aerospace Electrical Division, Lima Ohio.

13. Gowen, F. E. and E. W. Perkins, Drag of Circular Cylinders for a Wide Range of Reynolds Numbers and Mach Numbers, National Advisory Committee for Aeronautics Technical Note 2960, Washington, June 1953.

14. Electrical System Design Study for 300-KW Nuclear Dynamic Space Power System, Westinghouse Electric Corporation, Aerospace Electrical Division, Lima, Ohio. Report No. D-709353, March 1962.

15. Phase II Final Report for the SPUR AC Generator Development, Westinghouse Electric Corporation, Aerospace Electrical Division, Lima, Ohio. Report No. D-709549, January 1963.

16. SNAP 50/SPUR 467 KVA Experimental Generator Design Summary, USAF Systems Command Report AFAPL-TR-67-7, May 1967. Prepared by Westinghouse Electrical Corporation, Aerospace Electrical Division, Lima, Ohio.

17. Bagwell, D., TØSS, An IBM 7090 Code for Computing Transient or Steady State Temperature Distributions, U.S. Atomic Energy Commission Research & Development Report No. K-1494, December 1963.

18. SPUR Generator Stator Seal Development, Topical Report, USAF Systems Command Report ASD-TDR-63-677; Part I, August 1963; Part II, February 1967. Prepared by Westinghouse Electric Corporation, Aerospace Electrical Division, Lima, Ohio.

19. Bore Seal Technology Topical Report, NASA Lewis Research Center Report NASA-CR-54093, December 1964. Prepared by Westinghouse Electric Corporation, Aerospace Electrical Division, Lima, Ohio.

20. Alkali Metal Resistant Electrical Devices, USAF Report AFAPL-TR-68-61, June 1968. Prepared by Westinghouse Electric Corporation, Aerospace Electrical Division, Lima, Ohio.

21. Amateau, M. F. and E. A. Steigerwald, "Fracture Characteristics of Structural Metals", AD 611873, ER-5937-3, Thompson-Ramo-Wooldridge, January 1965.

22. Hanna, G. L. and E. A. Steigerwald, "Fracture Characteristics of Structural Metals, AD 411509, ER-5426, Thompson-Ramo-Wooldridge, June 1963.

23. Progress in Measuring Fracture Toughness and Using Fracture Mechanics, Fifth Report of the ASTM Special Committee on Research and Standards, March 1964, p. 113.

24. Wessel, E. T., W. G. Clark, and W. K. Wilson, "Engineering Methods for the Design and Selection of Materials Against Fracture", Final Technical Report, Contract No. DA-30-069-AMC-602 (T), June 1966.

25. Brown, Jr., W. F. and J. E. Srawley, "Plain Strain Crack Toughness Testing of High Strength Metallic Materials", ASTM Special Technical Publication No. 410.

26. Sprague, R. A., M. J. Donachie, Jr., and W. P. Danesi, "Effect of Creep Exposure on the Fracture Toughness of Two Low Alloy Steels", Journal of Basic Engineering, March 1966.

27. McGrew, J. M. et. al., "Part II Screw Seal Evaluation", AFAPL-TR-65-89 Part II, Prepared under Contract No. AF33(657)-8469 by Missile and Space Division of General Electric Company, Cincinnati, Ohio, September 1965.

28. Ludwig, L. P., et. al., "Gas Ingestion and Sealing Capacity of Helical Groove Fluid Film Seal (Viscoseal) Using Sodium and Water as Sealed Fluids", NAS TN D-3348, March 1966.

29. King, A. E., "Screw Type Shaft Seals for Potassium Lubricated Generators", IEEE Trans. on Aerospace, Vol. AS-3, Supplement pp. 471-479, June 1965.

30. Caldwell, R. T. and D. M. Walley, Physical and Thermodynamic Properties of Potassium, Technical Report AFAPL-TR-66-104, November 1966.

31. Organic Fluid Data for the Potassium Turboalternator Study, AiResearch Report APS-5268-R, August 31, 1967.

32. Stair, W. K., "Effect of Groove Geometry on Viscoseal Performance", ASME Paper 66-WA/FE-28, November 1966.

33. King, A. E., et. al., "SNAP-50/SPUR 467 KVA Experimental Generator Design Summary", Technical Report AFAPL-TR-67-7, May 1967.

34. King, A. E., "Screw Type Shaft Seals for Potassium Lubricated Generators", IEEE Transactions on Aerospace, Vol. AS-3, June 1965, Supplement pp. 471-479.

35. Lowry, R. A., "A Holweck Type Molecular Pump", Research Laboratories for Engineering Sciences, University of Virginia, Charlottsville, Virginia, August 1961.

36. Lessley, Hodgson, and Haglund, "SNAP-8 Seals to Space Test Program", NASA-CR-54234, Vol. IV, May 1964. See also ASME Paper No. 65-GTP-14.

37. Hodgson, "SNAP-8 Seals to Space Test Program", NASA-CR-54234, Vol. II, May 1964. See also ASME Paper No. 65-GTP-15.

38. Chadbourne, Kovacevich, and Riffle, "SNAP-50/SPUR Nuclear Mechanical Power Unit Experimental Research and Development Program", Technical Report AFAPL-TR-67-34, Part III, May 1967.

APPENDIX A

COMMENTS ON WINDAGE LOSS CALCULATIONS

A refinement of the windage power loss calculations was made for analysis of the KTA alternator base designs using model theory and experimental data from a rotor configuration similar to the KTA rotor configurations. A discussion of the analytical refinements is presented in the following paragraphs.

The windage power loss within a rotor cavity is necessarily predicted from test data obtained from an operating model. To accomplish this task, it is necessary to (1) describe the significant variables associated with the fluid which influence the losses, (2) describe the variables which define the dynamic state of the rotor, (3) describe the dependent variable of interest, (4) reduce the number of variables involved by using dimensional analysis, and (5) obtain the performance characteristics of the geometrically similar rotor configuration in terms of the dimensionless parameters defined by the analysis.

The dependent variable of interest from the standpoint of power loss is the windage torque, T. The independent variables associated with the fluid within the rotor cavity were assumed to be (1) the density, ρ, (2) the viscosity, μ, and (3) the velocity of progration of pressure impulses or the sonic velocity within the fluid, a^*. The dynamic state of the rotor was defined by speed of rotation, ω. The dimensions of the rotor configuration were represented by one characteristic dimension, R, or the radius of the rotor.

The torque on the rotor can be written as an infinite series:

$$T = \sum C_i \left[\omega^a, \rho^b, \mu^c, R^d, a^{*e}\right] \qquad (1)$$

In order for Eq. (1) to be correct, the dimensions of each of the series on the right must have the same dimensions as the dependent variable on the left side of the equation. Substituting the fundamental dimensions (M, L, and t) for each term, the dimensional equation becomes:

$$ML^2t^{-2} = \left(t^{-1}\right)^a, \left(ML^{-3}\right)^b, \left(ML^{-1}t^{-1}\right)^c, \quad L^d, \left(Lt^{-1}\right)^e \tag{2}$$

Equating exponents of M, L, and t gives:

$$\begin{aligned} 1 &= b + c \\ 2 &= -3b - c + d + e \\ -2 &= -a - c - e \end{aligned} \tag{3}$$

and solving this set of equations for c, d, and e in terms of a and b gives

$$\begin{aligned} c &= 1 - b \\ d &= 2 + a + b \\ e &= 1 - a + b \end{aligned} \tag{4}$$

Rewriting the series Eq. (2) for T using the exponents of Eq. 1, Eq. 4 gives:

$$T = C_i \left[\omega^a, \rho^b, \mu^{1-b}, R^{2+a+b}, a^{*1-a+b}\right] \tag{5}$$

Next, collecting terms of similar known and unknown exponents, one obtains

$$\frac{T}{R^2 a^* \mu} = f\left[\left(\frac{\omega R}{a^*}\right)^a, \left(\frac{\rho R a^*}{\mu}\right)^b\right] \tag{6}$$

With these three groups of dimensionless parameters, experimental data can be illustrated graphically as shown by the solid lines in Figure 1. The graphical solution offered by this treatment of quantitative data can be used to predict the windage power loss for a similar case even if the rotor has a different diameter and is operated within a strange fluid. The accuracy of this graphical solution is limited by the assumed variables. If pertinent variables were not included in the functional Eq. (5), the accuracy of the solution would be limited accordingly. The solution can be proved satisfactory only by experience.

A previous dimensional analysis of the problem by Smith[4,5*] did not consider the velocity of propagation of pressure impulses, a*, as a pertinent variable. The dimensionless groups of terms for this case can be obtained by setting e = 0 in the previous exponent equations, (4), and solving for a and c in terms of b. This gives

$$a = 1 + b$$
$$c = 1 - b$$
$$d = 3 + 2b$$

Rewriting the series Eq. (2) for T using these new exponent equations gives

$$T = C_i \left[\omega^{1+b}, \rho^{b}, \mu^{1-b}, R^{3+2b} \right] \tag{7}$$

Collecting terms of similar known and unknown exponents gives

$$\frac{T}{R^3 \omega \mu} = f\left(\frac{\rho \omega R^2}{\mu}\right)^b \tag{8}$$

*References for Appendix A are listed in Section 8 of the report.

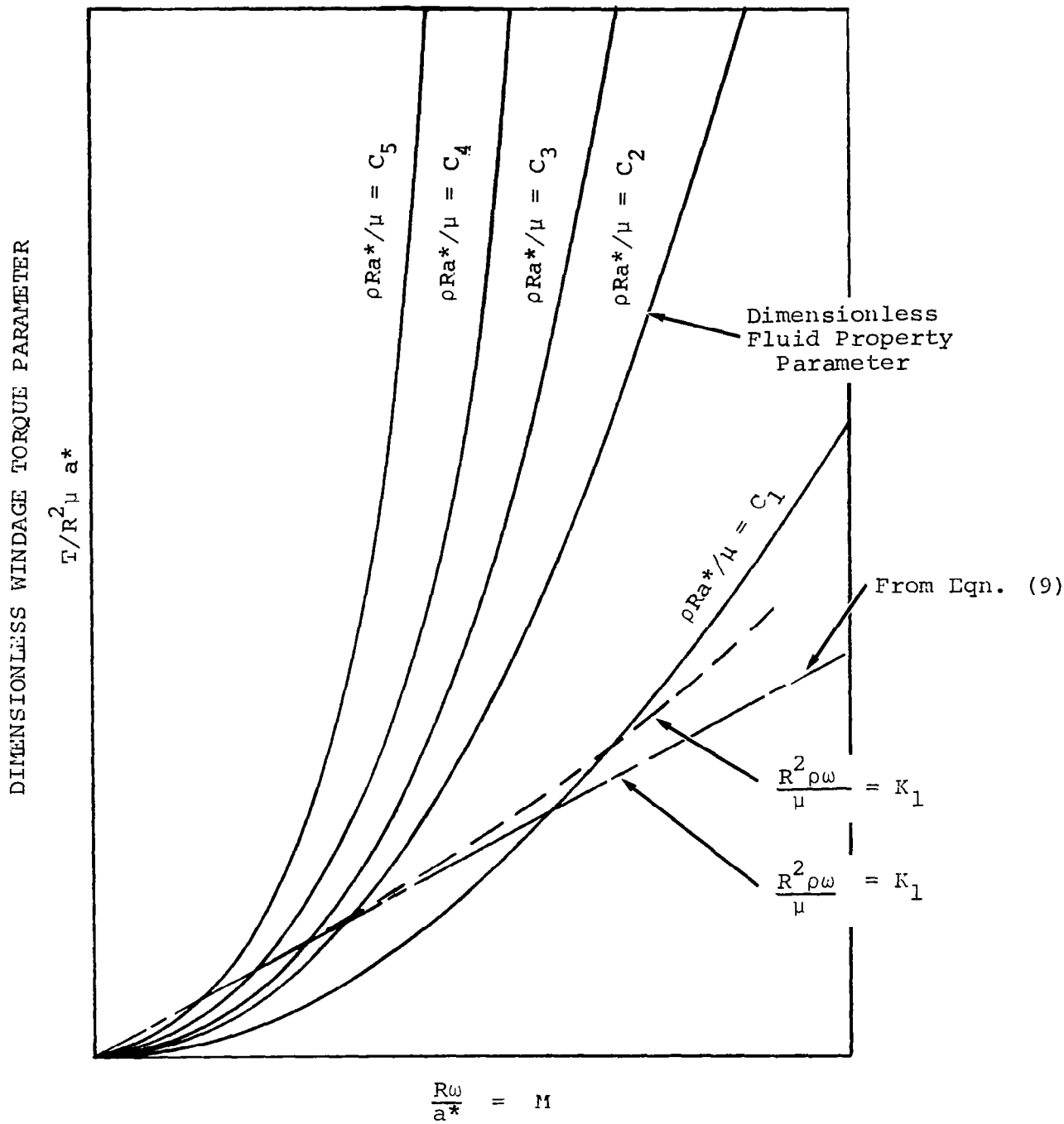
DIMENSIONLESS WINDAGE TORQUE PARAMETER
$T/R^2\mu\, a^*$
$\rho Ra^*/\mu = C_5$
$\rho Ra^*/\mu = C_4$
$\rho Ra^*/\mu = C_3$
$\rho Ra^*/\mu = C_2$
$\rho Ra^*/\mu = C_1$
Dimensionless Fluid Property Parameter
From Eqn. (9)
$\frac{R^2\rho\omega}{\mu} = K_1$
$\frac{R^2\rho\omega}{\mu} = K_1$
$\frac{R\omega}{a^*} = M$
DIMENSIONLESS ROTOR SPEED PARAMETER

FIGURE 1

In order to compare this functional equation with Eq. (6), which was obtained by considering a* to be a pertinent variable, both sides of Eq. (8) are multiplied by $R\omega/a^*$. This gives

$$\frac{T}{R^2 a^* \mu} = f\left[\frac{R\omega}{a^*}\left(\frac{\rho\omega R^2}{\mu}\right)^b\right] \tag{9}$$

This gives two functional relationships which contain the same dimensionless group of terms on the left-hand side of Eq. (6) and (9).

The dimensionless torque parameter in Eq. (9) is (1) an exponential function of the Reynolds No. $\rho\omega R^2/\mu$, and (2) a linear function of the Mach No., $R\omega/a^*$, associated with the pole tips. Experience has proved that the dimensionless torque parameter is an exponential function of the Reynolds number. However, experience has also proved that the dimensionless torque parameter is not a linear function of the Mach number. Thus, the accuracy of the functional equation obtained by a dimensional analysis, which does not include a*, is limited accordingly. The difference between the two functional relationships, Eq. (6) and (9), also can be illustrated graphically in Figure 1. After a plot of the quantitative data has been made as illustrated by the solid lines, a line through points of constant Reynolds number can be drawn as shown by the broken lines. In this instance, the Reynolds number equals the product of $R\omega/a^*$ and $\rho Ra^*/\mu$. This line may not be straight; it probably has an upward curvature when the Mach number is large. On the other hand, the functional relationship given by Eq. (9) infers that all of these points fall on a straight line as indicated. Thus, when experimental data is plotted according to the functional relationship defined by Eq. (9), the effects of Mach number are omitted. Error will be introduced when this data is used to predict the windage power loss for cases which have a Mach number different than the test case.

APPENDIX B

VISCOSEAL PARAMETRIC STUDY

1. GENERAL ANALYSIS OF VISCOSEAL PERFORMANCE

The performance of viscoseals for use in potassium and the organic fluids was obtained from results of tests using different fluids. To accomplish this, it was necessary to (1) describe the significant variables, associated with the fluid, which influence the performance of viscoseals, (2) describe the variables which define the dynamic state of seals, (3) describe the dependent performance variables of interest, (4) reduce the number of variables involved by using dimensional analysis, and (5) obtain the performance characteristics of the seals in terms of the dimensionless parameters defined by the dimensional analysis.

The dimensional analysis for this study did not include all of the variables which are required to describe the configuration of the seal, e.g., seal diameter, root depth, thread pitch, and number of threads. However, dimensionless parameters obtained from experimental data on seals with various configurations were compared to determine the influence of certain variables, e.g., root depth, thread pitch, and seal diameter on the dimensionless parameters. All of the significant variables associated with the fluid were included in the analysis.

The most important variable to viscoseal performance is the pressure drop per unit length of seal, or $\Delta P/L$; therefore, this quantity was treated as the dependent variable. The independent variables associated with the fluid were assumed to be (1) density, ρ, (2) the absolute viscosity, μ, and (3) surfaces tension, σ. The dynamic state of the seal was defined by the peripheral velocity of the rotating

shaft, V. The dimensions of the seal were represented by one characteristic dimension, S.

$\Delta P/L$ was written as an infinite series:

$$\frac{\Delta P}{L} = \sum C_i \left(V^a, \rho^b, \mu^c, \sigma^d, S^e\right) \qquad (1)$$

where

C_i = dimensionless constant
V, ρ, μ, σ, S = variables defined above
a, b, c, d, e = exponents for subsequent dimensionless analysis

For Eq. (1) to be correct, the dimensions of each of the series on the right must have the same dimensions as $\Delta P/L$ on the left. Substituting the fundamental dimensions, mass, length, and time (M, L, and T) for each of the terms, the dimensional equation becomes:

$$ML^{-2}T^{-2} = \left(LT^{-1}\right)^a \left(ML^{-3}\right)^b \left(ML^{-1}T^{-1}\right)^c \left(MT^{-2}\right)^d (L)^e$$

Equating exponents of M, L, and T gives:

$$1 = b + c + d$$
$$-2 = a - 3b - c + e$$
$$-2 = -a - c - 2d$$

or three equations and five unknowns. Solving the equations for b, c, and e gives:

$$b = 1 + a + d$$
$$c = 2 - a - 2d \qquad (2)$$
$$e = a + d - 3$$

Rewriting Eq. (1) for $\Delta P/L$ using Eq. (2) gives:

$$\frac{\Delta P}{L} = C_i\left(V^a, \rho^{-1+a+d}, \mu^{2-a-2d}, \sigma^d, S^{-3+a+d}\right)$$

which reduces to:

$$\frac{\Delta P}{L}\frac{S^3}{\mu^2} = f\left[\left(\frac{V S\rho}{\mu}\right)^a, \left(\frac{\rho\sigma S}{\mu^2}\right)^d\right] \qquad (3)$$

For this study, the total number of variables, n, was six, and the total number of fundamental dimensions, m, was three, which gave n-m=3, or three groups of dimensionless parameters. With these dimensionless parameters, experimental results can be graphically illustrated as shown in Figures 1, 2, and 3.

The seal data obtained with a test fixture[16*] is given in Figure 1 in terms of dimensionless parameters. One-half of the radial seal clearance (0.0039 in.) was used for the characteristic dimension, S, of the seal for all test points associated with the double-thread configuration. A characteristic dimension equal to the entire radial clearance (0.0072 in.) was used for the single-thread configuration. The turbulent flow points for all of the fluids fell on a straight line using a logarithmic scale and are represented empirically by the equation:

$$\frac{\Delta P}{L}\frac{\rho S^3}{\mu^2} = 7.8 \times 10^{-4}\left(\frac{\rho V S}{\mu}\right)^2 \qquad (4)$$

*References for this Appendix are listed in Section 8 of the report.

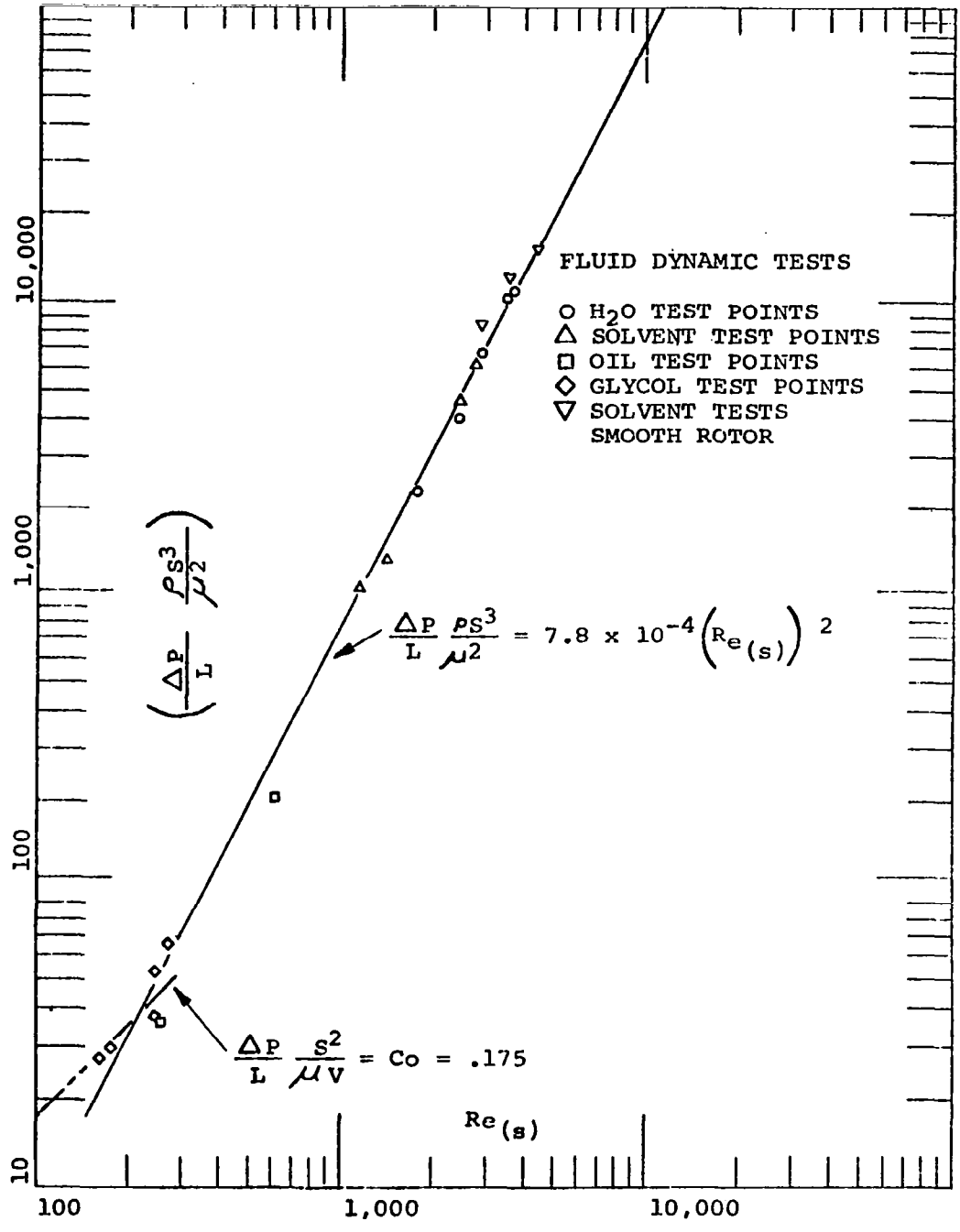

DIMENSIONLESS PLOT OF EXPERIMENTAL DATA FROM VISCOSEALS IN TEST FIXTURE DESCRIBED IN REFERENCE 16

FIGURE 1

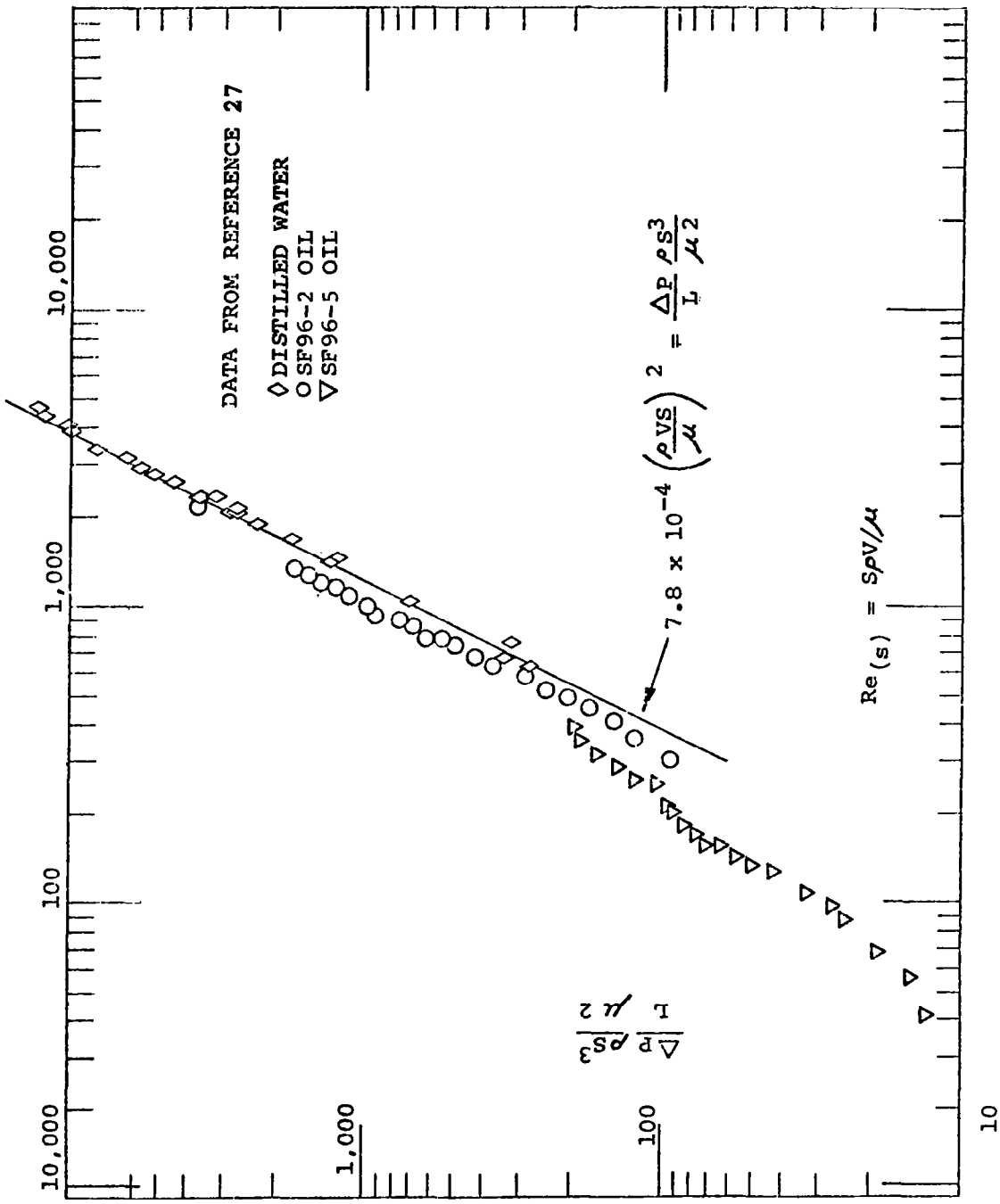

COMPARISON OF VISCOSEAL DATA OBTAINED IN TEST FIXTURE WITH OTHER DATA

FIGURE 2

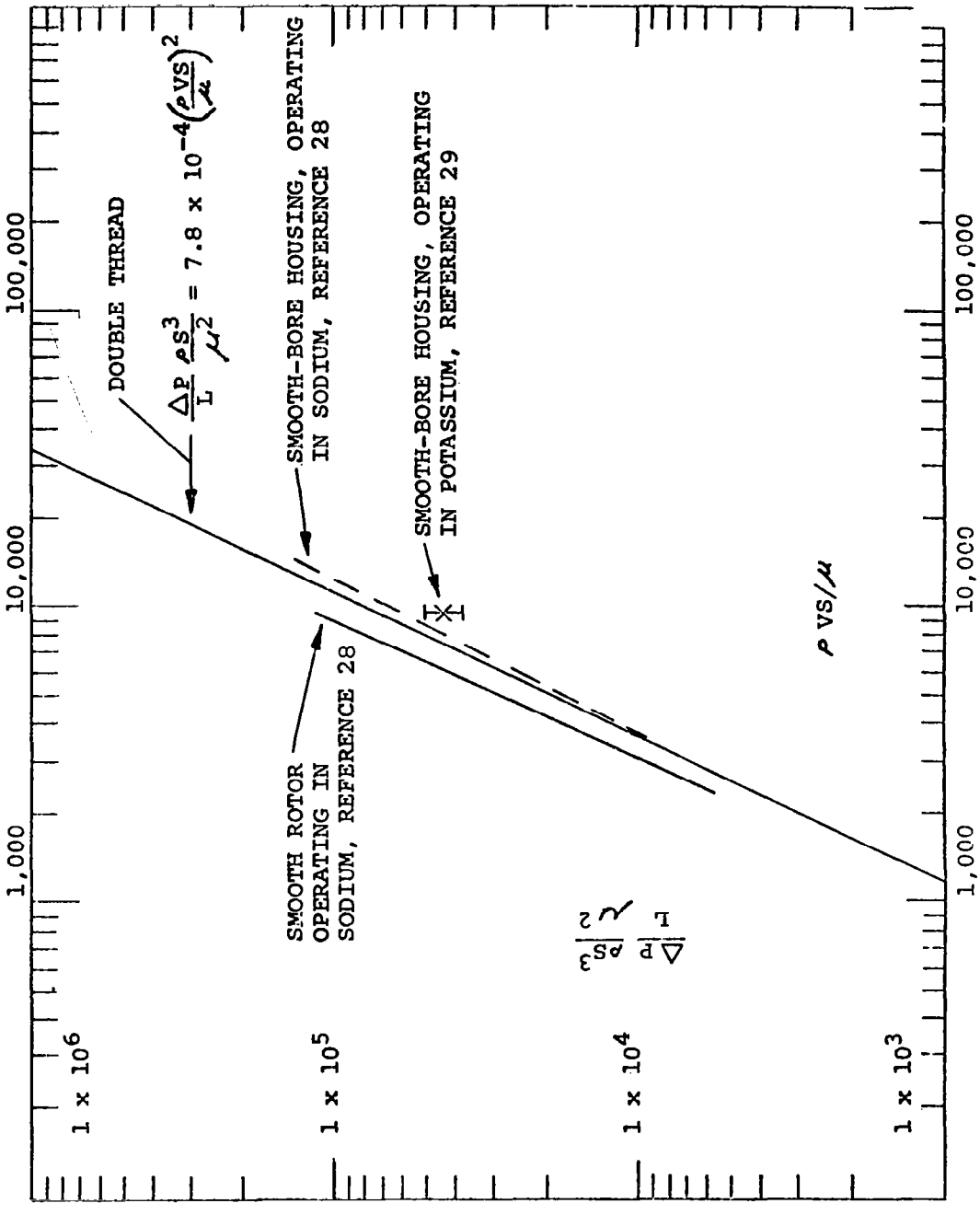

COMPARISON OF VISCOSEAL DATA OBTAINED IN TEST FIXTURE WITH DATA REPORTED FOR VISCOSEALS OPERATING IN LIQUID METALS

FIGURE 3

Three of the test points are for a single-thread configuration. A comparison of the dimensionless parameters shows that both the single- and double-thread configurations are represented by the same empirical equation if one-half of the radial clearance for the double-thread configuration is used. The accuracy of this conclusion may be questionable since it is based on only three test points with the single-thread configuration. Single-thread data from tests reported by McGrew[27], Ludwig[28], and King[29] are shown in Figures 2 and 3 in terms of the same dimensionless parameters. A comparison of the variables which describe each seal configuration is given in Table 1. The turbulent data of Figure 2 is also empirically represented by Eq. (4). A similar comparison is shown in Figure 3 for a smooth rotor and a smooth-bore housing. In this case, the empirical equation for a double- and single-thread configuration gave results which fell between experimental data for a grooved housing-smooth rotor and a grooved rotor-smooth housing operating in sodium.

An experimental data point for a smooth-bore housing operating in potassium is also shown in Figure 3. The location of the liquid-vapor interface within the seal for this data point was determined by examining the seal housing after the rig had been disassembled. The liquid in the clearance had polished the surface very similar to a liquid hone which left a demarcation area assumed to be the location of the liquid-vapor interface. The demarcation was 7/16 ±1/16 in. from the liquid end of the seal. It should be noted that this seal had a helix angle of 9.0 deg while the other experimental data was obtained with seals with helix angles between 14.5 and 15.7 deg. Better agreement would have been expected if the helix angle were in the same range as the other data.

TABLE 1

DESCRIPTION OF SEAL CONFIGURATIONS

Location of Helix	Diameter of Rotor, in.	Depth of Groove, in.	Radial Clearance, in.	Groove Width, in.	Land Width, in.	Helix Angle, deg	Number of Helix Starts
Rotor	0.994	0.010	0.0035	0.127	0.076	14.5	4
Rotor	1.993	0.013	0.004	0.190	0.130	14.5	5
Housing	1.993	0.013	0.004	0.190	0.130	14.5	5
Rotor	2.000	0.014	0.0034	0.125	0.125	9.0	4
Housing	2.050	0.015	0.0072	0.115	0.114	15.7	8
Housing and Rotor	2.0489	0.015	0.0078	0.115	0.114	15.7	8

In general, the results from these experiments support the conclusion that the total radial clearance is the significant dimension for a single thread configuration and one-half of the radial clearance is the significant dimension for a double-thread configuration. Also, it can be postulated that all of the significant variables for a seal with helix angle between 14.5 and 15.7 deg and with groove depth between 0.010 and 0.015 in. were included in the dimensionless parameters because the test data represented configurations with a 2:1 variation of seal diameter and radial clearance. A large variation of groove width, land width, and number of helix starts was also represented by this data.

Comparison of the performance of the seals in terms of the dimensionless parameters shows that the performance of a seal in a given fluid can be predicted from test results obtained with a different fluid. In the turbulent regime, the value of the dimensionless surface tension parameter, $\sigma\rho S/\mu^2$, does not have a significant influence upon the dimensionless dependent paramter, $(\Delta P/L)(\rho S^3/\mu^2)$.

It was found that the following empirical expression is satisfied by experimental data obtained using various fluids and viscoseal configurations operating in the turbulent regime.

$$\frac{\Delta P}{L}\frac{\rho C^3}{\mu^2 N^3} = 7.8 \times 10^{-4}\left(\frac{\rho VC}{\mu N}\right)^2 \qquad (5)$$

where C = radial clearance
N = 1 for a single-thread configuration
N = 2 for a double-thread configuration

This analysis showed that the sealing capacity per unit length of a seal with a double-thread configuration was approximately 100-percent greater than the sealing capacity of a single-thread configuration with a smooth rotor and the same radial clearance. Fluid density was the variable that influenced the sealing capacity of the seals in the turbulent regime of flow. Separating the variables in the equation gives:

$$\frac{\Delta P}{L} = 7.8 \times 10^{-4} \rho V^{2} \frac{N}{C} \qquad (6)$$

The name "viscoseal" is misleading for this type of seal when it is operated in the turbulent regime of flow because the experiments show that sealing capacity per unit length of the seal is independent of the viscosity of the fluid, provided the Reynolds No., $\rho VC/\mu N$, is greater than 300.

2. VISCOSEAL PARAMETRIC DATA

The following specifications were used to perform the viscoseal parametric study:

Fluid	Temp. °F	Seal Diameters, in.	Alternator Design Speeds, rpm	Maximum Pressure Differential
Potassium	800	2,3,4	16,000 to 32,000	25 psia-psat
Potassium	1100	2,3,4	16,000 to 32,000	25 psia-psat
Mineral Oil	400	2,3,4	16,000 to 32,000	50 psi
Polyphenyl Ether	800	2,3,4	16,000 to 32,000	50 psi

In addition, the study was based on the following conditions and/or assumptions:

(a) The required lengths for the seals were based on the condition that complete sealing of the liquids would be accomplished at 50 percent of the alternator design speed with maximum pressure differential across the seal.

(b) The wetted length of the seal at the 50-percent speed point was made equal to 60 percent of the overall length of the seal. The remaining 40 percent of the seal length is required for dams at the ends of the seal and for scavenging of any liquid which may break away from the interface.

(c) Radial clearance was assumed 0.3 percent of seal diameter.

(d) Double helical groove geometry was assumed; i.e., helical grooves on both the housing and the shaft.

(e) Potassium fluid property data and organic fluid property data were taken from sources[30,31] supplied by AiResearch.

(f) The sealing capacity per unit length = 7.8×10^{-4} $\rho V^2 N/C$.

The results of the viscoseal parametric study are displayed graphically in Figures 4 through 9.

Figures 4 and 5 give the required length of a seal for the condition indicated on each curve. Figures 6 and 7 give the power consumption within the seals as a function of shaft speed. Power losses were determined using the turbulent friction parameter determined by Stair[32]. This is according to journal bearing loss calculation techniques of Smith and Fuller with a constant multiplier to account for the thread geometries different from smooth bearing surfaces.

The required length of a seal varies linearly with the maximum pressure differential; therefore, the seal length required at any pressure differential other than that specified for this study can be obtained simply by ratioing; i.e.,

$$\text{New Seal Length} = \frac{\text{Old Seal Length}}{\text{Old } \Delta P} \times \text{New } \Delta P$$

where ΔP = pressure differential.

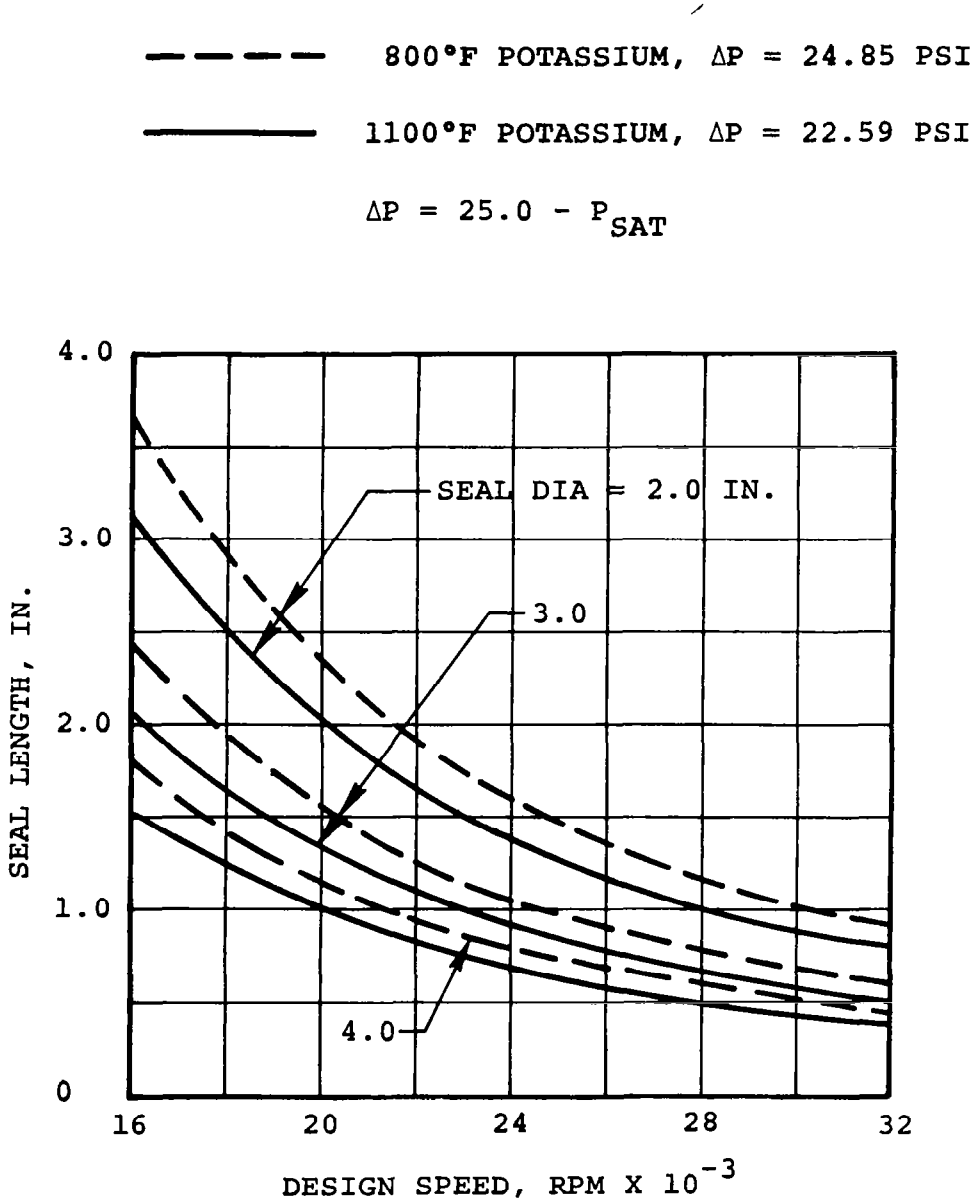

POTASSIUM VISCOSEAL LENGTH

FIGURE 4

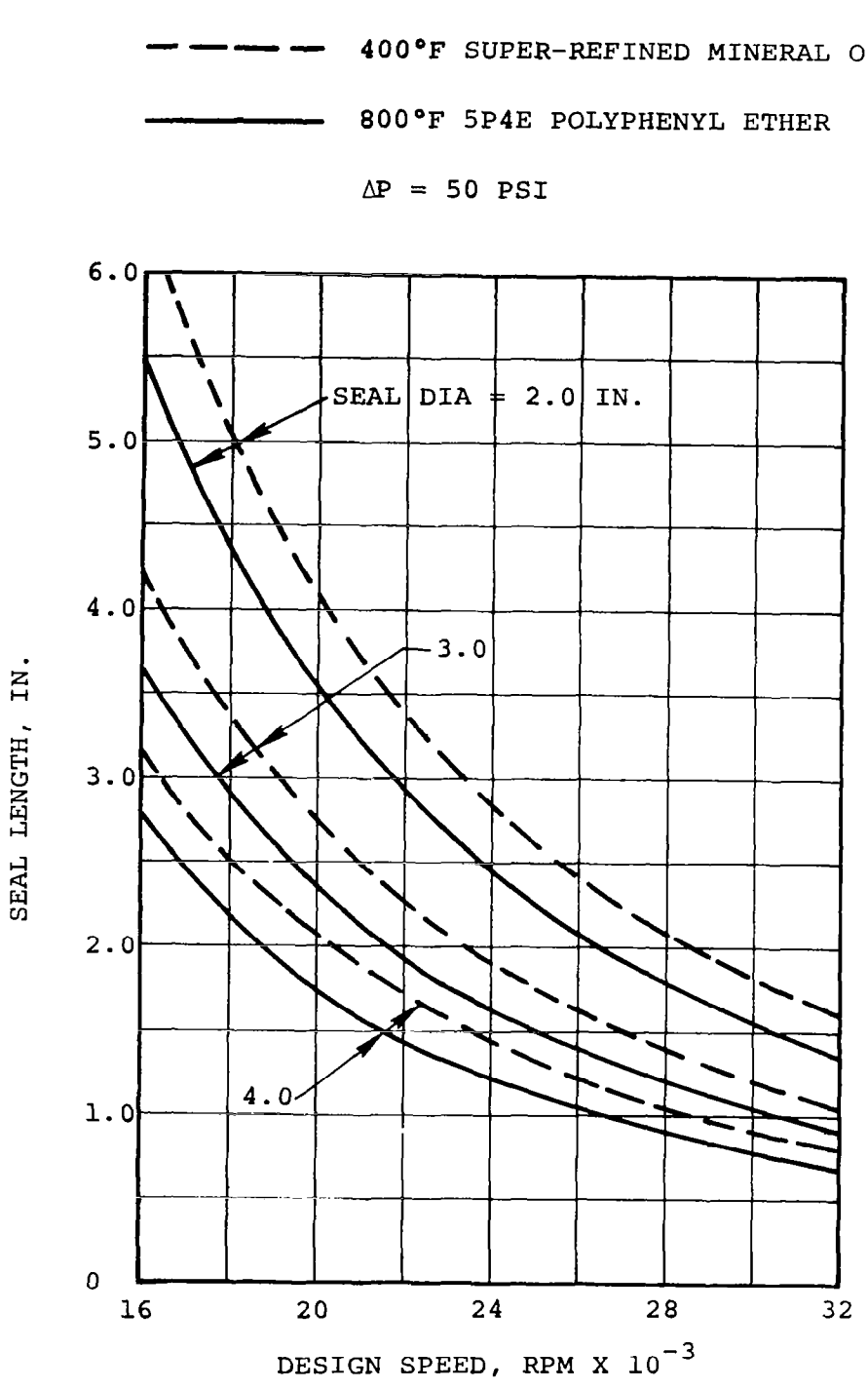

ORGANIC VISCOSEAL LENGTH

FIGURE 5

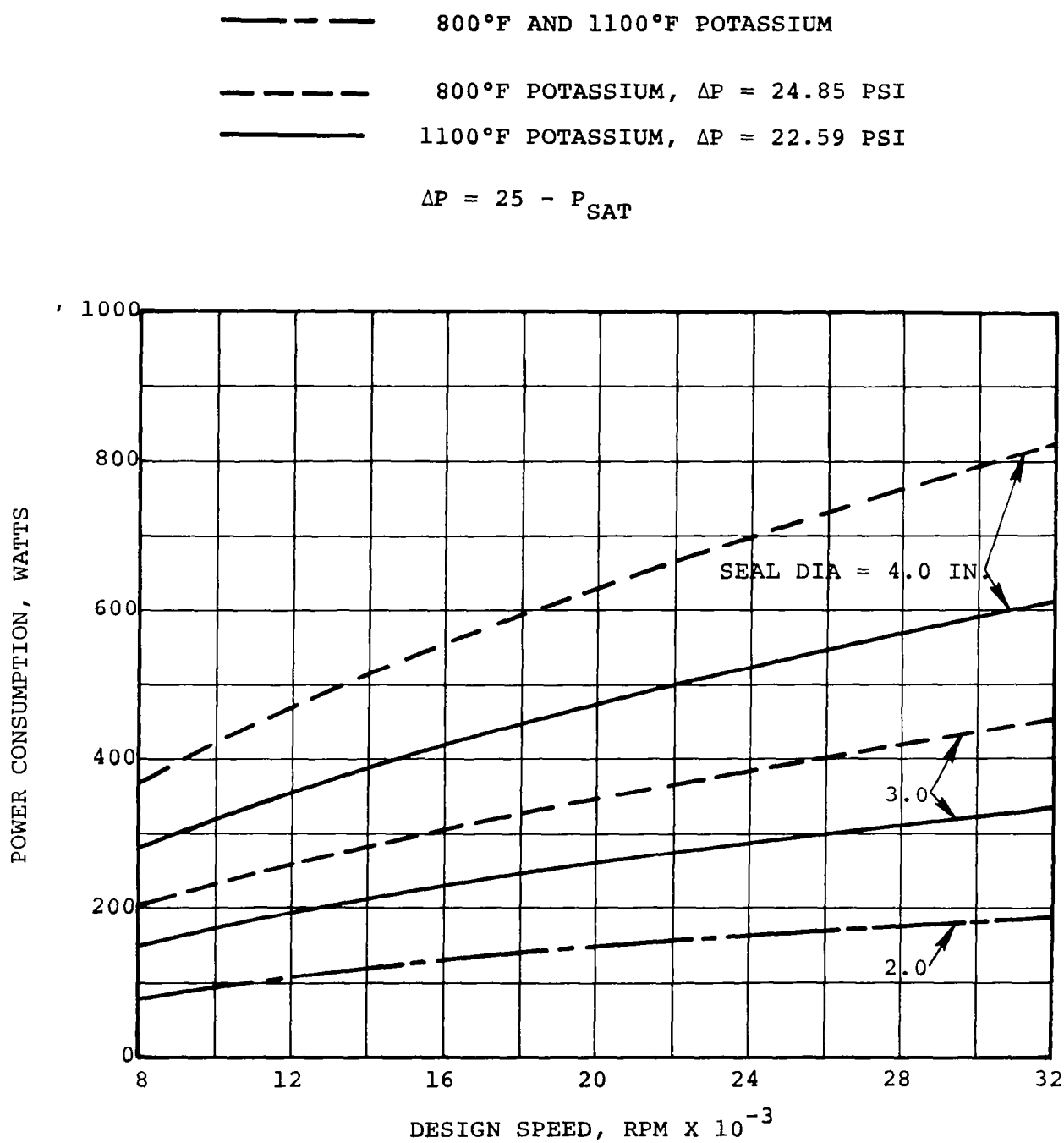

POTASSIUM VISCOSEAL POWER CONSUMPTION

FIGURE 6

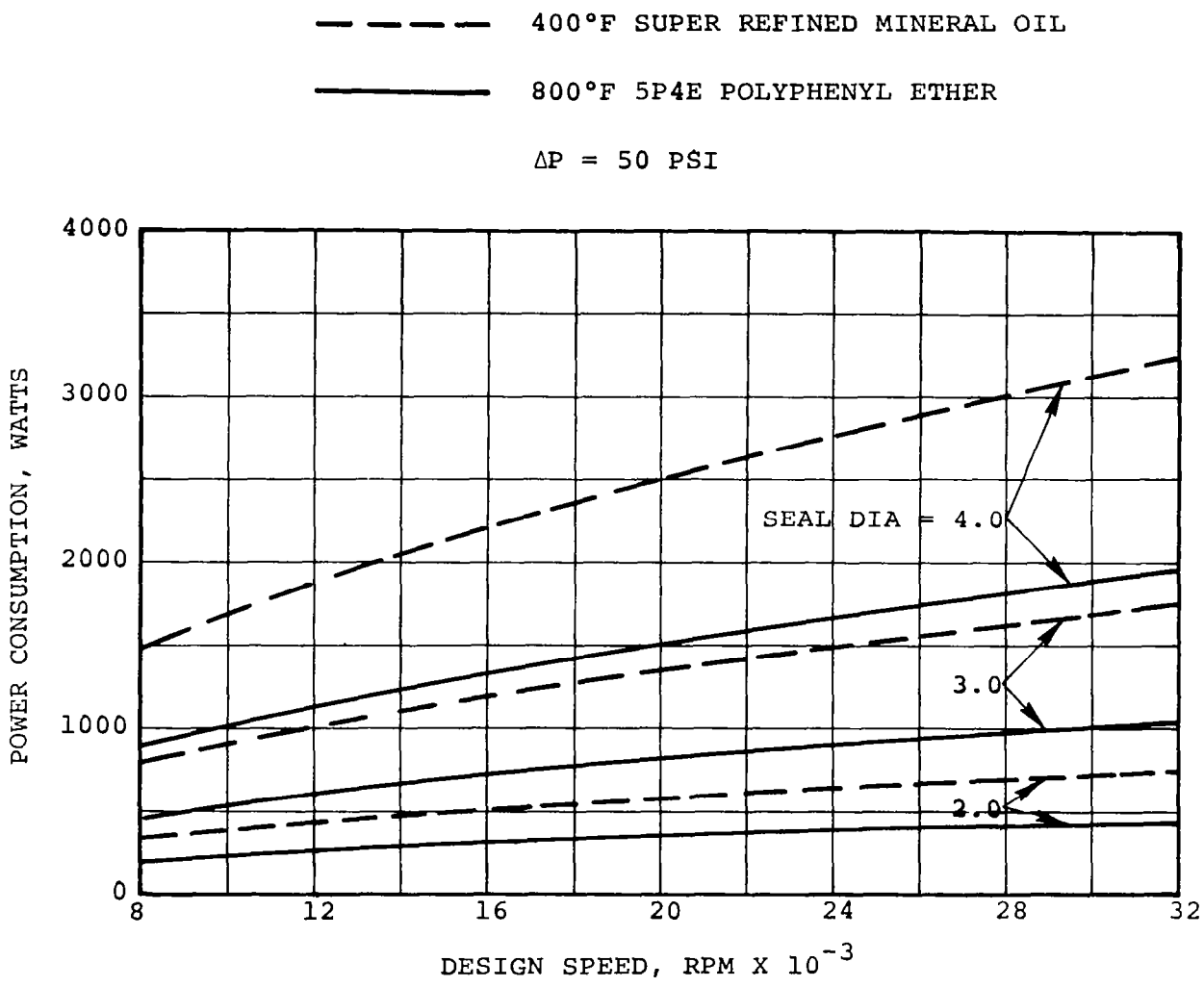

ORGANIC VISCOSEAL POWER CONSUMPTION

FIGURE 7

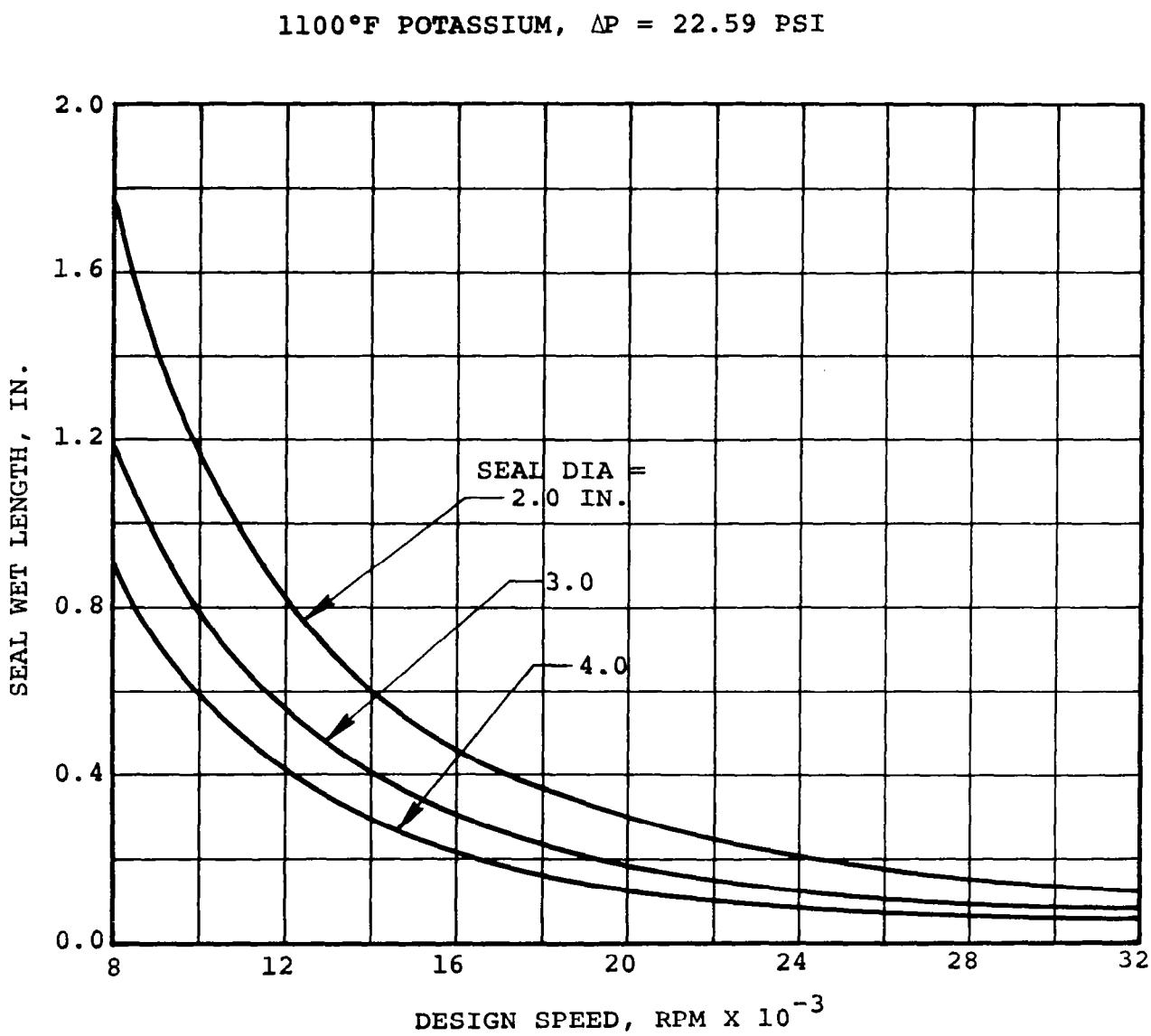

POTASSIUM VISCOSEAL WETTED LENGTH

FIGURE 8

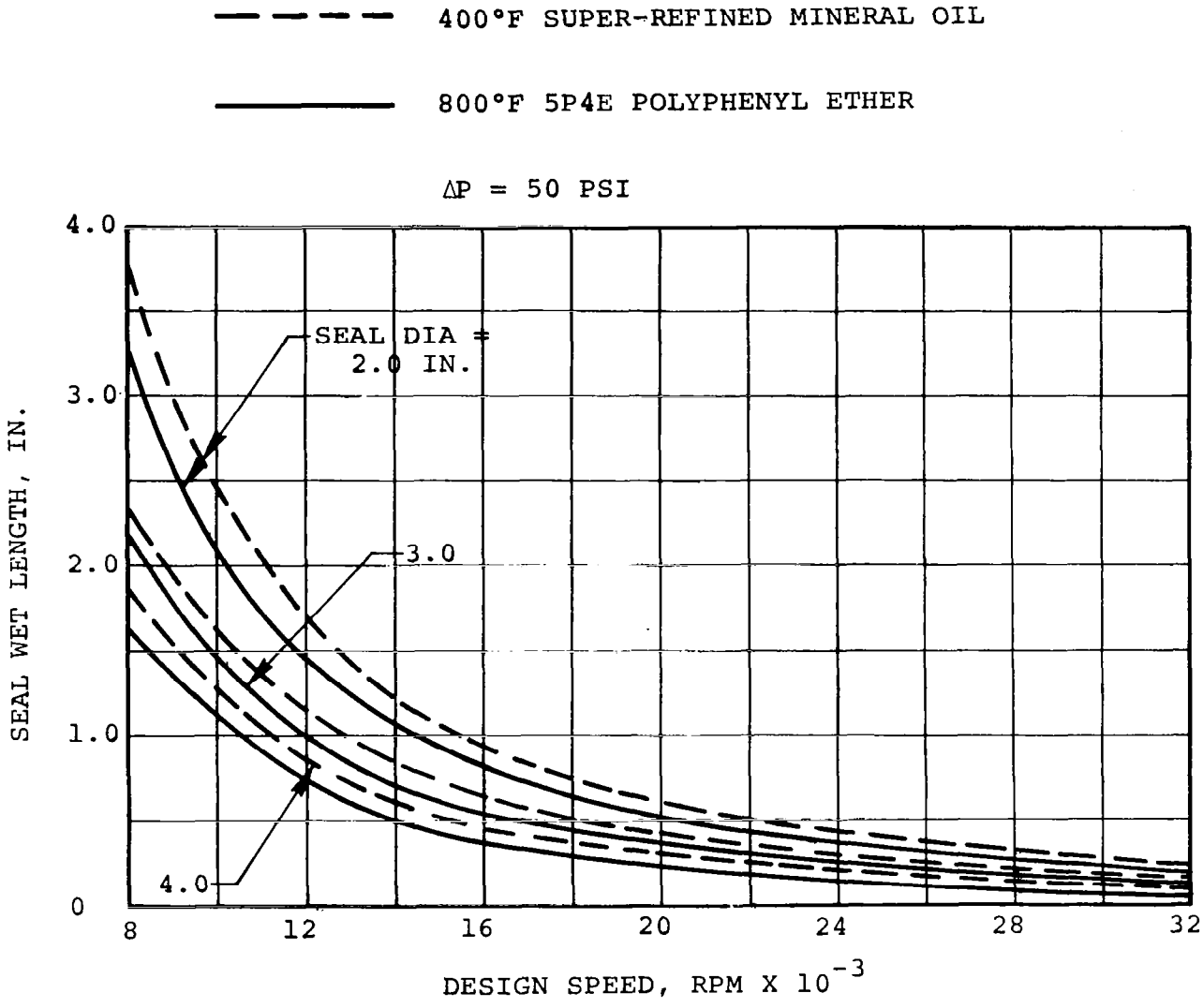

ORGANIC VISCOSEAL WETTED LENGTH

FIGURE 9

Power consumption also varies linearly with the pressure differential; therefore, power consumption at pressure differentials other than those used in this study can be obtained in an analogous manner to seal length above.

Figures 8 and 9 which give wet length of seal as a function of shaft speed and seal diameter, can be used to determine the speed range for which a liquid-vapor or liquid-gas interface will exist within the seal. Excessive leakage will occur when the entire seal is completely flooded.

The seal length, power consumption, and wetted length are based upon the assumption that the radial clearance of the seal is 0.3 percent of the seal diameter. The sealing capacity at other clearances can be determined by considering the differential pressure per unit length as inversely proportional to the radial clearances, provided the Reynolds number based upon one-half of the actual clearance is greater than 300.

APPENDIX C

PARAMETRIC DESIGN STUDY OF HOLWECK PUMP VAPOR SEALS

1. INTRODUCTION

1.1 Need for the Vapor Seal

One of the steps that can be taken to minimize windage losses in the alternator rotor cavity is to minimize the vapor density (and pressure) within the cavity. Since the bearing cavity shaft seals are usually of the noncontact-type where an open liquid-to-vapor interface exists, the vapor pressure on the rotor-cavity side of the bearing-cavity seal will be at least as great as the saturated vapor pressure of the bearing fluid. The magnitude of this saturated vapor is sufficient to cause prohibitive windage losses in most high-temperature, high-speed alternators, and provisions are usually made for reducing the rotor cavity pressure by connecting it to an external (or internal) vapor scavenging system.[33] With the reduced rotor cavity pressure, provision must be made to prevent free access of the interface saturated vapor to the rotor cavity. One method which has found application in the past is to restrict the vapor by inserting a Holweck-type molecular vacuum pump between the bearing cavity seal and the rotor cavity. The molecular pump head acting against the saturated vapor results in a superheated vapor on the suction side. The superheated vapor produces a secondary benefit by obviating the possibility of the fluid condensing in the rotor cavity and/or impinging on the ceramic bore seal.

1.2 Basic Configuration and Operation

The type of seal configuration envisioned is shown schematically in Figure 1. The molecular pump is cantilevered over the liquid seal

Pressure/Density Conditions
of Interest

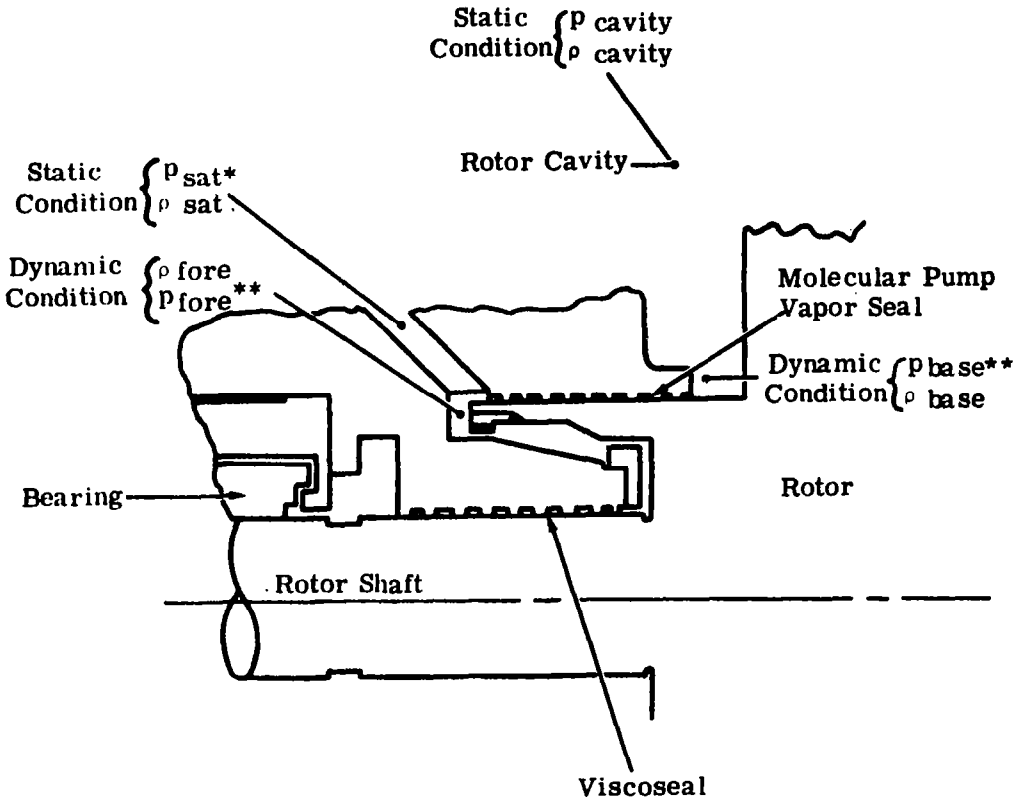

* Given low pressure sink conditions, saturated vapor pressure and density.

** Pressure difference across Holweck pump = $\Delta p_H = p_{fore} - p_{base}$.

BASIC SHAFT SEAL CONFIGURATION

FIGURE 1

to minimize stub shaft length. The arrangement shown has a single-stage pump; additional stages may be added by placing additional cantilevered pumps above the first stage. For example, a three-stage vapor pump is possible with one additional cantilevered impeller by using the underside of the impeller for one of the stages. The underside of the first-stage cantilevered impeller usually cannot be used as a vapor pump stage because it serves another function in the rotor cavity scavenging system. Pump staging is necessary to achieve the required vapor pressure differential at the saturated pressures being considered in the KTA (0.155 psia at 800°F potassium coolant). Examination of the pump operating principle and the particular form of flow theory involved (which is dependent on the magnitude of the vapor pressure) offers explanation of why the additional stages are needed to increase pump capacity.

As the name implies, the pumping principle involved is based on molecular flow theory that is usually restricted to high-vacuum conditions. The pump configuration consists of a smooth shaft running in a helical threaded-housing. The pumping action is derived from the collision of molecules with the moving surface of the shaft. The momentum exchange between the shaft and the molecules provides the molecules with an additional velocity component in the direction of rotation. Subsequent collisions induce a flow that is proportional to the peripheral speed of the shaft. The net flow between the high and the low pressure is less than the induced flow because the pressure gradient induces both a back-flow through the threads and a leakage flow across the thread lands. The pump maintains its maximum pressure differential when the net flow is zero; this is the condition desired when the pump is employed as a shaft seal.

The molecular pump calculation theories are dependent upon the flow regime of the pump. In continuous or viscous flow, the pressure generating capability is a small pressure differential; at molecular

flow, it is a large pressure ratio. Thus, the very mathematical form of the theory is dependent on the state of the flow. At low pressure, molecular-flow conditions (e.g., 0.01 psia or less typical of 600°F saturated K-vapor), pressure heads of 10:1 are easily achieved and heads of several thousand to one are not at all uncommon. Therefore, the pump can be considered reasonably effective as a vapor shaft seal at molecular flow conditions. However, the pump is not as effective at greater pressures (0.1 psia or more), and pressure heads as high as 10:1 are very difficult to achieve. The reason is that molecular flow no longer occurs at these high pressures, and viscous drag flow is predominant. As would be expected, viscous drag is not very effective with a gas. Since the saturated vapor pressures of the KTA are of the order of 0.1 psia or greater for the higher coolant temperatures, the pumps will require staging. An important additional feature of the staging is that, in each successive stage, the vapor pressure is lowered by the preceding one, and the successive stage becomes more effective. Typically, the pressure ratios across two equal successive stages might be 2:1 and 6:1, respectively. Obviously, the latter stage is the most effective. Of course, a long single stage would have the same effect but would require prohibitive stub shaft lengths.

In order to assess the extent of maximum permissible rotor cavity pressure required to minimize the windage losses in the KTA alternator cavity, a preliminary study was made of calculated windage losses versus saturated vapor pressures for potassium and mineral oil. The results are shown in Figure 2. As seen, the rotor cavity pressure must be in the order of 0.01 psia for potassium vapor and 0.005 psia for mineral oil vapor for the losses to be approximately 1 kw. The design limit of 1 kw was specified based on intuitive reasoning and past experience. In the final analysis of the KTA cooling designs,

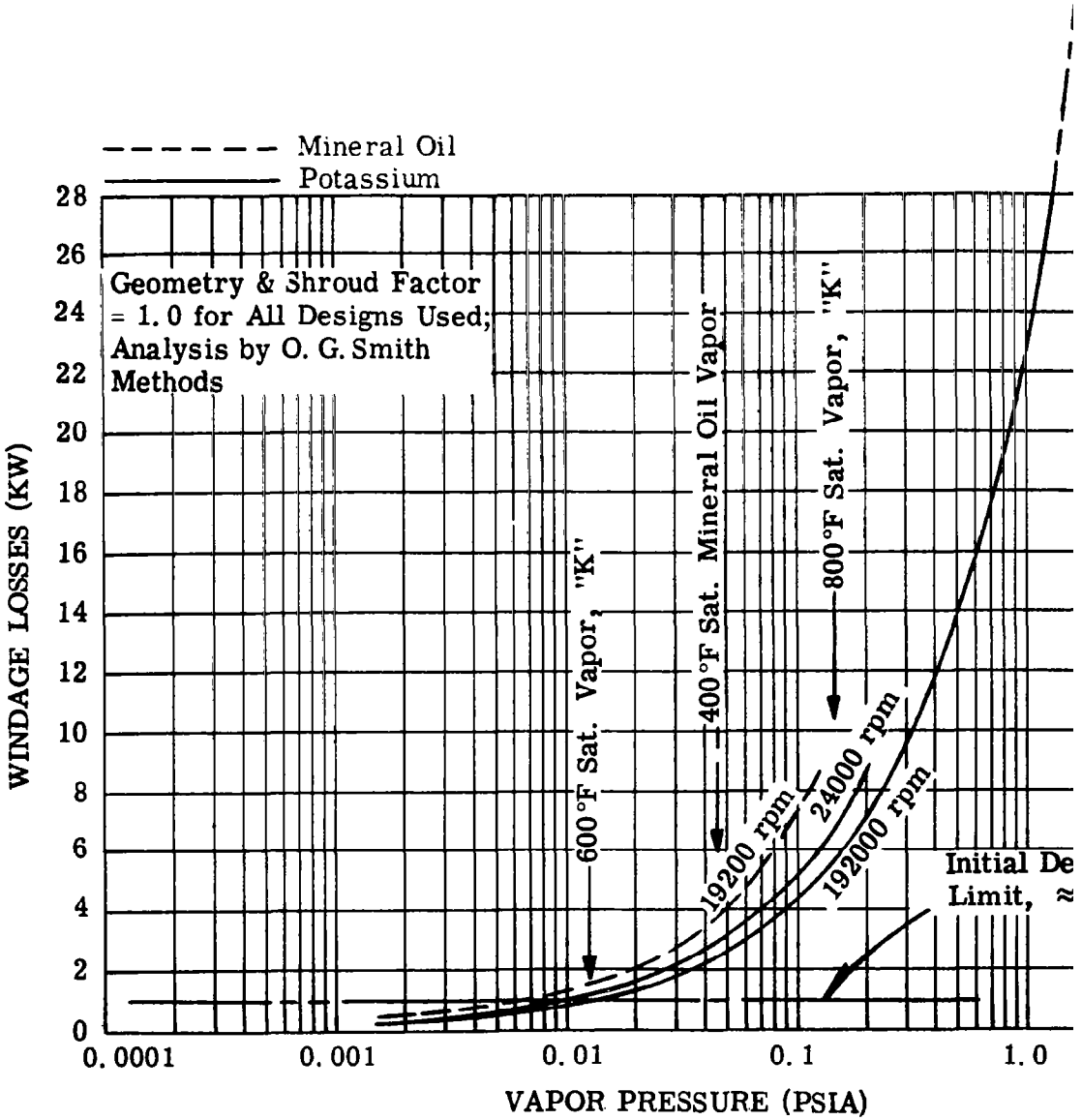

PRELIMINARY WINDAGE LOSS COMPARISON

FIGURE 2

this value proved to be too high.* However, it was also determined that sufficiently lower rotor cavity pressures and windage losses could be maintained with additional pump staging so that the procedure and conclusions of the study were unaffected.

*Final analyses on windage, rotor losses, and rotor cooling configuration later indicated that a few hundred watts (100 to 200) windage loss was all that could be tolerated. This requires potassium vapor pressures less than 0.004 psia and mineral oil vapor pressures less than that. However, requirements other than permissible windage losses precluded setting the rotor cavity pressure for mineral oil vapor.

2. PARAMETRIC PERFORMANCE STUDY

The parametric performance study was carried out in two steps. These steps were:

(a) Determine the best thread configuration for three different stub shaft diameters based on an assumed constant fluid state.

(b) Determine the performance of the thread configurations selected from (a) with and without multiple stages.

The constant fluid state assumed for these studies was 800°F saturated potassium vapor* corresponding to the fluid state at the low-pressure side of the viscoseal. Performance of the pump at conditions other than the 800°F saturated potassium vapor conditions included mineral oil vapor between 300° and 500°F and potassium vapor pressures from 600° to 1100°F. The latter extreme was analyzed to illustrate the problems associated with vapor pressures $\geq$ 2.0 psia. Pressure ratios of less than 1.5:1 are about the maximum that can be expected across a set of typical pumps. Because of this, application of Holweck pumps in the rotor cavity scavenging system appears undesirable for the 1100°F potassium coolant condition.

2.1 Optimum Geometry Study, Background

The object of designing a pump to act as a seal is to determine the configuration for maximum pressure head or minimum back-flow leakage, which are equivalent conditions. There are essentially four

*Potassium performance calculations were made using properties exclusively from AFAPL-TR-66-104 prior to notification of vapor viscosity change. Final designs will have to take the change into account.

variables that determine the configuration - the thread root width and depth, the radial thread land clearance, and the pitch (helix) angle - for any given set of operating conditions and constraints such as speed, diameter, length and vapor pressure/temperature. As these conditions change, the optimum thread configuration will change. Consider, for example, a case where the flow may deviate from the molecular flow regime; the optimum thread configurations predicted by molecular flow theory are no longer appropriate. Physically, molecular flow occurs when the molecular mean-free-path is greater than the channel dimensions. Thus, when pressure is increasing and flow is tending away from the molecular flow regime, any decrease in thread geometry that keeps the mean-free-path greater than the channel dimensions is an improvement. Thus, transition-flow optimum geometries always have channel dimensions less than molecular flow geometries; likewise, viscous-flow optimum geometries have channel dimensions less than transition-flow geometries (in theory only; actually, these latter differences may be infinitesimal).

The above example points out why it is so important to optimize for each case at hand and that what is best for one set of design conditions may not necessarily be best for another. Fortunately, the conditions for the KTA are typical of viscous and/or transition flow regimes and the thread geometries determined should be applicable over the ranges of the study.

Because most of the organic fluids being considered have vapor pressures of the same order of magnitude as potassium in the 600° to 800°F range, it was expected that the thread optimization analyses for potassium would be applicable to the organic fluids. Analyses were carried out to determine the actual performance around 400°F.

2.2 Optimum Geometry Study

The analysis used in the study was in the form of a computer performance program based on the work of King[34] and Lowry[35]. For viscous and transition flow conditions, the analysis and the subsequent computer program were experimentally verified by King using argon gas at several thermodynamic states (transition and viscous flow) for several thread configurations, most of which are applicable to the KTA requirements. Molecular flow conditions were not verified during the tests of King since the molecular flow equations were based on a previously verified analysis.[35]

The thread configuration nomenclature is shown in Figure 3. The radius and radial clearance were treated as independent parameters and fixed according to values previously specified for the viscoseal study. These are tabulated in Table 1. The length of the seal was specified to correspond to the seal radius. The pressure differential is directly proportional to the axial length except for a correction factor to account for incomplete threads at the entrance and exit. Since this factor changes as the thread geometry changes, it was not considered practical to perform the study in more general terms of pressure differential per unit length of seal. Also shown in Table 1 are the resulting optimum thread geometries from the studies below.

The first step was to determine the optimum pitch angle, γ, for the three diameters as a function of root depth-to-width ratio (SA/SB). The computed performance is shown in Figures 4 through 6 for either XLPR = 0.5 SA or XLPR = SA. A direct result of these figures is that the optimum pressure head occurs at SA = XLPR rather than at XLPR = 0.5 SA. Cross plots of these figures at the most promising pitch angles are shown in Figures 7 through 9. Sometimes, the curves were drawn using theoretical nonintegral threads as shown in Figure 10. Based on these figures, the optimum thread-root width-to-depth

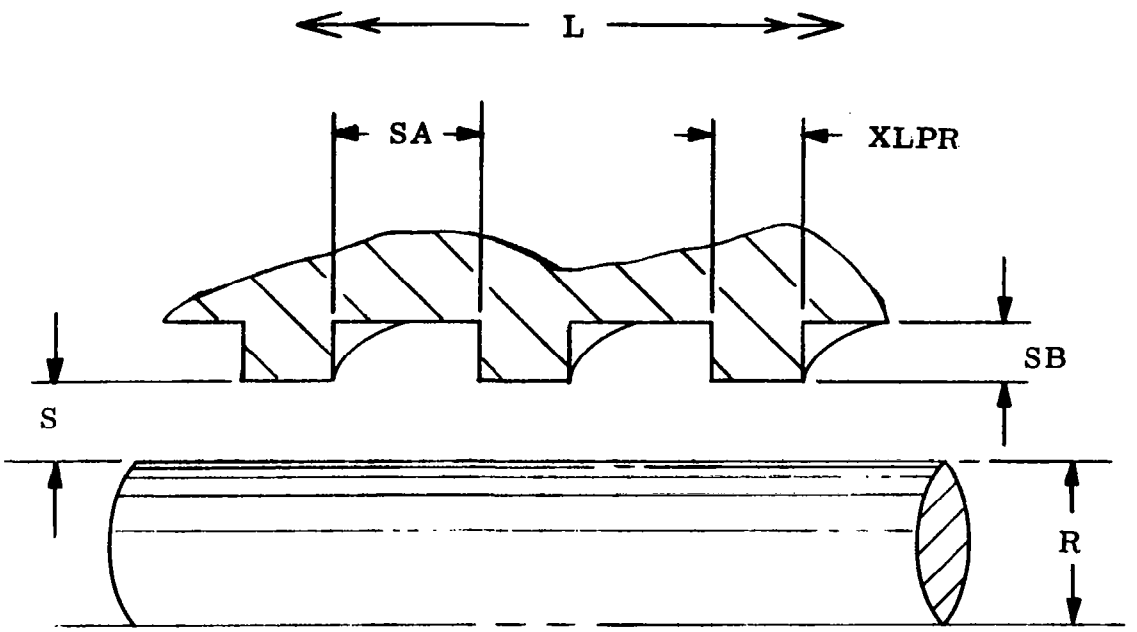

R = shaft radius

S = radial clearance

L = length of pump

SA = axial length of thread root

SB = thread root depth

XLPR = axial length of thread land

α = pitch angle (not shown)

G = number of parallel threads (not shown)

HOLWECK PUMP THREAD CONFIGURATION

FIGURE 3

TABLE 1

SUMMARY OF HOLWECK THREAD CONFIGURATIONS

800°F Saturated Potassium Vapor on
Low-Pressure Side of Viscoseal
24,000 ±8000-rpm Shaft Speed

	Symbol	Parameters		
Shaft Diameter[1] - in.	D	3.5	4.5	5.5
Seal Length[2] - in.	L	1.75	2.25	2.75
Radial Clearance[3] - in.	S	0.006	0.009	0.012
Corresponding Viscoseal				
Diameter, in.		2.0	3.0	4.0
Radial Cl., in.[4]		0.006	0.009	0.012
Optimum Thread Configuration				
Pitch Angle, deg		2.3437	2.1878	2.5765
Number of Parallel Threads	G	2	2	2
Optimum SB/S	-	12.5	10	12.5
Thread Root Depth, in.	SB	0.075	0.09	0.18
Optimum SA/SB	-	1.5	1.5	1.5
Axial Thread Root Width, in.	SA	0.1125	0.135	0.27
Optimum XLPR/SA	-	1.0	1.0	1.0
Axial Thread Land Width, in.	XLPR	0.1125	0.135	0.27

[1] Viscoseal Diameter plus 1.5 in.

[2] Specified as equal to seal radius

[3] Specified as equal to viscoseal radial clearance

[4] Equal to 0.3 percent of viscoseal diameter

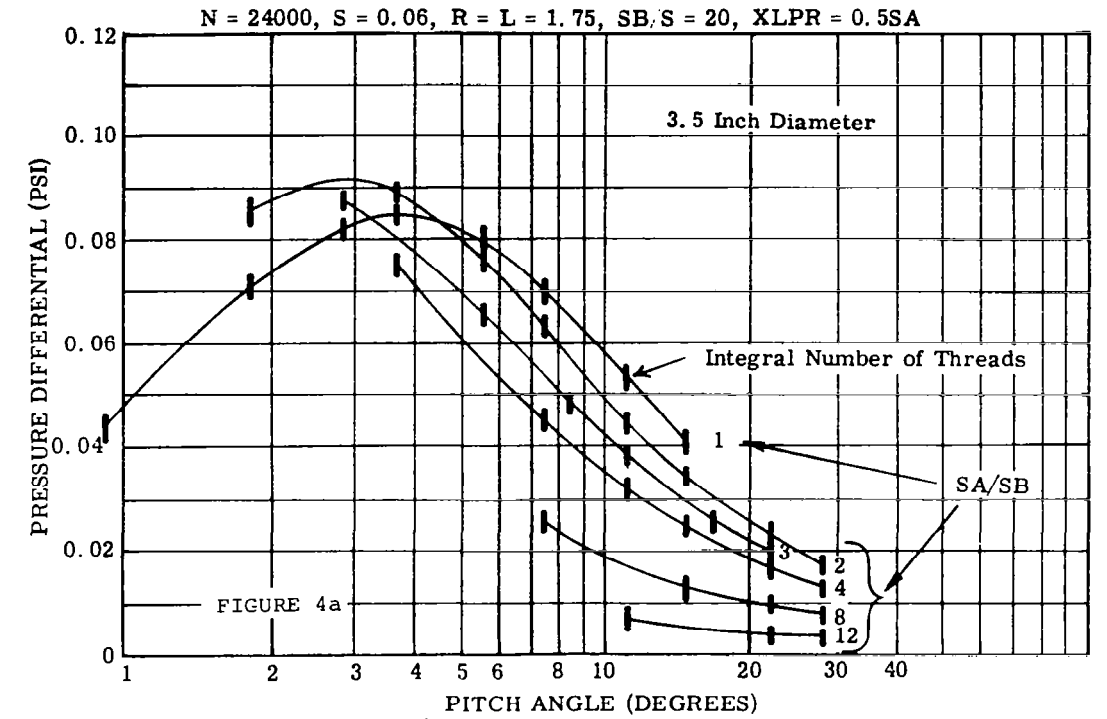

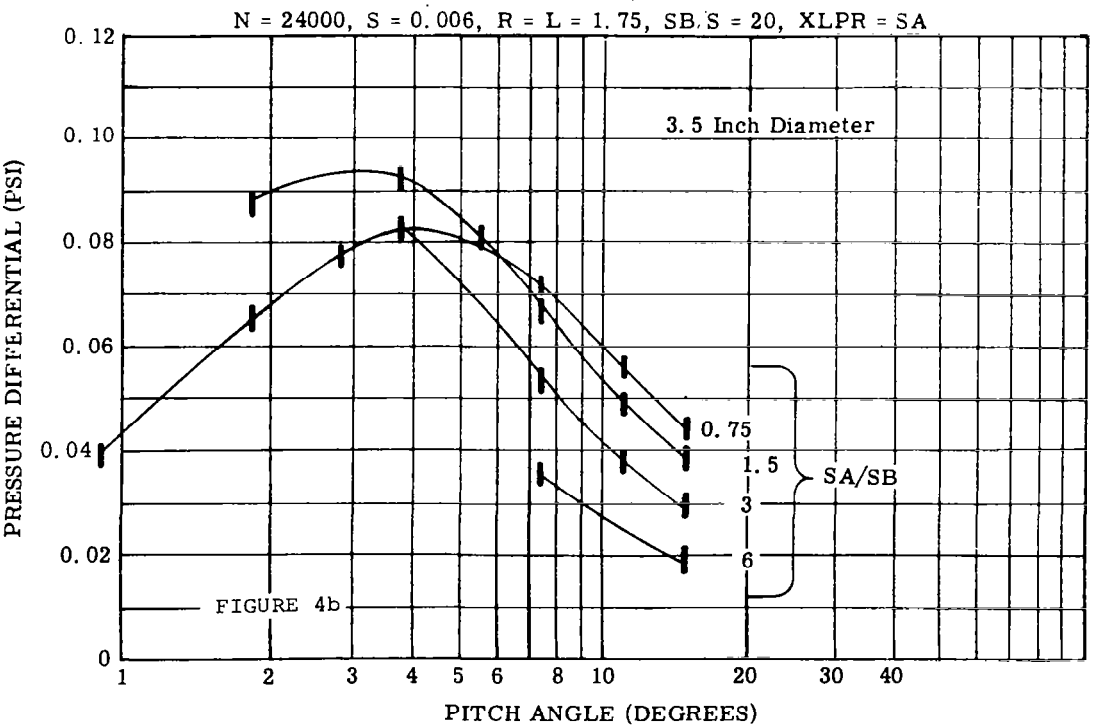

HOLWECK PUMP PARAMETRIC DATA,
EFFECT OF PITCH ANGLE, 3.5 IN. DIA

FIGURE 4

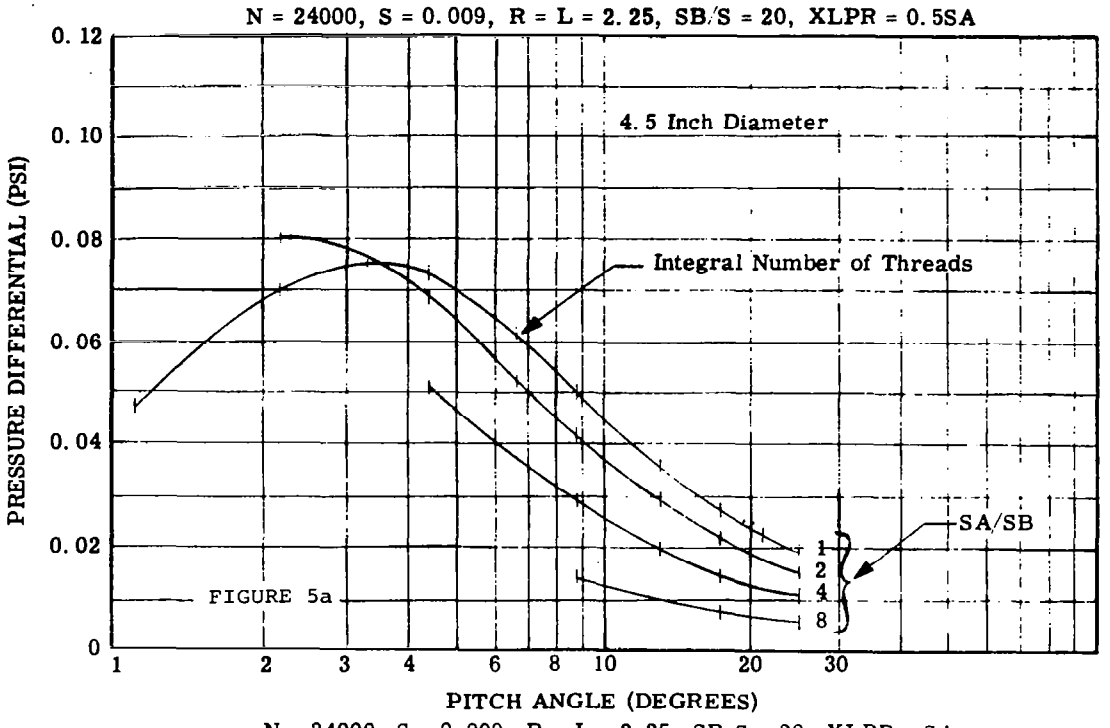

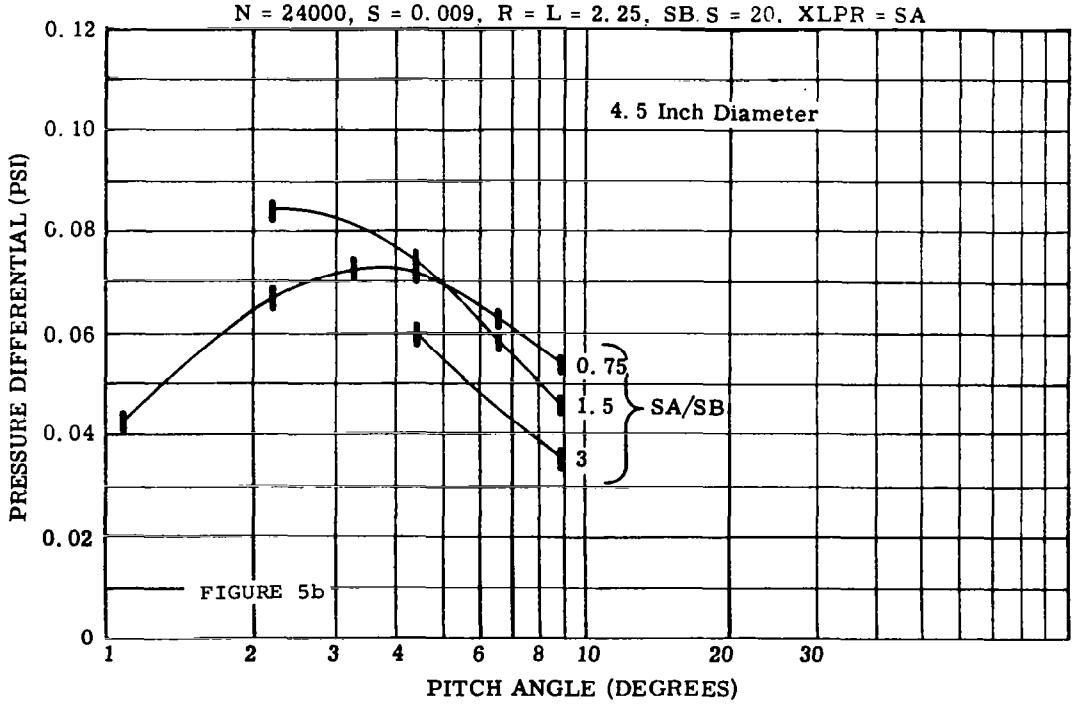

HOLWECK PUMP PARAMETRIC DATA,
EFFECT OF PITCH ANGLE, 4.5 IN. DIA

FIGURE 5

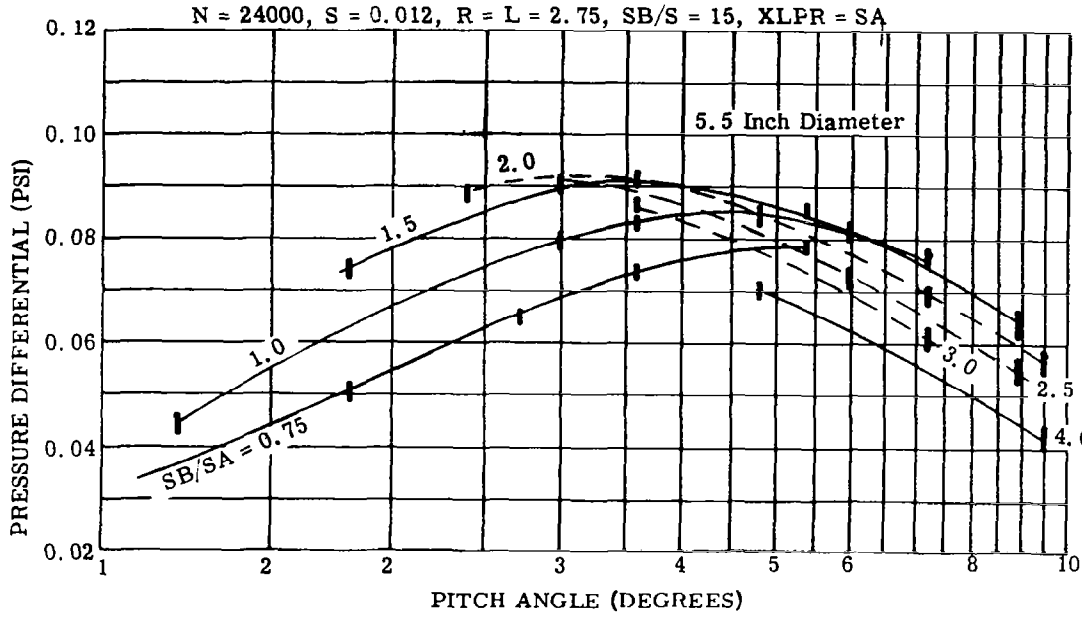

HOLWECK PUMP PARAMETRIC DATA,
EFFECT OF PITCH ANGLE, 5.5 IN. DIA

FIGURE 6

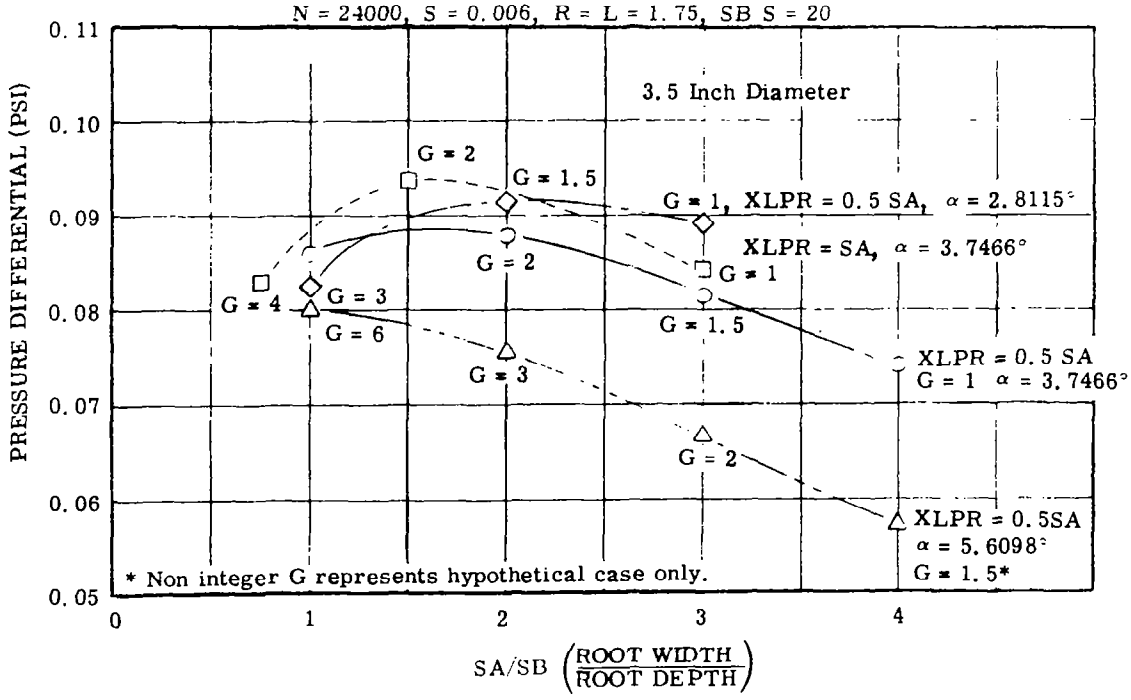

HOLWECK PUMP PARAMETRIC DATA,
EFFECT OF SA/SB, 3.5 IN. DIA

FIGURE 7

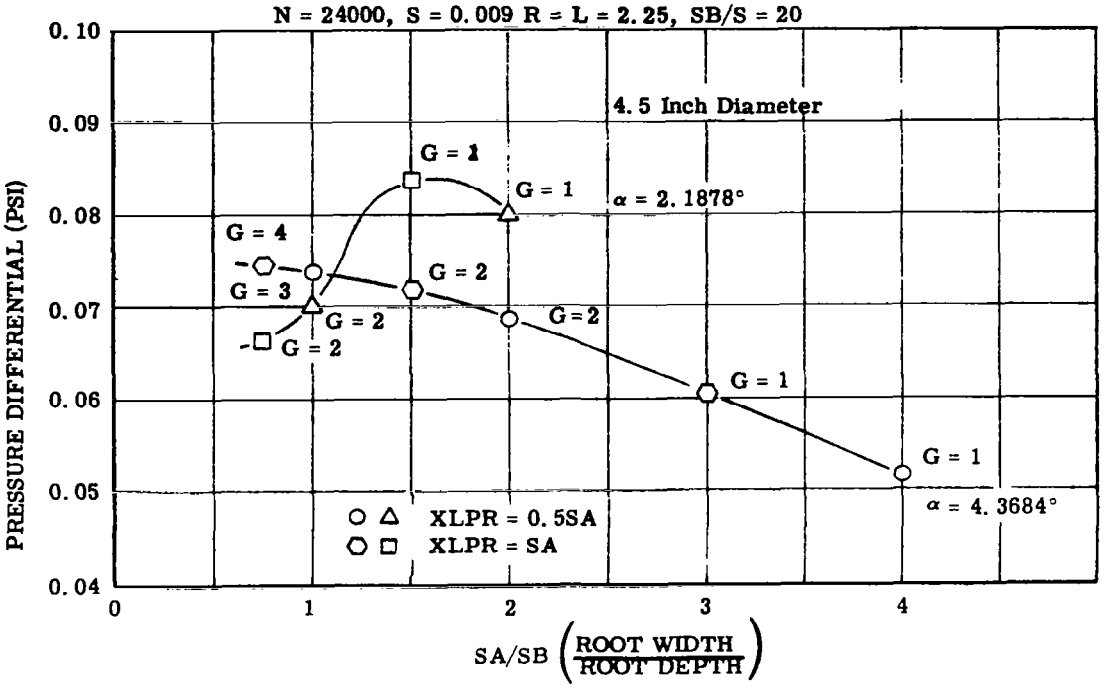

HOLWECK PUMP PERFORMANCE DATA,
EFFECT OF SA/SB, 4.5 IN. DIA

FIGURE 8

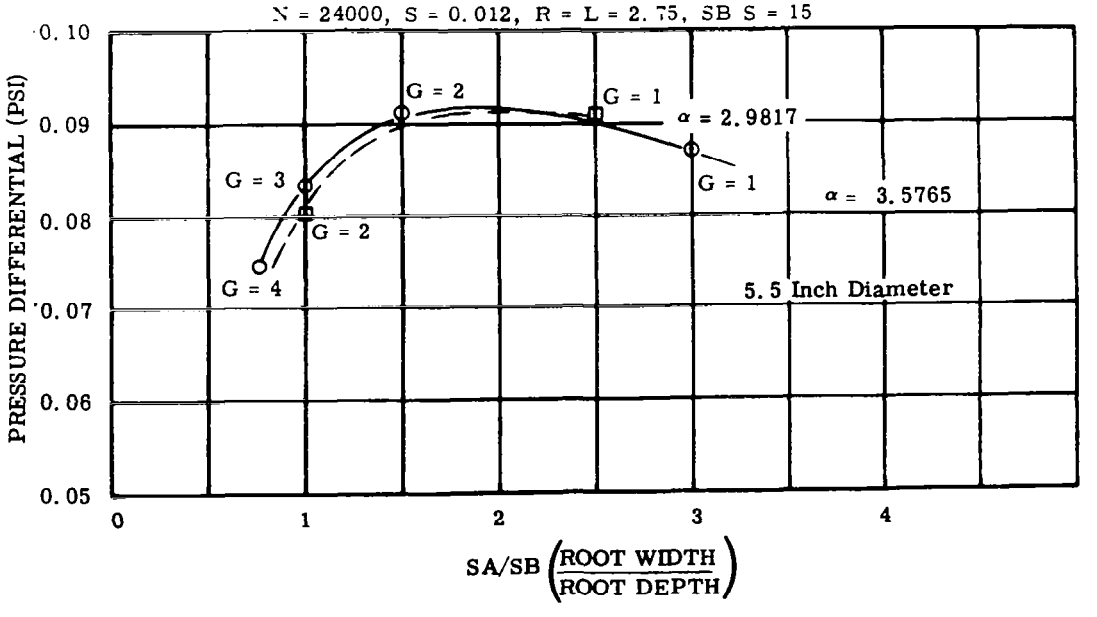

HOLWECK PUMP PERFORMANCE DATA,
EFFECT OF SA/SB, 5.5 IN. DIA

FIGURE 9

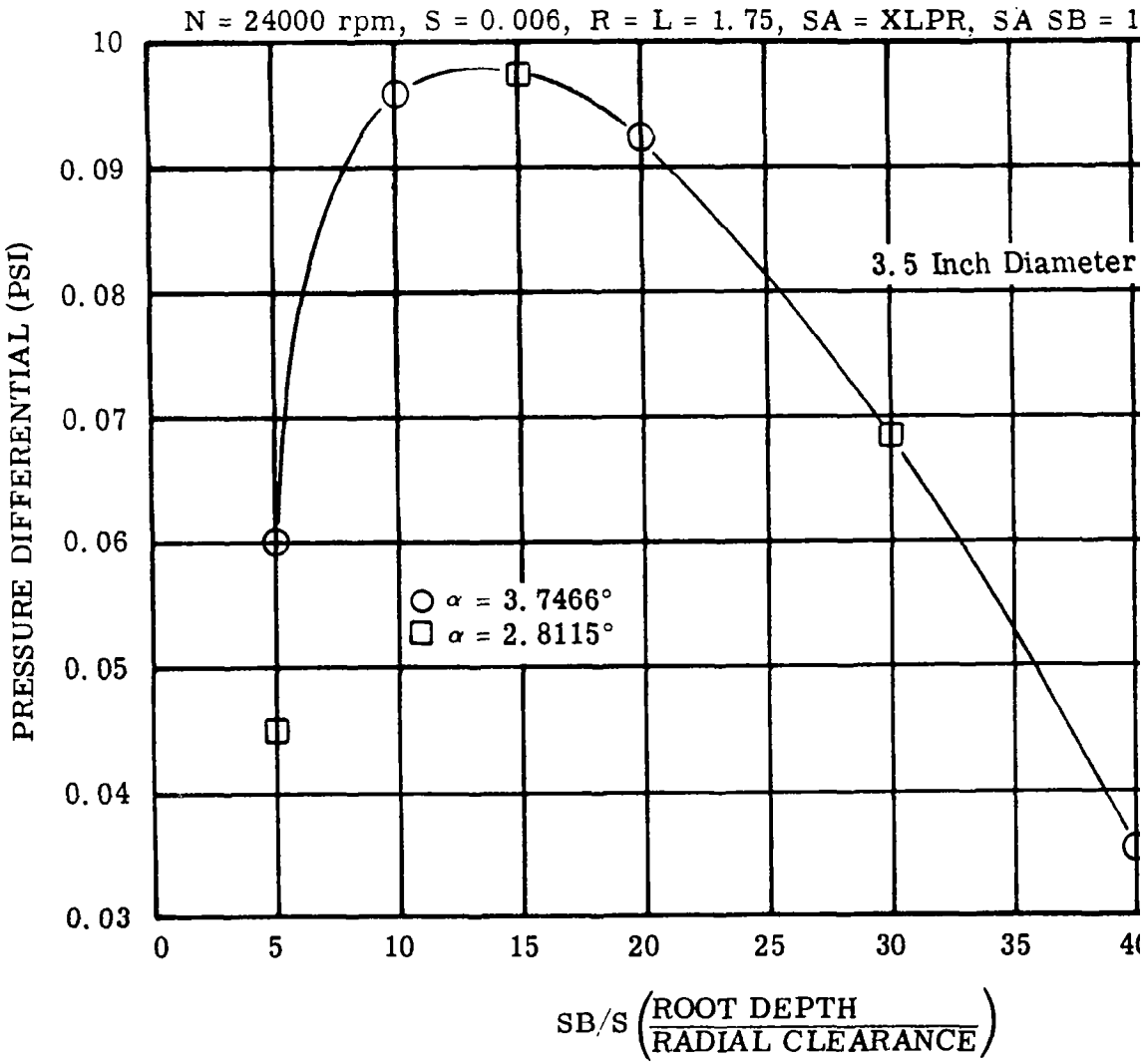

HOLWECK PUMP PARAMETRIC DATA,
EFFECT OF SB/S, 3.5 IN. DIA

FIGURE 10

ratio and approximate pitch angle were selected for the 3.5-, 4.5-, and 5.5-in.-diameter vapor pumps.

After determining the approximate pitch angle and the root width-to-depth ratio, the next step was to determine the optimum root depth to radial clearance ratio (SB/S). The results are shown on Figures 10, 11, and 12.

The resulting complete thread configuration is summarized in Table 1. The thread geometry parametric study results shown in the table are based on a shaft speed of 24,000 rpm but can be expected to hold over a full 16,000- to 32,000-rpm alternator speed range. For example, the pitch angle and root width-to-depth ratio at 16,000 and 32,000 rpm (Figure 13b) correspond to those for 24,000 rpm (Figure 4) except for the lower and higher pressure differentials. These pressure differentials change because of the lower and higher speeds.

2.3 Comparison With Other Geometries

Comparison of the configuration data, Table 1, with that of other investigators, Table 2, indicates that there is agreement among the various thread configuration ratios. The scatter can be attributed to a number of factors related to the various flow theories and to the integral selection choices. For instance, present investigations were carried out with XLPR/SA equal to one or one-half as constraints. An integral number of threads-per-inch appears to have been the constraint in the investigations of Lessley, Hodgson, and Haglund[36] and of Hodgson.[37] An integral value of the resulting pitch angle appears to have been the constraint in the investigations of Chadbourne, Kavacevich, and Riffle.[38] The net results of these various constraints is that the optimum thread configuration ratios will vary slightly because the various thread parameters are interdependent for integral numbers of threads.

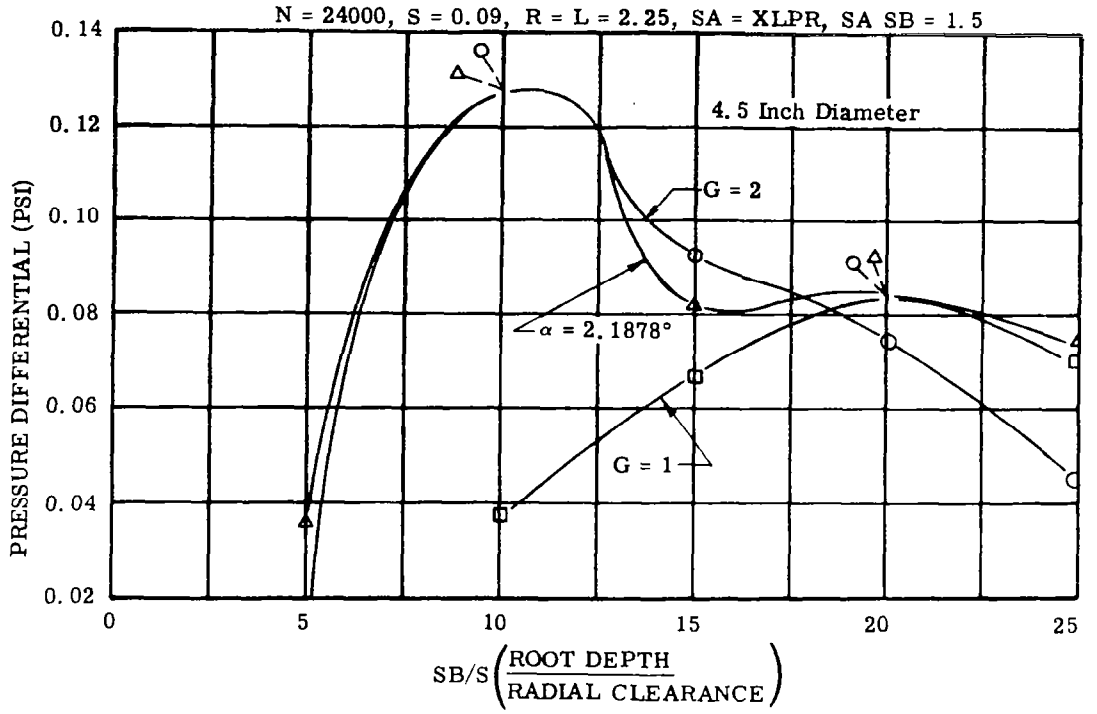

HOLWECK PUMP PARAMETRIC DATA,
EFFECT OF SB/S, 4.5 IN. DIA

FIGURE 11

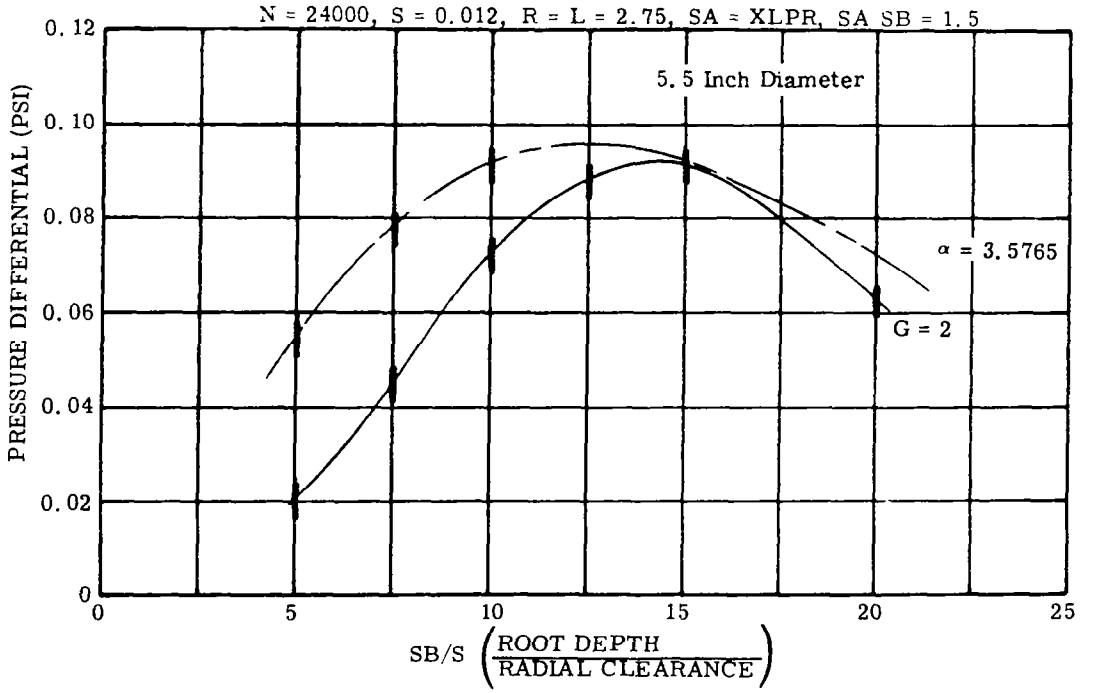

HOLWECK PUMP PARAMETRIC DATA,
EFFECT OF SB/S, 5.5 IN. DIA

FIGURE 12

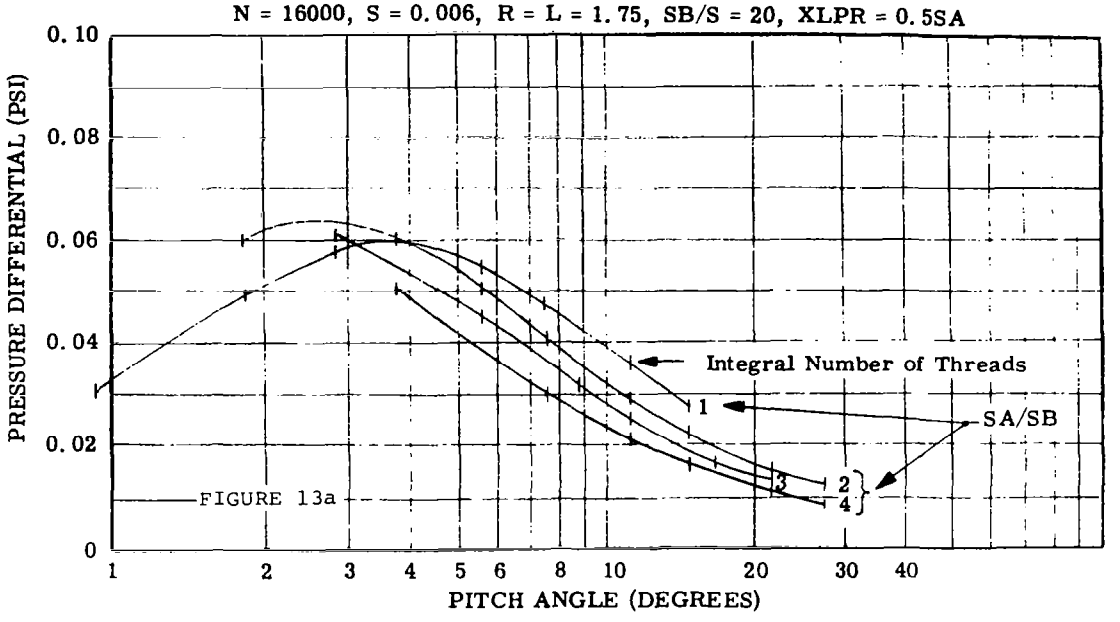

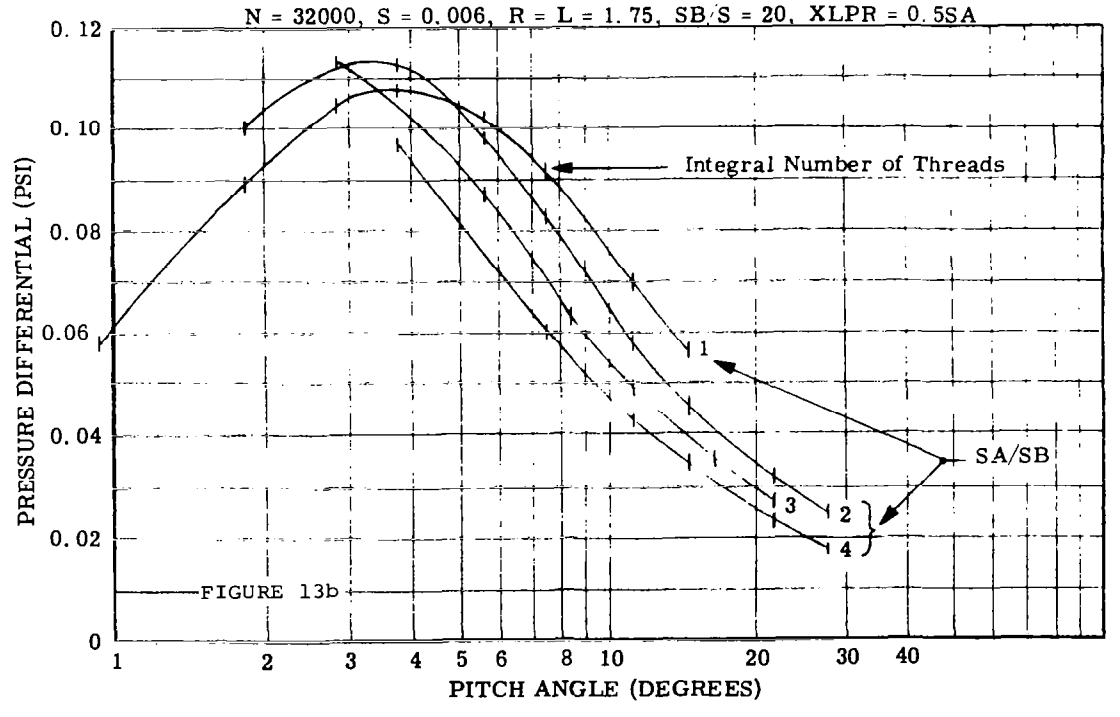

HOLWECK PUMP PARAMETRIC DATA,
EFFECT OF PITCH ANGLE AND SHAFT SPEED, 3.5 IN. DIA

FIGURE 13

TABLE 2

COMPARISON OF "OPTIMIZED" HOLWECK MOLECULAR PUMP THREADS

Investigator	Present			Reference (38)	Reference (36)	Reference (3
Vapor and Temperature	Potassium, 800°F	Potassium, 800°F	Potassium, 800°F	Potassium, 600°F	Dow ET 378, 300°F	Merc 70
Primary Flow	Viscous to transition	Viscous to transition	Viscous to transition	Transition	Molecular	Mole
Shaft Diameter	3.5	4.5	5.5	4	-	-
Radial Clearance	0.006	0.009	0.012	0.004	0.0045	0.
Pitch Angle	2.3437	2.1878	3.5765	7	-	-
Number Parallel Threads	2	2	2	3	-	-
Optimum SB/S Ratio	12.5	10	12.5	25	16	16
Optimum SA/SB Ratio	1.5	1.5	1.5	2	2.1	3.
Optimum XLPR/SA Ratio	1.0	1.0	1.0	0.638	1.43	0.

The thread root-depth geometries shown are for constant root depth over the entire length of the pump. As implied by the previous discussions, an improvement can be obtained by decreasing the root depth as the pressure increases along the length of the pump. Because of the mathematical complexities involved with including a variable thread depth in the original analysis, the configurations determined are for a constant thread depth. When final operating conditions become known, intuitive judgment can be used to arrive at a decreasing root depth, the nominal value being equal to the original constant depth; this has been done successfully in the past.[33, 36, 37] The theory presented in References 36 or 37 automatically predicts the decrease in root depth as the pressure rises but even then, the authors admit, intuitive judgment is sometimes required to arrive at the final optimum configuration.

2.4 Performance Study, Potassium

The performance of the three seals in Table 1 at variable speed and fore-pressure is shown in Figures 14, 15, and 16. As seen in the "a" figures, the pressure differential is a fraction of the fore-pressure at fore-pressures greater than 0.1 psia (order of magnitude). Below this pressure, the differential is of the same order of magnitude as the fore-pressure, and the performance is presented in the form of a pressure ratio in the "b" figures. The "c" figures show that the pressure differential is a linear function of speed.

Examination of the vapor seal performance at 20,000 rpm indicates that a cavity pressure of the order of magnitude of 0.01 psia is possible at potassium coolant temperatures as high as 850°F by series-staging three pumps (Figure 17). At 800°F, cavity pressures as low as 0.0002 psia appear possible with the staged pumps. The pressure ratios across the three stages are approximately 2.1:1, 3.7:1, and 95:1, respectively. The rapid jump in third-stage performance is due to the third-stage fore-pressure being reduced sufficiently by the

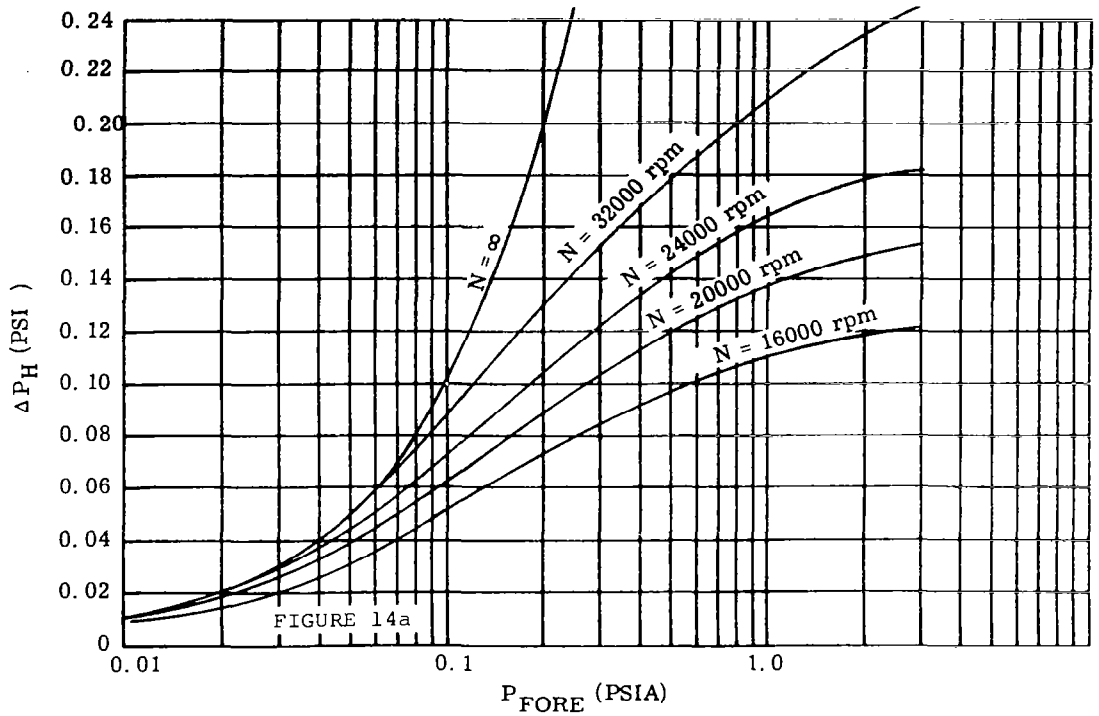

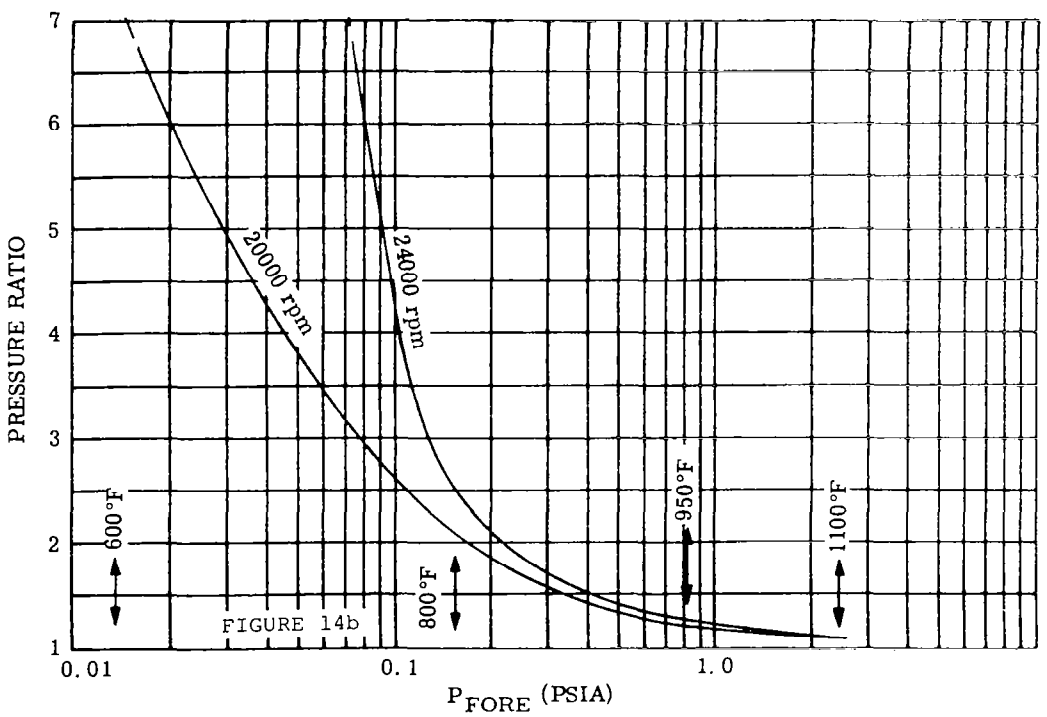

HOLWECK PUMP PERFORMANCE DATA,
3.5 IN.DIA, SATURATED POTASSIUM VAPOR

FIGURE 14

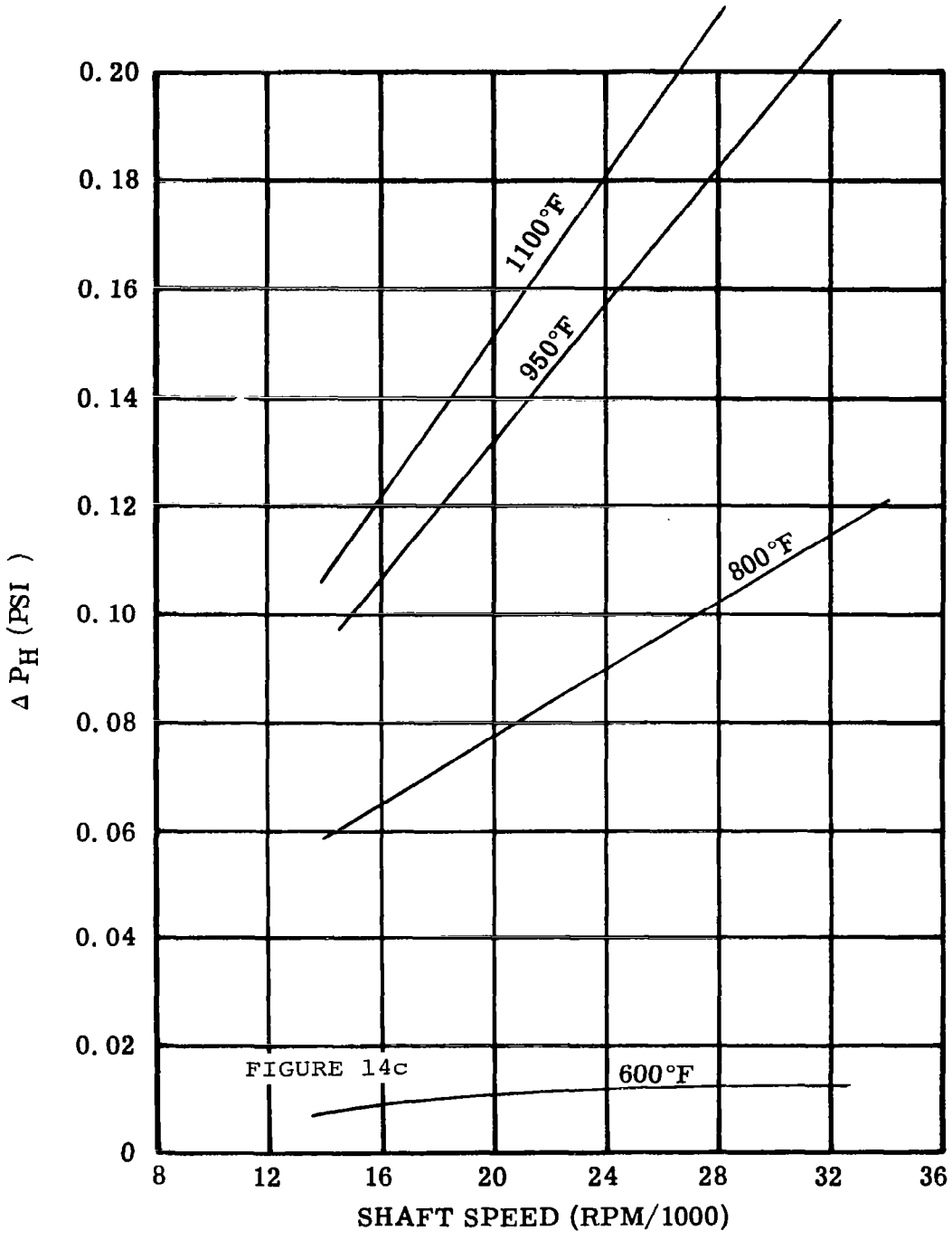

HOLWECK PUMP PERFORMANCE DATA,
3.5 IN.DIA, SATURATED POTASSIUM VAPOR

FIGURE 14 (Contd.)

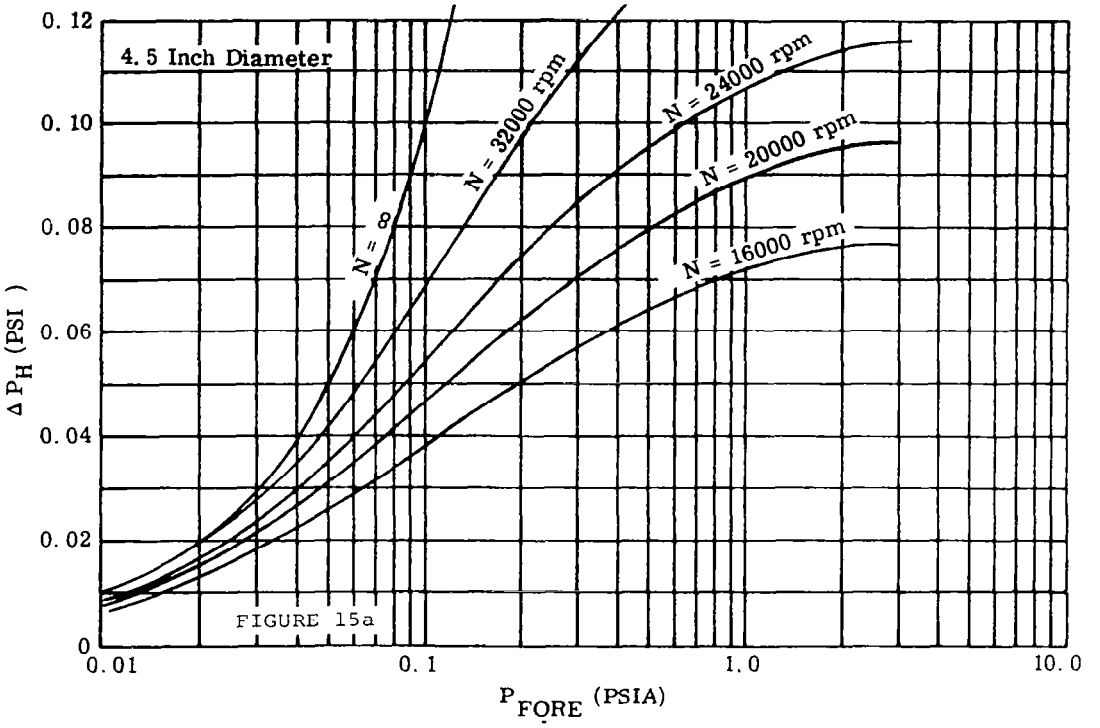

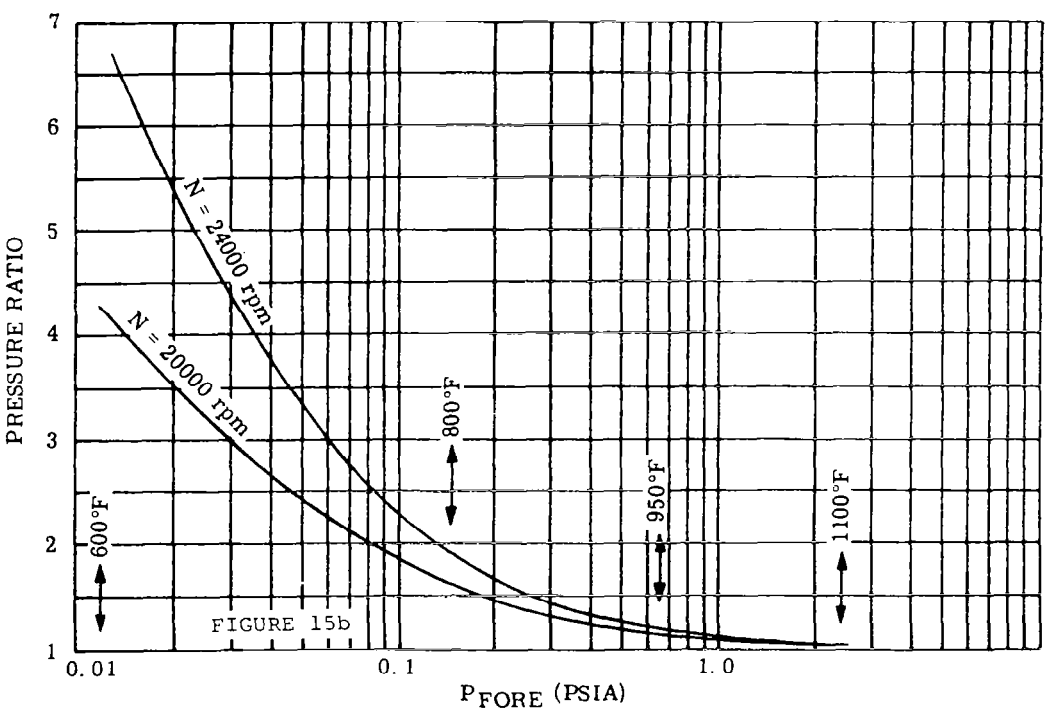

HOLWECK PUMP PERFORMANCE DATA,
4.5 IN.DIA, SATURATED POTASSIUM VAPOR

FIGURE 15

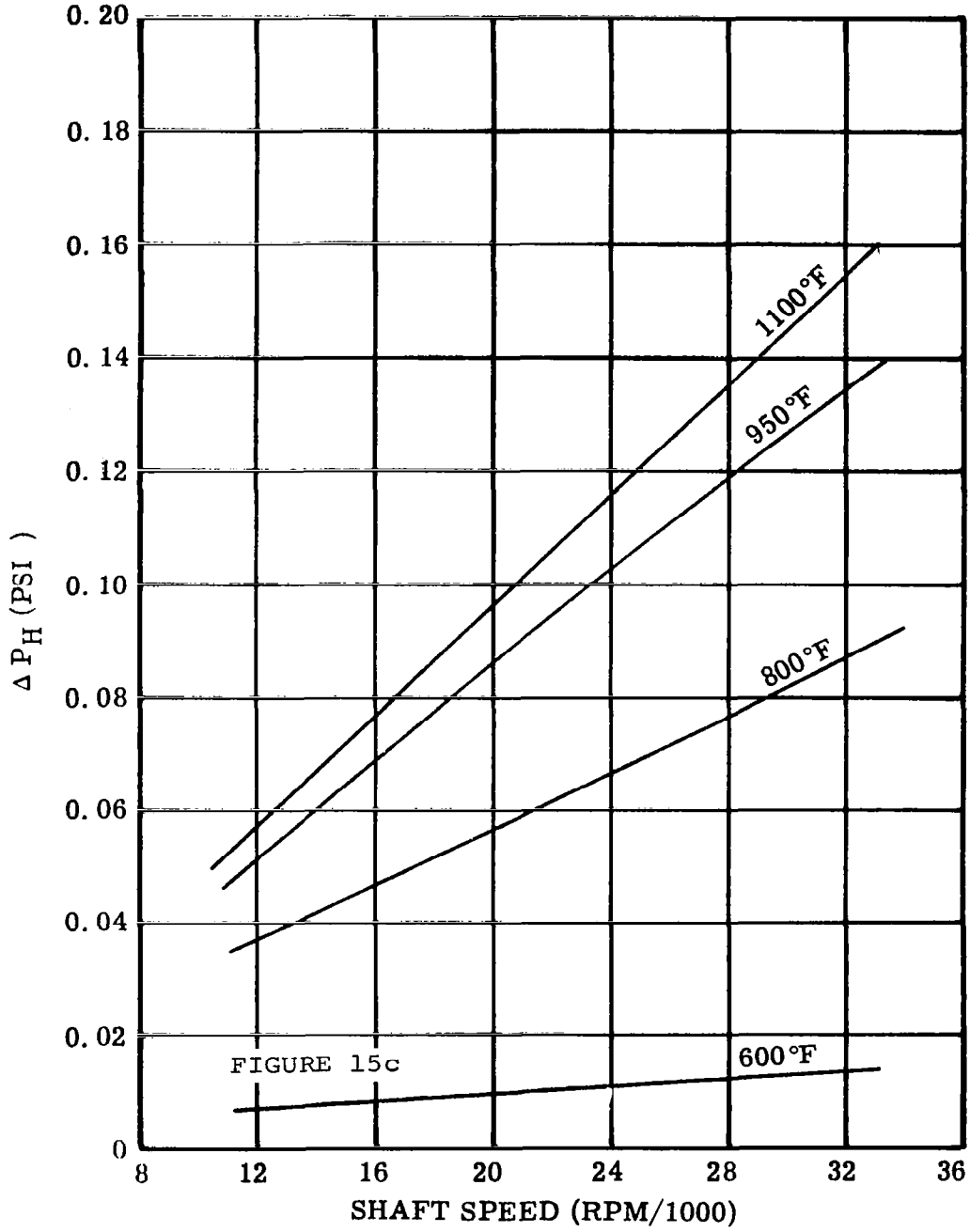

FIGURE 15c

HOLWECK PUMP PERFORMANCE DATA,
4.5 IN.DIA, SATURATED POTASSIUM VAPOR

FIGURE 15 (Contd.)

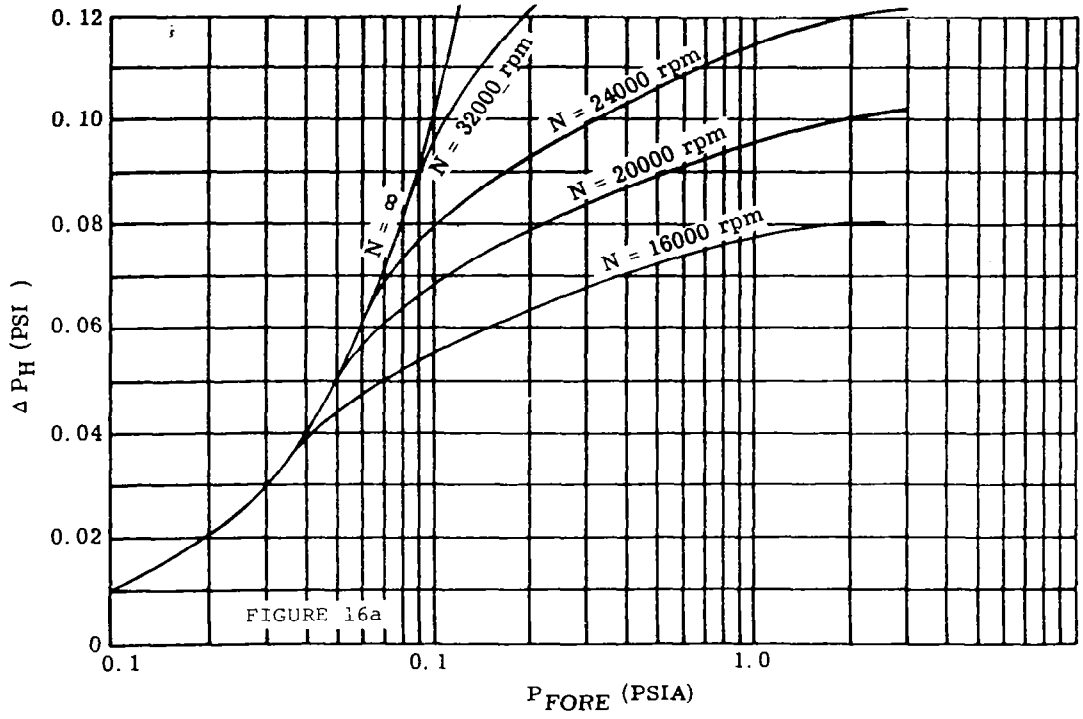

FIGURE 16a

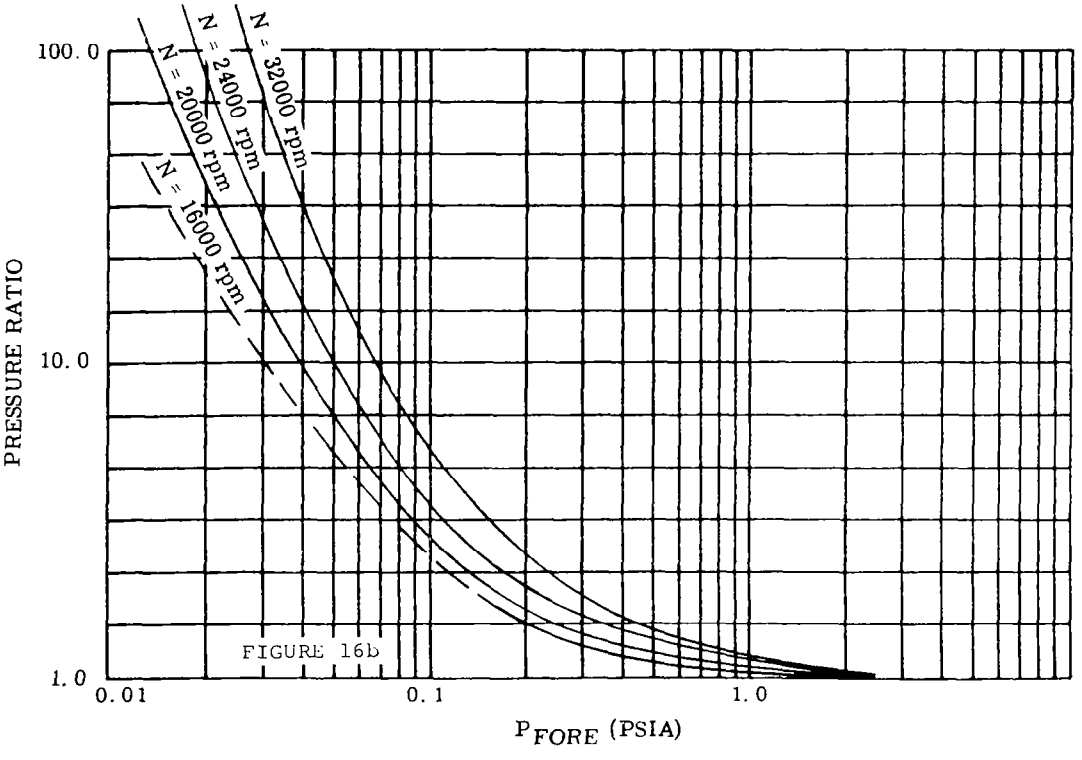

FIGURE 16b

HOLWECK PUMP PERFORMANCE DATA,
5.5 IN.DIA, SATURATED POTASSIUM VAPOR

FIGURE 16

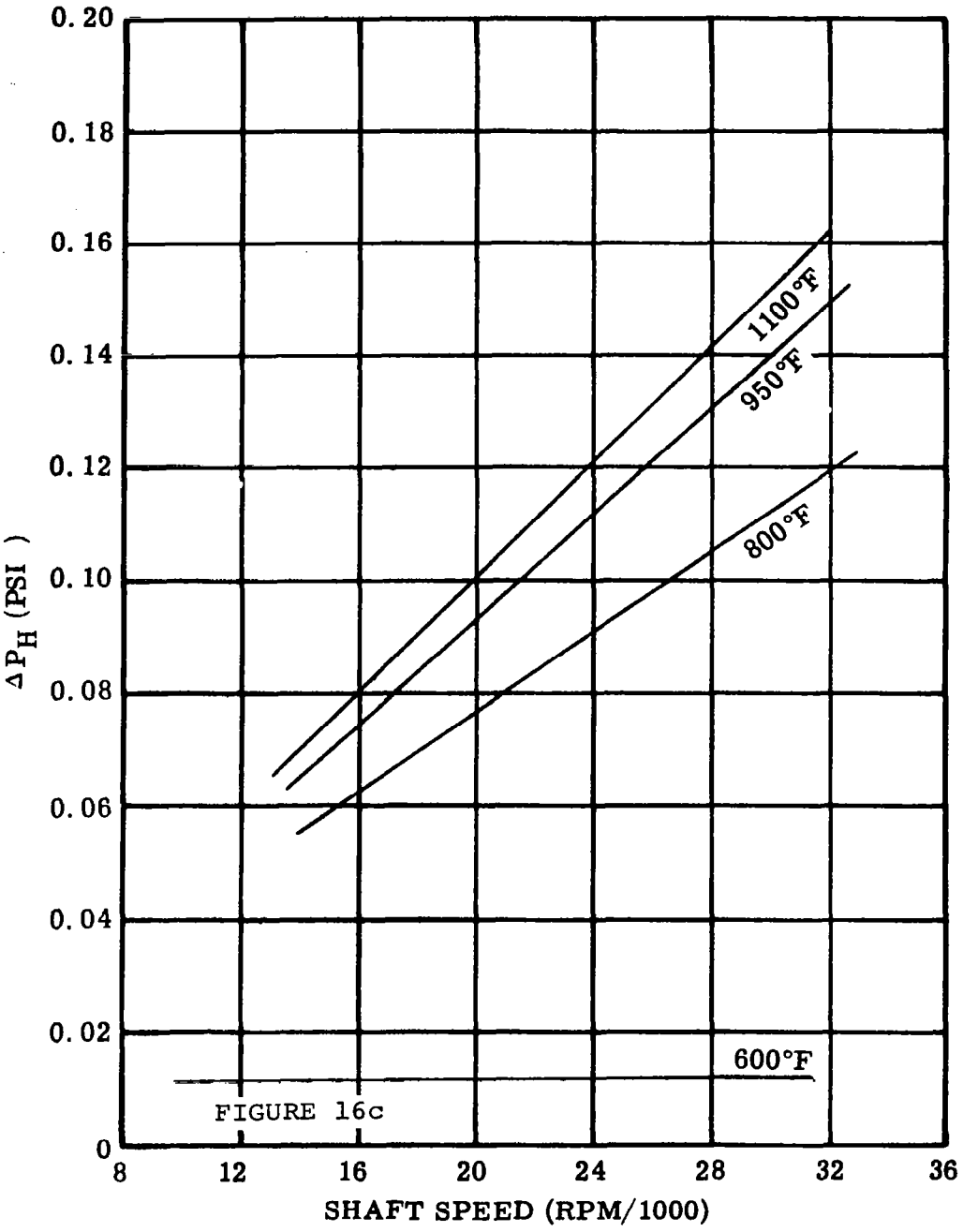

HOLWECK PUMP PERFORMANCE DATA,
5.5 IN.DIA, SATURATED POTASSIUM VAPOR

FIGURE 16 (Contd.)

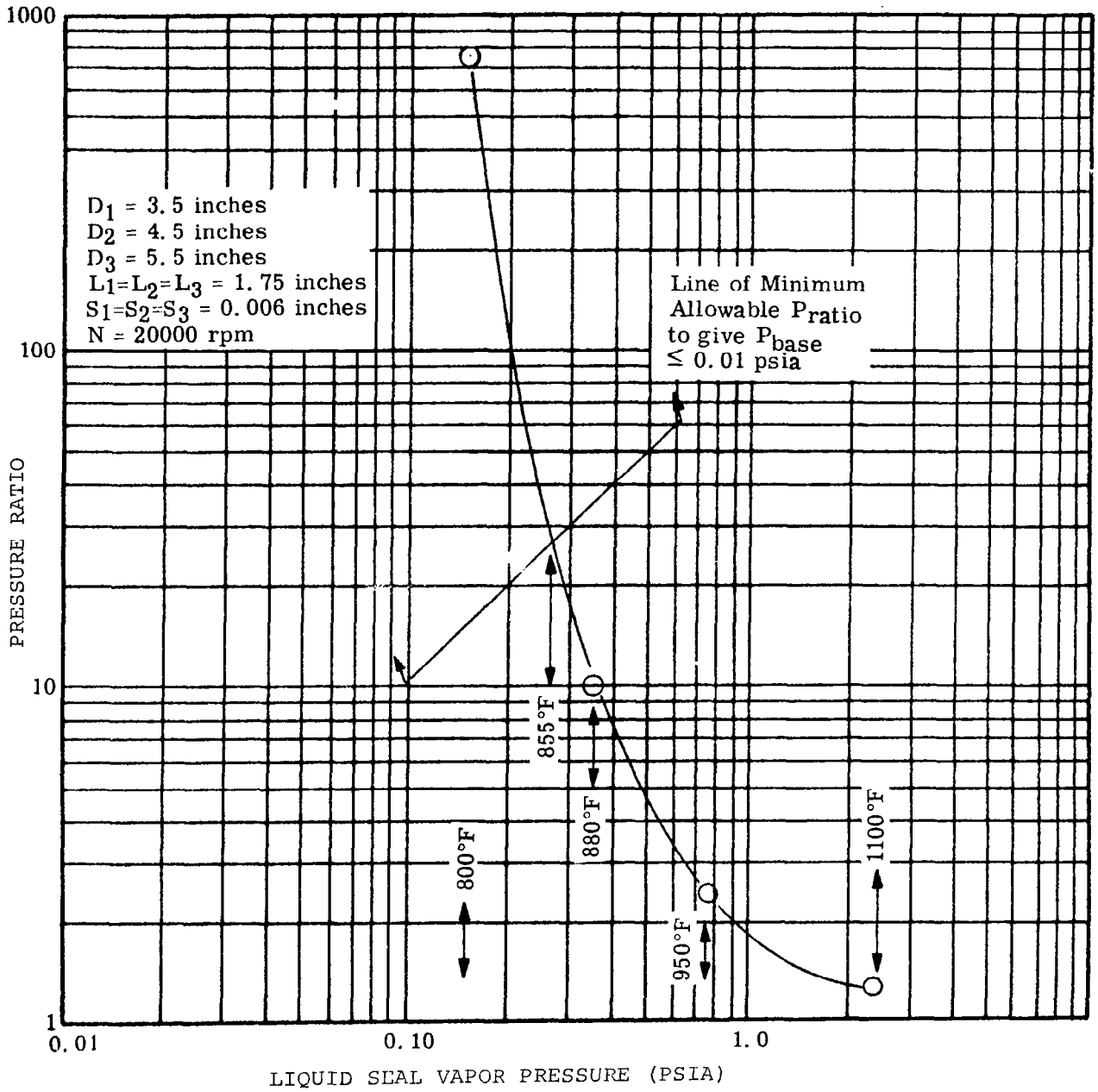

PRESSURE RATIO FOR THREE SUCCESSIVE STAGES OF HOLWECK PUMPS

FIGURE 17

first two stages so that molecular flow becomes predominant. Thus, at the minimum proposed potassium coolant temperature, 800°F, it can be stated that the Holweck molecular vacuum pumps can play a significant role in minimizing the rotor cavity pressure at speeds of interest to the KTA, e.g., 19,200 to 24,000 rpm. Of course, even greater pressure ratios can be achieved at 24,000 rpm. These are indicated in Table 3 along with the reduction in windage losses achievable with the molecular pump staging for the three-base designs.

At 600°F, the pressure ratio is usually of sufficient magnitude to obviate the need for three stages. However, if the staging is used, the total ratio may be well over a thousand as indicated in Figure 17.

At the other extreme of the proposed coolant temperature range, 1100°F, the minimum rotor cavity pressure that can be attained, even with three stages, is only on the order of 1.8 psia (down from 2.41 psia saturated vapor pressure). At these conditions, the windage losses will be in the order of tens of kilowatts. Thus if 1100°F coolant is used, some other means must be provided to reduce the rotor cavity pressure because the Holweck pumps will not contribute to reduction of the cavity pressure to an acceptable value.

2.5 Performance Study, Mineral Oil

The performance of the three seals at variable fore-pressure is shown in Figures 18, 19, and 20. At 20,000 and 24,000 rpm, the pressure differentials are near the fore-pressure for 400°F mineral oil. Thus, fewer stages are required to achieve low cavity pressures. At slightly lower seal temperatures, 380°F for instance, the flow is fully molecular, and, because of the relatively large molecule diameters and mean-free-paths of the molecules, pressure ratios of several hundreds- or thousands-to-one are readily achieved.

TABLE 3

HOLWECK PUMP STAGING AND WINDAGE POWER LOSS

Design No. 1 19,200 rpm, 800°F Potassium		Design No. 2 19,200 rpm, 400°F Mineral Oil		Desi 24,000 rpm,
Rotor Cavity Pressure, psia	Power Loss, w	Rotor Cavity Pressure, psia	Power Loss, w	Rotor Cavit Pressure, ps
0.155[a]	2850	0.036[f]	5050	0.155[a]
0.079[b]	1550	0.003[b]	420	0.062[b]
0.040[c]	830	0.00003[c]	0	0.021[c]
0.00465[d]	122			0.0003[d]
0.00005[e]	1			

[a]Saturation pressure of potassium at 800°F
[b]Rotor cavity pressure with a single-stage molecular pump
[c]Rotor cavity pressure with a two-stage molecular pump
[d]Rotor cavity pressure with a three-stage molecular pump
[e]Rotor cavity pressure with a four-stage molecular pump
[f]Saturation pressure of mineral oil at 400°F

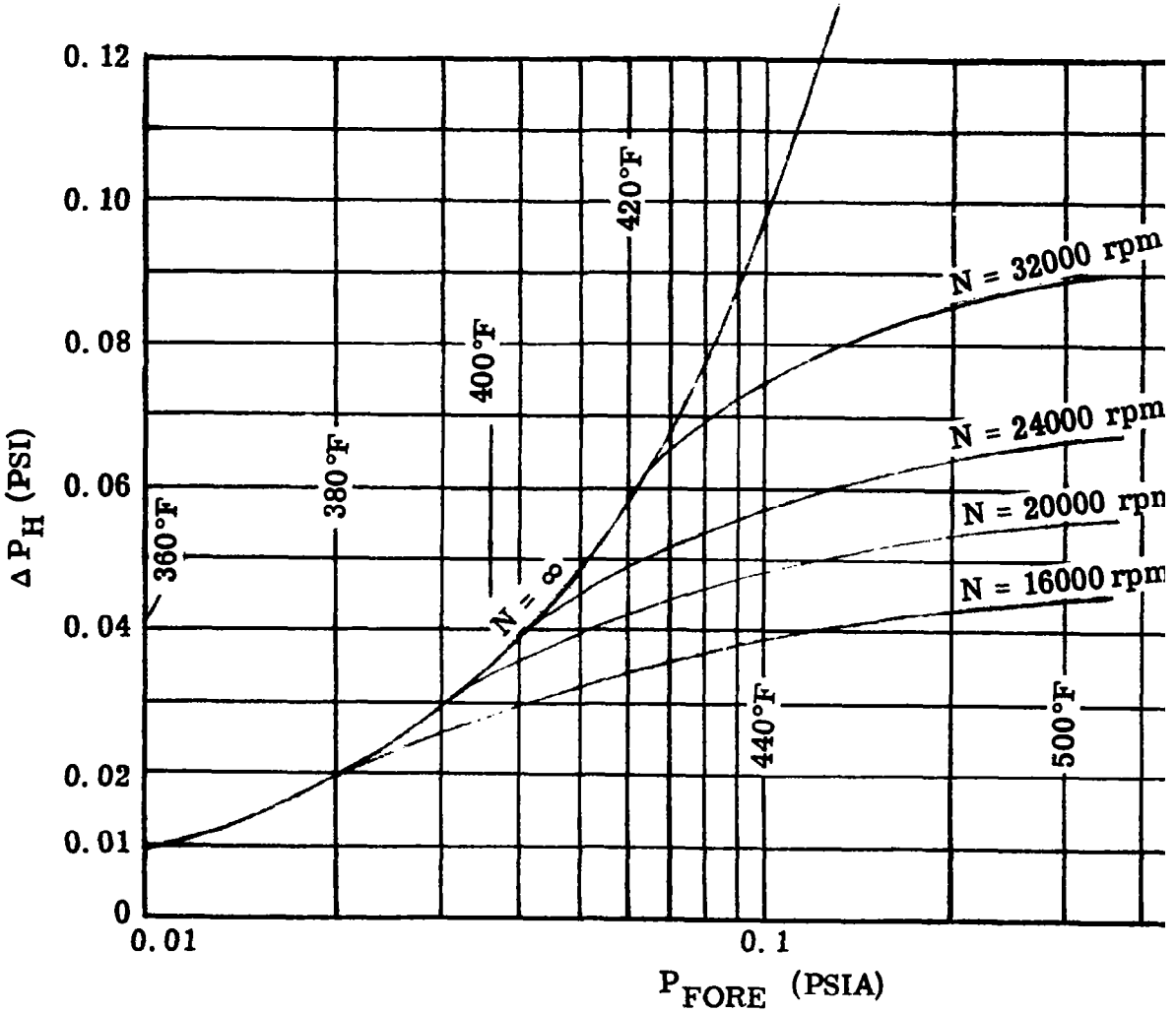

HOLWECK PUMP PERFORMANCE DATA,
3.5 IN. DIA SATURATED MINERAL OIL VAPOR

FIGURE 18

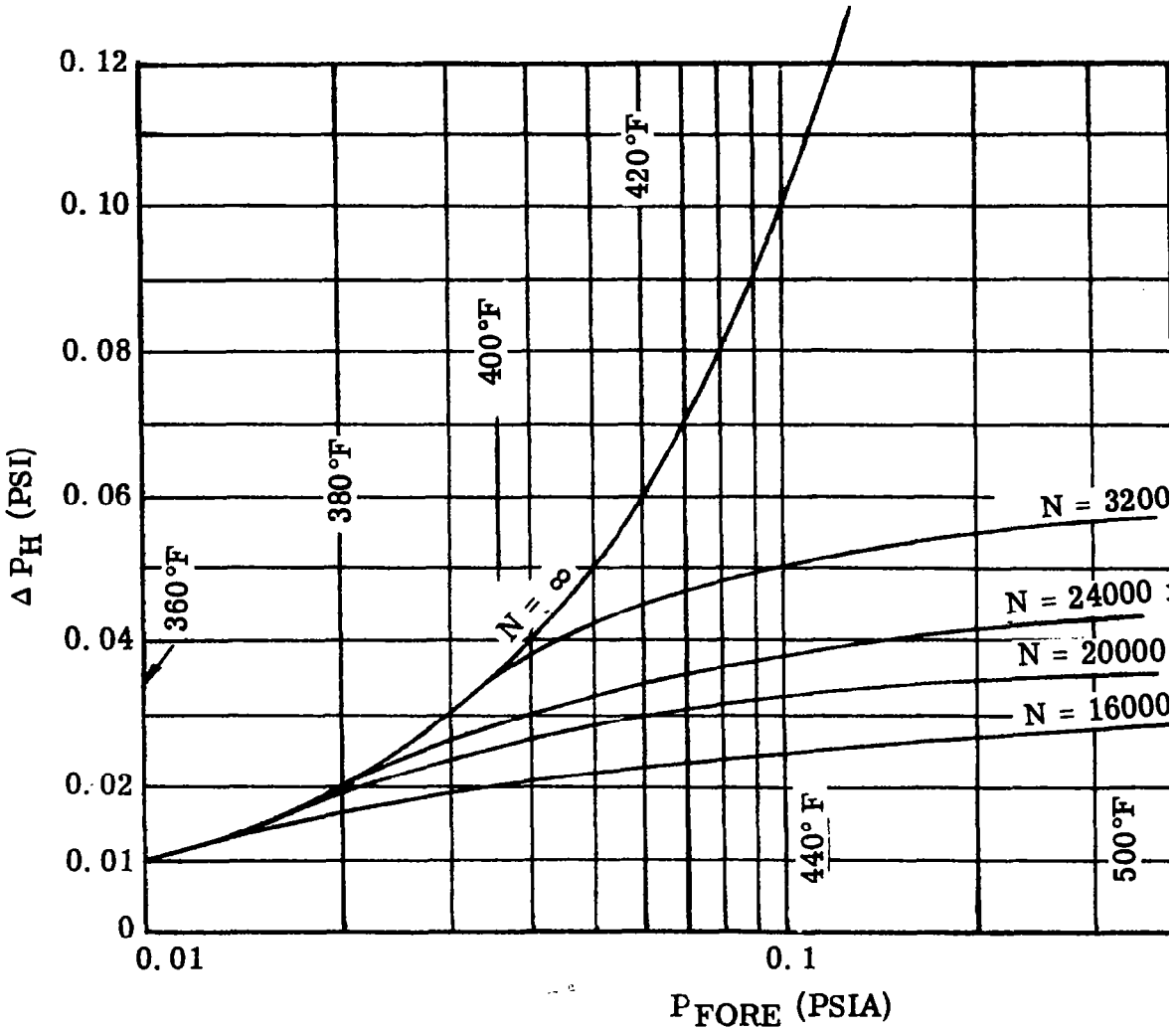

HOLWECK PUMP PERFORMANCE DATA,
4.5 IN. DIA SATURATED MINERAL OIL VAPOR

FIGURE 19

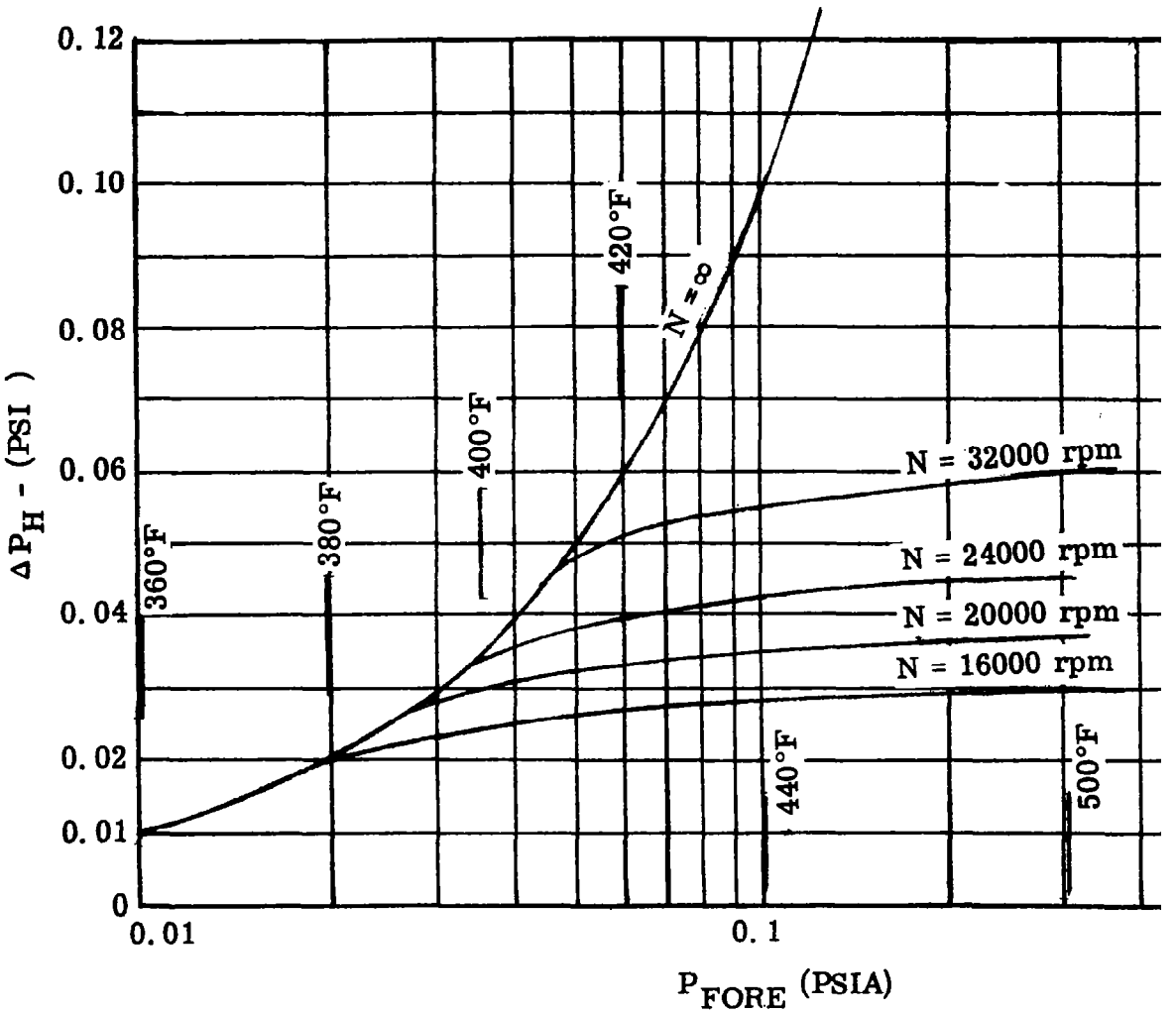

HOLWECK PUMP PERFORMANCE DATA,
5.5 IN. DIA SATURATED MINERAL OIL VAPOR

FIGURE 20

Alternate plots of pressure ratio as a function of fore-pressure were not made because of the extreme change in calculated pressure ratio in going from 400° to 380°F saturated fore-pressure. Additional analyses at four temperatures between 400° and 380°F did not reveal the shape of the curve in going from transition flow to molecular flow; a large finite jump existed in all cases analyzed.* Thus, it can be concluded that once molecular flow conditions become present, very large pressure ratios will be present.

At temperatures much above 500°F, the flow becomes turbulent, and the pressure differential generated will be greater than those shown in Figures 18, 19, and 20. However, the theory used is insufficient to predict these values.

*The computer program checks the performance as it goes, starting on the assumption of viscous flow, and once it determines that molecular flow conditions are present, it switches to a second set of equations for molecular flow theory; this switch sometimes results in a discontinuous performance curve calculation.

3. CONCLUSIONS

3.1 Temperatures Below 850°F

The maximum potassium vapor temperature at which the Holweck-type molecular pump appears feasible as a shaft seal is about 850°F with three stages. At any temperature below the 850°F, the molecular pumps can serve a useful function in the KTA alternator. The minimum temperature above which a molecular pump is needed to minimize windage is about 550°F; at this or below, staging of pumps appears unnecessary but may be desirable.

3.2 Temperature of 800°F

At 800°F potassium bearing/seal coolant temperature, the molecular pumps can reduce cavity pressures to less than 0.0002 psia, reducing the calculated windage losses to the order of a few watts.

3.3 Temperature of 1100°F

At 1100°F potassium bearing/seal coolant temperature, the molecular pumps can reduce cavity pressures to only about 1 to 2 psia which still gives windage losses of tens of kilowatts. If other means can be made to reduce the cavity pressure while maintaining the 1100°F rotor/bearing coolant, use of the molecular pump may again become feasible; such a situation must be examined on an individual basis.

3.4 Temperature of 400°F

A mineral oil vapor temperature of 400°F appears feasible for the molecular pumps to act as a shaft seal in the alternator.

3.5 Organic Fluid Performance

Because of the approximating analysis used for the mineral oil data shown, the conclusions drawn for organic fluid performance and design should be tempered with the knowledge that, once definite operating conditions and fluids are specified, the performance should be analyzed at those conditions using applicable flow theory (e.g., molecular or turbulent) for screw threads selected specifically for the organic fluid.

3.6 Preliminary Pump Design

For the preliminary designs, the parametric data included can be used to estimate the approximate envelope of volume required by the pumps to fulfill a specified performance. However, because the optimum configuration and subsequent performance are so dependent upon the vapor conditions, the actual design of the pump should be finalized after final operating conditions are specified.